

# **Influences on Hyporheic Exchange in a Small Coastal British Columbia Suburban Stream**

**by**  
**Jacquelyn Shrimmer**

B.Sc. (Environmental Science), Simon Fraser University, 2008

Thesis Submitted In Partial Fulfillment of the  
Requirements for the Degree of  
Master of Science

in the  
Department of Geography  
Faculty of Environment

**© Jacquelyn Shrimmer 2013**  
**SIMON FRASER UNIVERSITY**  
**Spring 2013**

All rights reserved.

However, in accordance with the *Copyright Act of Canada*, this work may be reproduced, without authorization, under the conditions for "Fair Dealing." Therefore, limited reproduction of this work for the purposes of private study, research, criticism, review and news reporting is likely to be in accordance with the law, particularly if cited appropriately.

# Approval

**Name:** Jacquelyn Shrimer  
**Degree:** Master of Science (Geography)  
**Title of Thesis:** *Influences on Hyporheic Exchange in a Small Coastal British Columbia Suburban Stream*  
**Examining Committee:** **Chair:** Kirsten Zickfeld  
Assistant Professor

**Dr. Ilja van Meerveld**  
Senior Supervisor  
Assistant Professor  
Faculty of Earth and Life Sciences, VU  
VU University Amsterdam

---

**Dr. Jeremy Venditti**  
Committee Member  
Associate Professor, Geography  
Simon Fraser University

---

**Dr. Diana Allen**  
External Examiner  
Professor  
Department of Earth Sciences  
Simon Fraser University

---

Date Defended: March 28, 2013

## Partial Copyright Licence



The author, whose copyright is declared on the title page of this work, has granted to Simon Fraser University the right to lend this thesis, project or extended essay to users of the Simon Fraser University Library, and to make partial or single copies only for such users or in response to a request from the library of any other university, or other educational institution, on its own behalf or for one of its users.

The author has further granted permission to Simon Fraser University to keep or make a digital copy for use in its circulating collection (currently available to the public at the "Institutional Repository" link of the SFU Library website ([www.lib.sfu.ca](http://www.lib.sfu.ca)) at <http://summit/sfu.ca> and, without changing the content, to translate the thesis/project or extended essays, if technically possible, to any medium or format for the purpose of preservation of the digital work.

The author has further agreed that permission for multiple copying of this work for scholarly purposes may be granted by either the author or the Dean of Graduate Studies.

It is understood that copying or publication of this work for financial gain shall not be allowed without the author's written permission.

Permission for public performance, or limited permission for private scholarly use, of any multimedia materials forming part of this work, may have been granted by the author. This information may be found on the separately catalogued multimedia material and in the signed Partial Copyright Licence.

While licensing SFU to permit the above uses, the author retains copyright in the thesis, project or extended essays, including the right to change the work for subsequent purposes, including editing and publishing the work in whole or in part, and licensing other parties, as the author may desire.

The original Partial Copyright Licence attesting to these terms, and signed by this author, may be found in the original bound copy of this work, retained in the Simon Fraser University Archive.

Simon Fraser University Library  
Burnaby, British Columbia, Canada

revised Fall 2011

## **Abstract**

This study examined how discharge, streambed topography, and channel planform influence hyporheic exchange in a coastal suburban stream in B.C. Tracer experiments were carried out in four reaches of Hoy Creek in Coquitlam using sodium chloride, and piezometers were installed to determine the vertical hydraulic gradient (VHG). The tracer data were used in OTIS, a transient storage model, to determine the following parameters: cross-sectional area of the stream and storage zone, dispersion, and the storage zone exchange coefficient ( $\alpha$ ). For the lower reaches, there was no significant relation between  $\alpha$  and discharge; however, there was a significant positive relation between  $\alpha$  and discharge for the upper reaches. Dispersion and the cross-sectional area of the storage zone did not change with discharge. VHG and streambed tracer breakthrough curves/data showed predominantly upwelling conditions. Hyporheic flow occurred mainly through meander bends, step-pool systems, and riffles.

**Keywords:** Hyporheic exchange; suburban stream; Hoy Creek; OTIS; tracer study; vertical hydraulic gradient

Soli Deo gloria.

## **Acknowledgements**

Thank you to everyone who has supported and encouraged me along the journey of completing this degree. I would like to thank Dr. Ilja van Meerveld for providing so much input and keeping me on track. I appreciate your direction, encouragement, and patience, especially when it came to OTIS. I would also like to thank Dr. Jeremy Venditti and Dr. Diana Allen for providing constructive feedback on my thesis.

Thank you to everyone who provided assistance in the field, rain or shine (Elizabeth Baird, Naomi Cummings, Katie Dodman, Terence Lai, Tabitha Li, Jenn Melatini, Fred Shrimmer, Sheena Spencer, Louise Steinway, Tanya Witzke, and Stephan Zimmerman). This project would not be complete without your help.

I would like to thank my parents for their support throughout this endeavor, starting with your help in the application process from half a world away, with minimal internet and phone access. This would not have been possible without your help.

Thanks to my family and friends for motivation, encouragement, lending a listening ear, and putting up with my busy and ever-changing schedule. Thanks to everyone in the Hydrology Lab and Department of Geography for the time spent bouncing ideas off one another, whether relevant to our research or otherwise.

I would like to acknowledge NSERC for funding for this research, Metro Vancouver for precipitation data, and the City of Coquitlam for various documents.

# Table of Contents

Approval.....	ii
Partial Copyright Licence .....	iii
Abstract.....	iv
Dedication.....	v
Acknowledgements.....	vi
Table of Contents.....	vii
List of Tables.....	ix
List of Figures.....	xiii
<b>1. Introduction .....</b>	<b>1</b>
1.1. Problem Statement .....	1
1.2. Research Objectives .....	3
1.2.1. Research Questions.....	3
1.2.2. Hypotheses.....	4
<b>2. Literature Review .....</b>	<b>5</b>
2.1. Introduction .....	5
2.2. Significance of the Hyporheic Zone .....	5
2.3. Controls on Hyporheic Exchange.....	7
2.3.1. Discharge .....	7
2.3.2. Geomorphic Features.....	10
2.3.3. Lateral Inflow and Hillslope Topography .....	12
2.4. Transport Processes and Modeling Hyporheic Exchange .....	13
<b>3. Study Site and Methodology .....</b>	<b>17</b>
3.1. Study Site.....	17
3.1.1. Hoy Creek, Coquitlam .....	17
3.1.2. Climate and Streamflow Normals .....	22
3.1.3. Description of the Study Reaches .....	23
3.1.3.1. Upper Study Reaches .....	23
3.1.3.2. Lower Study Reaches .....	24
3.2. Methodology.....	25
3.2.1. Tracer Experiments .....	25
3.2.2. Determination of Vertical Hydraulic Gradients.....	32
3.2.3. Determination of Inflow.....	36
3.2.4. Topographic Surveys.....	37
3.2.5. Modeling with OTIS and OTIS-P .....	37
3.2.5.1. Calibration .....	37
3.2.5.2. Validation.....	39
<b>4. Results and Discussion.....</b>	<b>41</b>
4.1. Streamflow .....	41
4.2. Steady State EC and Lateral Inflow .....	42
4.3. Vertical Hydraulic Gradients.....	51
4.4. Tracer Experiments.....	61

4.4.1. Breakthrough Curves.....	61
4.4.2. OTIS-P Calibration .....	66
4.4.3. Optimized Parameter Values.....	69
4.4.4. Storage Zone Exchange Coefficient.....	73
4.4.5. Cross-sectional Area of the Storage Zone and Stream.....	75
4.4.6. Dispersion.....	79
4.4.7. Storage Zone Residence Time.....	80
4.4.8. Hydraulic Retention Factor and Average Traveling Distance of a Water Molecule .....	81
4.5. Reliability of the Optimized Parameters .....	82
4.6. Model Validation.....	84
4.7. Issues with OTIS .....	89
<b>5. Conclusion and Recommendations .....</b>	<b>91</b>
5.1. Conclusion .....	91
5.2. Recommendations .....	92
<b>References.....</b>	<b>95</b>
<b>Appendices.....</b>	<b>101</b>
Appendix A: Temporal Stability Calculation .....	102
Appendix B: Steady State EC Maps .....	103
Appendix C: Calibration Results .....	107
Appendix D: Validation Results.....	138

## List of Tables

Table 2.1 Overview of studies on the influence of discharge on the size of the hyporheic zone (HZ).....	8
Table 2.2 Overview of studies on the influence of discharge on hyporheic exchange (HE). .....	9
Table 3.1 Upper (UA and UB) and lower (DA and DB) reach characteristics. ....	18
Table 3.2 Summary of the tracer experiments in the upper reach UA (EC measurements from the YSI and *ECH <sub>2</sub> O probes; the injection stopped at an unknown time on July 7, thus the duration of injection is an estimate). .....	27
Table 3.3 Summary of the tracer experiments in the upper reach UB (EC measurements from the YSI and *ECH <sub>2</sub> O probes). .....	27
Table 3.4 Summary of the tracer experiments in the lower reach DA (EC measurements from the YSI and *ECH <sub>2</sub> O probes). .....	28
Table 3.5 Summary of the tracer experiments in the lower reach DB (EC measurements from the YSI and *ECH <sub>2</sub> O probes). .....	28
Table 3.6 Distance of each probe from the injection site for the upper reaches. ....	31
Table 3.7 Distance of each probe from the injection site for the lower reaches.....	31
Table 3.8 R <sup>2</sup> values for the relation between EC (x) and concentration of NaCl (y) for the eleven probes used in this study.....	32
Table 3.9 Location and depth below the surface of the piezometers in the upper reaches UA and UB. Reach UA: piezometer 1 was installed outside of the reach. Reach UB: piezometers 2, 3, and 5 were washed away.....	34
Table 3.10 Location and depth below the surface of the piezometers in the lower reaches DA and DB. ....	35
Table 4.1 Discharge (Q), measurement uncertainty, and lateral inflow (Q <sub>lat</sub> ) for the lower reach tracer tests. Q <sub>YSI</sub> and YSI error are the discharge and the uncertainty in the discharge calculated from the EC measurements using the YSI probe. Q <sub>E5</sub> and E5 error are the discharge and the uncertainty in the discharge calculated from the EC measurements using the ECH <sub>2</sub> O 5 probe. In all but 5 cases (*) Q <sub>lat</sub> was less than the uncertainty in Q <sub>lat</sub> . For September 24, 2010 ECH <sub>2</sub> O data were unavailable. See Figure 3.7 and Table 3.7 for the location of the YSI and ECH <sub>2</sub> O probes.....	44

Table 4.2 Discharge (Q), measurement uncertainty, and lateral inflow ( $Q_{lat}$ ) for the upper reach tracer tests. $Q_{YSI}$ and YSI error are the discharge and the uncertainty in the discharge calculated from the EC measurements using the YSI probe. $Q_{E5}$ and E5 error are the discharge and the uncertainty in the discharge calculated from the EC measurements using the ECH <sub>2</sub> O 5 probe. (*indicates calculation from ECH <sub>2</sub> O 1 probe instead of the YSI probe). In all cases $Q_{lat}$ was less than the uncertainty in $Q_{lat}$ . See Figure 3.7 and Table 3.6. ....	45
Table 4.3 Time between the start of the injection (start) and steady state (SS), the start of the injection and the start of the increase in EC (start to rise), between the start of the increase in the rise in EC and steady state EC (rise to SS), and the ratio of rise to SS and start to rise (normalized) for the YSI probe measurements at upper reach UA. The Spearman rank correlation coefficient ( $r_s$ ) for the relation between these timing parameters and discharge is also given. ....	62
Table 4.4 Time between the start of the injection (start) and steady state (SS), the start of the injection and the start of the increase in EC (start to rise), between the start of the increase in the rise in EC and steady state EC (rise to SS), and the ratio of rise to SS and start to rise (normalized) for the YSI probe measurements at upper reach UB. The Spearman rank correlation coefficient ( $r_s$ ) for the relation between these timing parameters and discharge is also given. ....	63
Table 4.5 Time between the start of the injection (start) and steady state (SS), the start of the injection and the start of the increase in EC (start to rise), between the start of the increase in the rise in EC and steady state (rise to SS), and the ratio of rise to SS and start to rise (normalized) for the YSI probe measurements at lower reach DA. The Spearman rank correlation coefficient ( $r_s$ ) for the relation between these timing parameters and discharge is also given. ....	64
Table 4.6 Time between the start of the injection (start) and steady state (SS), the start of the injection and the start of the increase in EC (start to rise), between the start of the increase in the rise in EC and steady state (rise to SS), and the ratio of rise to SS and start to rise (normalized) for the YSI probe measurements at lower reach DB. The Spearman rank correlation coefficient ( $r_s$ ) for the relation between these timing parameters and discharge is also given. ....	65
Table 4.7 The correlation coefficient (R), Nash-Sutcliffe Efficiency (E), and Mean Squared Error (MSE) for the modeled and observed data at the YSI probe location and the range of R, E, and MSE for the ECH <sub>2</sub> O probe locations in reach UA. For Oct. 5, 2010 only the ECH <sub>2</sub> O-1 probe recorded data. The experiment on July 7, 2010 was not included due to the pump stopping at an unknown time. ....	67

Table 4.8 The correlation coefficient (R), Nash-Sutcliffe Efficiency (E), and Mean Squared Error (MSE) for the modeled and observed data at the YSI probe location and the range of R, E, and MSE for the ECH <sub>2</sub> O probe locations in reach UB (Oct. 27 parameters are not included because they would not stabilize in OTIS-P; *outlier).....	68
Table 4.9 The correlation coefficient (R), Nash-Sutcliffe Efficiency (E), and Mean Squared Error (MSE) for the modeled and observed data at the YSI probe location and the range of R, E, and MSE for the ECH <sub>2</sub> O probe locations in reach DA (Sept 28 and Nov 9 parameters were not included because the model simulations would not stabilize in OTIS-P; *outlier). .....	68
Table 4.10 The correlation coefficient (R), Nash-Sutcliffe Efficiency (E), and Mean Squared Error (MSE) for the modeled and observed data at the YSI probe location and the range of R, E, and MSE for the ECH <sub>2</sub> O probe locations in reach DB. ....	69
Table 4.11 The optimized parameter values for reach UA. For each date the first row shows the values for the first site (YSI probe) and second row for the last site (ECH <sub>2</sub> O 5 probe). The experiment on July 7, 2010 was not included due to the pump stopping at an unknown time. See Figure 3.7 and Table 3.6 for the probe locations. ....	70
Table 4.12 The optimized parameter values for reach UB (Oct. 27 parameters are not included because they would not stabilize in OTIS-P; *outlier). For each date the first row shows the values for the first site (YSI probe) and second row for the last site (ECH <sub>2</sub> O 4/5 probe). See Figure 3.7 and Table 3.6 for the probe locations. ....	71
Table 4.13 The optimized parameter values for reach DA (*estimate from a different probe location due to YSI probe malfunction; Sept. 28 and Nov. 9 parameters were not included because the model simulations would not stabilize in OTIS-P; **outlier). For each date the first row shows the values for the first site (YSI probe) and second row for the 6th site (ECH <sub>2</sub> O 5 probe). Dal for Nov. 16 is not given due to high uncertainty in the discharge calculation. See Figure 3.7 and Table 3.7 for the probe locations.....	72
Table 4.14 The optimized parameter values for reach DB. For each date the first row shows the values for the first site (YSI probe) and second row for the 6 <sup>th</sup> site (ECH <sub>2</sub> O 5 probe). See Figure 3.7 and Table 3.7 for the probe locations.....	73
Table 4.15 Correlation coefficient (R), Nash-Sutcliffe Efficiency (E), and Mean Squared Error (MSE) of the range of modeled versus observed DEC and piezometer data for reaches UA and UB (*outlier).....	85

Table 4.16 Correlation coefficient (R), Nash-Sutcliffe Efficiency (E), and Mean Squared Error (MSE) for the modeled and observed DEC and piezometer data for reaches DA and DB (\*outlier)..... 86

## List of Figures

Figure 1.1 Vertical and lateral exchange of water between the open channel and the surrounding saturated sediments of the hyporheic zone (shaded area; adapted from Findlay, 1995). .....	2
Figure 2.1 The four processes of solute transport in a stream.....	13
Figure 2.2 Conceptual framework for OTIS (from Runkel, 1998).....	14
Figure 3.1 Location of Hoy Creek in Coquitlam, BC. (Data source: Google Earth, Digital Globe, accessed June 8, 2012) .....	19
Figure 3.2 Photos of the upper (left two images) and lower (right two images) reaches of Hoy Creek during low flow conditions. ....	19
Figure 3.3 Main features in the upper and lower study reaches of Hoy Creek and locations of the piezometers. The trees that are labelled have a significant influence on the stream since they protrude into the flow. ....	20
Figure 3.4 Cumulative frequency of the B-axis of bed material based on a Wolman pebble counts for reaches UA, UB, DA, and DB. ....	21
Figure 3.5 Precipitation and discharge in upper and lower Hoy Creek. ....	21
Figure 3.6 Precipitation and daily average temperature normals from 1971-2000 for Coquitlam and Port Moody, B.C. respectively (Environment Canada, 2010). ....	22
Figure 3.7 Probe and piezometer locations for the four study reaches. Red to blue shading indicates higher to lower elevation. Distances of the probes below the top of each reach are given in Table 3.6 and Table 3.7. ....	30
Figure 3.8 Negative (left) and positive (right) VHG, indicating downwelling and upwelling hyporheic flow respectively (figure adapted from Baxter et al., 2003). ....	35
Figure 3.9 Piezometer network across and around a meander bend in reach UA. ....	36
Figure 4.1 Unexplained high discharge events (indicated by arrows). These streamflow responses were observed at the upper reach during periods without precipitation.....	42
Figure 4.2 Discharge (L/s) during the tracer experiments at reach UA.....	46
Figure 4.3 Discharge (L/s) during the tracer experiments at reach UB.....	47
Figure 4.4 Discharge (L/s) during the tracer experiments at reach DA.....	48

Figure 4.5 Discharge (L/s) during the tracer experiments at reach DB.....	49
Figure 4.6 Average rank of steady state EC for each reach. A high average rank indicates a relatively low steady state EC and thus a relatively high discharge. Refer to Figure 3.3 for an explanation of the features in the stream (different shades of blue represent riffles and pools). .....	50
Figure 4.7 Standard deviation (SD) of the rank of steady state EC at each probe location within each reach. A low SD indicates a more persistent rank, while a high SD indicates a highly variable rank for steady state EC.....	51
Figure 4.8 Vertical hydraulic gradients during the tracer experiments in reach UA. Negative values indicate downwelling. Positive values indicate upwelling. ....	54
Figure 4.9 Vertical hydraulic gradient during the tracer experiments in reach UB. Negative values indicate downwelling. Positive values indicate upwelling. ....	55
Figure 4.10 Vertical hydraulic gradient during the tracer experiments in reach DA. Negative values indicate downwelling. Positive values indicate upwelling. ....	56
Figure 4.11 Vertical hydraulic gradient during the tracer experiments in reach DB. Negative values indicate downwelling. Positive values indicate upwelling. ....	57
Figure 4.12 Average rank of the VHG for each reach. A low rank indicates a low (or more negative) VHG compared to the other sites in the reach, while a high rank indicates a relatively large positive VHG. ....	58
Figure 4.13 Standard deviation of the rank of the VHG in each reach. A low standard deviation of the rank indicates a persistent ranks. ....	59
Figure 4.14 Examples of the observed and modeled breakthrough curves at the YSI locations in the upper and lower reaches of Hoy Creek (UA and DB). Observed and modeled breakthrough curves of all experiments are provided in Appendix C.....	61
Figure 4.15 The time between the start of the increase in EC and steady state (rise to SS) divided by the time between the start of the experiment and the start of the increase in EC (start to rise) versus discharge (Q). Higher values of (rise to SS)/(Start to rise) indicate more transient storage and dispersion. The top figure shows the relation for the upper reaches and the bottom figure shows the relation for the lower reaches. ....	66

Figure 4.16 Relation between the optimized storage zone exchange coefficient ( $\alpha$ ) and discharge for the four reaches. Left column shows the data for the upper reaches (UA: filled symbols and UB: open symbols), the right columns show the data for the lower reaches (DA: filled symbols, DB: open symbols). The upper row shows the data for the YSI probe location, the bottom row for the ECH <sub>2</sub> O 5 probe location.....	75
Figure 4.17 The optimized (filled symbols) and estimated cross-sectional area (open symbols) of the stream (A) for the upper reaches (top row) and lower reaches (bottom row) as a function of discharge.....	76
Figure 4.18 The optimized storage zone cross-sectional area ( $A_s$ ) for the upper reaches (left column) and lower reaches (right column) as a function of discharge for the YSI probe location (upper row) and ECH <sub>2</sub> O-5 location (lower row) (UA and DA: filled symbols and UB and DB: open symbols).....	77
Figure 4.19 The ratio of the cross-sectional area of the hyporheic zone and the cross-sectional area of the stream ( $A_s/A$ ) as a function of discharge for the upstream reaches (left column) and downstream reaches (right column); YSI probe location (top row) and ECH <sub>2</sub> O-5 probe location (bottom row) (UA and DA: filled symbols and UB and DB: open symbols).....	79
Figure 4.20 Storage zone residence time as a function of discharge for the upper reaches (left column) and lower reaches (right column; UA and DA: filled symbols and UB and DB: open symbols). YSI probe location (top row) and ECH <sub>2</sub> O 5 probe location (bottom row).....	80
Figure 4.21 Hydraulic retention factor ( $R_h$ ) as a function of discharge at the YSI probe location (UA and DA: filled symbols and UB and DB: open symbols).....	81
Figure 4.22 The average distance a water molecule travels in the stream before entering transient storage ( $L_s$ ) as a function of discharge at the YSI probe location (top row) and ECH <sub>2</sub> O-5 location (bottom row) (UA and DA: filled symbols and UB and DB: open symbols). ....	82
Figure 4.23 The Damköhler number ( $Da_l$ ) as a function of discharge for the tracer tests in the upper and lower reaches. The area between the dashed lines is the ideal range of $Da_l$ values. ....	83
Figure 4.24 Validation graphs for the tracer experiment on July 30, 2010 in reach DA. For the locations of the probes, see Figure 3.7. All other validation graphs are given in Appendix D.....	88

# 1. Introduction

## 1.1. Problem Statement

The hyporheic zone is a hydrologically, biologically, and chemically distinct area between the stream and the surrounding streambed in which the exchange of water and dissolved material occurs. It is preferred by salmon for spawning habitat, and acts as natural filter for effluents, contaminants, and nutrients (Baxter and Hauer, 2000; Hancock, 2002; Gandy et al., 2007). Additionally, hyporheic exchange increases the degree of contact of subsurface water with the substrate and therefore increases the solute residence time (Bencala, 2000). While the hyporheic zone is not frequently significant in volume, it is significant for solute transport from the stream to the subsurface (Bencala et al., 2011).

Harvey and Bencala (1993) conceptualize hyporheic flow as predominantly horizontal flow outside of the stream and predominantly vertical flow beneath the stream (Figure 1.1). Horizontal exchange of water occurs commonly through meander bends in the stream. Longitudinal exchange occurs through step-pool and riffle-pool sequences in a stream, which are associated with complexity of the streambed. Head gradients are the driving force behind hyporheic exchange (Tonina and Buffington, 2009). The composition of streambed material also affects movement of water through it, thereby influencing the extent of the hyporheic zone and the amount of hyporheic exchange. For example, coarser material results in a greater water exchange between the stream and the hyporheic zone assuming there is a head gradient.

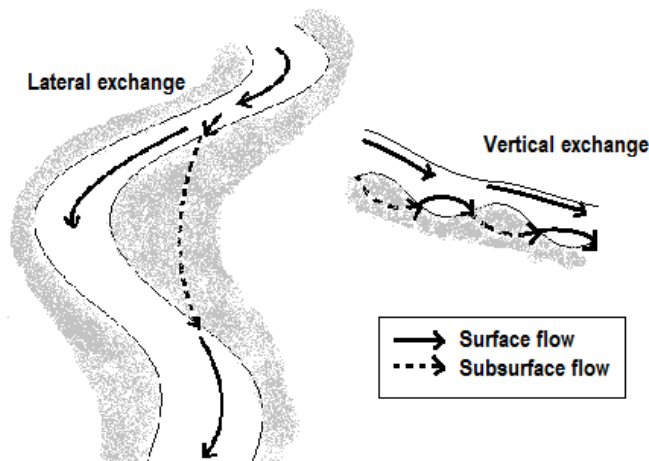


**Figure 1.1 Vertical and lateral exchange of water between the open channel and the surrounding saturated sediments of the hyporheic zone (shaded area; adapted from Findlay, 1995).**

A number of other factors also influence the extent of the hyporheic zone and the rate of hyporheic exchange. These include discharge, streambed topography, and channel planform (Harvey and Bencala, 1993; Harvey et al., 1996; Dahm et al., 2007). However, previous studies have yielded inconsistent results regarding how discharge influences the hyporheic zone and hyporheic exchange. Some studies have shown that the hyporheic zone increases with increasing discharge (Wondzell, 2006; Patschke, 1999; Scordo and Moore, 2009), while others indicate a decrease with increasing discharge (D'Angelo et al., 1993; Duineveld, 2008; Harvey et al., 1996). The same is true for the rate of hyporheic exchange (Wondzell, 2006; Harvey et al., 1996; Karwan and Saiers, 2009). Furthermore, some studies indicate no trend between the extent of the hyporheic zone or then amount of hyporheic exchange and discharge (Legrand-Marcq and Laudelout, 1985; Patschke, 1999; Scordo and Moore, 2009).

Despite an increase in the number of studies on hydrological processes within the hyporheic zone, there is a need to continue to advance our knowledge of the hyporheic zone. There is especially a need to compare results from different studies (different flow rates, different streambed topographies, different streambed materials, etc.) to derive generalities. According to Bencala (2000), "continuing advances in knowledge of the hydrological processes in hyporheic zones are critical to quantitative

analysis of stream ecosystems”. Findlay (1995) states that there has been “no attempt to uncover generalities across systems or to provide an organizing framework to simplify intersystem comparisons”, which is in agreement with White (1993) who states, “to my knowledge, a comparative examination of the hyporheic zones within any single, larger river system (e.g., 1<sup>st</sup> order to 6<sup>th</sup> or larger order streams) has never been attempted”. Krause et al. (2011a) add that one of the major issues with current and future research of hyporheic exchange involves understanding scale dependencies and variability in streambed properties. In addition, further research is needed on how hyporheic exchange is influenced by discharge, streambed topography, and streambed material.

Research is also lacking regarding the hyporheic zone in urban streams; most studies have been conducted under laboratory conditions or in forested areas. This study therefore examines hyporheic exchange in an urban setting and compares it to previous studies on hyporheic exchange in forested and laboratory settings.

## **1.2. Research Objectives**

The objective of this project was to gain a better understanding of hyporheic exchange in a suburban coastal British Columbia stream, and the factors that influence it.

### **1.2.1. *Research Questions***

The specific research questions for this study were:

1. How different is hyporheic exchange in high and low gradient reaches?
2. How do hyporheic exchange and transient storage change with discharge?
3. Can streambed topography and channel planform explain locations where hyporheic exchange and lateral inflow occur?

### **1.2.2. Hypotheses**

My hypotheses for this research were as follows:

**Hypothesis 1:** Hyporheic exchange will be greatest in high gradient reaches and lowest in low gradient reaches due to decreasing head differences and finer streambed sediment as a result of the lower stream velocities in the low gradient reaches. The hyporheic zone will be larger in lower gradient reaches because the stream is wider and streambed tends to be thicker in these areas.

**Hypothesis 2:** Hyporheic exchange will decrease with increasing discharge because the influence of head differences due to obstructions decreases. However, the extent of the hyporheic zone will increase with increasing discharge because the area available for hyporheic exchange increases as the stream width widens, as found in studies conducted in the Malcolm Knapp Research Forest in B.C. (Patschke, 1999; Scordo and Moore, 2009).

**Hypothesis 3:** Streambed topographical features (specifically riffle and step-pools), and channel planform (specifically meander bends) will be locations of increased hyporheic exchange and lateral inflow during low flow conditions, but anthropogenic features such as storm drains determine the locations of lateral inflows during high flow conditions.

## **2. Literature Review**

### **2.1. Introduction**

Different scientific fields study the hyporheic zone and its implications for biotic processes, filtration, and transformation of chemicals; as a result, a number of different definitions of the hyporheic zone have been proposed. The term “hyporheic” is derived from Greek, with “hypo” meaning “under”, and “rhe” meaning “flow” (Tonina and Buffington, 2009).

Hydrologically the hyporheic zone can be defined as the zone in between the stream and groundwater in which transient storage occurs. It can also be defined as the saturated area that is affected by stream water, whereas groundwater is defined as the saturated area unaffected by stream water (White, 1993). Harvey and Bencala (1993) define the hyporheic zone as the subsurface area into which the downwelling streamwater enters and is temporarily stored with the subsurface water already present before re-entering the stream. The definition used in this study will be this hydrologically relevant definition of the hyporheic zone, as this study will focus on the hydrological aspects of the hyporheic zone rather than the biogeochemical and ecological aspects.

### **2.2. Significance of the Hyporheic Zone**

The hyporheic zone is home to a diverse and unique set of organisms, especially invertebrates, and is the site of significant biogeochemical activity (Marmonier et al., 1993; Hancock, 2002). Different organisms inhabit the stream, groundwater, and hyporheic zones. The aquatic invertebrates in the hyporheic zone are termed the “hyporheos” and include crustaceans, water mites, worms, and juvenile stages of aquatic insects (Boulton et al., 1998). Exchange of water from the stream to the hyporheic zone changes stream water chemistry once water upwells from the hyporheic

zone. This is due to the anaerobic and aerobic metabolic processes, and a combination of biogeochemical processes that occur in the hyporheic zone (Findlay, 1995). Dissolved oxygen generally decreases within the hyporheic zone due to metabolic processes by organisms that inhabit the hyporheic zone (Findlay, 1995). Additionally, due to retention of water in the hyporheic zone, remineralization can delay the loss of nutrients (such as nitrogen) from the stream, which can lead to increases in overall primary production (Findlay, 1995).

The hyporheic zone has also been studied for its significance to fish, in particular, salmon. Hyporheic exchange is more likely in areas characterized by gravels and a complex streambed (ie. obstructions, step-pool and riffle-pool sequences), which is also where salmon tend to spawn (Baxter and Hauer, 2000; Dauble and Geist, 2000; Woessner, 2000; Hanrahan, 2008). Salmon and trout bury their eggs for incubation in gravels in the hyporheic zone (Tonina and Buffington, 2009) because of the temperature and porosity of the bed sediment. In winter, water is warmer due to hyporheic exchange (assuming groundwater is warmer than stream water). This enhances incubation by accelerating the growth and development of eggs (Hanrahan, 2008). Fish tend to inhabit these areas in summer as well because of the upwelling of colder groundwater. Additionally, when hyporheic exchange increases, the sediment becomes more oxygenated due to advective flow, creating optimal conditions for embryos (Soulsby et al., 2009; Tonino and Buffington, 2009).

The hyporheic zone can act as a natural filter for stream water. Hancock (2002) identifies three main filtering mechanisms: physical, biological, and chemical. The hyporheic zone acts as a physical filter by removing silt and particulate matter from stream water that enters it. It acts as a biological filter by taking up or transforming nutrients. The efficiency of this mechanism depends on the microbial activity in the hyporheic zone. The hyporheic zone acts as a chemical filter by enabling chemical reactions, such as redox processes and metal precipitation, to occur. This depends on the chemical conditions within the hyporheic zone. Hyporheic retention and subsequent remineralization can delay the loss of nutrients from a stream reach and thus influence stream nutrient budgets (Findlay, 1995).

## **2.3. Controls on Hyporheic Exchange**

Streambed composition and porosity, channel topography, topography of the surrounding area, and discharge all determine the extent of the hyporheic zone (Harvey and Bencala, 1993; Harvey et al., 1996; Hancock, 2002; Dahm et al., 2007). This literature review will give an overview of the results of previous studies conducted on the influences on hyporheic exchange.

### **2.3.1. Discharge**

Many studies have found that discharge affects hyporheic exchange. However, the results are inconsistent (Table 2.1 and Table 2.2); some studies indicated that hyporheic exchange increases with increasing discharge, while others found the opposite. Wondzell (2011) showed that hyporheic exchange is greater in smaller streams compared to larger streams, because in larger streams with greater discharge, the processes driving the exchange become hydrologically constrained. Ryan et al. (2010) investigated the effects of riparian land cover on the hyporheic zone at various discharge levels in a third order urban stream in Maryland and found that exchange between the stream and groundwater was greater during summer baseflow than during spring; they also found that less riparian forest cover resulted in a greater influence of discharge on the exchange and transient storage due to the effects of vegetation within the stream. Hart et al. (1999) speculate that the small size of the hyporheic zone in their study site was the reason that they did not find evidence of a trend in the change of the hyporheic zone with increasing discharge.. Another suggested explanation for the variations in study results is that streams have different morphologies, and solute exchange may not scale with discharge in the same way for each stream (Schmid et al., 2010). D'Angelo et al. (1993) hypothesized that increased hyporheic exchange with increased discharge may be the result of the increased availability of the solute over time, and flushing of hyporheic exchange site when discharge is high. They also gave two explanations for why the hyporheic zone decreased with increased discharge. The first is decreased channel complexity between headwaters and downstream sites, which results in a smaller transient storage area due to the elimination of potential transient storage zones that could have formed behind these features. The second explanation is

**Table 2.1 Overview of studies on the influence of discharge on the size of the hyporheic zone (HZ).**

Author	Date	Location	Effect on size of HZ	Range of size of HZ (m <sup>2</sup> ) and discharge (L/s)	Number of comparisons
<b>Patschke</b>	1999	Malcolm Knapp Research Forest, Maple Ridge, BC	HZ increased with increased discharge in more complex reaches, no clear trend in less complex reaches	Discharge: 1.6-92 HZ: 0.0192-0.2200	Compared 4 reaches at high and low flow, 12 tests
<b>Schmid et al.</b>	2010	Small streams (suburban and urban), Austria and Italy	HZ increased with increased discharge	Discharge: 0.0031-0.00005	4 reaches; 28 tests
<b>Scordo and Moore</b>	2009	Malcolm Knapp Research Forest, Maple Ridge, BC	HZ increased with increased discharge	Discharge: 0.21-30.6 HZ: 0.006-0.135	Compared 2 reaches at high and low flow, 10 tests total
<b>Hart et al.</b>	1999	Tennessee, small woodland stream	No clear trend	Discharge: 2.6-40 HZ: 0.006-0.024	1 reach; 20 tests
<b>Wondzell</b>	2006	Steep mountain streams in Oregon	No clear trend	Discharge: 1.04-11.46 HZ: 0.007-1.86	Compared 4 reaches at low and high baseflow
<b>D'Angelo et al.</b>	1993	Appalachian Mountain stream in North Carolina and Cascade Mountain stream in Oregon	HZ decreased with increased discharge	Discharge: 0.00024-2 HZ: 0.0005-2	16 sites; 22 tests
<b>Duineveld</b>	2008	Malcolm Knapp Research Forest, Maple Ridge, BC	HZ decreased with increased discharge	Discharge: 0.1-20.5 HZ: 0.0134-0.0555	1 reach; 10 tests
<b>Fabian et al.</b>	2011	Cascade stream, Honduras	HZ decreased with increased discharge	Discharge: 1.0-14.5 HZ: 0.12-0.18	1 reach; 3 tests
<b>Harvey et al.</b>	1996	Rocky Mountain stream, Colorado	HZ decreased with increased discharge	Discharge: 0.008-0.096 HZ: 0.025-0.21	1 reach
<b>Karwan and Saiers</b>	2009	Second order streams, Connecticut	HZ decreased with increased discharge	Discharge: 0.007-0.327 HZ: 0.62-2.20	1 reach
<b>Morrice et al.</b>	1997	Headwater streams in western and north-central New Mexico	HZ decreased with increased discharge	Discharge: 0.75-75 HZ: 0.004-0.23	3 reaches of different streams
<b>Ryan et al.</b>	2010	Small urban stream, Baltimore, Maryland	HZ decreased with increased discharge	Discharge: 0.82-29.8 HZ: 0.131-1.89	2 reaches (upper and lower)
<b>Wroblicky et al.</b>	1998	Headwater streams, New Mexico	HZ decreased with increased discharge	HZ: 1-4	2 streams

**Table 2.2 Overview of studies on the influence of discharge on hyporheic exchange (HE).**

Author	Date	Location	Effect on HE	Range of HE	Range of discharge (L/s) and number of measurements
<b>Argerich et al.</b>	2011	Second order stream, Iberian Peninsula	HE increased with increased discharge	0.8-5.0 ( $10^{-4}$ /s)	Range: 4.6-119.5 Measurements: 23
<b>D'Angelo et al.</b>	1993	Mountain streams, North Carolina and Oregon	HE increased with increased discharge	0-20 ( $10^{-4}$ /s)	Range: 0.0002-2 Measurements: 2 (summer and winter)
<b>Duineveld</b>	2008	Malcolm Knapp Research Forest, Maple Ridge, BC	HE increased with increased discharge	1.20-16.0 ( $10^{-4}$ /s)	Range: 0.1-20.5 Measurements: 10
<b>Fabian et al.</b>	2011	Cascade stream, Honduras	HE increased with increased discharge	3.34-12.2 ( $10^{-4}$ /s)	Range: 1.0-14.5 Measurements: 3 (dewatered, dry, transition, and wet seasons)
<b>Hart et al.</b>	1999	Small woodland stream, Tennessee	HE increased with increased discharge	0.5-15.8 ( $10^{-4}$ /s)	Range: 2.6-40 Measurements: 20
<b>Harvey et al.</b>	1996	Rocky Mountain stream, Colorado	HE increased with increased discharge	0.082-0.4 ( $10^{-3}$ /s)	Range: 0.0075-0.096 Measurements: 2 (high and low)
<b>Schmid et al.</b>	2010	Small streams (suburban and urban), Austria and Italy	HE increased with increased discharge		Range: 0.0031-0.00005 Measurements: 28
<b>Patschke</b>	1999	Malcolm Knapp Research Forest, Maple Ridge, BC	No clear trend	0.90-34.3 ( $10^{-4}$ /s)	Range: 1.6-92 Measurements: 12
<b>Legrand-Marcq and Laudelout</b>	1985	Forest stream, France	No clear trend	0.051-0.605 (/s)	Range: 25-750 (L/min)
<b>Scordo and Moore</b>	2009	Malcolm Knapp Research Forest, Maple Ridge, BC	No clear trend	0.8-3.5 ( $10^{-4}$ /s)	Range: 0.21-30.6 Measurements: 6
<b>Wondzell</b>	2006	Steep mountain streams in Oregon	No clear trend	2.18-62.41 ( $10^{-5}$ /s)	Range: 1.04-11.46 Measurements: 2 (high and low)
<b>Ryan et al.</b>	2010	Third order urban stream, Baltimore, Maryland	HE decreased with increased discharge	0.691-7.79 ( $10^{-5}$ /s)	Range: 6.8-620 Measurements: 2
<b>Karwan and Saiers</b>	2009	Second order streams, Connecticut	HE decreased with increased discharge	0.433-2.82 ( $10^{-4}$ /s)	Range: 0.007-0.327 Measurements: 3 (drought, summer, spring)
<b>Tonina and Buffington</b>	2007	Lab setting (flume)	HE decreased with increased discharge		Range: 12.50-32.83 Measurements: 3
<b>Morrice et al.</b>	1997	Headwater streams, New Mexico	HE decreased with increased discharge	0.61-5 ( $10^{-4}$ /s)	Range: 0.75-75 Measurements: 4 (fall, summer, winter, spring)

that transient storage zones act more independently during low discharge periods compared to high flow periods when transient storage zones might be incorporated into the stream. More data are needed to determine if these explanations are correct.

More studies need to be conducted on the size of the hyporheic zone during storms and over a longer period to determine the degree of hyporheic and surface water interaction. Boano et al. (2010) showed that mean discharge can be used to estimate the average properties of hyporheic exchange under unsteady conditions. Additionally,

discharge fluctuations were found to cause variations in the rate of exchange and subsurface residence time distributions. Maier and Howard (2011) found that stream-stage fluctuations increased the rate and amount of groundwater-stream water mixing, increased the depth that particles penetrate into the streambed, and increased the size of the hyporheic zone.

### **2.3.2. Geomorphic Features**

The amount of horizontal and longitudinal exchange depends on the extent of the hyporheic zone and the composition of the streambed material. Areas confined by hillslopes consisting mainly of bedrock with low hydraulic conductivity have small hyporheic zones, whereas areas on a floodplain with high conductivity alluvial sediments have large hyporheic zones (Tonina and Buffington, 2009). The following key factors control vertical and lateral hyporheic exchange in the alluvial zone: (a) hydraulic conductivity of the alluvium, (b) hydraulic gradient between either end of the riffle, and (c) the influx of groundwater to the alluvium from its surroundings (Storey et al., 2003).

Most studies that have investigated the influence of geomorphic features (step-pool and riffle-pool sequences, meanders, obstructions) on hyporheic exchange have found that when the stream is more complex, hyporheic exchange is enhanced, depending on the hydraulic conductivity of the streambed (Gooseff et al., 2007). Large woody debris can increase hyporheic exchange by increasing complexity and enhancing vertical connectivity in the stream (Sawyer et al., 2012). Tonina and Buffington (2007) showed that hyporheic exchange is the result of a complex interaction between discharge and bedform topography. Jones et al. (2008) found that features such as side channels, backwaters, tributaries, and springs outside the stream channel were also critical drivers of hyporheic flow. Baxter and Hauer (2000) and Kasahara and Wondzell (2003) showed that channel morphology (stream size and channel constraint) controlled hyporheic exchange. Lautz et al. (2010) described three scenarios where hyporheic exchange occurs: upstream of an impoundment, rapid flow through shallow hyporheic flow cells, and rapid downwelling through riffles. The topography of the valley floor controls the development of the flow system, which in turn predicts the location and extent of the hyporheic zone (Wondzell and Swanson, 1996). Krause et al. (2011b) found that the vertical hydraulic gradient (VHG) is affected by high pressure at different

points along a riffle-pool system due to obstacles on the streambed: surface water infiltrates into the pore space of the bed upstream of the obstacle, and exfiltrates downstream of the obstacle, suggesting that streambed topography significantly influences the exchange of water between the stream and the subsurface. Wondzell (2011) found that hyporheic exchange is smaller in low gradient streams in comparison to high gradient streams.

Examining hyporheic exchange requires knowledge of the streambed topography as the depth and spatial pattern of hyporheic exchange are controlled by the amplitude and wavelength of the head surface along the streambed (Tonina and Buffington, 2007). An obstruction may create a high pressure zone upstream that can drive hyporheic exchange and circulation (Tonina and Buffington, 2007). In general, if the curvature of the streambed is concave, upwelling from the hyporheic zone occurs; if the curvature is convex, downwelling into the hyporheic zone occurs (Tonina and Buffington, 2007). This correlates to riffle and pool systems in that the convex riffle portion of the stream is a downwelling area, and the concave pool portion of the stream is an upwelling area (Kasahara and Hill, 2008). Other structures like large wood and debris dams, large boulders, and pool and boulder steps, function in this manner as well (Harvey and Bencala, 1993; Stofleth et al., 2008; Lautz et al., 2010). If depth of alluvium is not limiting, high amplitude and long wavelength head variations will result in deeper hyporheic flow compared with areas of limited alluvium (smaller depth to bedrock or other layer with a very low conductivity) (Kasahara and Wondzell, 2003; Tonina and Buffington, 2009). Shorter wavelength/amplitude head variations create more circulation cells with reduced path lengths and exchange times (Tonina and Buffington, 2009). More complex streambed topography and variation in bed material can lead to more variable residence time distributions as well as smaller streambed fluxes (Ward et al., 2012).

Horizontal features, such as meander bends and gravel bars are also areas of enhanced hyporheic exchange (Harvey and Bencala, 1993; Wroblicky et al., 1998; Kasahara and Hill, 2007; Cardenas, 2008; Takahashi et al., 2008). Takahashi et al. (2008), for example, found that strong preferential flow through the hyporheic zone occurred across meander bends. However, Harvey and Bencala (1993) found that while hyporheic flow occurred across a meander bend due to the curvature of the stream, it was less pronounced in comparison to hyporheic flow driven by streambed topography.

### **2.3.3. Lateral Inflow and Hillslope Topography**

Lateral inflow includes water contribution to the stream from groundwater, overland flow, interflow, or small springs (Runkel, 1998). Few studies have investigated lateral inflow into streams. Beven (2006) stated “we need more studies of the incremental discharge into stream channels, so that we are encouraged to explore the reasons for the heterogeneity of inputs”. Some studies suggest that topography determines the location of lateral inflow to streams. Lateral inflows can be expected to be a function of stream topography, substrate and stream bank porosity, total subsurface water volume and flow, as well as water table height (D’Angelo et al., 1993). D’Angelo et al. (1993) found that lateral inflow was greatest in larger streams, but speculated that its importance in regulating temperature and nutrient concentrations in the stream may be greater in small streams, especially during low flows.

Different topographic features, such as spurs and hollows, result in different wetness conditions, and therefore may be associated with different relative runoff amounts (Anderson and Burt, 1978). Due to convergence of hydrologic flowpaths, hollows were wetter, which led to more runoff in comparison to spurs amounts in the study of Anderson and Burt (1978). Huff et al. (1982) also found that topography had a significant influence on lateral inflow to streams. Their results indicated that significant inflow occurred just opposite of a hollow, supporting the idea that hollows contribute more subsurface flow to the stream in comparison to spurs or planar slopes. In addition, Huff et al. (1982) found that the underlying bedding planes of the bedrock also affect subsurface flow by providing a lateral flowpath along the strike towards the stream channel. Fractures and dikes may provide a means of lateral transport of water to the stream channel and may control the locations of lateral inflow.

In an urban stream, culverts and other drainage structures may have a greater influence on lateral inflow compared to lateral inflow of subsurface flow from hillslopes and groundwater, especially during rain events. Impervious surfaces, such as streets, direct runoff into the stream via culverts and other drainage structures, and therefore may have a greater influence on streamflow during rainfall conditions compared to natural lateral inflows from the riparian zone surrounding the stream (Paul and Meyer, 2001; Wheeler et al., 2005). As a watershed becomes more urbanized, peak streamflow

volume also increases, indicating that lateral inflow due to drainage networks that feed directly into the stream may be more prominent and efficient in routing rainfall to the stream than hillslope and groundwater inflows (Wheeler et al., 2005).

## 2.4. Transport Processes and Modeling Hyporheic Exchange

The four main solute transport processes in streams are advection, dispersion, groundwater inflow, and storage-zone exchange; advection and dispersion can also occur in groundwater and the storage zone (Wagner and Harvey, 1997; Figure 2.1). Advection is the movement of solutes with the bulk movement of water and dispersion is the movement of solutes within the water due to mixing of the solutes in the water and velocity differences. Groundwater flows into the stream through the sediment below the streambed or the surrounding streambanks. Storage-zone exchange results in mixing of solutes in stagnant or very slow moving areas in the stream (e.g. pools) or the hyporheic zone (Wagner and Harvey, 1997). The model used in this study assumes that advection and dispersion occur only in the stream.

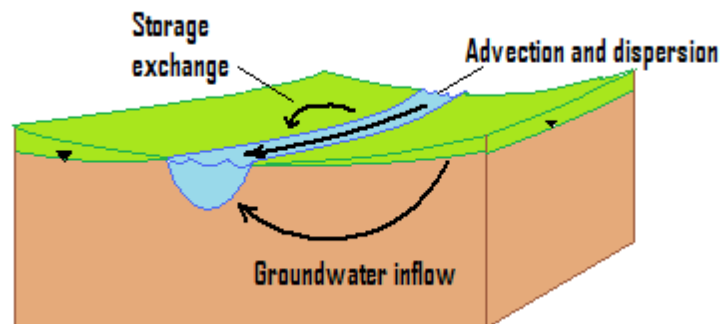


**Figure 2.1** *The four processes of solute transport in a stream.*

The United States Geological Survey (USGS) developed the One-dimensional Transport with Inflow and Storage (OTIS) model (U.S. Geological Survey, 2000; Runkel, 1998) to simulate the movement of a solute through a stream and to quantify transient

storage. OTIS uses mass balance equations for the main channel (including advection and dispersion) and the storage zone (transient storage including the hyporheic zone and stagnant water zones) (Figure 2.2). Lateral inflow is included in the model, and represents water entering the stream as overland flow, interflow, and groundwater inputs (Figure 2.2).

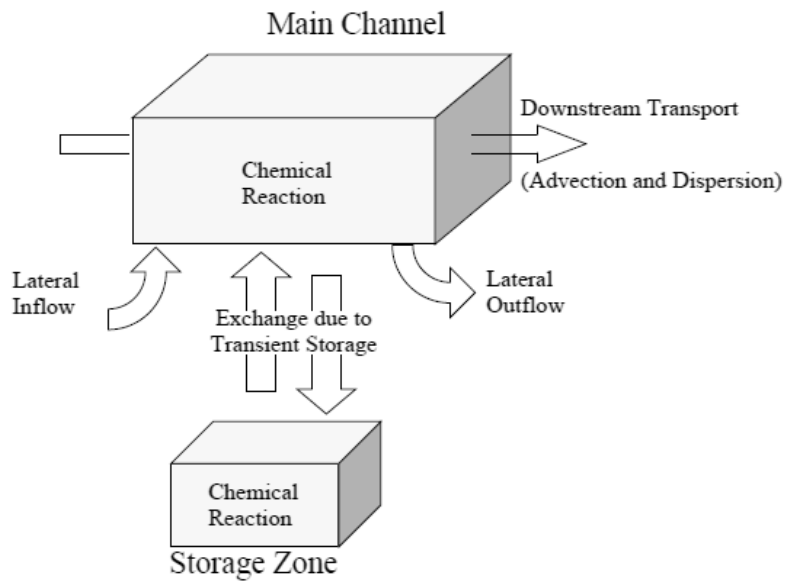


**Figure 2.2 Conceptual framework for OTIS (from Runkel, 1998).**

The model is based on the advection-dispersion equation with additional terms that take transient storage and lateral inflow into consideration. Two differential equations are used in the model to estimate tracer concentrations in the main channel and storage zone respectively (Runkel, 1998):

$$\frac{\partial C}{\partial t} = -\frac{Q}{A} \frac{\partial C}{\partial x} + \frac{1}{A} \frac{\partial}{\partial x} \left[ AD \frac{\partial C}{\partial x} \right] + \underbrace{\frac{Q_L}{A} (C_L - C)}_{lateral\_flux} + \underbrace{\alpha (C_S - C)}_{transient\_storage} \quad (1)$$

and

$$\frac{\partial C_s}{\partial t} = \alpha \frac{A}{A_s} (C - C_s) \quad (2)$$

where  $A$  and  $A_s$  are the main channel and storage zone cross-sectional areas, respectively ( $\text{m}^2$ );  $C$ ,  $C_L$ , and  $C_s$  are the main channel, lateral inflow, and storage zone solute concentrations, respectively ( $\text{mg/L}$ );  $D$  is the dispersion coefficient for the stream channel ( $\text{m}^2/\text{s}$ );  $Q$  is the volumetric stream flow rate ( $\text{m}^3/\text{s}$ );  $Q_L$  is the lateral inflow rate ( $\text{m}^3/\text{s}/\text{m}$ );  $t$  is time (s);  $x$  is distance (m); and  $\alpha$  is the storage zone exchange coefficient ( $\text{s}^{-1}$ ). The equations are solved using the Crank-Nicolson method because of its accuracy, efficiency, and stability (Runkel, 1998; USGS, 2000). OTIS-P is a modified version of OTIS that uses optimization to automatically select optimal values of unknown parameters using non-linear least squares regression.

The main assumption of OTIS is that the concentration of the tracer varies only in the longitudinal direction (downstream) and not within the cross-section (width or depth) (Runkel, 1998). OTIS assumes one-dimensional transport, which implies that the solute mass is uniformly distributed over the stream's cross-sectional area (i.e. fully mixed). With regards to the main channel, OTIS assumes that the physical processes that affect solute concentration are advection, dispersion, lateral inflow and outflow, as well as transient storage. OTIS assumes for the storage zone that advection, dispersion, and lateral inflow and outflow do not occur and that all model parameters that describe transient storage and chemical reactions may be spatially variable but are temporally constant (Runkel, 1998). OTIS can account for chemical reactions that affect the concentrations of solutes in the main channel and storage zone due to sorption and first-order decay. It assumes that all mass that leaves the channel into the transient storage zone returns to the same part of the channel, as it applies the same characteristics to each reach (Bencala et al., 2011).

OTIS is highly used in hydrological studies on the hyporheic zone. A study conducted by Wondzell (2006), however, showed very different results between the observations and those predicted by OTIS-P. Observations indicated that residence times in an unconstrained stream were longer than in a constrained stream, and that the location and extent of the hyporheic zone changed little during high and low baseflow. OTIS-P however, indicated that both the size and residence time of transient storage

were greater in reaches with few large steps compared to reaches with more frequent small steps. Wondzell (2006) suggested that the observations and predicted values were different due to the insensitivity of OTIS-P to long residence-time exchange flows and its high sensitivity to discharge changes. Scordo and Moore (2009) found that their “scaled-up” estimate of hyporheic exchange based on Darcy’s law was an order of magnitude lower than the estimates of transient storage from OTIS-P. They suggested that this may have been due to lateral fluxes, horizontal exchange that was not quantified at the channel-unit scale, or the fact that storage exchange estimated by OTIS-P includes transient storage in pools as well as in the hyporheic zone. They stated that a limitation of OTIS-P is that “one cannot safely equate modeled transient storage with storage in the hyporheic zone in streams with a steep step-pool morphology”. Bencala et al. (2011) also stated that one of the major limitations of transient storage models (TSMs) is their inherent simplicity of not being able to separate different types of transient storage zones in the stream and subsurface (e.g. eddies, channel and pool margins, and hyporheic exchange). The stream storage zones can have very different conditions compared to the subsurface storage zone, and within each different type of transient storage zone, heterogeneity can have a significant impact on the range of residence times within that zone. OTIS also oversimplifies connectivity and the interaction between the stream, riparian zone, and hillslope, by only taking into consideration significant lateral inflow (Bencala et al., 2011). Despite its limitations, OTIS is widely used due to its accessibility and ease of use, and it because it is currently one of the only models that quantifies hyporheic exchange.

## **3. Study Site and Methodology**

### **3.1. Study Site**

#### **3.1.1. *Hoy Creek, Coquitlam***

This research took place in Hoy Creek in Coquitlam, B.C. (Figure 3.1). The two research sites are located within an urban setting: one in an upstream, steeper portion of Hoy Creek and one in a downstream, meandering portion. The upper part of Hoy Creek is located at about 270 m. asl, and the lower part of Hoy Creek at about 40 m. asl (data from the World Geodetic System of 1984 datum and Earth Gravitational Model 1996 Geoid). Each study area consisted of two study reaches. Studying multiple reaches of the same stream increases the statistical power compared to studying the stream as a whole and is also more practical.

Hoy Creek provides an interesting study location for studying hyporheic exchange in a suburban stream as it is a known salmon spawning stream with a fish hatchery. Streams with considerable hyporheic exchange are preferred by salmon for spawning (Baxter and Hauer, 2000). All studied reaches are fish-bearing reaches (CH2M Hill, 2012). The Hoy Scott Watershed Society maintains Hoy Creek (Houghton, 2008).

Hoy Creek is bordered on both sides by housing. It originates in North Hoy Creek near the top of Westwood Plateau in Coquitlam and flows southward into Scott Creek, a tributary of the Coquitlam River. Due to urban development in the Lower Coquitlam River Watershed and around Hoy Creek, a significant portion of the watershed's drainage is carried through the storm drain system. Numerous culverts direct flow into the creek. In 1999, 20.8% of the watershed area of Hoy Creek was effectively impermeable (Fraser River Action Plan, 1999). In 2005, the Scott-Hoy Creek Watershed had a total impervious area (TIA) of 40%, and a riparian forest integrity (RFI) of 40% (CH2M Hill,

2012). All four study reaches are classified as having medium compaction (CH2M Hill, 2012). RFI values given in the Scott Creek Integrated Watershed Management Plan (CH2M Hill, 2012) were 75% from Parkway Boulevard to Camelback Court (Reach UA), 100% from Camelback Court to Plateau Boulevard (Reach UB), and 39% from David Avenue to Guildford Way (Reaches DA and DB). Comparison of calculated TIA values from 1996 and 2005 indicate that the Scott Creek Watershed, which includes Hoy Creek, has declined from fair to poor health due to the effects of urbanization (i.e. loss of riparian forest habitat). This is more notable in the lower portion of Hoy Creek than the upper portion since more development has occurred in the upper watershed since 1999.

The upper portion of Hoy Creek is quite different in comparison to the lower portion (Figure 3.2, Figure 3.3, and Table 3.1). The upper part has a considerably larger amount of woody debris. Steeper forested slopes surround it, and it has a coarser grained streambed compared to the downstream reaches of Hoy Creek (Figure 3.4 and Table 3.1). The lower part of Hoy Creek is located on Capilano sediments of glacial gravel and sand, while the upper part is located on Vashon drift of glacial till (Geological Survey of Canada, 1997). Discharge is lower in the upper reaches of Hoy Creek compared to the lower reaches (Figure 3.5 and Table 3.1).

**Table 3.1 Upper (UA and UB) and lower (DA and DB) reach characteristics.**

Characteristic	UA	UB	DA	DB
D <sub>50</sub> (mm)	4.6	7.5	3.9	4.0
D <sub>84</sub> (mm)	10.0	27.0	7.0	7.6
Length (m)	51.2	49.7	62.8	54.7
Stream slope (%)	31.2	38.7	20.7	18.6
Near-stream hillslope (%)	7	8	3	5
Watershed hillslope (%)	13	23	6	5
Average channel width (m)	2.5	3.1	4.5	4.0
Average discharge (Jul-Sept 2010) (L/s)	3.3	9.7	30.1	53.0
Average discharge (Jul-Sept 2010) (mm/day)	0.6	1.5	0.7	1.3
Average discharge (Oct-Dec 2010) (L/s)	25.7	30.1	279.8	104.0
Average discharge (Oct-Dec 2010) (mm/day)	4.7	4.7	7.2	2.3

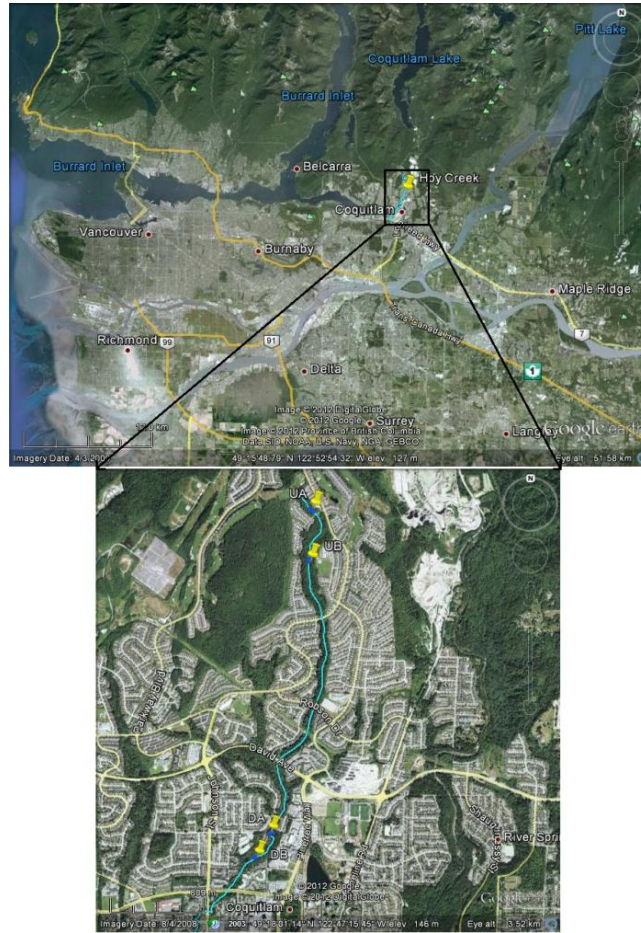


**Figure 3.1** Location of Hoy Creek in Coquitlam, BC. (Data source: Google Earth, Digital Globe, accessed June 8, 2012)



**Figure 3.2** Photos of the upper (left two images) and lower (right two images) reaches of Hoy Creek during low flow conditions.

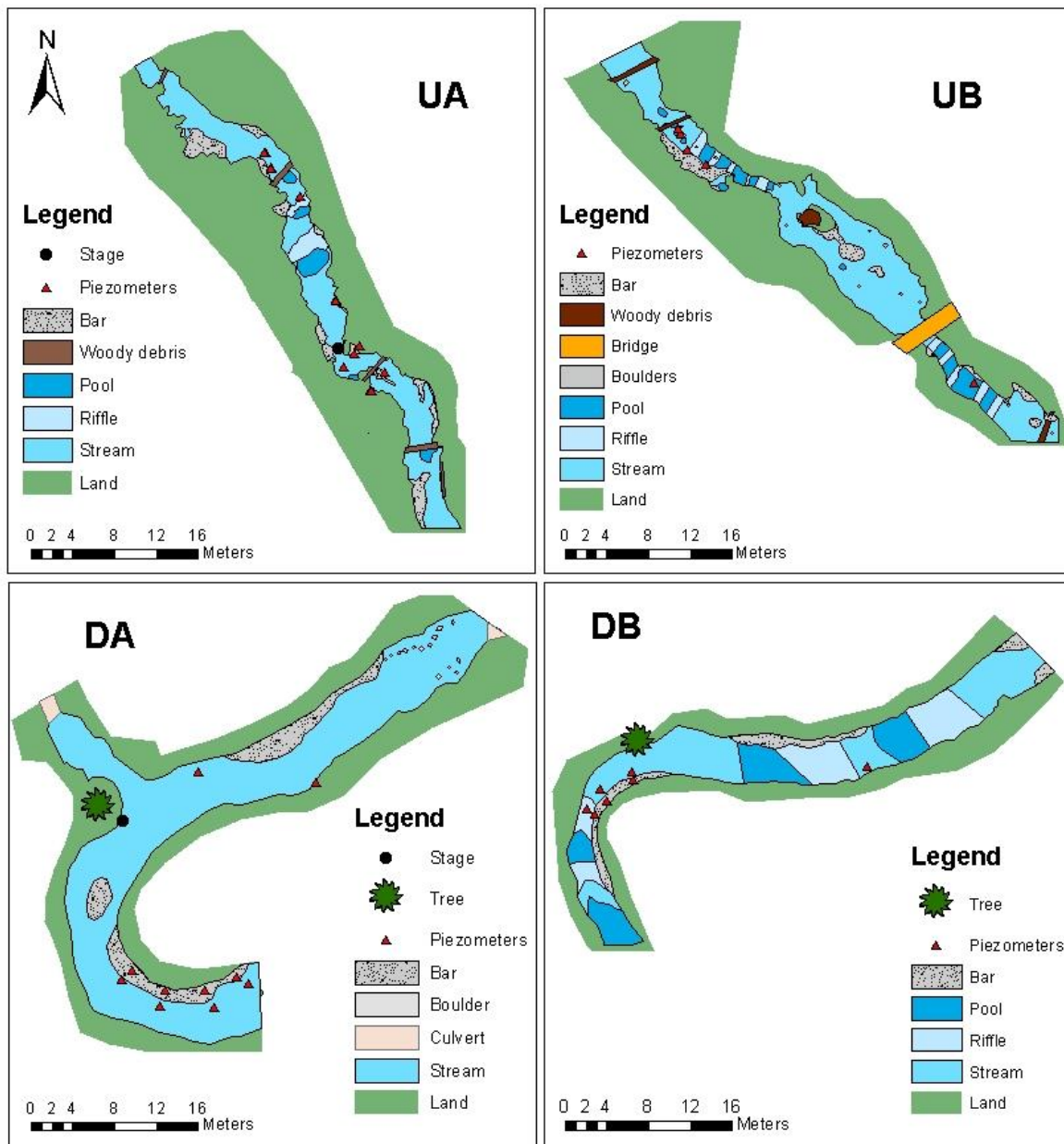


**Figure 3.3** Main features in the upper and lower study reaches of Hoy Creek and locations of the piezometers. The trees that are labelled have a significant influence on the stream since they protrude into the flow.

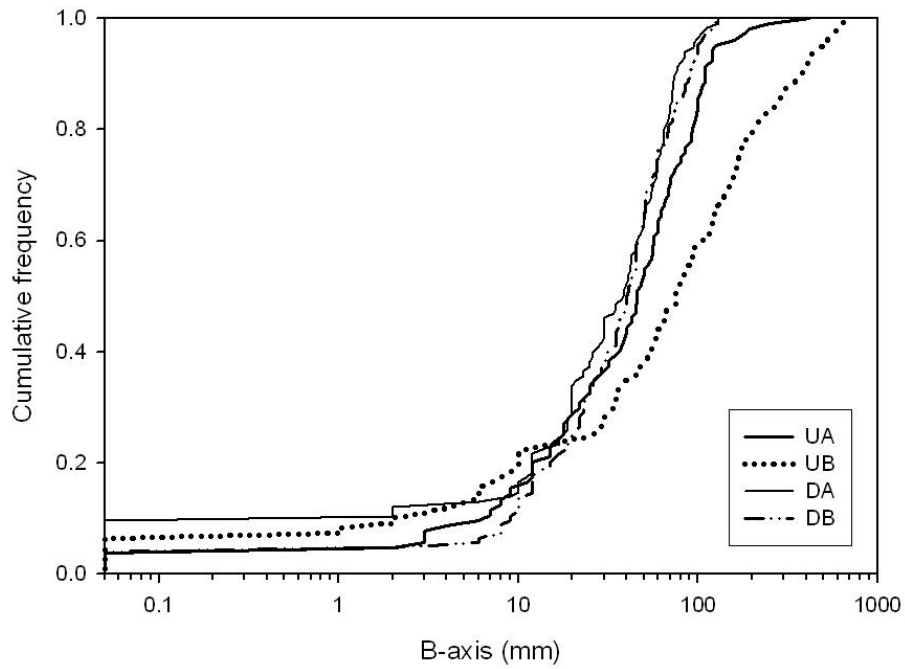


**Figure 3.4 Cumulative frequency of the B-axis of bed material based on a Wolman pebble counts for reaches UA, UB, DA, and DB.**

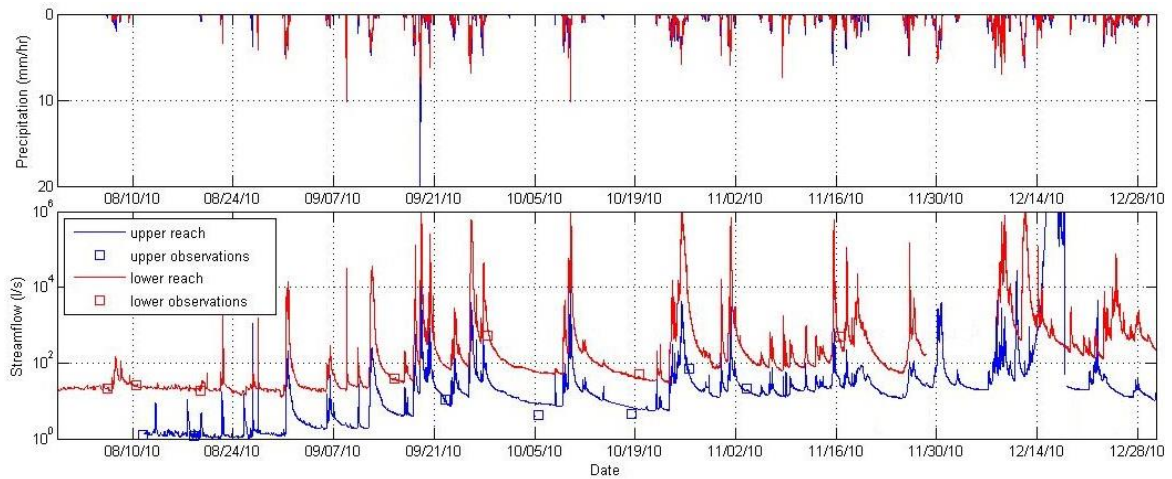


**Figure 3.5 Precipitation and discharge in upper and lower Hoy Creek.**

### 3.1.2. Climate and Streamflow Normals

Hoy Creek is located within the Coastal Western Hemlock biogeoclimatic zone (Pojar et al., 1991). Average annual precipitation for Coquitlam is 1859 mm (Environment Canada, 2010). The months of June to August are relatively dry with average precipitation ranging from 62-92 mm/month; October to January is wet, with average precipitation ranging between 182-299 mm/month (Figure 3.6). Average monthly temperature data for Coquitlam was unavailable, but the data for the neighbouring community of Port Moody, which is located 4 km west of Hoy Creek, was used instead (Figure 3.6). The average daily temperature in Port Moody ranged between 3-10.5°C between October and January, and between 14.8-17.8°C between June to September (Environment Canada, 2010).

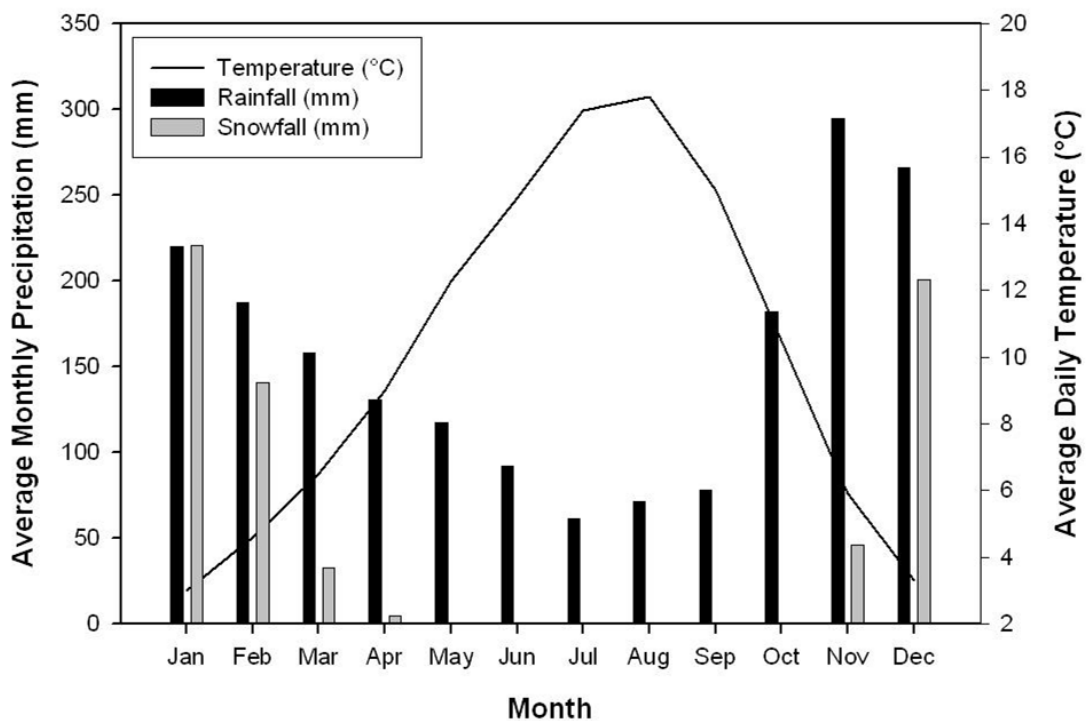


**Figure 3.6** Precipitation and daily average temperature normals from 1971-2000 for Coquitlam and Port Moody, B.C. respectively (Environment Canada, 2010).

### **3.1.3. Description of the Study Reaches**

The reaches were selected based on their characteristics. Multiple locations were scouted. The four reaches selected have limited dead zones (i.e. transient storage zones in the stream) or bifurcation within their 50-60 meter length. They were also chosen to be representative of the upstream and downstream parts of Hoy Creek: the upstream study reaches are steeper, have coarser bed material, with steps, pools and riffles, whereas the downstream study reaches are meandering with finer bed material (Figure 3.3 and Figure 3.4).

#### **3.1.3.1. Upper Study Reaches**

Riparian vegetation at the upper reaches includes mostly vine maple, red alder, birch, cedar, and hemlock trees, and salmon-berry and huckleberry bushes. The upper reaches are located on Vashon drift (Va), described as a till, glaciofluvial, glaciolacustrine, and ice-contact deposit, a lodgement till (with sandy loam matrix), and minor flow till containing lenses and interbeds of glaciolacustrine laminated stony silt (Geological Survey of Canada, 1980).

Reach UA is the uppermost site in this study and is 51 m long. A townhouse complex and other housing bound the reach on either side. There is one meander bend within the stream about 30 m downstream from the top of the reach. There are two step-pool sequences formed by woody debris are located 12 m and 45 m downstream from the top of the reach, respectively (Figure 3.3). The  $D_{50}$  and  $D_{84}$  grain sizes are 46 mm and 100 mm, respectively (Figure 3.4 and Table 3.1).

Reach UB is located 440 m downstream from reach UA and is 50 m long. Reach UB is bound by steeper slopes compared to reach UA (Table 3.1). Reach UB is bound on one side by housing and on the other side by an elementary school and sports field. It splits 17 m from the top of the reach and merges again after 18 m (Figure 3.3). The  $D_{50}$  of the bed material is 75 mm, while the  $D_{84}$  is 270 mm (Figure 3.4; Table 3.1).

### **3.1.3.2. Lower Study Reaches**

Riparian vegetation at the lower reaches includes numerous tree species (cedar, hemlock, red alder, birch, broadleaf maple, and vine maple), salmon-berry, huckleberry, salal, and blackberry bushes. Reach DB is located in a stretch of Hoy Creek identified as having a major invasive species intrusion of mainly Himalayan blackberry and Japanese knotweed (CH2M Hill, 2012). Reach DA has been identified as a site of severe erosion defined with an area of more than 10 m<sup>2</sup> (CH2M Hill, 2012). Reaches DA and DB are both located downstream of a wetland area. According to the Geological Survey of Canada mapping (1980), these lower reaches are located on Capilano sediments (Cc), described as a raised deltaic and channel till with medium sand to cobble gravel up to 15 m thick deposited by proglacial streams, which is in most places underlain by silty to silty clay loam.

Reach DA is the uppermost of the two downstream reaches. A bridge crosses the stream just upstream from the top of the reach, which is located about half way around a meander bend. There is another meander bend towards the end of the reach. Two culverts enter the stream in this reach, one near the top of the reach and another about half-way down the reach (Figure 3.3). One side of the stream is bordered by a high school and a post-secondary school, while a townhouse complex is located on the opposite side. The  $D_{50}$  of the bed material is 39 mm, while the  $D_{84}$  is 70 mm (Figure 3.4).

Reach DB is the furthest downstream study reach in Hoy Creek. A townhouse complex and a well-used gravel trail border one side of the stream, while the other side contains a riparian buffer zone of smaller shrubs and trees, approximately 80 m wide. This reach contains one meander bend near the downstream end of the reach (Figure 3.3). The  $D_{50}$  of the bed material is 40 mm; the  $D_{84}$  is 75 mm (Figure 3.4).

## **3.2. Methodology**

### **3.2.1. Tracer Experiments**

Steady state tracer experiments were used to characterise the movement of water through the stream and hyporheic zone. Tracer experiments are a common method to assist in determining where and how fast water is flowing. Steady state (i.e. constant injection) tracer experiments are more reliable than slug injections because the rising and falling limb data from slug injections are cumulatively less informative than those of steady state injections, thereby influencing the estimate of the lateral volumetric groundwater inflow rate (Wagner and Harvey, 1997). The tracer experiments were conducted during low and high discharge conditions. The low discharge period lasted from June to mid-September 2010, and the high discharge period from mid-September to December 2010 (Figure 3.5). In total 40 tracer tests were conducted, 10 in each reach. Experiments were conducted in a random order, based on the time available for the experiment and rotation of sites (Table 3.2-Table 3.5).

Sodium chloride, a conservative solute tracer, was injected into the stream at each of the reaches until steady state electrical conductivity (EC) was reached at the downstream end of the reach. According to the Canadian Water Quality Guidelines (Nagpal et al., 2003), the concentration of sodium chloride should not exceed 150 mg/L to protect freshwater aquatic life from chronic effects. To ensure protection of freshwater aquatic life from acute and lethal effects, the Canadian Water Guidelines suggest that the concentration of sodium chloride should not exceed 600 mg/L at any time. The maximum increase in concentration of sodium chloride in the stream during an experiment was 87 mg/L. For one test the sodium chloride increased to a maximum concentration of 240 mg/L for 3 hours, and for three tests it increased to a maximum concentration between 170-185 mg/L for 1-2 hours, all of which are well below the maximum allowable concentration of sodium chloride for protection against acute and lethal effects. The maximum concentrations during the other tests were below 150 mg/L (Table 3.2-Table 3.5). The concentration of the injected tracer solution required for the tracer tests was determined using the equation:

$$C_{is} = \frac{Q_{est}}{q} C_s \quad (3)$$

where  $C_{is}$  is the concentration of the injection solution (g/L),  $Q_{est}$  is an estimate of the discharge based on a slug test or previous measurements (L/s),  $q$  is the injection rate (L/s), and  $C_s$  is the desired maximum tracer concentration in the stream (g/L) (Moore, 2004).

Stream water was pumped into a 120 L plastic container onsite to dissolve a pre-weighed amount of salt. A Global Water SP200 peristaltic sampling pump powered by a 12 V battery was used to inject the tracer into the stream at a constant rate (approximately 0.5-1 L/min; Table 3.2-Table 3.5). Injections lasted 1-3 hours, depending on the time required for the EC readings at the furthest downstream measurement point of the reach to remain constant for at least 10 minutes.

Thorough mixing before injection is required to reduce uncertainty from injection of inconsistent tracer concentrations into the stream. To ensure that the tracer solution remained well mixed, water was pumped from the bottom of the container to the top using a bilge pump connected to a separate 12 V battery. Additionally, the solution was stirred continuously when the injection solution was supersaturated, and less frequently (e.g. every 5 minutes) when it had a lower concentration.

**Table 3.2 Summary of the tracer experiments in the upper reach UA (EC measurements from the YSI and \*ECH<sub>2</sub>O probes; the injection stopped at an unknown time on July 7, thus the duration of injection is an estimate).**

Date (2010)	Discharge (L/s)	Average injection rate (mL/min)	Solute concentration (g/L)	Duration of injection (h)	Maximum EC (µS/cm)	Background EC (µS/cm)
Jul 2	2	356	16	2.0	*400	*260
Jul 7	2	291	56	~1.6	*360	*260
Jul 15	1	340	21	3.0	528	326
Aug 11	1	310	17	3.1	448	309
Aug 18	1	318	17	2.7	421	273
Sept 22	11	522	27	2.2	177	136
Oct 5	4	477	25	1.8	294	199
Oct 18	4	577	61	1.9	444	175
Oct 26	72	584	70	1.2	85	66
Nov 3	22	583	100	1.5	184	94

**Table 3.3 Summary of the tracer experiments in the upper reach UB (EC measurements from the YSI and \*ECH<sub>2</sub>O probes).**

Date (2010)	Discharge (L/s)	Average injection rate (mL/min)	Solute concentration (g/L)	Duration of injection (h)	Maximum EC (µS/cm)	Background EC (µS/cm)
Jul 23	1	441	17	3.7	366	240
Jul 26	1	298	17	2.7	329	208
Aug 5	4	314	17	2.4	*290	*190
Aug 12	1	320	17	3.4	388	262
Sept 29	40	500	74	0.9	109	78
Oct 13	18	574	73	1.3	181	102
Oct 27	52	589	117	1.2	112	67
Nov 10	27	578	124	1.4	177	88
Dec 4	29	620	133	1.1	183	85
Dec 6	25	608	134	1.2	202	90

**Table 3.4 Summary of the tracer experiments in the lower reach DA (EC measurements from the YSI and \*ECH<sub>2</sub>O probes).**

Date (2010)	Discharge (L/s)	Average injection rate (mL/min)	Solute concentration (g/L)	Duration of injection (h)	Maximum EC (µS/cm)	Background EC (µS/cm)
Jul 14	46	333	73	2.1	171	153
Jul 22	36	559	76	1.7	185	145
Jul 30	23	579	89	2.0	234	157
Aug 6	27	554	75	2.3	223	158
Aug 10	26	499	73	3.0	215	167
Aug 19	19	556	87	1.8	247	159
Sept 15	40	592	97	1.9	209	161
Sept 28	335*	717	281	0.9	100	87
Oct 19	49	733	185	1.2	237	144
Nov 9	233	600	356	1.3	150	118
Nov 16	266*	658	366	1.4	104	88

**Table 3.5 Summary of the tracer experiments in the lower reach DB (EC measurements from the YSI and \*ECH<sub>2</sub>O probes).**

Date (2010)	Discharge (L/s)	Average injection rate (mL/min)	Solute concentration (g/L)	Duration of injection (h)	Maximum EC (µS/cm)	Background EC (µS/cm)
Jul 20	23	588	62	2.0	215	160
Jul 27	21	552	64	2.4	211	154
Aug 4	23*	583	83	2.4	*230	*160
Aug 16	25	537	86	2.4	221	158
Sept 24	144	728	169	0.9	132	103
Oct 12	114	658	151	1.3	137	110
Oct 20	64	732	159	1.3	217	155
Oct 29	61	656	290	1.2	212	107
Nov 12	83	654	382	1.1	224	122
Dec 3	158	708	374	1.1	175	118

The electrical conductivity (EC) was measured at multiple locations along the reach (about every 5 m) using five ECH<sub>2</sub>O-TE probes, one YSI 6920-V2 EC probe, and five homemade EC and temperature probes that are similar in design to the Campbell Scientific CS547A probes (Figure 3.7). The ECH<sub>2</sub>O probes are named ECH<sub>2</sub>O 1- ECH<sub>2</sub>O 5 hereafter, with the ECH<sub>2</sub>O 1 probe always being located furthest upstream. The YSI 6920-V2 EC probe is named YSI and the homemade probes are named DEC 1-DEC 5 hereafter.

Brilliant blue dye was injected into the stream at the upstream end of each reach to assess whether there was sufficient mixing in the stream and to determine where the first measurement site could be located. Distances between probe locations are provided in Table 3.6 and Table 3.7. Once steady state was reached, EC and temperature measurements were taken approximately every 5 meters throughout the reach using a Hanna pH/EC/TDS/Temperature probe (resulting in about 10 measurements in each reach). These measurements were used to determine where lateral inflow might occur because the tracer becomes more diluted where lateral inflow occurs and were mapped in ArcGIS and used to determine the locations of lateral inflow. Lateral outflow is more difficult to determine as the tracer method is insensitive to losses from the stream because the water leaving the stream does not change the concentration of tracer within the stream (Bencala et al., 2011).

EC measurements were converted to concentration values (g/L of salt) by calibrating the probes in the lab using water from Hoy Creek. R<sup>2</sup> values of the dilution standard were good for the ECH<sub>2</sub>O and YSI probes, and a bit lower for the DEC probes (Table 3.8). The EC data collected during the tracer tests were used to create breakthrough curves.

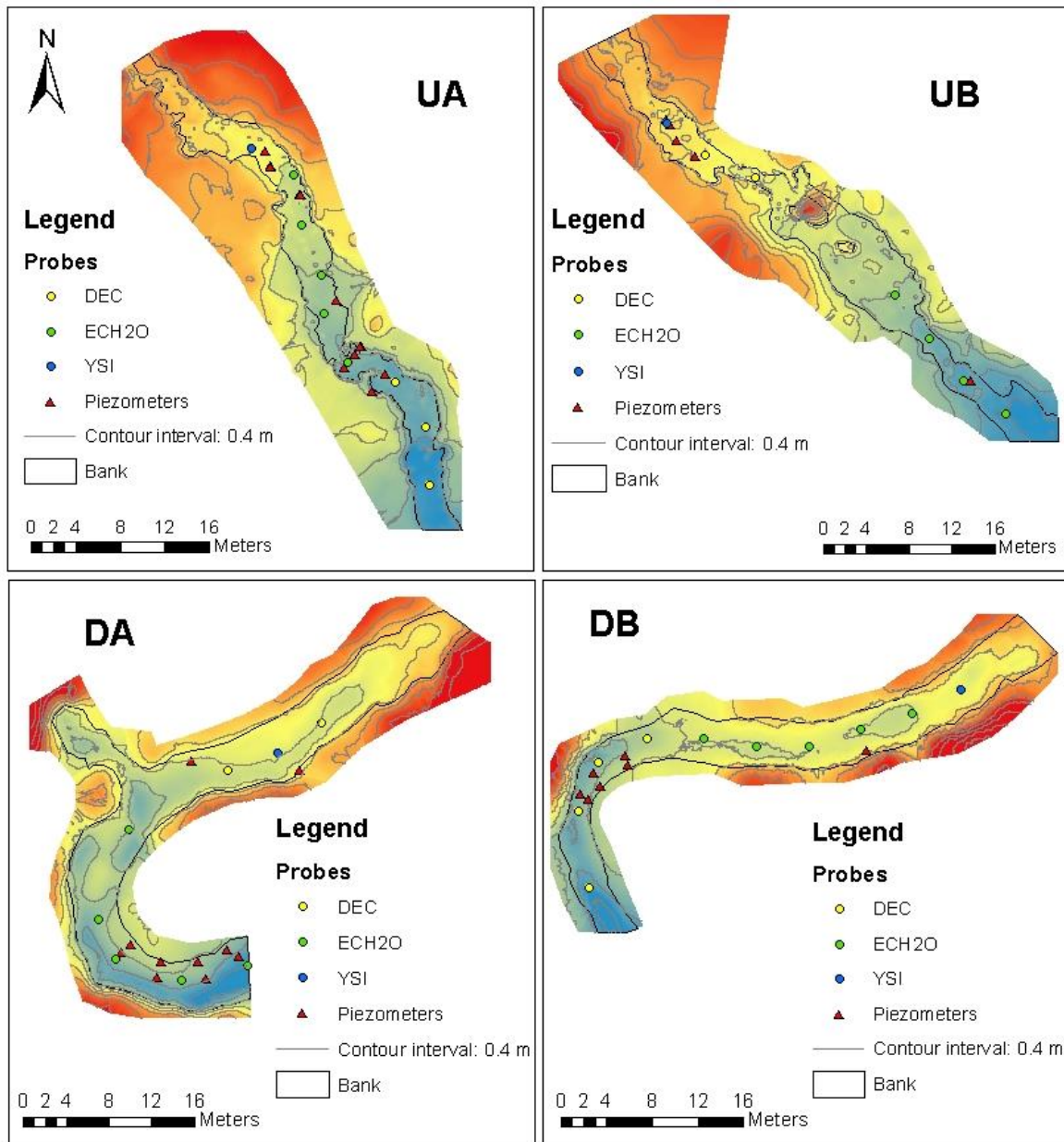


**Figure 3.7** Probe and piezometer locations for the four study reaches. Red to blue shading indicates higher to lower elevation. Distances of the probes below the top of each reach are given in Table 3.6 and Table 3.7.

**Table 3.6 Distance of each probe from the injection site for the upper reaches.**

Reach UA		Reach UB	
Probe	Distance from injection site (m)	Probe	Distance from injection site (m)
YSI	12.0	YSI	7.2
ECH <sub>2</sub> O 1	15.7	DEC 1	11.7
ECH <sub>2</sub> O 2	20.7	DEC 3	16.7
ECH <sub>2</sub> O 3	25.7	ECH <sub>2</sub> O 1	34.7
ECH <sub>2</sub> O 4	30.7	ECH <sub>2</sub> O 2	39.7
ECH <sub>2</sub> O 5	35.7	ECH <sub>2</sub> O 3	44.7
DEC 3	41.7	ECH <sub>2</sub> O 4/5	49.7
DEC 5	46.2		
DEC 4	51.2		

**Table 3.7 Distance of each probe from the injection site for the lower reaches.**

Reach DA		Reach DB	
Probe	Distance from injection site (m)	Probe	Distance from injection site (m)
DEC 1	18.0	YSI	7.7
YSI	23.0	ECH <sub>2</sub> O 1	12.7
DEC 2/3	28.0	ECH <sub>2</sub> O 2	17.7
ECH <sub>2</sub> O 1	33.8	ECH <sub>2</sub> O 3	22.7
ECH <sub>2</sub> O 2	48.8	ECH <sub>2</sub> O 4	27.7
ECH <sub>2</sub> O 3	52.8	ECH <sub>2</sub> O 5	32.7
ECH <sub>2</sub> O 4	57.8	DEC 1	37.7
ECH <sub>2</sub> O 5	62.8	DEC 5	42.7
		DEC 3	47.7
		DEC 4	54.7

**Table 3.8  $R^2$  values for the relation between EC (x) and concentration of NaCl (y) for the eleven probes used in this study.**

Probe	Equation	$R^2$
YSI	$y = 0.0005x - 0.0391$	0.99993
ECH20 1	$y = 0.5031x - 0.0369$	0.99990
ECH20 2	$y = 0.4901x - 0.0405$	0.99981
ECH20 3	$y = 0.4922x - 0.0413$	0.99943
ECH20 4	$y = 0.4935x - 0.0412$	0.99969
ECH20 5	$y = 0.5007x - 0.0354$	0.99997
DEC 1	$y = 0.0030x - 0.1282$	0.99936
DEC 2	$y = 0.0034x - 0.2242$	0.99735
DEC 3	$y = 0.0044x - 0.3795$	0.98099
DEC 4	$y = 0.0035x - 0.2167$	0.99839
DEC 5	$y = 0.0043x - 0.3743$	0.99411

While tracer tests are frequently used to assess hyporheic exchange, several problems are associated with the method. Harvey et al. (1996) showed that the accuracy of the tracer method for characterization of hyporheic exchange can be lower during high discharge; however, they found that the tracer method was sufficiently accurate and reliable to characterize hyporheic exchange during high baseflow (96 L/s) in their study. The maximum flow measured during the tracer experiments in this study was less than 335 L/s at the lower reaches. The maximum flow during the tracer experiments at the upper reaches was 72 L/s.

### **3.2.2. Determination of Vertical Hydraulic Gradients**

A network of piezometers was installed to determine vertical hydraulic gradients (VHG) during each tracer test (Figure 3.7 and Figure 3.8). The piezometers were made from 25 mm diameter PVC pipes and had a 10 cm slotted zone at the bottom covered with perforated tape to reduce the inflow of sediment. These were installed predominantly in sand and gravel bars and banks (Figure 3.7). Thirteen piezometers were installed in reach UA: one network of four piezometers along a longitudinal cross-

section of a step, and one network of six piezometers across a meander bend (Figure 3.9 and Table 3.9). The depths varied between 13 cm and 29 cm below the streambed. Two piezometers were also installed in the stream bank at 59 cm and 62 cm below the surface. Six piezometers were installed in reach UB. Installation was difficult due to the shallow depth of the streambed and the presence of very coarse-grained material. Depths varied from 14 cm to 29 cm below the surface (Table 3.9 and Table 3.10). Ten piezometers were installed in reach DA at depths varying between 12.2 cm and 52.6 cm. One piezometer was installed in the left bank, and another one in a gravel bar (which repeatedly had to be reinstalled). The other piezometers were installed in a meander bend. Seven piezometers were installed in reach DB at depths ranging between 15.6 cm and 28.3 cm below the streambed. One was installed in the stream along a straight part of the reach while the other piezometers were installed in the bend.

The EC and temperature of the water inside the piezometers and the stream next to them were measured with a Hanna probe at regular intervals (ranging from every 10 to 30 minutes) during the tracer experiments to determine tracer concentrations in the streambed and stream. When the Hanna pH/EC/TDS/Temperature probe was unavailable (tests on Jul. 2, 7, 14, 15, Aug. 18, Nov. 3, 9, 12, 16, and Dec. 3, 4, and 6), water samples were taken from the piezometers before injection of the tracer, at steady state, and after the test using a small hand sampler. Water levels inside and outside the piezometers were measured using a measuring tape connected to a sounding device. The VHG was calculated as follows:

$$VHG = \frac{\Delta h}{\Delta l} \quad (4)$$

where  $\Delta h$  is the difference in the elevation of the water level inside and outside the piezometer (cm) and  $\Delta l$  is the depth from the surface of the streambed to the middle of the slotted zone in the piezometer (cm) (Baxter et al., 2003). A positive VHG indicates upwelling conditions (Scordo and Moore, 2009; Figure 3.8). The VHG measurements were plotted in ArcGIS and related to streambed curvature and stream planform.

**Table 3.9 Location and depth below the surface of the piezometers in the upper reaches UA and UB. Reach UA: piezometer 1 was installed outside of the reach. Reach UB: piezometers 2, 3, and 5 were washed away.**

UA			UB		
Piezometer	Distance from injection site (m)	Depth (cm)	Piezometer	Distance from injection site (m)	Depth (cm)
2	38.7	58.8	1	71.6	19
3	38.7	19.1	4	44.7	22
4	38.7	25.2	6	11.7	16
5	35.5	20.7	7	7.2	14
6	35.7	20.5	8	7.2	15
7	35.7	61.5			
8a	30.4	26.6			
8b	27.0	14.4			
9	21.0	13.0			
10	18.0	19.5			
11	15.0	28.8			
12	14.5	20.5			
13	14.0	18.5			

**Table 3.10 Location and depth below the surface of the piezometers in the lower reaches DA and DB.**

DA			DB		
Piezometer	Distance from injection site (m)	Depth (cm)	Piezometer	Distance from injection site (m)	Depth (cm)
1	62.8	18.4	1	17.7	16.4
2	62.8	28.6	2	40.2	21.6
3	59.5	29.4	3	40.2	23.9
4	59.5	22.0	4	43.9	28.3
5	56.8	32.7	5	43.9	17.1
6	56.8	14.7	6	45.5	19.4
7	51.9	27.2	7	45.5	15.6
8	51.9	12.2			
9	30.0	19.9			
10	24.5	52.6			

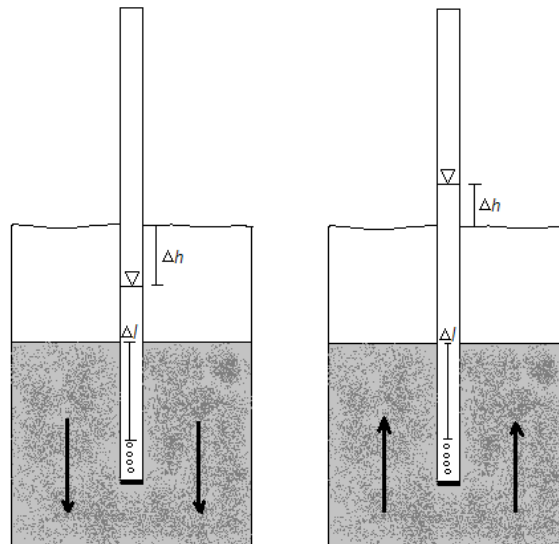


**Figure 3.8 Negative (left) and positive (right) VHG, indicating downwelling and upwelling hyporheic flow respectively (figure adapted from Baxter et al., 2003).**



**Figure 3.9 Piezometer network across and around a meander bend in reach UA.**

Two additional piezometers were installed at stream stage measurement sites (one at upper reach UA and one at lower reach DA). These piezometers were equipped with Odyssey Water Level Loggers from July to December 2010 (see Figure 3.3).

### **3.2.3. Determination of Inflow**

Lateral and vertical inflow into the stream was estimated using the data from the tracer experiments and the following equation (Scordo and Moore, 2009):

$$Q_L = \frac{Q_{ds} - Q_{us}}{L_T} \quad (5)$$

where  $Q_L$  is the net lateral inflow rate (L/s/m),  $Q_{ds}$  is the streamflow measured at the furthest downstream location (L/s),  $Q_{us}$  is the streamflow measured at the furthest upstream location within the reach (L/s), and  $L_T$  is the length of the reach (m).

Streamflow was calculated for each measurement location using the following equation (Moore, 2004):

$$Q = \frac{q}{k(EC_{ss} - EC_{bg})} \quad (6)$$

where  $Q$  is discharge (L/s),  $q$  is the injection rate (L/s),  $k$  is the slope of the relation between the relative concentration at steady state and EC (where the relative concentration is equal to the injection rate divided by the sum of the injection rate and stream discharge), and  $EC_{bg}$  and  $EC_{ss}$  are the electrical conductivities of stream water at background (before injection of tracer) and steady state (during the tracer injection) respectively.

### **3.2.4. Topographic Surveys**

The reaches were surveyed using a Topcon total station. For reach UA 1247 points were surveyed, for reach UB 1105 data points, for DA 1042 points, and reach DB 830 data points. These data points were mapped in ArcGIS to create various maps showing probe and piezometer locations, as well as DEMs of each reach. These topographic surveys were used to determine the gradient of each reach in order to determine whether or not topography could predict the location of lateral inflows in each reach. All culverts and other drainage features were mapped as well (Figure 3.3).

### **3.2.5. Modeling with OTIS and OTIS-P**

#### **3.2.5.1. Calibration**

OTIS and OTIS-P (see section 2.4) were used to model the movement of the tracer through the stream and streambed, and to determine transient storage in the stream and the rate of hyporheic exchange. OTIS-P solves equations 1 and 2 to estimate advection, dispersion, lateral inflow, and transient storage. The parameters that were optimized using OTIS-P are: the cross-sectional area of the stream ( $A$ ), the cross-sectional area of the storage zone ( $A_s$ ), the dispersion ( $D$ ), and storage zone exchange coefficient ( $\alpha$ ). OTIS-P adjusts these values to create a curve that best fits the observed

breakthrough data at the YSI and ECH<sub>2</sub>O probe locations (Table 3.6 and Table 3.7) during the tracer experiments. The Spearman rank correlation coefficient ( $r_s$ ) was determined for the relation between the optimized parameters and discharge.

Other parameters can be estimated based on the values of the parameters that were optimized in OTIS-P. These include the standardized storage zone to stream cross-sectional area ( $A_s/A$ ) that allows for comparisons between streams and reaches, and the storage zone residence time ( $T_{SZ}$ ), which is the average time a molecule is stored in transient storage (Thackston and Schnelle, 1970):

$$T_{SZ} = \frac{A_s}{A\alpha} \quad (7)$$

The hydraulic retention factor ( $R_h$ ), a measure of the average time a water molecule is stored relative to the hydraulic turnover length, can be calculated using the following equation (Morrice et al., 1997):

$$R_h = \frac{A_s}{Q}, \quad (8)$$

where  $Q$  is the discharge (m<sup>3</sup>/s). Finally, the average distance a water molecule travels in the stream before entering transient storage ( $L_s$ ) can be calculated using the equation (Fabian et al., 2011):

$$L_s = \frac{Q}{A\alpha} \quad (9)$$

Parameter uncertainty is an inevitable part of any transient storage model. By analyzing the Damköhler number ( $DaI$ ), stream velocity and reach length, an appropriate reach length can be chosen. The  $DaI$  is a dimensionless combination of the rates of exchange between stream and storage zones and is computed using the following equation:

$$DaI = \frac{\alpha \left( 1 + \frac{A}{A_s} \right) L}{u}, \quad (10)$$

where  $L$  is the length of the reach (m),  $u$  is the average water velocity (m/s),  $\alpha$  is the stream-storage exchange coefficient ( $s^{-1}$ ), and  $A_s$  is the storage zone cross-sectional area ( $m^2$ ) (Wagner and Harvey, 1997). Uncertainty in the optimized hyporheic exchange parameters is lowest when  $Da=1$ , and increases as  $Da$  values deviate from 1.  $Da$  less than '1' have a higher uncertainty because only small amounts of tracer interact with the storage zones in the reach and indicate that reach length may be too long or the velocity is too high.  $Da$  greater than '1' have a higher uncertainty because all solute interacts with the storage zones in the reach and indicate that the reach lengths may be too short or the velocity is too low.

Input files for OTIS-P include the *control* file (used to specify the file names of the input and output files), *parameter* file (which has information on the time, reach/sub-reach length data, and  $A_s$ ,  $D$ , and  $\alpha$  estimates), *flow* file (which contains discharge data and estimates for the  $A$  parameter), *data* file (which contains concentration data from the YSI and ECH<sub>2</sub>O probes), and the *STARPAC* input file (which is used to indicate which parameters are optimized and which parameters are held constant). There were too many concentration data points for the *data* input file. Therefore not all data points were included in the *data* file and only those data points just before the injection of the solute started until steady state was reached were included. Initial values for the  $A$ ,  $A_s$ ,  $D$ , and  $\alpha$  parameters were based on previous OTIS-P runs; the OTIS-P runs were carried out in order from the experiment with the lowest to highest discharge. At the start of each calibration run, the same parameter values were assigned for all segments of the reach. Once OTIS-P was run, the optimized parameter values were inserted into the *parameter* input files and OTIS-P was run again. This process was repeated until OTIS-P yielded stable optimized parameter values.

### **3.2.5.2. Validation**

Using the calibrated parameter values from OTIS-P, OTIS was used for validation of the model. OTIS requires fewer input files than OTIS-P, which include the *control* file (used to specify the filenames of the remaining input and output files), *parameter* file (contains the time, reach/sub-reach length data and the parameter values for  $A_s$ ,  $D$ , and  $\alpha$ ), and *flow* file (contains the discharge data and the optimized value of  $A$ ). All additional data (DEC probes and stream and streambed data from the piezometer

sites) were used for validation of the model. Goodness of fit statistics included the correlation coefficient (R), Nash-Sutcliffe Efficiency (E), and Mean Squared Error (MSE).

## 4. Results and Discussion

### 4.1. Streamflow

Forty tracer tests were conducted: 10 at each reach. However, because of rain events, unforeseen flooding, and equipment malfunction, not all tests could be used for analysis (September 28 and July 7, 2010 (UA), August 4, 2010 (DB), October 27, 2010 (UB), and November 9, 2010 (DA)). Discharge during the tracer tests varied between 1 and 72 L/s for the upstream reaches and between 19 and 335 L/s for the downstream reaches (Table 4.1 and Table 4.2). Previous tracer studies have been conducted for discharge varying from <1-250 L/s (Webster and Valett, 2007). Not many studies that examined hyporheic exchange have been conducted under high flow conditions that are comparable to the high flows in the downstream reaches during this study. The highest discharge in tracer studies relating specifically to hyporheic exchange ranged between 30-75 L/s (Morrice et al., 1997; Hart et al., 1999; Patschke, 1999; Scordo and Moore, 2009; Ryan et al., 2010).

The urban setting was initially thought to be “more controlled” than a natural forest setting, but in fact was less controlled. Unknown drainage networks and crossings led to more unknowns than in a relatively untouched forest setting. For example, there were regular rapid increases in discharge during the summer despite a lack of precipitation (Figure 4.1). Streamflow increased by 1.1-29 L/s during twenty of these events between July 10 and August 31, 2010. The volume added to the stream ranged from 14 to 457 m<sup>3</sup>. Inquiries were made to the City of Coquitlam concerning these flow increases; however, their responses regarding the source of this water do not seem plausible (e.g. it was suggested that this was due to the spray park, which is located downstream of the study reaches; diversion of water from the park would not contribute to the stream reaches at a higher elevation). Other examples of potential sources of flow changes included obstructions placed into the stream, such as rocks, to create small

dams which changed flow on a micro-scale. On another occasion (June 9, 2010), a bench was thrown into the river at site DA, adding “streambed complexity”.

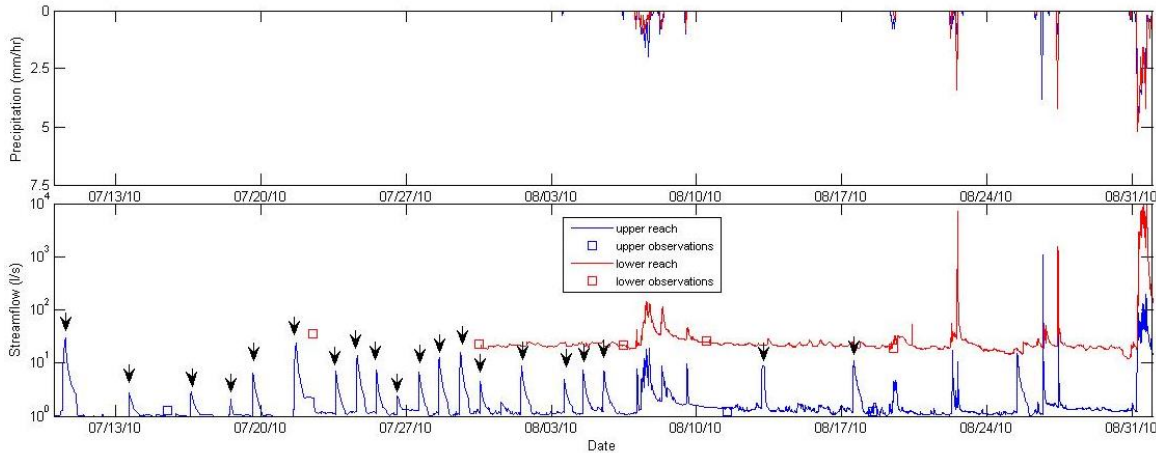


**Figure 4.1 Unexplained high discharge events (indicated by arrows). These streamflow responses were observed at the upper reach during periods without precipitation.**

## 4.2. Steady State EC and Lateral Inflow

Discharge at each probe location was calculated from the steady state EC measurements taken during the tracer tests and plotted in ArcGIS. These plots show that there was relatively little lateral inflow to the reaches (Figure 4.2-Figure 4.5). The estimated maximum error in the discharge calculations was usually greater than the amount of lateral inflow estimated from the changes in discharge calculated from the steady state EC data. Some of the higher discharge values had an error that was higher than the discharge itself (Table 4.1 and Table 4.2). Two notable tests are November 16, 2010 (reach DA, where the error was nearly half the calculated discharge value) and September 22, 2010 (reach UA, where the error was larger than the calculated discharge). The error in the calculated discharge increased as the discharge increased and depended mostly on the fluctuation in the EC at background and steady state, and the amount by which the EC increased from background to steady state.

The maps of steady state discharge (Figure 4.2-Figure 4.5) and steady state EC measured with the handheld probe (or YSI, ECH<sub>2</sub>O, and DEC probes when the handheld probe was unavailable; Appendix B) reveal no clear pattern as to whether discharge increased along the reaches or not and instead show high variability in discharge on the different days. The average rank of the steady state EC values and standard deviation (SD) of the rank were calculated to determine the temporal stability (i.e. temporal persistence) of the variation in discharge along the reach (Figure 4.6 and Figure 4.7). This was done by assigning a rank to the steady state EC value at each probe location for each test, and then determining the average and standard deviation (SD) of the rank for each specific probe location (see Appendix A for the calculation). A high average rank indicates a persistently low steady state EC (and therefore high discharge), while a low average rank indicates a persistently high steady state EC (and therefore low discharge). An intermediate average rank, with a high standard deviation in rank indicates a highly variable rank, and thus no persistent pattern in the steady state EC values.

For reach UA, steady state EC was relatively similar throughout the reach. The average rank varied between 4.0 and 5.9 (SD ranged from 1.9-3.8), indicating little persistent variation in steady state EC throughout the reach. In the step-pool near the beginning of the reach and through the bend downstream, discharge was generally lowest, with an average rank between 4.1 and 4.3.

The average rank for reach UB varied between 2.1 and 5.6 (SD ranged from 1.3-2.3), indicating more persistent variation in steady state EC between sites within the reach. Sites just before the bifurcation in the middle of reach UB had the lowest average rank (2.05, SD of 1.3) (and thus the lowest discharge); the site just after the convergence of the stream had the highest average rank (5.6, SD of 2.1) (thus highest discharge). Where the reach was narrower, the average rank varied between 2.1 and 4.2.

Average rank for reach DA varied between 1.6 and 5.2 (SD ranged from 2.1-2.7), indicating some persistent differences in steady state EC between sites. The average rank of steady state EC decreased somewhat towards the end of the reach, indicating decreasing streamflow in the slow moving part of the stream after a meander bend.

The average rank of steady state EC for reach DB ranged between 3.8 and 6.7 (SD ranged from 1.3-4.0), indicating some persistent differences in steady state EC between sites. The average rank of steady state EC values was highest through the meander bend for DB, indicating the lowest discharge in the meander bend.

While the plotting of the discharge on the different measurement days showed that there was no clear pattern in the spatial variation in discharge across the reaches, the data does suggest that there was a significant spatial and temporal variability in discharge across the study reaches.

**Table 4.1 Discharge (Q), measurement uncertainty, and lateral inflow ( $Q_{lat}$ ) for the lower reach tracer tests.  $Q_{YSI}$  and YSI error are the discharge and the uncertainty in the discharge calculated from the EC measurements using the YSI probe.  $Q_{E5}$  and E5 error are the discharge and the uncertainty in the discharge calculated from the EC measurements using the ECH<sub>2</sub>O 5 probe. In all but 5 cases (\*)  $Q_{lat}$  was less than the uncertainty in  $Q_{lat}$ . For September 24, 2010 ECH<sub>2</sub>O data were unavailable. See Figure 3.7 and Table 3.7 for the location of the YSI and ECH<sub>2</sub>O probes.**

DA						DB					
Date (2010)	$Q_{YSI}$ (L/s)	YSI Error (L/s)	$Q_{E5}$ (L/s)	E5 Error (L/s)	$Q_{lat}$ (L/s)	Date (2010)	$Q_{YSI}$ (L/s)	YSI Error (L/s)	$Q_{E5}$ (L/s)	E5 Error (L/s)	$Q_{lat}$ (L/s)
Jul 14	46.0	10.5	40.7	8.4	5.4	Jul 20	22.6	1.8	20.3	4.2	2.3
Jul 22*	35.9	4.2	28.2	7.4	7.7	Jul 27	20.6	3.3	19.5	3.7	1.4
Jul 30	22.7	2.9	19.0	3.8	3.6	Aug 16	25.0	3.1	22.1	2.0	2.9
Aug 6	21.7	2.1	23.0	1.2	1.4	Sept 24	143.6	34.9	n/a	n/a	n/a
Aug 10	25.7	2.3	24.3	2.1	1.5	Oct 12	114.3	20.8	101.0	19.8	13.3
Aug 19	18.7	2.8	23.0	9.1	4.4	Oct 20*	63.6	8.3	38.7	6.3	24.9
Sept 15	39.8	5.0	38.2	9.2	1.7	Oct 29*	61.5	4.5	126.8	32.9	65.3
Oct 19	49.5	8.0	50.2	8.7	0.7	Nov 12	83.1	11.4	92.5	14.6	9.4
Nov 16*	510.0	208.2	267.1	46.8	242.9	Dec 3*	157.7	20.4	294.1	126.5	136.5

Locations of lateral inflow may be more distinct during events than during the tracer test experiments. Significant inflow from the culverts and storm drains was not observed during the experiments because the tracer tests were generally carried out during dry periods so that discharge would not change rapidly during the test. Streambed temperature recorded in Hoy Creek during events showed that stream and streambed temperature changed rapidly in response to precipitation and urban runoff entering the stream (Zimmerman, 2011).

**Table 4.2 Discharge (Q), measurement uncertainty, and lateral inflow ( $Q_{lat}$ ) for the upper reach tracer tests.  $Q_{YSI}$  and YSI error are the discharge and the uncertainty in the discharge calculated from the EC measurements using the YSI probe.  $Q_{E5}$  and E5 error are the discharge and the uncertainty in the discharge calculated from the EC measurements using the ECH<sub>2</sub>O 5 probe. (\*indicates calculation from ECH<sub>2</sub>O 1 probe instead of the YSI probe). In all cases  $Q_{lat}$  was less than the uncertainty in  $Q_{lat}$ . See Figure 3.7 and Table 3.6.**

UA						UB					
Date (2010)	$Q_{YSI}$ (L/s)	YSI Error (L/s)	$Q_{E5}$ (L/s)	E5 Error (L/s)	$Q_{lat}$ (L/s)	Date (2010)	$Q_{YSI}$ (L/s)	YSI Error (L/s)	$Q_{E5}$ (L/s)	E5 Error (L/s)	$Q_{lat}$ (L/s)
Jul 2	1.6	0.1*	1.6	0.1	0.01	Jul 23	1.5	0.1	1.7	0.2	0.2
Jul 15	1.2	0.03	1.2	0.1	0.1	Jul 26	1.7	0.2	1.7	0.4	0.01
Aug 11	1.2	0.1	1.4	0.2	0.2	Aug 5	3.6	0.6*	4.0	0.4	0.4
Aug 18	1.2	0.1	1.3	0.1	0.1	Aug 12	1.5	0.1	1.6	0.2	0.2
Sept 22	10.9	11.5	14.6	7.5	3.7	Sept 29	40.4	8.1	41.0	5.7	0.6
Oct 5	4.2	0.3	4.9	1.3	0.7	Oct 13	17.9	1.8	17.4	1.5	0.5
Oct 18	4.4	0.1	4.3	0.3	0.1	Nov 10	27.2	4.1	29.7	2.0	2.5
Oct 26	72.3	16.3	67.5	41.7	4.9	Dec 4	28.4	2.9	30.4	5.6	2.0
Nov 3	21.9	2.2	21.5	1.7	0.4	Dec 6	24.7	2.2	27.1	6.7	2.5

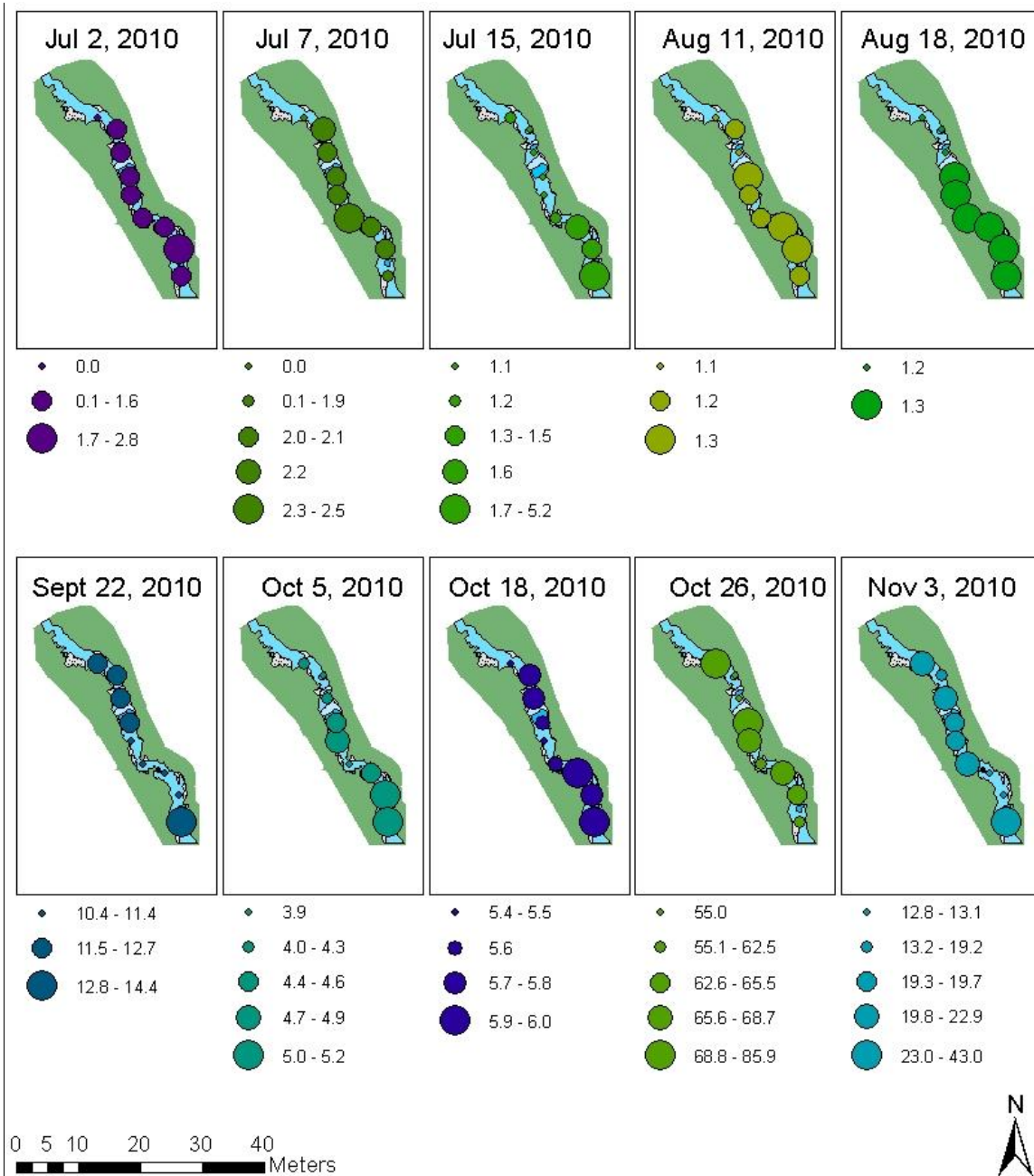


**Figure 4.2 Discharge (L/s) during the tracer experiments at reach UA.**

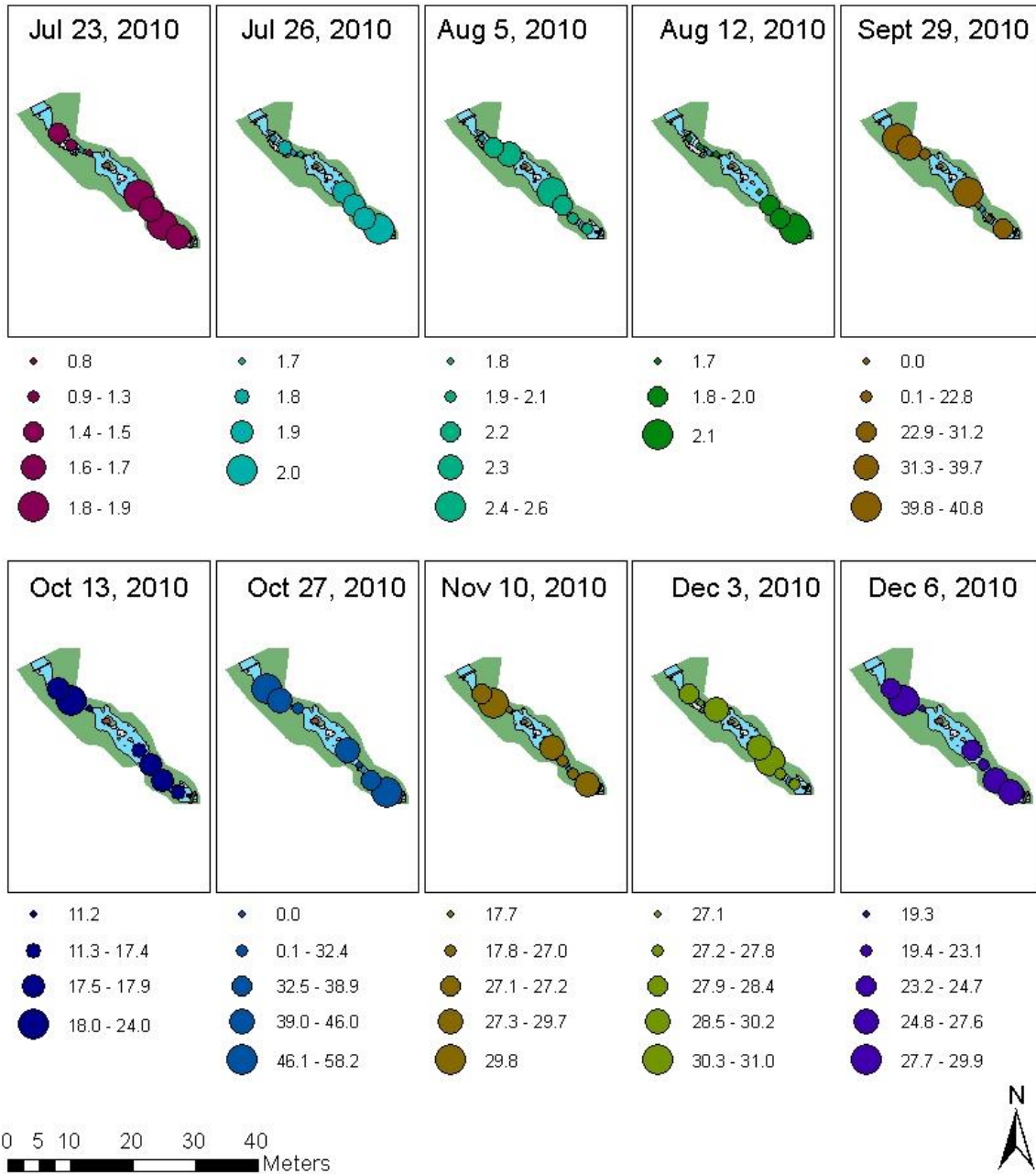


**Figure 4.3 Discharge (L/s) during the tracer experiments at reach UB.**

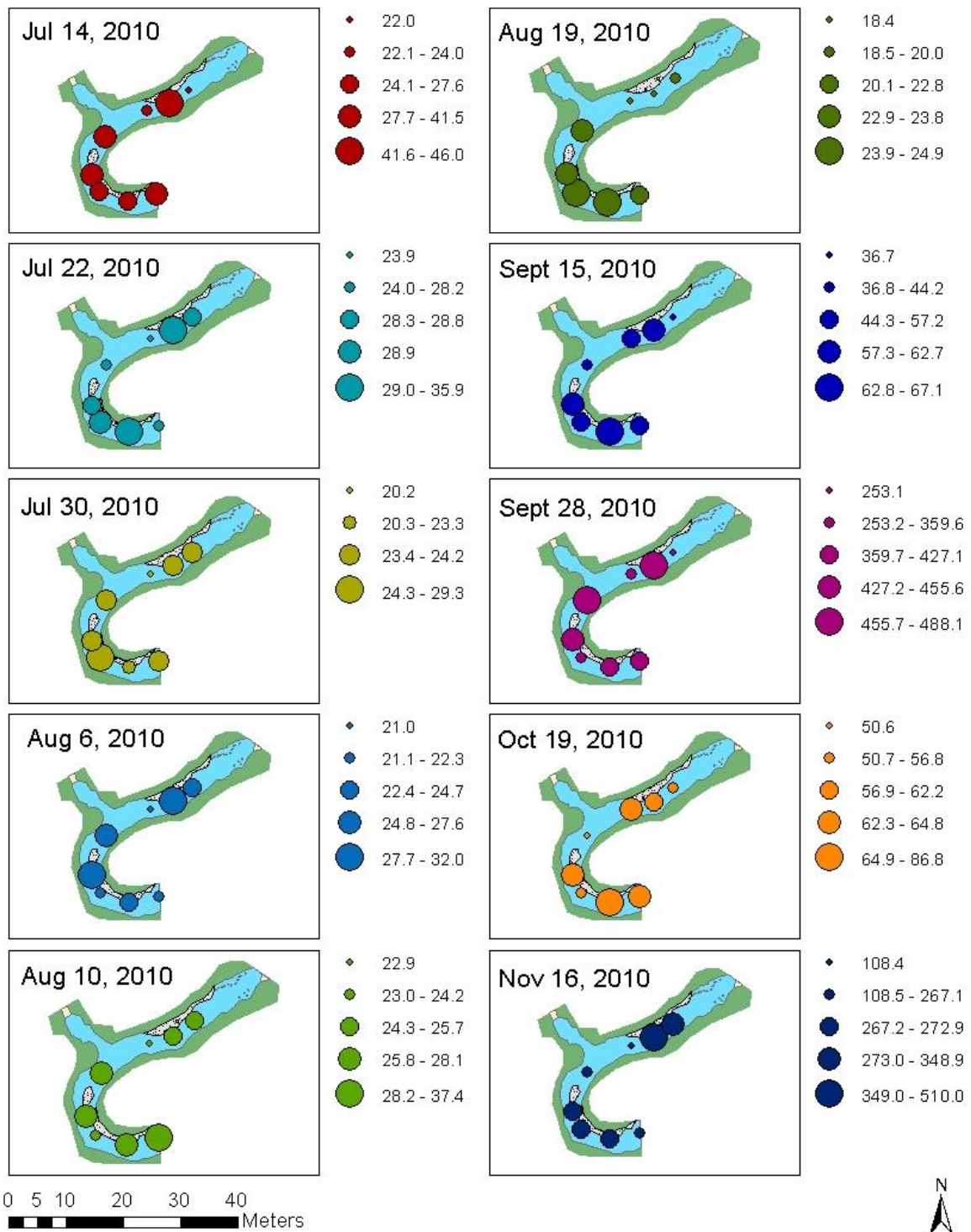


**Figure 4.4 Discharge (L/s) during the tracer experiments at reach DA.**

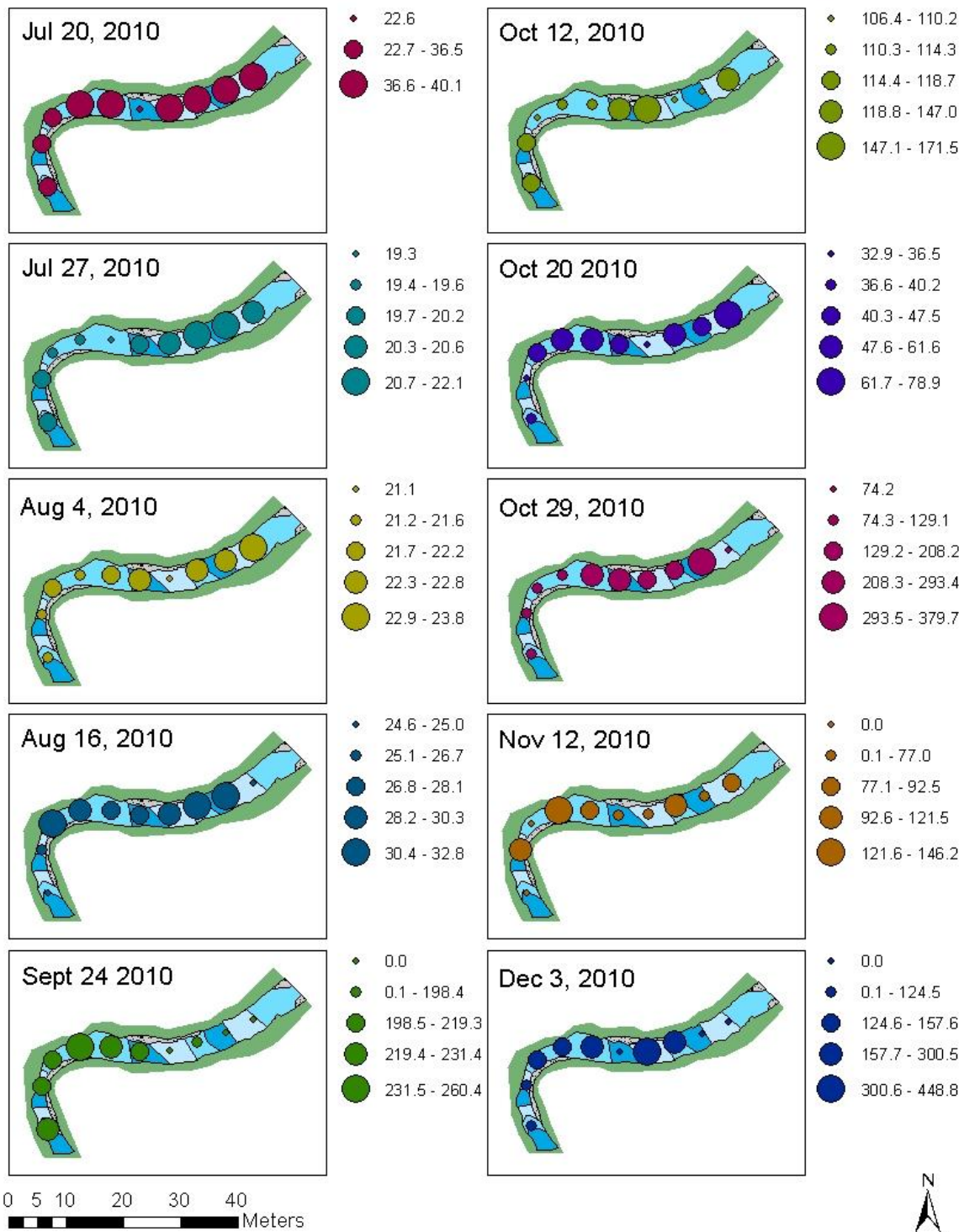


**Figure 4.5 Discharge (L/s) during the tracer experiments at reach DB.**

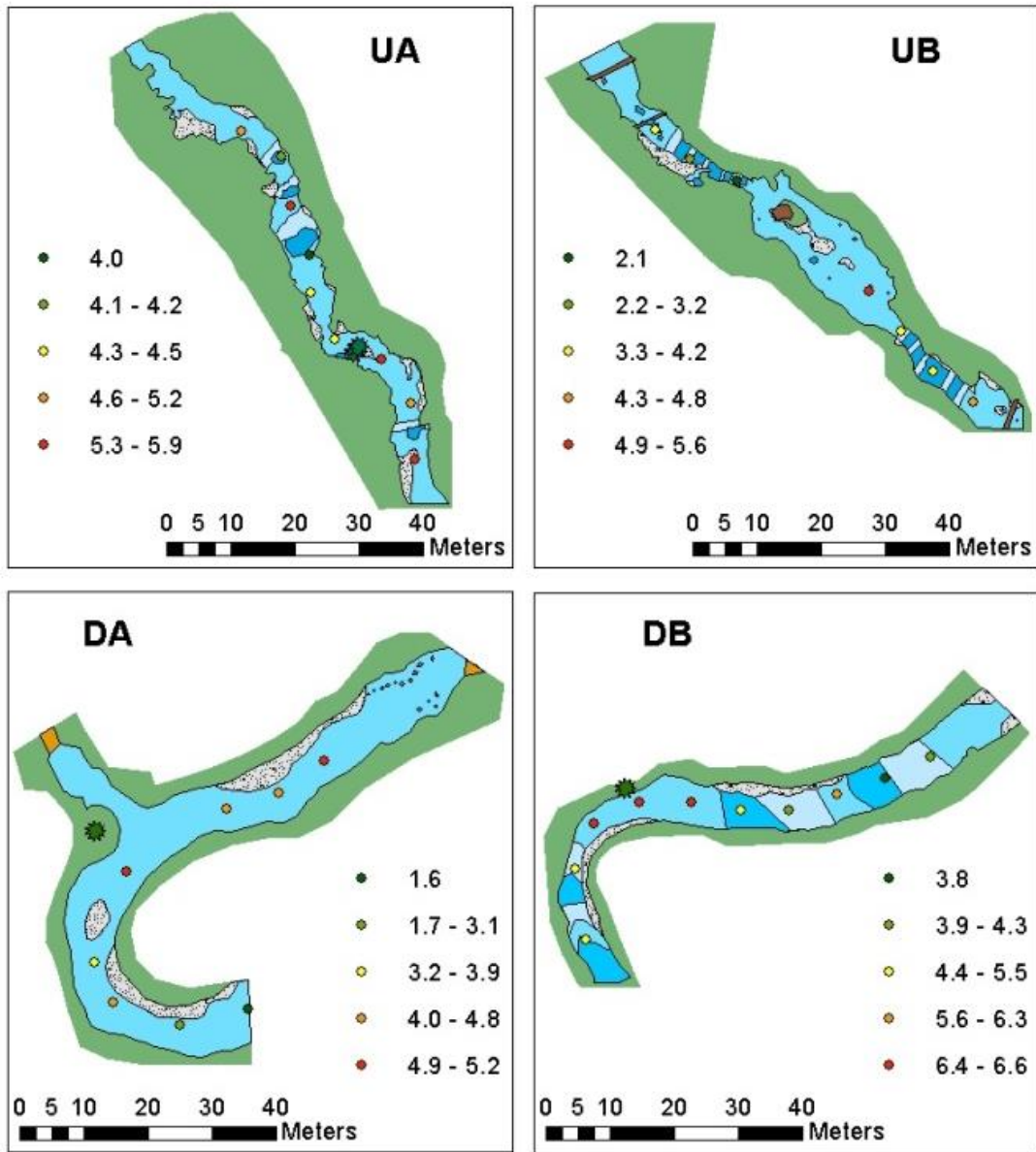


**Figure 4.6 Average rank of steady state EC for each reach. A high average rank indicates a relatively low steady state EC and thus a relatively high discharge. Refer to Figure 3.3 for an explanation of the features in the stream (different shades of blue represent riffles and pools).**

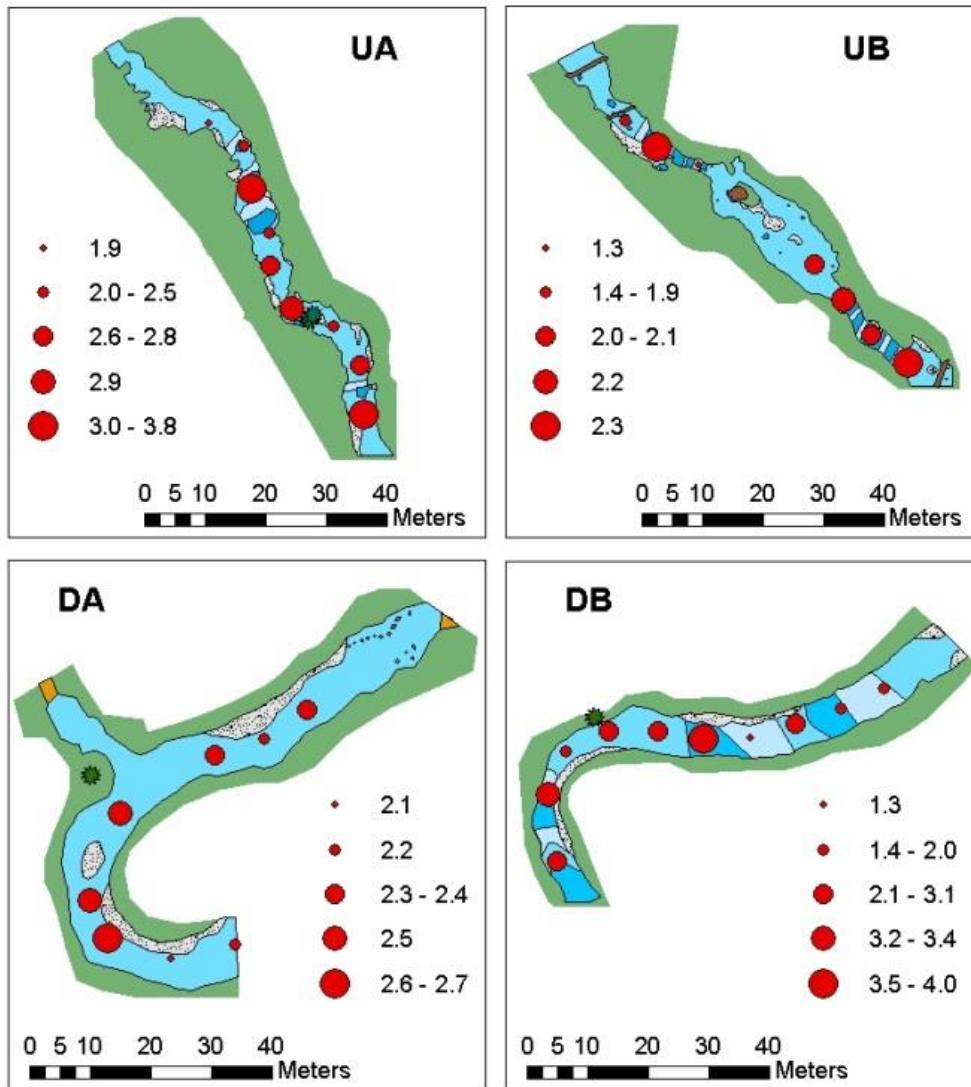


**Figure 4.7** Standard deviation (SD) of the rank of steady state EC at each probe location within each reach. A low SD indicates a more persistent rank, while a high SD indicates a highly variable rank for steady state EC.

### 4.3. Vertical Hydraulic Gradients

VHGs during tracer tests ranged from nearly 0 to 0.96, indicating upwelling, except for at piezometers 1-8 in the bend of reach DA in which a negative VHG (indicating downwelling) was measured (Figure 4.8-Figure 4.11). There was no

noticeable difference in the VHG between the reaches as the range was quite similar, except for the negative VHG for reach DA. This indicates that there may be similar amounts of hyporheic exchange in each of these reaches, with the exception of reach DA, which exhibits strong downwelling.

The average rank of the VHG values and associated SD in rank were calculated to determine the variation in VHG along the reach at the piezometers (Figure 4.12 and Figure 4.13) using the ranking method described in section 4.2 for ranking the steady state EC measurements (see Appendix A for the calculation). A high average rank indicates a persistently high VHG, while a low average rank indicates a persistently low VHG. An intermediate average rank, with a high standard deviation indicates a highly variable rank, and thus no persistent pattern in the VHG.

In reach UA, VHG was generally 0 in the straight portion of the reach as well as in the small bend towards the end of the reach, indicating no measurable upwelling or downwelling (Figure 4.8). Upward gradients increased across the bend, with the smallest gradients occurring in the stream and the largest gradients towards the bank of the stream. As discharge increased, VHG decreased slightly, indicating a decrease in upwelling. There was a high spatial variability in the VHG in the area around the bend, as well as at the step-pool in the upper part of the reach. For reach UA, the average rank in VHG varied between 0.9 and 7.4 (SD ranged from 0.0-2.3), revealing considerable persistent variation in VHG.

Upwelling also occurred in UB. However, there is no clear trend or pattern for the relation between VHG and stream morphology or discharge. Piezometers were difficult to install in reach UB and were dislodged on a regular basis, resulting in only a few data points (Figure 4.9). The range of VHG was quite variable between experiments. Additionally, the variability of VHG near the beginning of the reach was considerable for such a small area: the VHG in the cluster of four piezometers within four meters from each other ranged from 0 to 0.5 at low discharge. At higher discharge (when two of these piezometers were dislodged), the range was smaller (0-0.1). For reach UB, the average rank varied between 1.0 and 3.1 (SD ranged from 0.0-1.1), revealing little persistent variation in VHG across the reach.

Reach DA is the only reach for which negative VHGs were measured, indicating downwelling (Figure 4.10). Positive VHGs were measured in the straight part of reach DA upstream from the meander bend. VHGs were greatest (-0.113 to 0.327) at the upstream end of the bend, and downwelling was stronger at the downstream end of the meander bend. There was no trend between VHG and discharge for the piezometers along the straight part of the reach (VHG was highly variable, ranging from 0.0 to 0.74). However, in the bend, downwelling generally became stronger (more negative VHGs) with higher discharge. This may indicate that this part of reach DA is a losing reach in Hoy Creek. For reach DA the average rank varied between 1.2 and 8.8 (SD ranged from 0.4-2.9), indicating considerable persistent variation in VHG across the reach.

For reach DB, VHG was 0.0 along the straight stretch of the reach and did not change with discharge (Figure 4.11). Gradients were generally greater at the upstream end of the bend than further downstream, except for the September 24, 2010 measurements. Increasing discharge resulted in smaller gradients in the meander bend. Unfortunately, piezometers around the meander bend next to the piezometers within the bar were washed away during high streamflow conditions so that only limited data were available for this site. The few data points that were collected suggest that upwelling is stronger in the bend compared to the straight stretch of the reach. For reach DB the average rank varied between 1.0 and 6.0 (SD ranged from 0.0-1.8), revealing persistent variation between piezometers, but not as much as for reaches in DA and UA.

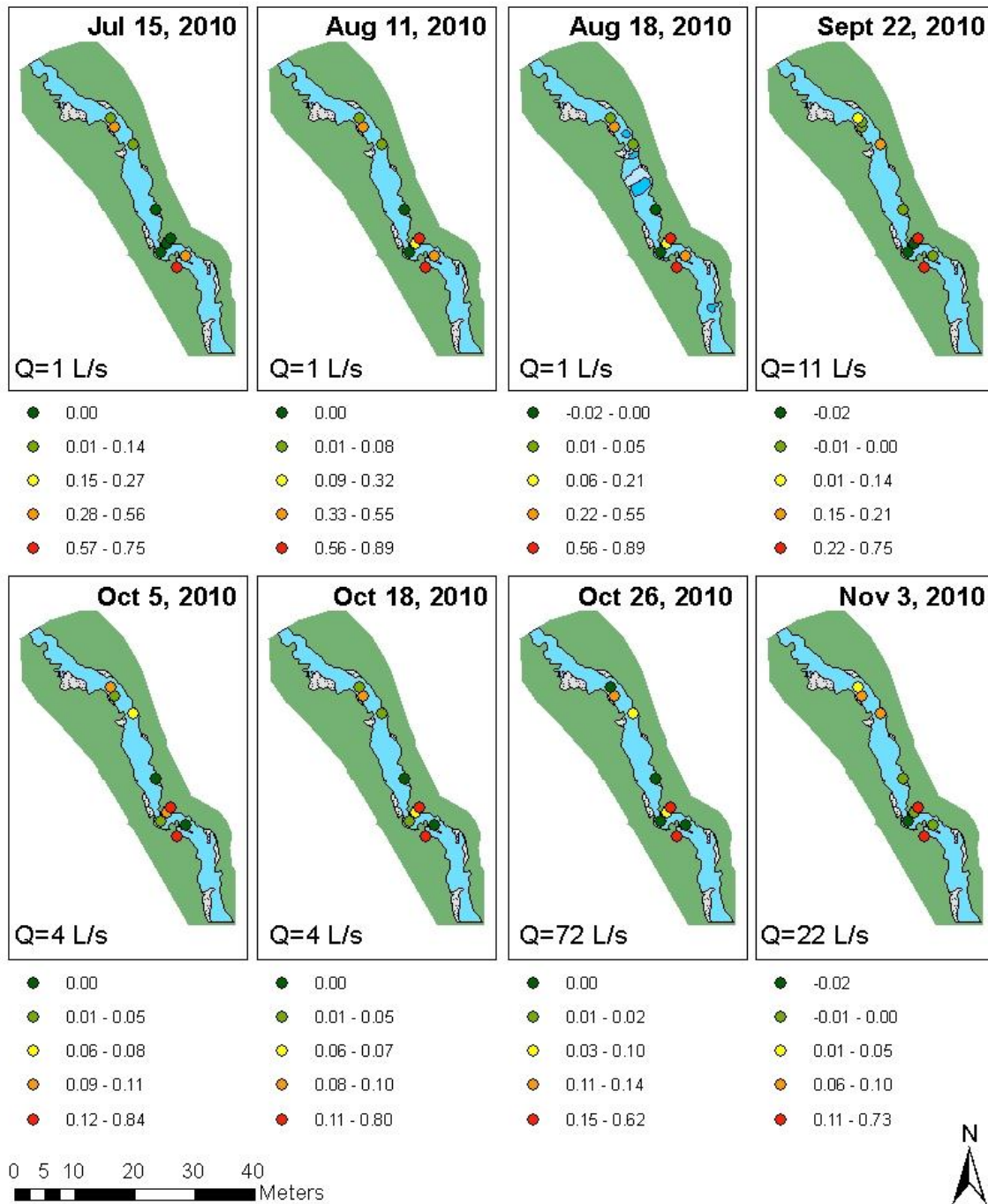


**Figure 4.8 Vertical hydraulic gradients during the tracer experiments in reach UA. Negative values indicate downwelling. Positive values indicate upwelling.**

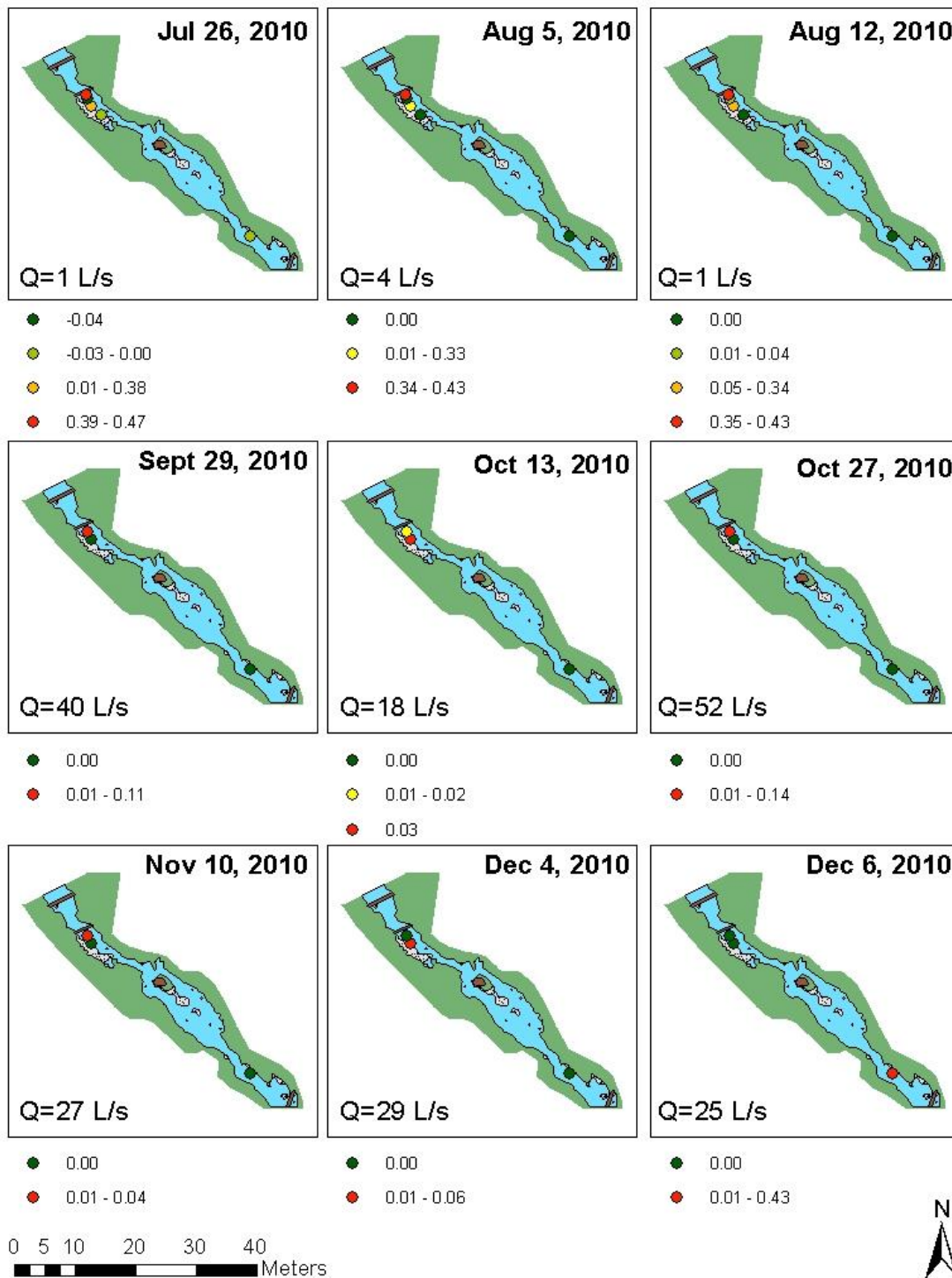


**Figure 4.9 Vertical hydraulic gradient during the tracer experiments in reach UB. Negative values indicate downwelling. Positive values indicate upwelling.**

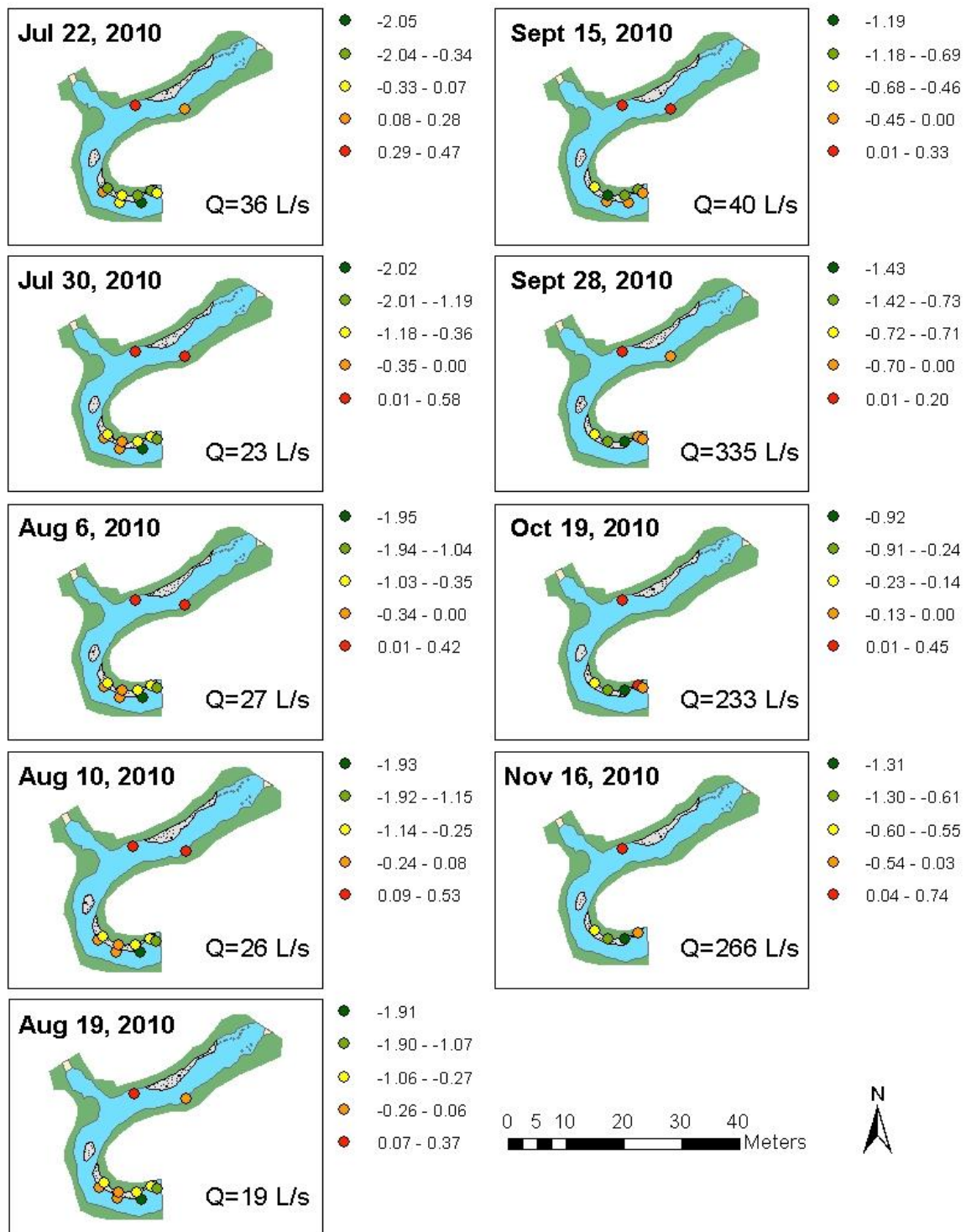


**Figure 4.10 Vertical hydraulic gradient during the tracer experiments in reach DA. Negative values indicate downwelling. Positive values indicate upwelling.**

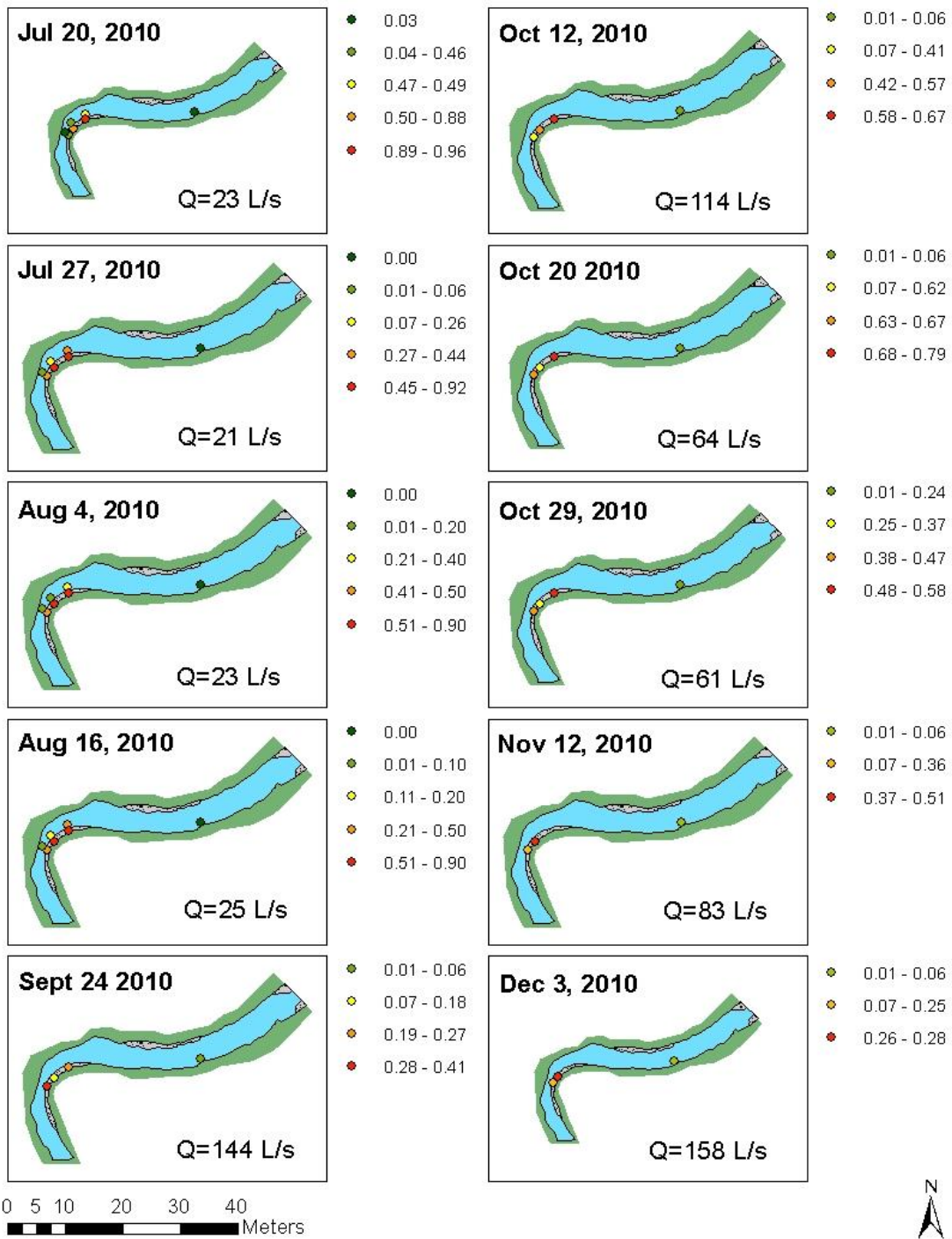


**Figure 4.11 Vertical hydraulic gradient during the tracer experiments in reach DB. Negative values indicate downwelling. Positive values indicate upwelling.**

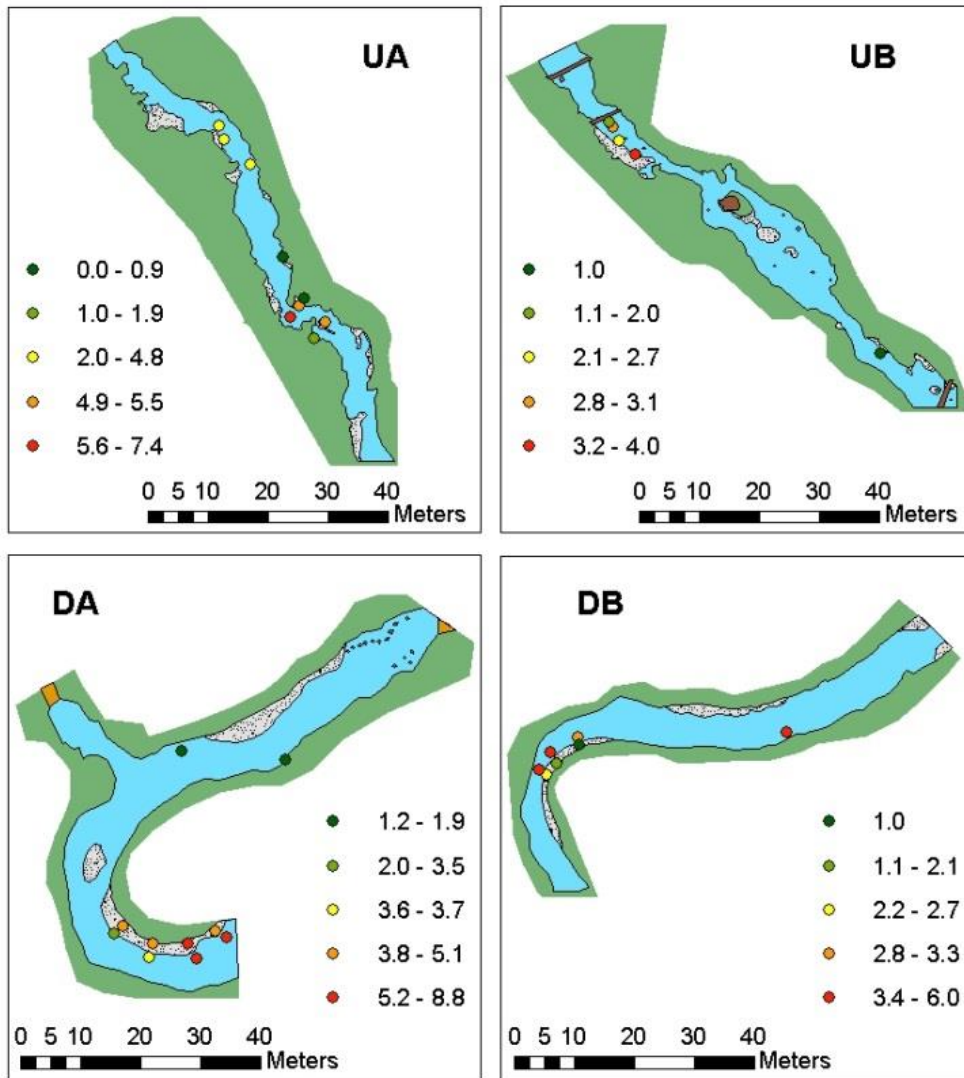


**Figure 4.12** Average rank of the VHG for each reach. A low rank indicates a low (or more negative) VHG compared to the other sites in the reach, while a high rank indicates a relatively large positive VHG.

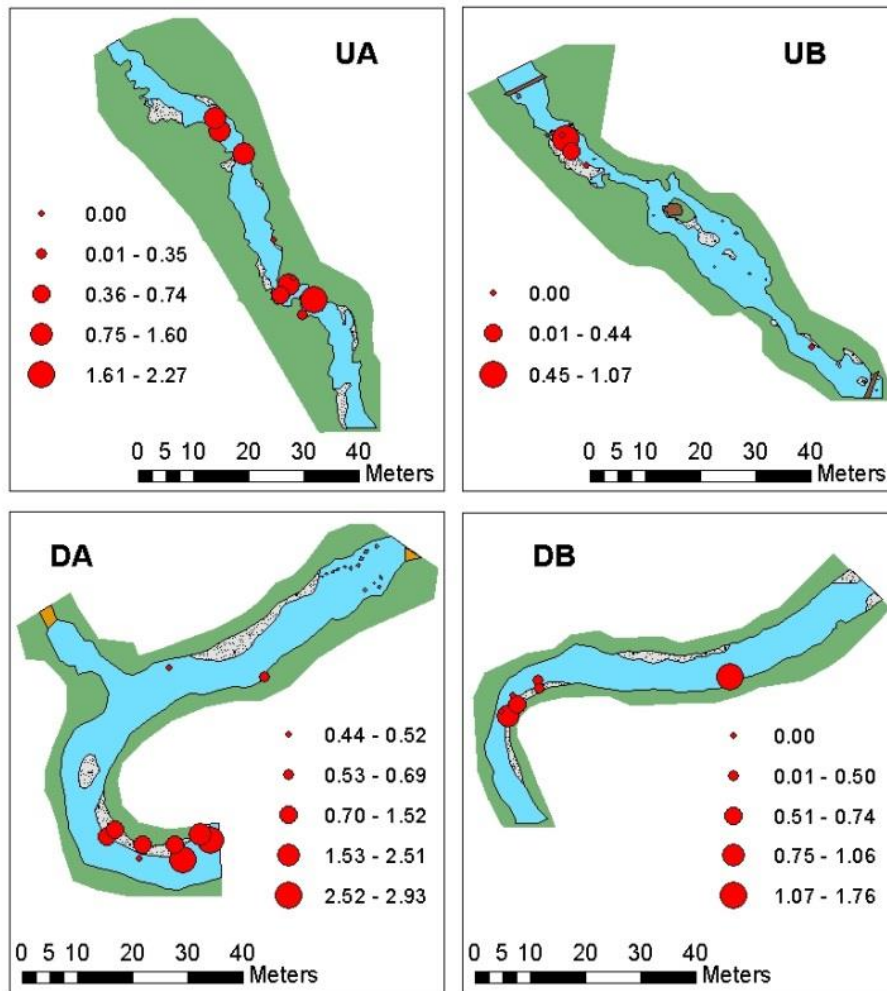


**Figure 4.13 Standard deviation of the rank of the VHG in each reach. A low standard deviation of the rank indicates a persistent ranks.**

VHGs decreased towards the bank in reach DB and UA and became larger towards the bank at the upstream end of the meander bend in reach UA. In contrast, it increased towards the bank at the upstream and downstream end of the meander bend in reach DA. VHGs increased through the meander bend (stronger upwelling) in both downstream reaches. These VHG results indicate a general trend of stronger upwelling through a meander bend in reaches DB and UA and larger gradients on the downstream end of the meander bend compared to the upstream part. This indicates that upwelling from the hyporheic zone and/or groundwater inflow was larger towards the downstream end of the meander bends for these reaches.

Upwelling occurred in the pool of the step near the upstream end of the reach. The positive VHGs in the pool downstream of the step near the upstream end of reach UA indicate inflow of hyporheic water and/or groundwater to the stream at that location. Munz et al. (2011) showed that at the head of riffles and within pools, average VHG did not exceed 0.025, indicating slight upwelling conditions. At the end of the riffle, VHG increased to an average of 0.1, indicating increased upwelling. At the downstream end of a pool, VHG decreased to 0.05-0.1, which is larger than upstream of the pool. For reach UA, slight upwelling occurred in the pool near the beginning of the reach; this observation was also supported by observations of tracer movement through the piezometers located in the step and just downstream of the pool. These results support the findings of Tonina and Buffington (2007) who noted that an obstruction creates high pressure upstream, which drives hyporheic exchange. Munz et al. (2011) also observed higher VHG variability as a result of sediment heterogeneity, which could explain the high VHG variability at certain locations in the studied reaches in Hoy Creek (Figure 4.8-Figure 4.11).

VHGs decreased as discharge increased in reaches UA and DB (weaker upwelling). However, in reach DA, VHG decreased (stronger downwelling) as discharge increased, similar to the results of Fabian et al. (2011), who showed that upwelling was enhanced in upwelling zones at higher discharge. However, Fabian et al. (2011) also noted weakened upwelling and downwelling zones during the transition from dry to wet season due to a disruption of the equilibrium between groundwater and streamwater levels, and different (ie. Deeper and longer) flow paths are used to reach different upwelling and downwelling zones during different seasons, which is perhaps what occurs in reaches UA and DB, where upwelling weakens with increasing discharge.

However, Fabian et al. (2011) also noted weaker upwelling and downwelling during the transition from dry to wet season due to a disruption of the equilibrium between groundwater and streamwater levels, and different (ie. deeper and longer) flow paths to reach different upwelling and downwelling zones during different seasons. Perhaps this occurred in reaches UA and DB, where upwelling weakened with increasing discharge.

## 4.4. Tracer Experiments

### 4.4.1. Breakthrough Curves

More time was required to reach steady state during low flow conditions than during high flow conditions (Table 4.3-Table 4.6), indicating a higher advection rate and/or more dispersion during high flow conditions. It also took more time to reach steady state at reach UA compared to UB because the path between the injection site and the YSI probe location in UB is straight and shorter compared to that in UA (7 versus 12 m). The time required to reach steady state in the lower reaches, however, was comparable, likely due to similar site conditions and reach length. The breakthrough curves (Figure 4.14 and Appendix C) suggest significant dispersion and/or transient storage in reach UB. Some tests in reaches DA and DB also suggest significant dispersion and transient storage because they do not have an immediate rise and fall.

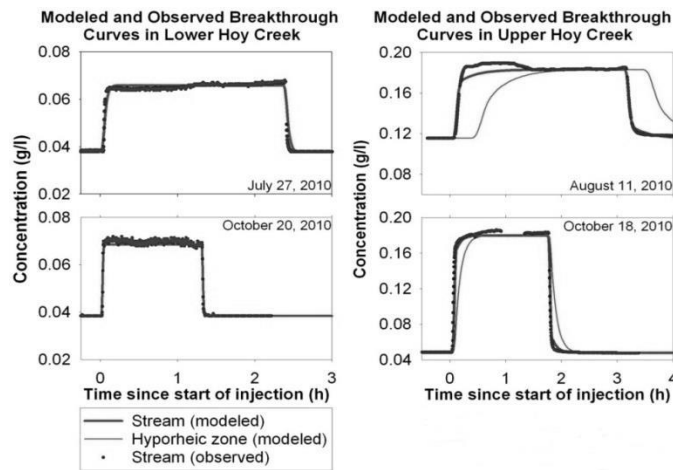


**Figure 4.14** Examples of the observed and modeled breakthrough curves at the YSI locations in the upper and lower reaches of Hoy Creek (UA and DB). Observed and modeled breakthrough curves of all experiments are provided in Appendix C.

**Table 4.3 Time between the start of the injection (start) and steady state (SS), the start of the injection and the start of the increase in EC (start to rise), between the start of the increase in the rise in EC and steady state EC (rise to SS), and the ratio of rise to SS and start to rise (normalized) for the YSI probe measurements at upper reach UA. The Spearman rank correlation coefficient ( $r_s$ ) for the relation between these timing parameters and discharge is also given.**

Date (2010)	Q (L/s)	Start to SS (min)	Start to rise (min)	Rise to SS (min)	Normalized
Jul 15	1	13.3	3.6	9.7	3.2
Aug 11	1	17.5	4.1	13.3	3.2
Aug 18	1	20.9	5.0	15.8	2.7
Sept 22	11	8.8	0.7	8.2	0.8
Oct 5	4	8.8	3.3	5.5	1.7
Oct 18	4	12.2	2.5	9.7	3.8
Oct 26	72	3.2	3.1	0.1	0.03
Nov 3	22	4.2	2.3	1.8	12.3
$r_s$		-0.91	-0.77	-0.85	-0.41
p-value		<0.01	0.03	<0.01	0.32

**Table 4.4 Time between the start of the injection (start) and steady state (SS), the start of the injection and the start of the increase in EC (start to rise), between the start of the increase in the rise in EC and steady state EC (rise to SS), and the ratio of rise to SS and start to rise (normalized) for the YSI probe measurements at upper reach UB. The Spearman rank correlation coefficient ( $r_s$ ) for the relation between these timing parameters and discharge is also given.**

Date (2010)	Q (L/s)	Start to SS (min)	Start to rise (min)	Rise to SS (min)	Normalized
Jul 23	1	6.3	1.5	4.8	3.2
Jul 26	1	5.3	1.7	3.7	2.2
Aug 12	1	6.0	1.5	4.5	3.0
Sept 29	40	2.0	1.0	1.0	1.0
Oct 13	18	3.8	0.5	3.3	7.7
Nov 10	27	4.3	3.0	1.3	0.4
Dec 4	29	2.7	0.3	2.3	7.0
Dec 6	25	2.8	0.6	2.3	4.2
$r_s$		-0.90	-0.39	-0.90	-0.05
p-value		>0.01	0.34	>0.01	0.91

**Table 4.5 Time between the start of the injection (start) and steady state (SS), the start of the injection and the start of the increase in EC (start to rise), between the start of the increase in the rise in EC and steady state (rise to SS), and the ratio of rise to SS and start to rise (normalized) for the YSI probe measurements at lower reach DA. The Spearman rank correlation coefficient ( $r_s$ ) for the relation between these timing parameters and discharge is also given.**

Date (2010)	Q (L/s)	Start to SS (min)	Start to rise (min)	Rise to SS (min)	Normalized
Jul 22	36	4.3	2.5	1.8	0.7
Jul 30	23	5.2	1.9	3.3	1.8
Aug 6	27	5.8	2.5	3.3	1.3
Aug 10	26	4.7	2.5	2.2	0.9
Aug 19	19	5.8	2.8	3.0	1.1
Sept 15	40	3.5	2.2	1.3	0.6
Oct 19	49	3.5	2.5	1.0	0.4
Nov 16	510*	2.8	2.2	0.7	0.3
$r_s$		0.87	0.17	0.83	0.88
p-value		0.01	0.69	0.01	<0.01

**Table 4.6 Time between the start of the injection (start) and steady state (SS), the start of the injection and the start of the increase in EC (start to rise), between the start of the increase in the rise in EC and steady state (rise to SS), and the ratio of rise to SS and start to rise (normalized) for the YSI probe measurements at lower reach DB. The Spearman rank correlation coefficient ( $r_s$ ) for the relation between these timing parameters and discharge is also given.**

Date (2010)	Q (L/s)	Start to SS (min)	Start to rise (min)	Rise to SS (min)	Normalized
Jul 20	23	6.3	2.3	3.5	1.6
Jul 27	21	5.3	2.7	3.7	1.2
Aug 16	25	6.0	1.8	3.0	1.5
Sept 24	144	2.0	1.5	0.5	1.4
Oct 12	114	3.8	2.0	0.8	0.4
Oct 20	64	4.3	1.5	2.7	0.4
Oct 29	61	2.7	2.5	1.5	1.8
Nov 12	83	2.8	2.7	1.2	0.6
Dec 3	158	5.4	2.4	2.9	0.3
$r_s$		-0.69	0.13	-0.73	-0.58
p-value		0.04	0.73	0.02	0.10

The ratio of the time between the start of the rise in EC and the time of steady state EC and the time between the start of the experiment and the start of the rise in EC (rise to SS/start to rise) can be used as a measure of transient storage and dispersion. If this ratio is large, then there is more transient storage and/or dispersion. While there appears to be a relation between discharge and this ratio for reaches DA, DB, and UA (Figure 4.15), suggesting a decrease in transient storage and dispersion with increasing discharge, this trend was only significant for reach DA ( $r_s=0.88$ ;  $p=0.004$ ) (Figure 4.15; Table 4.3-Table 4.6).

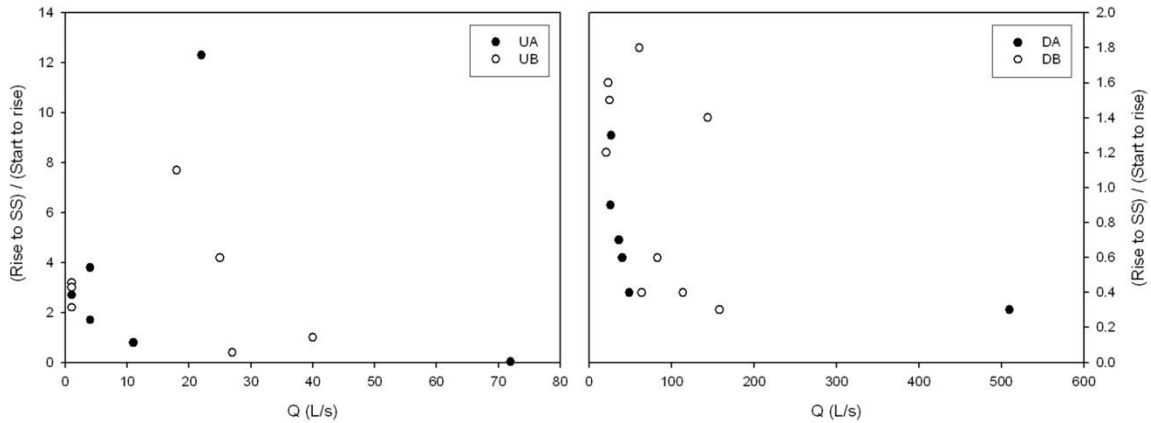


**Figure 4.15** The time between the start of the increase in EC and steady state (rise to SS) divided by the time between the start of the experiment and the start of the increase in EC (start to rise) versus discharge (Q). Higher values of (rise to SS)/(Start to rise) indicate more transient storage and dispersion. The top figure shows the relation for the upper reaches and the bottom figure shows the relation for the lower reaches.

#### 4.4.2. OTIS-P Calibration

OTIS-P could fit the observed breakthrough curves reasonably well for the first (YSI) EC measurement location in each reach, but less so at the locations further downstream (Figure 4.14, Appendix C, and Table 4.7-Table 4.10). In general, the fit between the modeled and observed data was slightly better for the experiments in the upper reaches than for the lower reaches, but the goodness of fit statistics (Table 4.7-Table 4.10) indicate that OTIS-P could represent the data relatively well for most experiments. The correlation coefficient for the relation between the modeled and observed EC data at the YSI probe location ranged between 0.909 and 0.997 for the experiments at the upper reaches (mean of 0.984), and between 0.815 and 0.999 (mean of 0.970) for the experiments at the lower reaches, excluding the July 23 experiment for reach UB, for which OTIS-P could not find a parameter set that fit the data. The Nash-Sutcliffe efficiency ranged between 0.786 and 0.991 (mean of 0.954) for the experiments at the upper reaches, again excluding the July 23 experiment in reach UB and between 0.468 and 0.997 (mean of 0.920) for the experiments in the lower reaches (excluding the July 14 experiment in reach DA), which is within the acceptable range of model fits. The

mean squared error ranged from  $4.53 \times 10^{-7}$  and  $4.63 \times 10^{-3} \text{ g}^2/\text{L}^2$  (mean of  $3.29 \times 10^{-5} \text{ g}^2/\text{L}^2$  for the experiments at the upper reaches and  $3.28 \times 10^{-4}$  and  $4.48 \times 10^{-7} \text{ g}^2/\text{L}^2$  (mean of  $4.09 \times 10^{-5} \text{ g}^2/\text{L}^2$  for the experiments at the lower reaches. July 30, August 19, and December 4 were also outliers due to poor parameter estimation by OTIS-P. November 16 is considered an outlier due to the high discharge uncertainty.

**Table 4.7 The correlation coefficient (R), Nash-Sutcliffe Efficiency (E), and Mean Squared Error (MSE) for the modeled and observed data at the YSI probe location and the range of R, E, and MSE for the ECH<sub>2</sub>O probe locations in reach UA. For Oct. 5, 2010 only the ECH<sub>2</sub>O-1 probe recorded data. The experiment on July 7, 2010 was not included due to the pump stopping at an unknown time.**

Date (2010)	UA (YSI)			UA (Range for ECH <sub>2</sub> O 1-5)		
	R	E	MSE	R	E	MSE
Jul 2	0.964	0.901	9.95E-05	0.964-0.996	0.887-0.972	3.12E-5-1.42E-4
Jul 15	0.995	0.986	7.12E-06	0.968-0.974	0.718-0.846	2.74E-4-5.83E-4
Aug 11	0.996	0.989	1.22E-05	0.969-0.996	-19.1-0.977	2.37E-5-6.40E-3
Aug 18	0.977	0.928	6.83E-05	0.965-0.974	0.880-0.903	8.71E-5-9.84E-5
Sept 22	0.991	0.955	3.83E-06	0.986-0.989	0.725-0.922	8.55E-6-2.12E-5
Oct 5	0.991	0.981	2.51E-05	0.988	0.924	4.12E-5
Oct 18	0.996	0.991	3.42E-05	0.995-0.996	0.988-0.991	3.52E-5-5.18E-5
Oct 26	0.991	0.974	4.53E-07	0.927-0.997	0.268-0.988	2.82E-7-2.16E-5
Nov 3	0.995	0.986	7.12E-06	0.989-0.996	0.938-0.975	1.36E-5-3.39E-5

**Table 4.8 The correlation coefficient (R), Nash-Sutcliffe Efficiency (E), and Mean Squared Error (MSE) for the modeled and observed data at the YSI probe location and the range of R, E, and MSE for the ECH<sub>2</sub>O probe locations in reach UB (Oct. 27 parameters are not included because they would not stabilize in OTIS-P; \*outlier).**

Date (2010)	UB (YSI)			UB (Range for ECH <sub>2</sub> O 1-5)		
	R	E	MSE	R	E	MSE
Jul 23*	0.355	-6.37	4.63E-03	0.062-0.355	-2.96- -0.936	1.09E-3-9.17E-4
Jul 26	0.909	0.786	1.46E-04	0.954-0.975	0.837-0.893	5.01E-5-8.47E-5
Aug 5	0.973	0.936	3.06E-05	0.841-0.970	0.526-0.919	3.99E-5-6.83E-4
Aug 12	0.987	0.957	3.88E-05	0.987-0.989	0.927-0.965	2.08E-5-4.69E-5
Sept 29	0.995	0.989	6.26E-07	0.884-0.905	0.397-0.661	1.97E-5-3.50E-5
Oct 13	0.987	0.969	1.12E-05	0.988-0.992	0.930-0.975	2.35E-5-9.01E-6
Nov 10	0.994	0.987	5.98E-06	0.985-0.991	0.969-0.976	1.12E-5-1.40E-5
Dec 4*	0.989	0.977	1.08E-05	0.974-0.993	0.946-0.985	6.18E-6-2.16E-5
Dec 6	0.997	0.920	5.69E-05	0.984-0.991	0.778-0.977	2.67E-5-1.20E-4

**Table 4.9 The correlation coefficient (R), Nash-Sutcliffe Efficiency (E), and Mean Squared Error (MSE) for the modeled and observed data at the YSI probe location and the range of R, E, and MSE for the ECH<sub>2</sub>O probe locations in reach DA (Sept 28 and Nov 9 parameters were not included because the model simulations would not stabilize in OTIS-P; \*outlier).**

Date (2010)	DA (YSI)			DA (Range for ECH <sub>2</sub> O 1-5)		
	R	E	MSE	R	E	MSE
Jul 14*	0.815	0.223	7.39E-05	0.862-0.910	-0.141-0.016	1.28E-4-1.53E-4
Jul 22	0.988	0.967	3.31E-06	0.695-0.790	0.402-0.509	6.63E-5-7.58E-5
Jul 30*	0.883	0.725	8.55E-05	0.904-0.914	0.601-0.676	8.46E-5-1.44E-4
Aug 6	0.994	0.988	2.75E-06	0.982-0.992	0.940-0.975	5.73E-6-1.44E-5
Aug 10	0.992	0.954	4.51E-06	0.915-0.969	0.674-0.916	7.41E-6-2.98E-5
Aug 19*	0.990	0.977	1.06E-05	0.796-0.969	0.474-0.887	2.97E-5-1.48E-4
Sept 15	0.999	0.997	4.48E-07	0.991-0.998	0.917-0.968	7.01E-6-1.12E-5
Oct 19	0.974	0.940	2.68E-05	0.936-0.983	-0.325-0.912	5.21E-5-6.77E-4
Nov 16 *	0.958	0.891	1.41E-06	0.883-0.952	-0.446-0.303	4.32E-5-7.44E-5

**Table 4.10 The correlation coefficient (R), Nash-Sutcliffe Efficiency (E), and Mean Squared Error (MSE) for the modeled and observed data at the YSI probe location and the range of R, E, and MSE for the ECH<sub>2</sub>O probe locations in reach DB.**

Date (2010)	DB (YSI)			DB (Range for ECH <sub>2</sub> O 1-5)		
	R	E	MSE	R	E	MSE
<b>Jul 20</b>	0.975	0.949	8.10E-06	0.988-0.994	0.775-0.836	4.71E-5-6.19E-5
<b>Jul 27</b>	0.996	0.989	1.48E-06	0.880-0.997	0.774-0.971	6.27E-6-5.35E-5
<b>Aug 16</b>	0.983	0.963	5.81E-06	0.885-0.912	0.660-0.725	9.97E-5-1.89E-4
<b>Sept 24</b>	0.952	0.901	4.58E-06	No ECH <sub>2</sub> O Probe data		
<b>Oct 20</b>	0.998	0.992	1.84E-06	0.614-0.996	-1.27-0.944	8.78E-5-1.01E-3
<b>Oct 29</b>	0.979	0.468	3.28E-04	0.911-0.980	0.761-0.940	6.26E-6-2.46E-5
<b>Oct 12</b>	0.990	0.971	1.20E-06	0.939-0.968	0.593-0.862	3.33E-6-2.91E-5
<b>Nov 12</b>	0.987	0.972	1.64E-05	0.939-0.971	-0.021-0.935	4.42E-5-2.37E-4
<b>Dec 3</b>	0.998	0.995	9.04E-07	0.907-0.913	0.748-0.815	1.06E-5-1.38E-5

#### **4.4.3. Optimized Parameter Values**

The following parameters were optimized in OTIS-P based on the observed concentration data at the YSI and ECH<sub>2</sub>O probe locations: storage zone exchange coefficient ( $\alpha$ , s<sup>-1</sup>), the cross-sectional area of the stream ( $A$ , m<sup>2</sup>), the cross-sectional area of the storage zone ( $A_s$ , m<sup>2</sup>), and dispersion ( $D$ , m<sup>2</sup>/s) (Table 4.11-Table 4.14). The values of the standardized storage zone to stream cross-sectional area ( $A_s/A$ ) and the storage zone residence time ( $T_{sz}=A_s/A/\alpha$ , min) were calculated using the optimized parameter values.

**Table 4.11 The optimized parameter values for reach UA. For each date the first row shows the values for the first site (YSI probe) and second row for the last site (ECH<sub>2</sub>O 5 probe). The experiment on July 7, 2010 was not included due to the pump stopping at an unknown time. See Figure 3.7 and Table 3.6 for the probe locations.**

Date (2010)	Q (L/s)	A (m <sup>2</sup> )	$\alpha$ (s <sup>-1</sup> )	A <sub>s</sub> (m <sup>2</sup> )	A <sub>s</sub> /A	T <sub>sz</sub> (min)	D (m <sup>2</sup> /s)	Dal
UA								
Jul 2	1.7	0.08	3.6e-3	0.029	0.38	107	0.01	3.20e-3
		0.05	4.9e-4	0.024	0.48	975	0.01	
Jul 15	1.3	0.05	4.9e-4	0.024	0.48	976	0.01	4.87e-4
		0.01	1.9e-2	0.028	2.38	123	0.01	
Aug 11	1.2	0.05	4.9e-4	0.024	0.48	976	0.01	5.04e-4
No ECH <sub>2</sub> O data available								
Aug 18	1.2	0.05	4.9e-4	0.024	0.48	976	0.01	5.21e-4
		0.01	1.9e-2	0.028	2.97	125	0.01	
Sept 22	10.9	0.19	8.5e-4	0.013	0.07	82	0.01	6.89e-5
		0.05	1.05e3	0.038	0.72	7e-4	0.43	
Oct 5	4.2	0.11	9.1e-4	0.010	0.09	100	0.01	1.35e-4
		0.09	6.0e-5	0.019	0.20	3170	0.01	
Oct 18	4.4	0.08	8.7e-4	0.013	0.16	184	0.01	1.49e-4
		0.06	2.0e-5	0.127	2.03	86300	0.16	
Oct 26	72.3	0.94	1.5e-3	0.946	1.01	670	0.01	1.03e-3
		0.22	3.5e-4	0.007	0.03	93	0.10	
Nov 3	21.9	0.32	4.8e-4	0.022	0.07	142	0.01	3.11e-5
		0.03	2.1e-2	0.026	1.00	49	1.52	

**Table 4.12 The optimized parameter values for reach UB (Oct. 27 parameters are not included because they would not stabilize in OTIS-P; \*outlier). For each date the first row shows the values for the first site (YSI probe) and second row for the last site (ECH<sub>2</sub>O 4/5 probe). See Figure 3.7 and Table 3.6 for the probe locations.**

Date (2010)	Q (L/s)	A (m <sup>2</sup> )	$\alpha$ (s <sup>-1</sup> )	A <sub>s</sub> (m <sup>2</sup> )	A <sub>s</sub> /A	T <sub>sz</sub> (min)	D (m <sup>2</sup> /s)	Dal
UB								
Jul 23*	1.5	0.16	5.7e-2	4.090	25.1	442	0.01	7.75
		1606	1.6e3	0.021	2e-5	9e-9	2.9e4	
Jul 26	1.7	0.03	2.5e-4	0.033	1.28	1920	0.01	7.59e-4
		0.03	4.2e-3	0.004	0.12	29	0.01	
Aug 5	3.6	0.02	2.8e-2	0.108	0.48	17	0.01	1.08e-1
		0.08	2.5e-4	0.041	0.54	2140	0.01	
Aug 12	1.5	0.03	1.6e-3	0.054	1.68	1030	0.01	3.06e-3
		0.01	3.9e-2	0.039	6.42	166	0.01	
Sept 29	40.4	0.33	1.2e-2	0.213	0.64	54	0.01	3.23e-3
		0.20	3.2e-3	0.434	2.17	674	0.01	
Oct 13	17.9	0.13	3.7e-3	0.039	0.30	79	0.08	4.28e-4
		0.05	8.3e-2	0.255	5.13	62	0.01	
Nov 10	27.2	0.31	2.4	0.484	1.54	0.7	0.01	2.11
		0.07	2.0e-1	0.200	2.86	14	0.01	
Dec 4*	28.9	0.18	1.1e-3	0.0001	0.001	0.5	0.06	6.96e-6
		0.08	1.2e-1	0.522	6.51	53	0.01	
Dec 6	24.7	0.07	1.9e-1	0.064	0.85	5	0.01	2.45e-2
		0.15	3.4e-2	0.092	0.61	18	0.01	

**Table 4.13 The optimized parameter values for reach DA (\*estimate from a different probe location due to YSI probe malfunction; Sept. 28 and Nov. 9 parameters were not included because the model simulations would not stabilize in OTIS-P; \*\*outlier). For each date the first row shows the values for the first site (YSI probe) and second row for the 6th site (ECH<sub>2</sub>O 5 probe). Dal for Nov. 16 is not given due to high uncertainty in the discharge calculation. See Figure 3.7 and Table 3.7 for the probe locations.**

Date (2010)	Q (L/s)	A (m <sup>2</sup> )	$\alpha$ (s <sup>-1</sup> )	A <sub>s</sub> (m <sup>2</sup> )	A <sub>s</sub> /A	T <sub>sz</sub> (min)	D (m <sup>2</sup> /s)	Dal
DA								
Jul 14**	46.0	0.27	1.4e-2	0.077	0.28	21	0.01	1.28e-3
		0.30	7.8e-3	0.278	0.93	119	0.01	
Jul 22	35.9	0.27	1.3e-3	0.190	0.72	567	0.01	3.61e-4
		0.27	1.6e-2	0.028	0.10	6	0.01	
Jul 30**	22.7	0.98	3.0	4.5e4	4.6e4	15100	1.4e+4	3.18e5
		0.09	4.2e-4	0.027	0.30	714	0.01	
Aug 6	21.6	0.20	6.0e-4	0.159	0.79	1310	0.05	2.38e-4
		0.16	7.0e-3	0.031	0.20	28	0.01	
Aug 10*	25.7	0.19	7.0e-3	0.031	0.17	24	0.01	5.00e-4
		0.20	2.9e-3	0.479	2.40	838	0.01	
Aug 19**	18.7	0.15	1.3e-9	26.90	183.0	1.41e11	0.03	9.85e-8
		0.30	2.9e-3	0.479	1.60	559	0.01	
Sept 15	39.8	0.29	2.8e-4	0.193	0.68	2430	0.05	7.27e-5
		0.50	2.9e-3	0.479	0.96	335	0.01	
Oct 19	49.5	0.31	2.1e-3	0.041	0.13	63	0.03	1.02e-4
		0.50	2.9e-3	0.479	0.96	335	0.01	
Nov 16**	510.0	3.42	7.8e1	0.0003	7.3e-5	9e-7	0.03	
		1.50	7.8e-3	0.278	0.19	24	0.01	

**Table 4.14 The optimized parameter values for reach DB. For each date the first row shows the values for the first site (YSI probe) and second row for the 6<sup>th</sup> site (ECH<sub>2</sub>O 5 probe). See Figure 3.7 and Table 3.7 for the probe locations.**

Date (2010)	Q (L/s)	A (m <sup>2</sup> )	$\alpha$ (s <sup>-1</sup> )	A <sub>s</sub> (m <sup>2</sup> )	A <sub>s</sub> /A	T <sub>sz</sub> (min)	D (m <sup>2</sup> /s)	Dal
DB								
Jul 20	22.6	0.45	4.6e1	0.003	0.01	2e-4	0.01	1.27
		0.41	4.5e1	0.003	0.01	1e-4	0.01	
Jul 27	21.0	0.43	4.5e1	0.049	0.12	3e-3	0.01	6.70
		0.002	4.2e1	0.288	136.0	3	4.60	
Aug 16	25.0	0.31	4.6e1	0.293	0.94	2e-2	0.01	30.00
		0.28	4.6e1	3.5e-5	1.2e-4	3e-6	0.01	
Sept 24	143.6	0.40	4.6e1	0.001	0.004	8e-5	0.03	0.15
No ECH <sub>2</sub> O data available								
Oct 12	114.3	2.02	7.9e-4	0.790	0.39	493	0.01	3.13e-4
		0.40	1.2e-4	0.176	0.44	3640	0.01	
Oct 20	63.6	0.72	4.0e-2	0.245	0.34	9	0.01	8.91e-3
		0.49	1.7e-3	0.020	0.04	24	0.01	
Oct 29	61.5	0.50	2.9e-3	0.479	0.96	335	0.01	1.24e-3
		0.48	2.0e-3	0.490	1.02	515	0.01	
Nov 12	83.1	1.90	2.3e-2	0.515	0.27	12	0.01	8.36e-3
		0.30	1.2e-4	0.176	0.59	4860	0.01	
Dec 3	157.6	2.75	3.6e-4	1.830	0.67	186	0.01	2.35e-3
		1.00	1.1e-7	4.670	4.69	4e7	0.01	

#### **4.4.4. Storage Zone Exchange Coefficient**

The optimized storage zone exchange coefficient ( $\alpha$ ) for the location of the YSI probe ranged between  $2.5 \times 10^{-4}$  and  $2.4 \text{ s}^{-1}$  for the upstream reaches and between  $2.8 \times 10^{-4}$  and  $4.6 \times 10^1 \text{ s}^{-1}$  for the downstream reaches (Table 4.11-Table 4.14; Figure 4.16). The highest optimized value for  $\alpha$  in previous studies was  $0.605 \text{ s}^{-1}$  (Legrand-Marcq and Laudelout, 1985), and the lowest  $0.691 \times 10^{-5} \text{ s}^{-1}$  (Ryan et al., 2010). In this

study, the highest value of  $\alpha$  was  $4.6 \cdot 10^1 \text{ s}^{-1}$  and the lowest  $2.5 \cdot 10^{-4} \text{ s}^{-1}$ , which is higher than the values of  $\alpha$  in previous studies, but within the optimized studies at the low end of the range of values. The range in the optimized value of  $\alpha$  was much wider for the experiments in the downstream reaches compared to those in the upstream reaches but for a comparable discharge, the optimized value of  $\alpha$  was similar for both sites.

This result is not in agreement with the findings of Wondzell (2011), who found that hyporheic exchange was slower in low gradient streams compared to high gradient streams. The difference in the range in the optimized values of  $\alpha$  for the downstream and upstream reaches could be due to differences in bed material. The lower reaches were characterized by finer bed material (e.g.  $D_{50}$  of 4.6-7.5 mm at the upper reaches compared to  $D_{50}$  values of 3.9-4.0 mm at the lower reaches, and  $D_{84}$  of 10.0-27.0 mm at the upper reaches compared to 7.0-7.6 mm at the lower reaches) and a thicker streambed than the upper reaches. It could also be due to more variable discharge in the lower reaches.

No significant trend was found between the optimized value of  $\alpha$  and discharge for the lower reaches ( $r_s = -0.35$  and  $p = 0.21$  for the data from reaches DA and DB combined) but a significant trend was found for the upper reaches ( $r_s = 0.52$  and  $p = 0.03$  for the data from reaches UA and UB combined).

The lack of a clear relation between discharge and the storage zone exchange coefficient for the lower reaches agrees with the findings of Legrand-Marcq and Laudelout (1985), Patschke (1999), Wondzell (2006), Scordo and Moore (2009). Patschke (1999) and Scordo and Moore (2009) conducted their studies in Malcolm Knapp Research Forest in Maple Ridge located ~17 km east of Hoy Creek in the same biogeoclimatic zone; Wondzell (2006) conducted his studies in steep mountain streams in Oregon. The significant relation between  $\alpha$  and discharge for the steeper upper reaches of Hoy Creek agrees with the findings of D'Angelo et al. (1993), Harvey et al. (1996), Hart et al. (1999), Duineveld (2008), Argerich et al. (2011), Fabian et al. (2011).

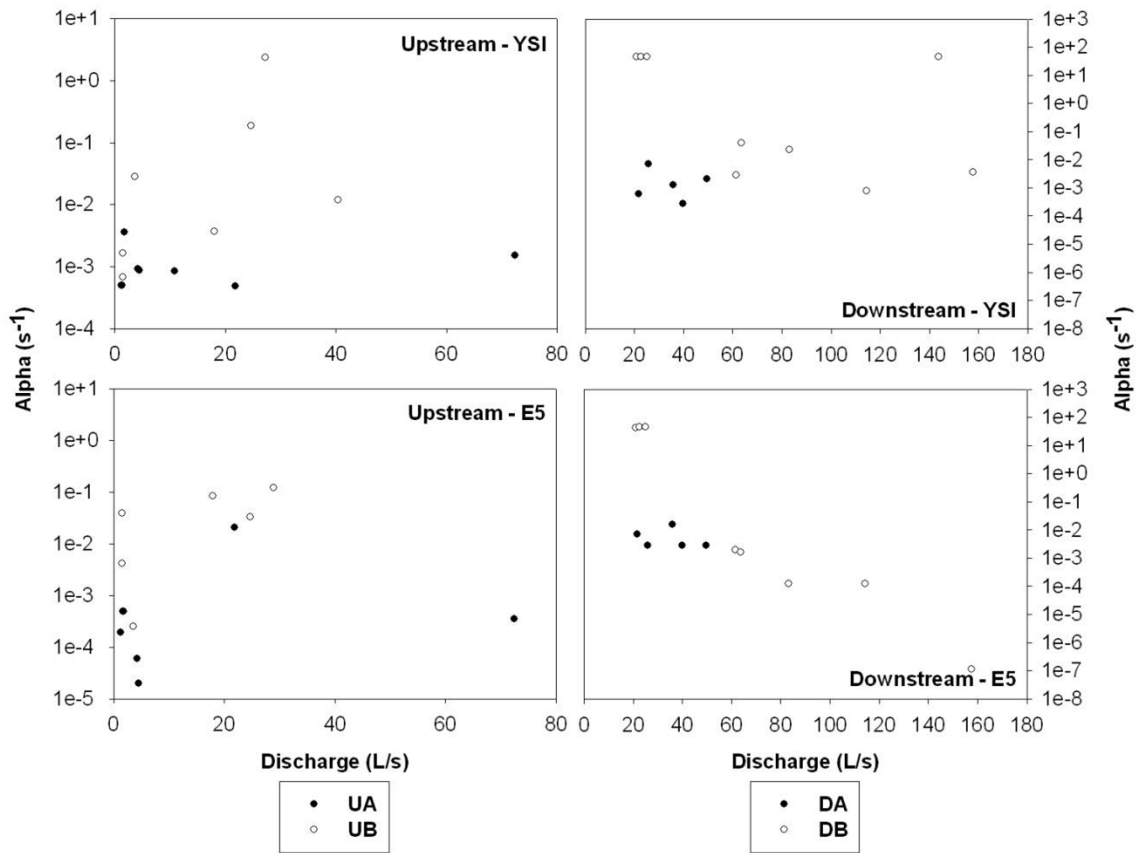


**Figure 4.16** Relation between the optimized storage zone exchange coefficient ( $\alpha$ ) and discharge for the four reaches. Left column shows the data for the upper reaches (UA: filled symbols and UB: open symbols), the right columns show the data for the lower reaches (DA: filled symbols, DB: open symbols). The upper row shows the data for the YSI probe location, the bottom row for the ECH<sub>2</sub>O 5 probe location.

#### 4.4.5. Cross-sectional Area of the Storage Zone and Stream

The optimized stream cross sectional area ( $A$ ) varied between 0.02 and 0.94 m<sup>2</sup> at the upstream reaches and between 0.19 and 3.42 m<sup>2</sup> at the lower reaches, and generally increased with discharge. The OTIS-P optimized stream cross-sectional areas were compared to estimated stream cross-sectional areas based on the water level, stream width, and streambed topography (Figure 4.17 and Figure 4.18). The optimized values from OTIS-P do not agree well with the estimated values and appear to underestimate the stream cross-sectional area for reach UA, whereas there is no

relation between the optimized cross-sectional area and discharge for the UB reach. This indicates that OTIS-P could not determine the correct values for the cross-sectional area of the stream.

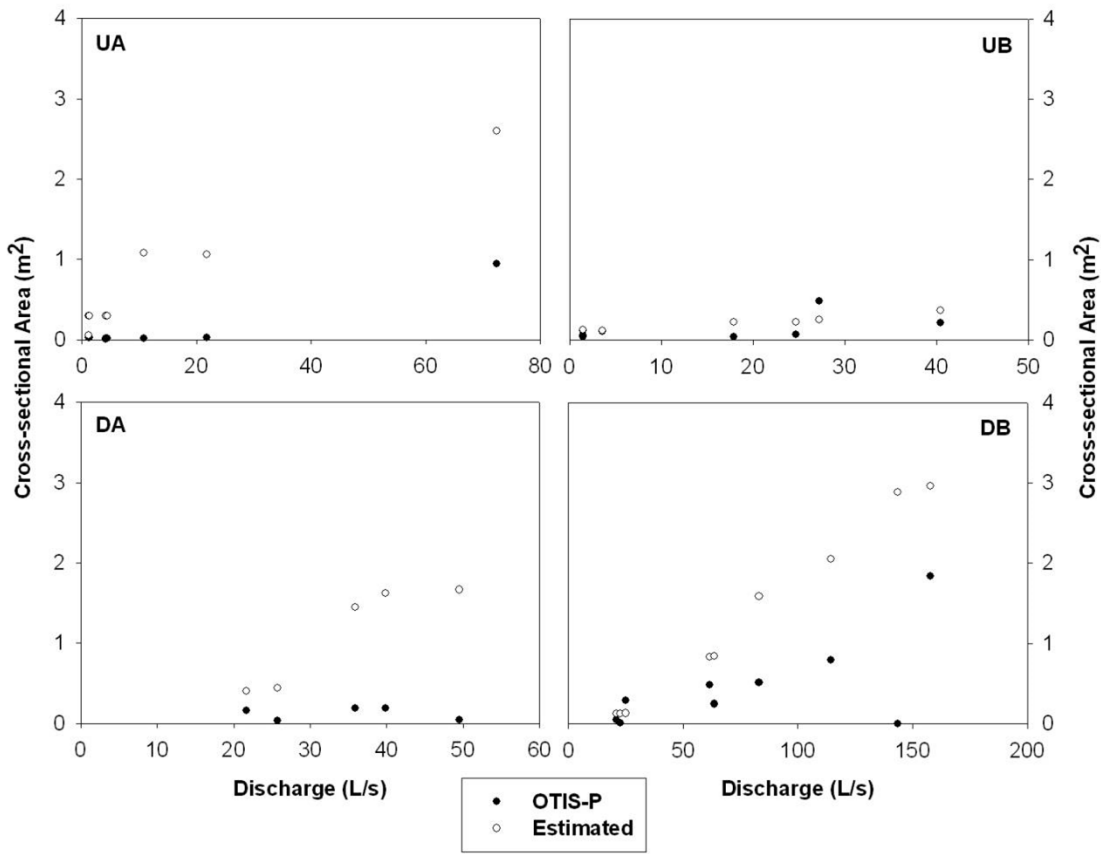


**Figure 4.17** The optimized (filled symbols) and estimated cross-sectional area (open symbols) of the stream (A) for the upper reaches (top row) and lower reaches (bottom row) as a function of discharge.

The optimized cross-sectional area of the hyporheic zone ( $A_s$ ) was generally smaller for the upstream reaches compared to the downstream reaches, which fits well with the narrower stream and the shallower depth of streambed material for the upper reaches. The optimized cross-sectional area of the storage zone ranged between 0.01 and 0.946 m<sup>2</sup> for the upstream reaches and between 0.001 and 1.8 m<sup>2</sup> for the downstream reaches. The largest cross-sectional area of the hyporheic zone in previous

studies was  $2.20 \text{ m}^2$  (Karwan and Saiers, 2009), and the smallest was  $5 \cdot 10^{-4} \text{ m}^2$  (D'Angelo et al., 1993). The optimized cross-sectional areas of the hyporheic zone in this study are both larger and smaller than those in previous studies.

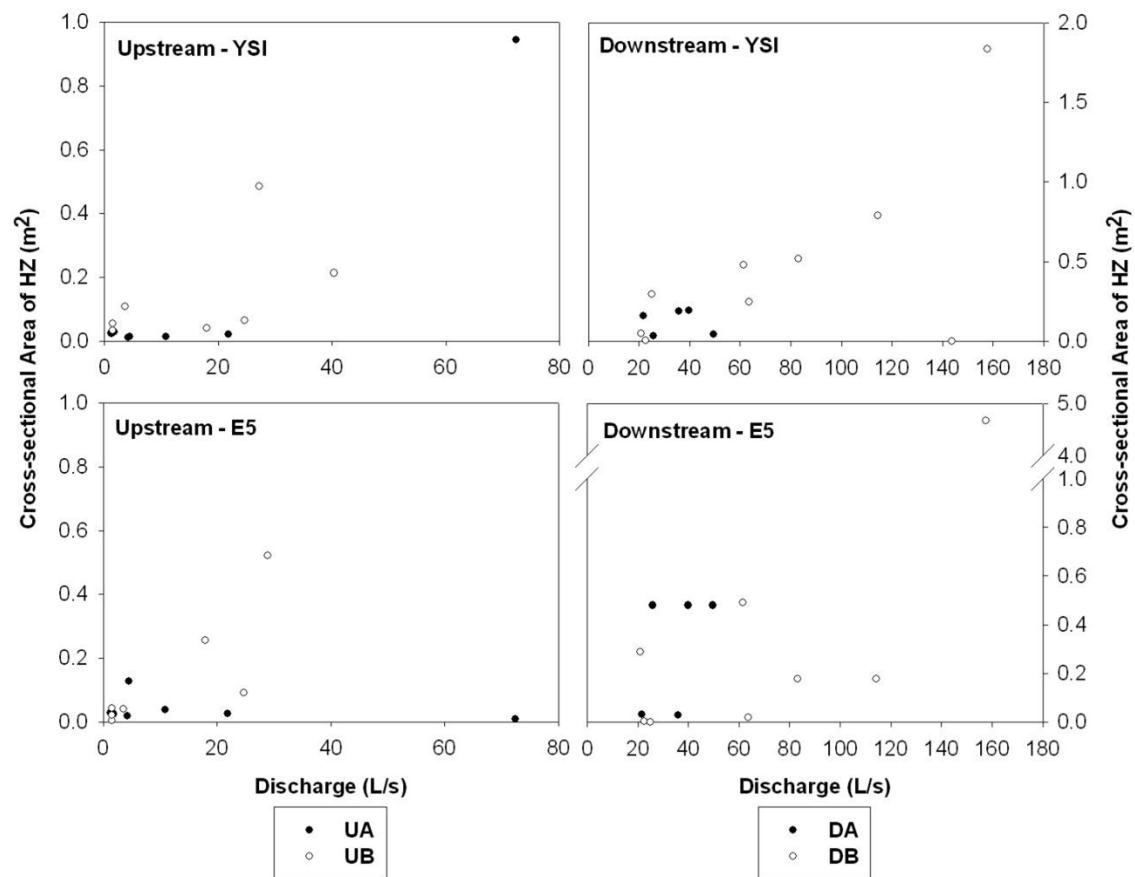


**Figure 4.18** The optimized storage zone cross-sectional area ( $A_s$ ) for the upper reaches (left column) and lower reaches (right column) as a function of discharge for the YSI probe location (upper row) and  $\text{ECH}_2\text{O-5}$  location (lower row) (UA and DA: filled symbols and UB and DB: open symbols).

The cross-sectional area of the storage zone increased with discharge for the downstream reaches; it remained fairly constant with increasing discharge at low flows, but increased with discharge at higher flows. The Spearman rank correlation coefficient for the relation between discharge and the cross-sectional area of the hyporheic zone

was 0.45 ( $p=0.09$ ) for the downstream reaches and 0.29 ( $p=0.26$ ) for the upstream reaches, indicating no significant relation for either the downstream or upstream reaches. However, the Pearson product moment correlation coefficient was 0.68 for the downstream reaches and 0.82 for the upstream reaches ( $p$ -values of  $5 \cdot 10^{-3}$  and  $5.39 \cdot 10^{-5}$  respectively), suggesting a significant linear relation between discharge and the cross-sectional area of the hyporheic zone for both reaches and that the relation is influenced by an outlier/outliers. Patschke (1999) and Scordo and Moore (2009), who conducted their study in the Malcolm Knapp Research Forest in Maple Ridge showed that the cross-sectional area of the hyporheic zone increased with increasing discharge. However, results from Duineveld (2008) in the same research forest, but a smaller stream, showed that the area decreased with increasing discharge. This indicates that trends may be different for different streams. Additionally, this does not confirm the explanations provided by D'Angelo et al. (1993) about why the hyporheic zone decreases with increased discharge (see section 2.3.1).

The ratio of the cross-sectional area of the hyporheic zone and the cross-sectional area of the stream ( $A_h/A$ ) standardizes the storage zone cross-sectional area, allowing for a comparison between the reaches. The range in  $A_h/A$  was fairly similar for the upstream and downstream reaches (Figure 4.19). There was no apparent relation between  $A_h/A$  and discharge for any of the reaches (Spearman's rank correlation coefficient was -0.05 for the downstream reaches and -0.10 at the upstream reaches;  $p$ -values were 0.8 and 0.7, respectively).

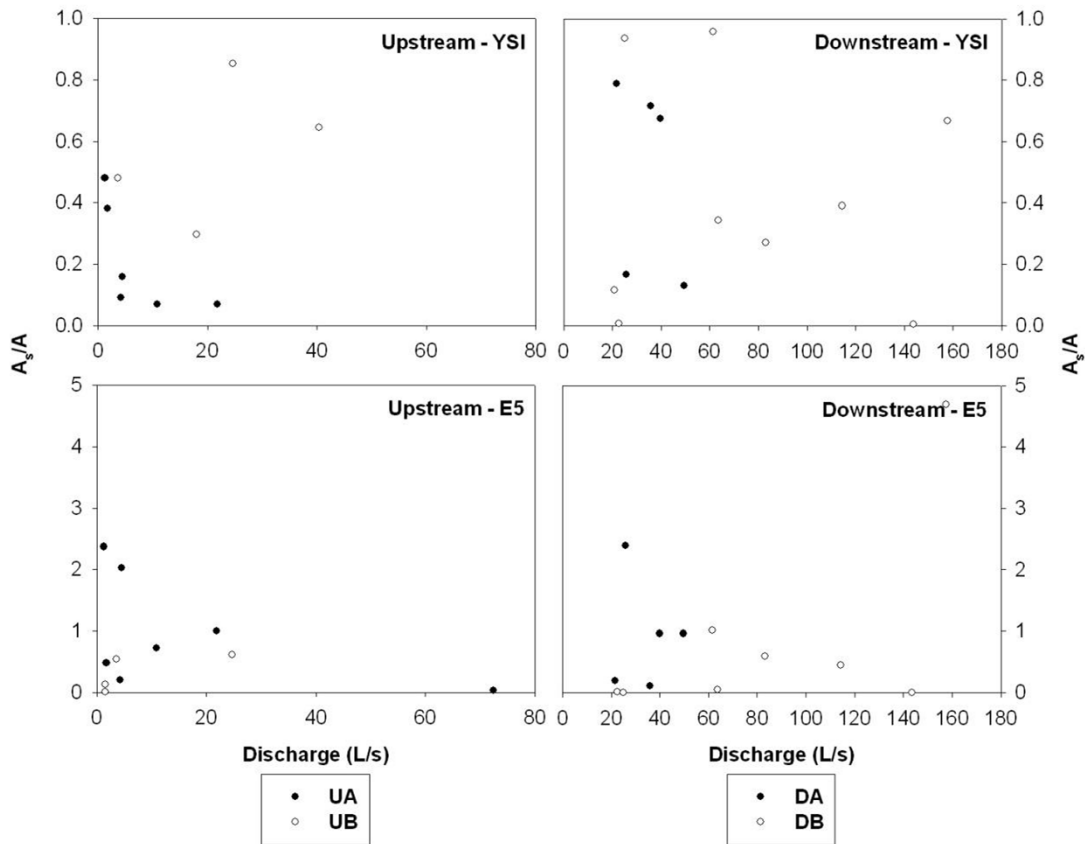


**Figure 4.19** The ratio of the cross-sectional area of the hyporheic zone and the cross-sectional area of the stream ( $A_s/A$ ) as a function of discharge for the upstream reaches (left column) and downstream reaches (right column); YSI probe location (top row) and ECH<sub>2</sub>O-5 probe location (bottom row) (UA and DA: filled symbols and UB and DB: open symbols).

#### 4.4.6. Dispersion

The OTIS-P estimated dispersion rates ranged between 0.010 and 0.077 m<sup>2</sup>/s for the upper reaches (average: 0.017 m<sup>2</sup>/s), and between 0.010 and 0.050 m<sup>2</sup>/s for the lower reaches (average: 0.019 m<sup>2</sup>/s). The majority of the dispersion rates were 0.010 m<sup>2</sup>/s (Table 4.11-Table 4.14). There was no trend in the OTIS-P optimized dispersion rates with discharge.

#### 4.4.7. Storage Zone Residence Time

For a similar discharge, the storage zone residence time ( $T_{sz}$ ) was similar for all reaches. The range of  $T_{sz}$  was larger for the downstream reaches ( $9 \times 10^{-7}$  to 2430 minutes) compared to the upstream reaches (0.7-1920 minutes), perhaps because of the wider range in discharge or the different streambed properties, (i.e. larger streambed width and smaller average grain size in the lower reaches compared to the upper reaches). For the upper reaches the storage zone residence time decreased with increasing discharge ( $r_s = -0.68$ ,  $p = 0.003$ ), while there was no trend for the downstream reaches ( $r_s = 0.04$ , with a  $p = 0.90$ ; Figure 4.20).

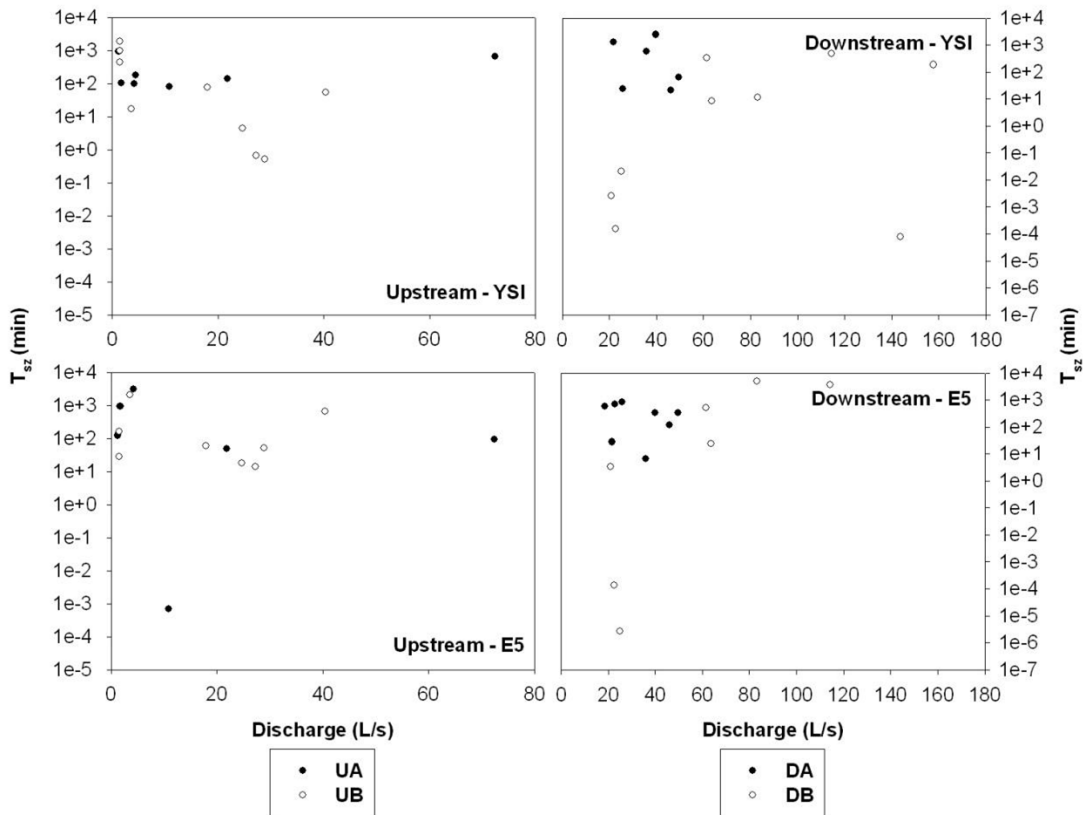


**Figure 4.20** Storage zone residence time as a function of discharge for the upper reaches (left column) and lower reaches (right column; UA and DA: filled symbols and UB and DB: open symbols). YSI probe location (top row) and ECH<sub>2</sub>O 5 probe location (bottom row).

#### 4.4.8. Hydraulic Retention Factor and Average Traveling Distance of a Water Molecule

The hydraulic retention factor ( $R_h=A_s/Q$ ) varied between 1.0 and 37.4 s/m at the upper reaches, and between  $4.9 \cdot 10^{-4}$  and 11.7 s/m at the lower reaches (Figure 4.21). There was a significant relation between  $R_h$  and discharge for the upper reaches ( $r_s=-0.59$ ,  $p=0.015$ ) but not for the lower reaches ( $r_s=0.11$ ,  $p=0.71$ ).

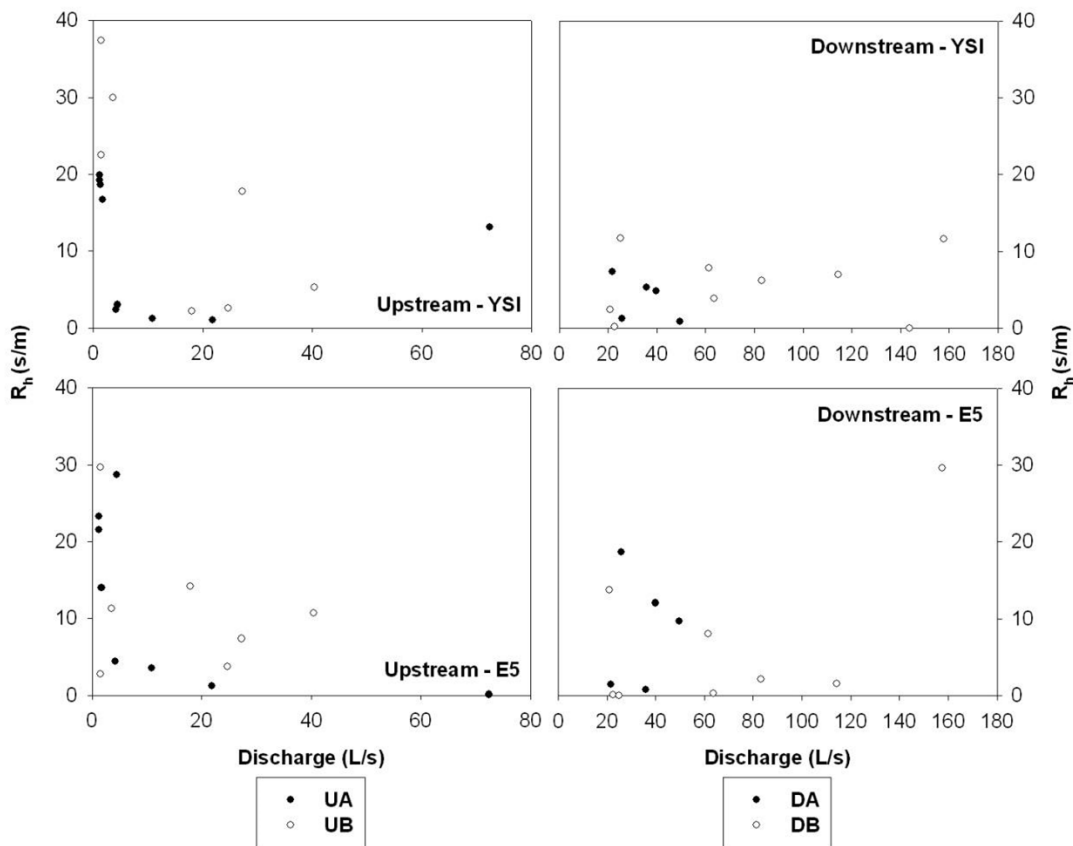


**Figure 4.21 Hydraulic retention factor ( $R_h$ ) as a function of discharge at the YSI probe location (UA and DA: filled symbols and UB and DB: open symbols).**

The average distance a water molecule travels in the stream before entering transient storage ( $L_s=Q/A/\alpha$ ) varied between 0.6 and 144 m at the upper reaches, and between  $1.1 \cdot 10^{-3}$  and 503 m at the lower reaches (Figure 4.22). There was no significant

relation between  $L_s$  and discharge for any of the reaches (upper reaches:  $r_s=-0.20$ ,  $p=0.45$ ; lower reaches:  $r_s=0.09$ ,  $p=0.75$ ).

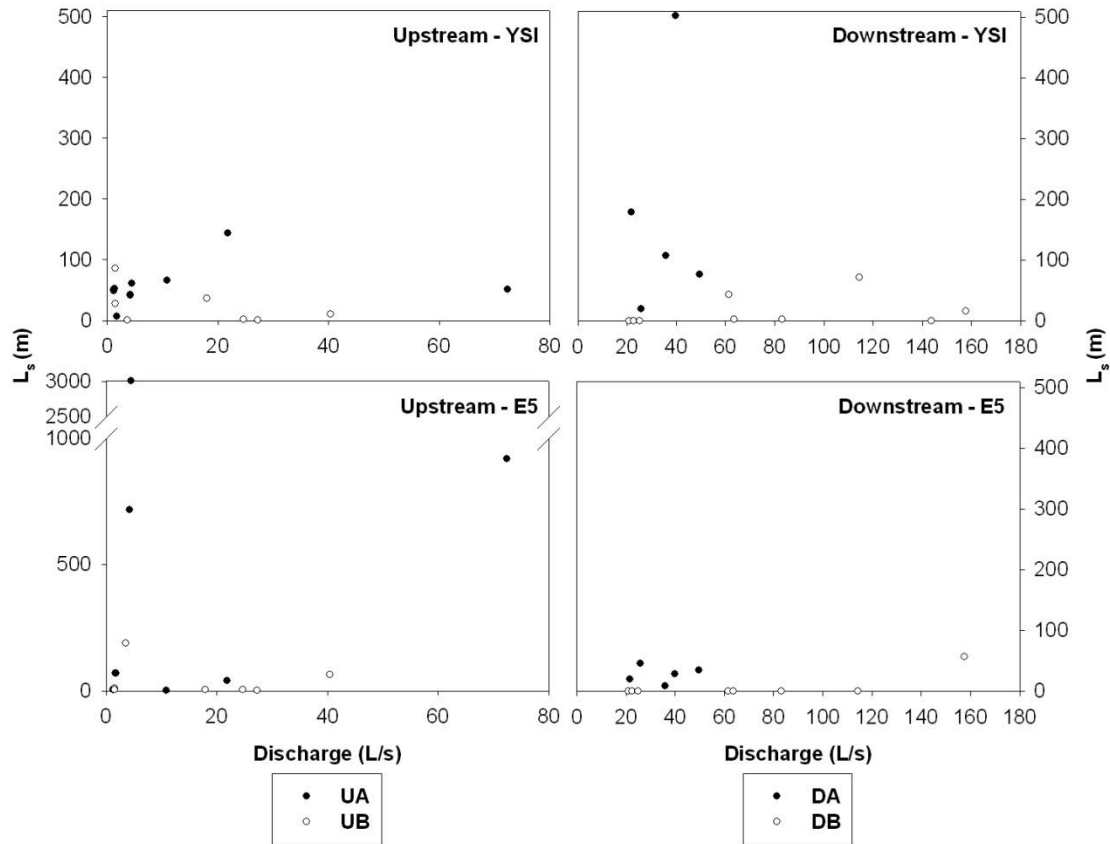


**Figure 4.22** The average distance a water molecule travels in the stream before entering transient storage ( $L_s$ ) as a function of discharge at the YSI probe location (top row) and ECH<sub>2</sub>O-5 location (bottom row) (UA and DA: filled symbols and UB and DB: open symbols).

## 4.5. Reliability of the Optimized Parameters

The Damköhler number ( $Da$ ), (equation 10), can be used to assess the uncertainty in the optimized parameter values (Wagner and Harvey, 1997). The  $Da$  values for the optimized parameters from OTIS-P (Figure 4.23; Table 4.11-Table 4.14) suggest a high level of uncertainty. Wagner and Harvey (1997) suggested that the reach



## 4.6. Model Validation

Validation of OTIS was done by using the optimized parameter values from OTIS-P to model the concentrations at the DEC probes and in the piezometers in OTIS. The modeled results were compared with the observed data to determine how well OTIS predicted the stream concentrations at the DEC locations and the concentrations in the streambed. An example of the modeled and observed data is shown in Figure 4.24; all other validation graphs can be found in Appendix D. A summary of the goodness of fit parameters is given in Table 4.15 and Table 4.16.

The OTIS validation results indicate poor model performance for the DEC sites and the streambed. The R, E, and MSE values indicate a much poorer fit for the DEC and piezometer sites compared to the sites that were used in the calibration (Table 4.15 and Table 4.16). For some (15-19 out of 35) piezometers, concentration data indicated a lack of interaction (or very slow interaction) with the stream as streambed EC did not change significantly during the tracer test. In only a few piezometers and during a few tests, there was a delay in the increase in concentrations during the experiment. For reach DA, there were 3 piezometers that indicated that the tracer moved through the bed (P9, P8, and P3). P9 is located in the bank along a straight stretch of the reach; P8 is located within the stream at the edge of a bar along a meander bend; P3 is located in a bar at the end of a meander bend. In reach DB, there were two piezometers that showed that the tracer moved through the bed (P6 and P1) during higher flow events. These piezometers are both located in a bar along a meander bend.

**Table 4.15 Correlation coefficient (R), Nash-Sutcliffe Efficiency (E), and Mean Squared Error (MSE) of the range of modeled versus observed DEC and piezometer data for reaches UA and UB (\*outlier).**

UA				UB			
Date (2010)	R	E	MSE	Date (2010)	R	E	MSE
Jul 2	0.989- 0.998	-17.5- 0.472	3.32E-3-5.39E- 3	Jul 23*	0.481	-2.48- 1.08	4.75E-3- 1.63E-2
Jul 15	0.694- 0.944	-22.5- 6.621	6.66E-3-1.20E- 2	Jul 26	0.503- 0.962	-9.24- 0.685	2.34E-4- 3.19E-3
Aug 18	0.593- 0.995	-4.64- 0.821	1.26E-4-1.26E- 4	Aug 5	-0.289- 0.120	-9.17- 6.01	1.73E-3- 6.84E-3
Sept 22	0.817- 0.907	-0.221- 0.262	6.62E-5-4.26E- 3	Aug 12	-0.922- 0.981	-27.4- 0.111	1.60E-3- 9.91E-3
Oct 5	-0.122- 0.860	-0.674- 0.688	9.54E-5-4.26E- 3	Sept 29	0.652- 0.995	-1.22- 0.978	1.16E-6- 2.32E-4
Oct 18	0.801	-1.04	9.01E-4	Oct 13	0.971- 0.981	0.147- 0.184	1.83E-4- 6.83E-4
Oct 26	0.887- 0.973	-2.95- 0.821	3.98E-6-3.60E- 4	Dec 4*	0.952- 0.963	0.672- 0.894	2.10E-4- 5.25E-5
Nov 3	0.930- 0.963	0.010- 0.619	4.53E-4-1.42E- 3				

**Table 4.16 Correlation coefficient (R), Nash-Sutcliffe Efficiency (E), and Mean Squared Error (MSE) for the modeled and observed DEC and piezometer data for reaches DA and DB (\*outlier).**

DA				DB			
Date (2010)	R	E	MSE	Date (2010)	R	E	MSE
Jul 30*	0.945	0.884	1.08E-5	Jul 20	0.941- 0.989	-1.25- 0.198	2.91E-4-1.22E- 3
Aug 6	0.601	-5.53	3.08E-4	Jul 27	0.733- 0.988	-3.27- 0.042	1.95E-3-1.98E- 4
Aug 10	0.888	0.325	3.69E-5	Aug 16	0.927- 0.941	-0.249- 0.357	4.89E-3-2.97E- 4
Aug 19*	0.273	-0.217	1.45E-4	Oct 12	0.975- 0.440	-20.9- 0.933	9.08E-4-3.24E- 6
				Oct 20	0.984- 0.995	-3.07- 1.703	5.10E-3-4.33E- 3
				Oct 29	0.844- 0.973	-4.05- 0.035	3.37E-3-2.76E- 4

For reach UA, eight piezometers (P9-P13, P8b, P6, and P5) indicated tracer movement through the bed and two piezometers (P4 and P3) showed that the tracer moved through the bed during high flow events. P11-P13 are located at the top of a step created by woody debris. P10 is located at the bottom of the step in a pool. P9 and P8b are located within a straight stretch of the reach, while P6 and P5 are located in a meander bend (Figure 3.7).

In reach UB, three of the piezometers (P8, P7, and P6) indicated tracer movement during higher flow events and two of the piezometers (P6 and P4) indicated that the tracer moved through the bed during some high flow events. P8, P6, and P7 are located within riffles that have a shallow gravel bed. The tracer movement through the streambed in these reaches supports previous research that hyporheic flow occurs through step-pool systems and meander bends. For all reaches, it appears that higher discharge can cause an increase in the exchange of water in the stream with water in the hyporheic zone, but only in certain locations and at certain times.

For the majority of the experiments, OTIS predicted incorrect concentrations in the hyporheic zone. For reach UA, the observed data for piezometers P5, P6, P9, P10, P11, P12, and P13 were fit reasonably well for only 3-4 experiments. For reach UB, only the streambed concentrations at P4, P7, and P8 were predicted reasonably well. Piezometer P8 was the only piezometer in reach DA for which OTIS could predict the streambed concentrations reasonably well ( $R^2 > 0.9$ ). For reach DB, concentrations were not predicted well for any of the piezometers. In most cases, the model fit the data just after the initiation of the tracer injection and after the end of the injection reasonably well but did not accurately reflect the rise in concentration very well. The observed streambed concentration data showed in most cases a slow exchange, if any at all, while the modeled data predicted a fast exchange between the main channel and the storage zones. Thus, it appears that the model overestimated the rate of hyporheic exchange.

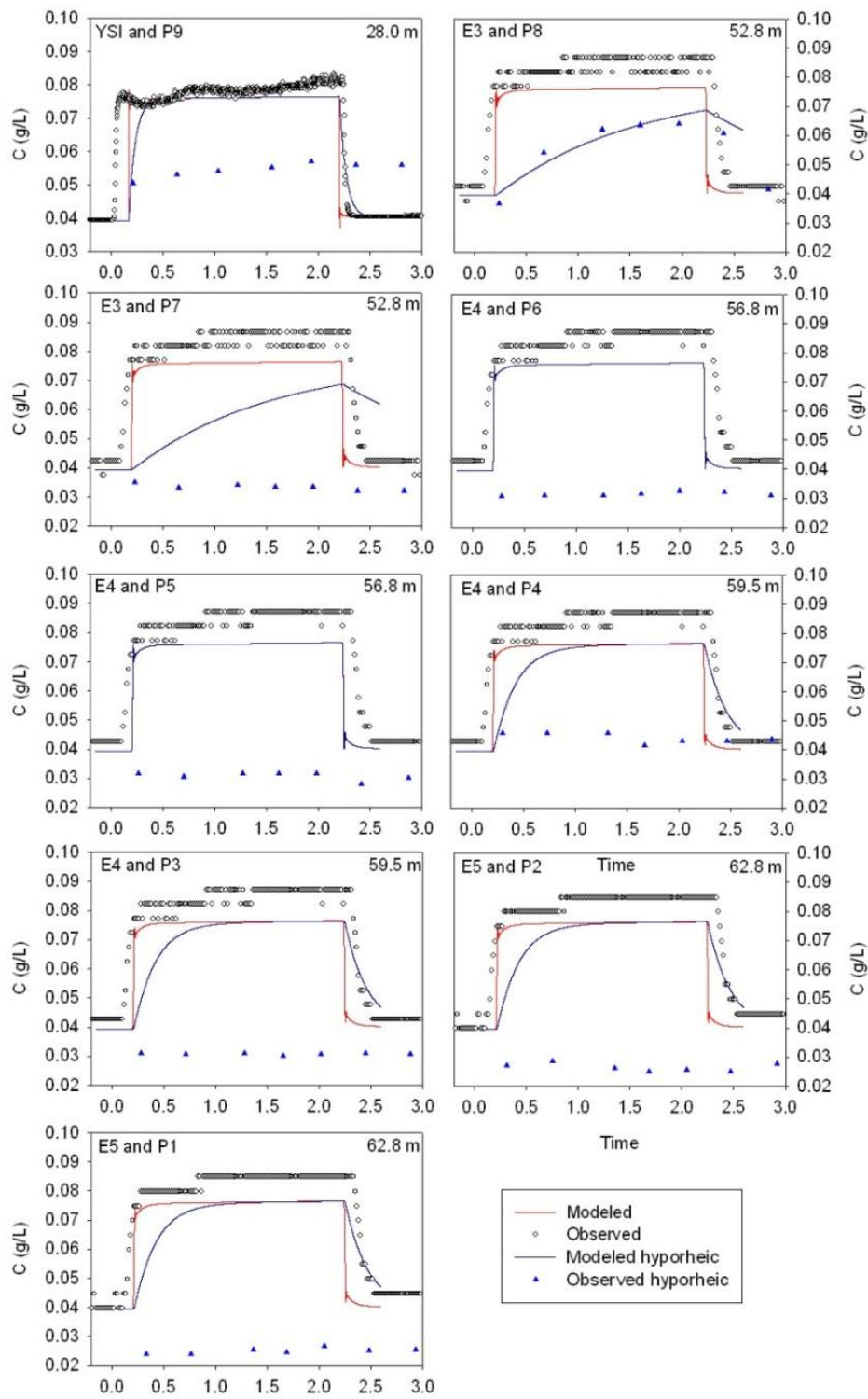


**Figure 4.24** Validation graphs for the tracer experiment on July 30, 2010 in reach DA. For the locations of the probes, see Figure 3.7. All other validation graphs are given in Appendix D.

## 4.7. Issues with OTIS

Parameter estimation was difficult, largely due to parameter equifinality. When running OTIS-P to optimize the  $A$ ,  $A_s$ ,  $D$ , and  $\alpha$  parameter values, different values would yield similar modeled concentrations and similar goodness of fit values. Ward et al. (2012) stated that equifinality can be the result of simplification of heterogeneity within the subsurface of the stream in a model.

Validation of the model using the DEC probe and piezometer data indicated that the optimized parameter values did not fit the data well and that therefore the estimated parameter values were not correct or that the model structure was wrong. In some cases, (i.e. at 16-20 piezometers) the modeled data fit the observed data, but in other cases they did not. The model therefore does not consistently and accurately estimate the correct parameters.

Szeftel et al. (2011) identified a number of issues that can arise when using transient storage models, which include (a) incorrect estimates of transient storage parameters due to uncertainties in analyzing breakthrough curves, (b) incorrect identification of spatial patterns of inflow and outflow, and (c) poorly defined boundary conditions. They state that model parameterization is highly dependent on the structure of the model. Additionally, OTIS does not incorporate streambed topography, which is a very important aspect to consider when predicting storage zone exchange parameters (Stonedahl et al., 2012).

Drummond et al. (2010) highlighted that the majority of stream tracer experiments have truncated breakthrough curves. OTIS uses an exponential residence time distribution for residence time distribution, which was found to be useful only for stream reaches with limited storage, and therefore limited transient storage exchange. Process-based models that incorporate hyporheic exchange as a fractal process seem to be more appropriate for modeling hyporheic exchange because they characterize the hyporheic residence time distribution as a power law. Additionally, OTIS tends to underestimate hyporheic solute retention, mean travel time, dispersion, and solute storage time as a result of truncation of the tracer experiments and overestimation of reaction rates (Drummond et al., 2010). Ward et al. (2012) also noted that if subsurface

characteristics are simplified, or idealized, hyporheic exchange and residence time distributions can be overestimated or underestimated.

## 5. Conclusion and Recommendations

### 5.1. Conclusion

The objective of this study was to determine how discharge, streambed topography, and channel planform influence hyporheic exchange in a coastal suburban stream in British Columbia. Tracer experiments were carried out in four reaches of Hoy Creek, and the tracer breakthrough curves were modelled in OTIS to determine the channel and storage zone cross-sectional areas, dispersion coefficient, and storage zone exchange coefficient. However, validation of OTIS using the EC measurements in the stream and streambed indicated poor model performance; the modeled data did not fit the observed data well. This highlights that one must take caution when using OTIS to estimate stream and storage zone parameters.

The optimized value of the rate of hyporheic exchange ( $\alpha$ ) was similar for the high and low gradient reaches during comparable discharge conditions, which disagrees with hypothesis one. The range of the rate of hyporheic exchange, however, was larger for the lower gradient reaches due to a wider range of discharge conditions compared to the upper higher gradient reaches. The optimized values of the storage zone exchange coefficient were larger than expected based on previous studies. The hyporheic zone was generally smaller for the upstream reaches compared to the downstream reaches due to the upstream reaches being narrower and having shallower streambed material depth. This agrees with hypothesis one.

Increasing discharge led to an increase in the rate of hyporheic exchange at the steeper upper reaches but there was no relation between discharge and the hyporheic exchange coefficient for the lower reaches. The tracer breakthrough curves for the measurements in the piezometers indicated more exchange when discharge increased as the tracer was observed in more piezometers during high flow conditions. There was no relation between discharge and the extent of the hyporheic zone for any of the

reaches. These results disagree with hypothesis two as hyporheic exchange was expected to decrease with increasing discharge and the extent of the hyporheic zone was expected to increase with increasing discharge. Increasing discharge led to decreased upwelling in reaches UA and DB and increased downwelling in the meander bend in reach DA. However upwelling conditions cannot directly be related to hyporheic exchange and may also indicate groundwater inflow.

The vertical hydraulic gradient measurements and streambed tracer movement showed that hyporheic flow occurred through meander bends, step-pool systems, and riffles, which is consistent with the results from previous research. Spatial variation in hyporheic exchange, however, was considerable within each reach and between the reaches. Streambed topography and channel planform increased hyporheic exchange; there was increased upwelling in reaches UA and DB, and increased downwelling in reach DA through meander bends, as well as increased upwelling and downwelling through step-pool systems. These results support the first part of hypothesis three. However, it remains difficult to determine whether or not this upwelling is hyporheic exchange or also in part groundwater upwelling. The second part of hypothesis three could not be answered because there was limited lateral inflow in any of the studied reaches (relative to the maximum uncertainty in the calculated discharge).

## **5.2. Recommendations**

If this study were to be repeated in the future, experiments in a wider range of streamflow conditions, specifically in the transition between the low and high flow conditions in this study are recommended. The difficulty with this is that this urban stream is very responsive: part of the urban runoff drains directly into the stream instead of naturally making its way slowly through forests soils. Experiments conducted during rainfall events will allow for the determination of these lateral inflows. Using EC probes with a higher accuracy or a different tracer (e.g. a fluorescent tracer) would allow for more accurate streamflow measurements and thus a better estimate of (lateral) inflows. Independent discharge measurement (e.g. using a current meter during high flow conditions) would have provided more confidence in the calculated discharge values as well. The tracer dilution method cannot detect a decrease in discharge due to streambed

losses and can result in an apparent increase in discharge along a study reach when independent area-velocity discharge measurements remain fairly constant as a result of double counting of the solute load that returns to the stream downstream (Bencala et al., 2011). Other methods, such as electrical resistivity measurements during the tracer experiments could be useful for “imaging” the subsurface solute distribution in either 2- or 3-dimensions (Bencala et al., 2011). Additionally, future research should involve analysis of the causes of the spatial and temporal variability of vertical hydraulic gradients and discharge instead of focussing only on the patterns in the vertical hydraulic gradients within the reach.

More spatially discrete measurements of tracer concentrations, combined with increased sampling of the streambed are also recommended. A more expansive piezometer network installed at a sufficient depth, or at multiple depths within the stream and in the bank in each reach, is also recommended. The data gathered from the limited number of piezometers in this study provided useful insights into the vertical hydraulic gradients and tracer movement through the streambed, but they could have been more useful for determining the relation between hyporheic exchange and streambed topography and channel planform if there were more spatially representative data.

The calculated Damköhler numbers ( $Da$ ), and other parameters calculated from these experiments should be used to determine the appropriate reach length to obtain more reliable parameter estimates in OTIS. However, the results of this study suggest that due to parameter equifinality, calibration of OTIS based on streamflow breakthrough curves alone may not provide reliable estimates of hyporheic exchange and that additional data (e.g. streambed concentrations) are needed. While OTIS is frequently used to analyze stream tracer tests and estimate hyporheic exchange parameters, the results of this study suggest that more validation is necessary and that previous calibration results without independent validation should be treated with caution.

Depending on the type of hyporheic exchange and the movement of tracer within the stream, another transient storage model should be considered, preferably one that incorporates both types of transient storage (dead zones within the stream and the hyporheic zone) separately. Several other models have been used to analyse transient storage, including an exponential residence time distribution, power law residence time

distribution, log normal residence time distribution, and the two storage zone version of the transient storage model (Bencala et al., 2011). These models all yield reasonable modeled versus observed fits, but each has a different interpretation of how transient storage influences solute transport in the stream and the subsurface. OTIS was used in this study because it is the simplest and most commonly used model. To reduce problems with truncation of breakthrough curves, Drummond et al. (2012) recommended measuring concentrations in the stream for a day before and after the experiments, because background variability of the tracer can contribute to sensitivity truncation (when there is little difference between the tracer and background concentrations). This may require the use of another tracer that can be measured more accurately (e.g. rhodamine or other fluorescent dye tracers) and a more sophisticated application system to maintain a constant concentration during varying discharge conditions.

More studies on urban stream characteristics are also recommended. Since urban streams are very responsive to precipitation events, it would be interesting to survey the streambed and surrounding area before and after the tracer studies to characterize whether and by how much the streambed changed. Preliminary studies may also highlight how urban streams may differ from forested streams and may indicate unexpected or illegal discharge to the stream (e.g. the unexpected increases in streamflow during dry days).

Additionally, it would be interesting to incorporate an ecological aspect to the study because Hoy Creek is a salmon-bearing stream that is sensitive to the anthropogenic activities within its immediate setting. This could be achieved by examining how improving hyporheic exchange (e.g. by incorporating more step-pools and meander bends into the stream) would affect and benefit salmon, as salmon prefer streams with hyporheic exchange for spawning (Dauble and Geist, 2000; Woessner, 2000; Hanrahan, 2008; Soulsby et al., 2009; Tonina and Buffington, 2009). Additionally, mapping salmon spawning areas may provide a map of potential locations of hyporheic exchange, which could then be studied in more detail.

## References

- Anderson, M.G. and Burt, T.P. 1978. "The role of topography in controlling throughflow generation". *Earth Surface Processes*. 3:331-344.
- Argerich, Alba, Marti, Eugenia, Sabater, Francesc, Haggerty, Roy, and Ribot, Miquel. 2011. "Influence of transient storage on stream nutrient uptake based on substrata manipulation". *Aquatic Sciences*. 73: 365-376.
- Baxter, Colden V., Hauer, Richard F, and Woessner, William W. 2003. "Measuring Groundwater-Stream Water Exchange: New Techniques for Installing Minipiezometers and Estimating Hydraulic Conductivity". *Transactions of the American Fisheries Society*. 132: 493-502.
- Baxter, Colden V. and Hauer, Richard F. 2000. "Geomorphology, hyporheic exchange, and selection of spawning habitat by bull trout (*Salvelinus confluentus*)". *Canadian Journal of Fisheries and Aquatic Sciences*. 57:1470-1481.
- Bencala, K. 2000. "Hyporheic zone hydrological processes". *Hydrological Processes*. 14: 2797-2798.
- Bencala, Kenneth E., Gooseff, Michael N., and Kimball, Briant A. 2011. "Rethinking hyporheic flow and transient storage to advance understanding of stream catchment connections". *Water Resources Research*. 47: W00H03.
- Beven, Keith. 2006. *Streamflow Generation Processes*. Wallingford: International Association of Hydrological Sciences.
- Boano, Fulvio, Revelli, Roberto, and Ridolfi, Luca. 2010. "Effect of streamflow stochasticity on bedform-driven hyporheic exchange". *Advances in Water Resources*. 33: 1367-1374.
- Boulton, Andrew, Findlay, Stuart, Marmonier, Pierre, Stanley, Emily, and Valett, H. Maurice. 1998. "The Functional Significance of the Hyporheic Zone in Streams and Rivers". *Annual Review of Ecology, Evolution, and Systematics*. 29: 59-81.
- Cardenas, M. 2008. "The effect of river bend morphology on flow and timescales of surface water-groundwater exchange across pointbars". *Journal of Hydrology*. 362: 134-141.
- CH2M Hill. 2012. *Scott Creek Integrated Watershed Management Plan*. Prepared for the City of Coquiltam.
- D'Angelo, D. J., Webster, J. R., Gregory, S. V., and Meyer, J. L. 1993. "Transient storage in Appalachian and Cascade mountain streams as related to hydraulic characteristics". *Journal of the North American Benthological Society*. 12 (3): 223-235.

- Dauble, Dennis and Geist, David. 2000. "Comparison of mainstem spawning habitats for two populations of fall Chinook salmon in the Columbia River Basin". *Regulated Rivers: Research and Management*. 16:345-361.
- Dahm, Clifford N., Valett, H. Maurice, Baxter, Colden V., and Woessner, William W. 2007. "Hyporheic Zones". *Methods in Stream Ecology*. Edited by Hauer, F. Richard and Lamberti, Gary A. Second Edition. Academic Press, Burlington.
- Drummond, J.D., Covino, T.P., Aubeneau, A.F., Leong, D., Patil, S., Schumer, R., and Packman, A.I. 2012. "Effects of solute breakthrough curve tail truncation on residence time estimates: A synthesis of solute tracer injection studies". *Journal of Geophysical Research*. 117: G00N08.
- Duineveld, Marieke. 2008. *Transient storage in a headwater stream in Coastal British Columbia*. Report. Simon Fraser University, Burnaby, B.C.
- Environment Canada. 2010. "Canadian Climate Normals or Averages 1971-2000". Retrieved May 8, 2010. <[http://www.climate.weatheroffice.gc.ca/climate\\_normals/index\\_e.html](http://www.climate.weatheroffice.gc.ca/climate_normals/index_e.html)>
- Fabian, Mark W., Endreny, Theodore A., Bottacin-Busolin, Andrea, and Lautz, Laura. 2011. "Seasonal variation in cascade-driven hyporheic exchange, northern Honduras". *Hydrological Processes*. 25: 1630-1646.
- Findlay, Stuart. 1995. "Importance of surface-subsurface exchange in stream ecosystems: The hyporheic zone". *Limnology and Oceanography*. 40 (1): 159-164.
- Fraser River Action Plan. 1999. "Lower Fraser Valley Streams Strategic Review". Retrieved September 28, 2011. <<http://www.dfo-mpo.gc.ca/Library/240006.pdf>>
- Gandy, C. J., Smith, J. W. N. and Jarvis, A. P. 2007. "Attenuation of mining-derived pollutants in the hyporheic zone: A review." *Science of the Total Environment*. 373: 435-446.
- Geological Survey of Canada. 1997. "GeoMap Vancouver". Retrieved May 18, 2010. [http://gsc.nrcan.gc.ca/urbgeo/geomapvan/index\\_e.php](http://gsc.nrcan.gc.ca/urbgeo/geomapvan/index_e.php)
- Geological Survey of Canada. 1980. "Map 1484A Surficial Geology, New Westminster West of Sixth Meridian".
- Google Earth 6.2. 2012. *Hoy Creek, 49°18'01.14"N, 122°47'15.45"W, elevation 146m*. Digital Globe data layer. Available through: <http://www.google.com/earth/index.html> [Accessed June 8, 2012]
- Gooseff, Michael N., Hall, Robert O. Jr, and Tank, Jennifer L. 2007. "Relating Transient Storage to Channel Complexity in Streams of Varying Land Use in Jackson Hole, Wyoming". *Water Resources Research*. 43: 1-10.
- Hancock, Peter J. 2002. "Human Impacts on the Stream-Groundwater Exchange Zone." *Environmental Management*. 29: 763-781.
- Hanrahan, Timothy. 2008. "Effects of river discharge on hyporheic exchange flows in salmon spawning areas of a large gravel-bed river". *Hydrological Processes*. 22:127-141.

- Hart, D. R., Mulholland, P. J., Mazolf, E. R., DeAngelis, D.L., and Hendricks, S.P. 1999. "Relationship between hydraulic parameters in a small stream under varying flow and seasonal conditions". *Hydrological Processes*. 13: 1497-1510.
- Harvey, Judson W. and Bencala, Kenneth E. 1993. "The Effect of Streambed Topography on the Surface-Subsurface Water Exchange in Mountain Catchments". *Water Resources Research*. 29:89-98.
- Harvey, Judson W, Wagner, Brian J. and Bencala, Kenneth E. 1996. "Evaluating the reliability of the stream tracer approach to characterize stream-subsurface water exchange." *Water Resources Research*. 32: 2441-2451.
- Houghton, Jahlie. 2008. "The Story of the Coquitlam River Watershed Past, Present and Future". *JR Environmental*. October 24, 2008.
- Huff, D.D., O'Neill, R.V., Emanuel, W.R., Elwood, J.W., and Newbold, J.D. 1982. "Flow variability and hillslope hydrology". *Earth Surface Processes and Landforms*. 7: 91-94.
- Jones, Krista L., Poole, Geoffrey C., Woessner, William W., Vitale, Matt V., Boer, Brian R., O'Daniel, Scott J., Thomas, Steven A., and Geffen, Brook A. 2008. "Geomorphology, hydrology, and aquatic vegetation drive seasonal hyporheic flow patterns across a gravel-dominated floodplain." *Hydrological Processes*. 22: 2105-2113.
- Karwan, D.L. and Saiers, J.E. 2009. "Influences of seasonal flow regime on the fate and transport of fine particles and dissolved solute in a New England stream". *Water Resources Research*. 45: W11423.
- Kasahara, Tamao and Hill, Alan. 2007. "Instream restoration: Its effects on lateral stream-subsurface water exchange in urban and agricultural streams in southern Ontario". *River Research and Applications*. 23: 801-814.
- Kasahara, Tamao and Hill, Alan. 2008. "Modeling the effects of lowland stream restoration projects on stream-subsurface water exchange". *Ecological Engineering*. 32: 310-319.
- Kasahara, Tamao and Wondzell, Steven. 2003. "Geomorphic controls on hyporheic exchange flow in mountain streams". *Water Resources Research*. 39:1005.
- Krause, S., Hannah, D. M., Fleckenstein, C. M., Heppell, D. Kaeser, Pickup, R., Pinay, G, Robertson, A. L., and Wood, P. J. 2011a. "Inter-disciplinary perspectives on processes in the hyporheic zone". *Ecohydrology*. 4: 481-499.
- Krause, Stefan, Hannah, David M., and Blume, Theresa. 2011b. "Interstitial pore-water temperature dynamics across a pool-riffle-pool sequence". *Ecohydrology*. 4: 549-563.
- Lautz, Laura, Kranes, Nathan, and Siegel, Donald. 2010. "Heat tracing of heterogeneous hyporheic exchange adjacent to in-stream geomorphic features". *Hydrological Processes*. 24: 3074-3086.
- Legrand-Marcq, Catherine and Laudelout, H. 1985. "Longitudinal Dispersion in a Forest Stream". *Journal of Hydrology*. 78: 317-324.
- Maier, Herb S., and Howard, Ken W.F. 2011. "Influence of Oscillating Flow on Hyporheic Zone Development". *Ground Water*. 49 (6): 830-844.

- Marmonier, Pierre, Vervier, Philippe, Gibert, Janine, and Dole-Olivier, Marie-José. 1993. "Biodiversity in Ground Waters". *TREE*. 8 (11): 392-395.
- Martinez-Fernandez, J and Ceballos, A. 2005. "Mean soil moisture estimation using temporal stability analysis". *Journal of Hydrology*. 312: 28-38.
- Moore, Dan. 2004. "Introduction to Salt Dilution Gauging for Streamflow Measurement Part 2: Constant-rate Injection". *Streamline Watershed Management Bulletin*. 8 (1): 11-15.
- Morrice, John, Valett, Maurice, Dahm, Clifford, and Campana, Michael. 1997. "Alluvial Characteristics, Groundwater-surface Water Exchange and Hydrological Retention in Headwater Streams". *Hydrological Processes*. 11:253-267.
- Munz, Matthias, Krause, Stefan, Tecklenburg, Christina, and Binley, Andrew. 2011. "Reducing monitoring gaps at the aquifer-river interface by modelling groundwater-surface water exchange flow patterns". *Hydrological Processes*. 25:3547-3562.
- Nagpal, N. K., Levy, D. A., and MacDonald, D. D. 2003. "Water Quality: Ambient Water Quality Guidelines for Chloride". Canadian Water Quality Guidelines. Retrieved March 17, 2010. <<http://www.env.gov.bc.ca/wat/wq/BCguidelines/chloride/chloride.html>>.
- Patschke, S. N. 1999. *Hyporheic exchange in a forested headwater stream*. Master's thesis, Simon Fraser University, Burnaby, B.C.
- Paul, Michael J. and Meyer, Judy L. 2001. "Streams in the Urban Landscape". *Annual Review of Ecology and Systematics*. 32: 333-365.
- Pojar, J., Kinka, K., and Demarchi, D.A. (1991). "Chapter 6: Coastal Western Hemlock Zone". *Ecosystems of British Columbia*. Edited by Meidinger, D.V. and Pojar, J. Research Branch, Ministry of Forests. Victoria, B.C.
- Runkel, R.L. 1998. One-dimensional transport with inflow and storage (OTIS): a solute transport model for streams and rivers. U.S. Geological Survey. Water-Resources Investigations Report 98-4018. Denver, Colorado.
- Ryan, Robert, Welty, Claire, and Larson, Philip. 2010. "Variation in surface water-groundwater exchange with land use in an urban stream". *Journal of Hydrology*. 392: 1-11.
- Sawyer, Audrey H., Cardenas, M. Bayani, and Buttles, Jim. 2012. "Hyporheic temperature dynamics and heat exchange near channel-spanning logs". *Water Resources Research*. 48: W01529.
- Schmid, Bernhard H., Innocenti, Ilaria, and Sanfilippo, Umberto. 2010. "Characterizing solute transport with transient storage across a range of flow rates: The evidence of repeated tracer experiments in Austrian and Italian streams". *Advances in Water Resources*. 33: 1340-1346.
- Scordo, Elisa B. And Moore, Dan R. 2009. "Transient storage processes in a steep headwater stream". *Hydrological Processes*. 23:2671-2685.
- Soulsby, C., Malcolm, I. A., Tetzlaff, D., and Youngson, A. F. 2009. "Seasonal and inter-annual variability in hyporheic water quality revealed by continuous monitoring in a salmon spawning stream". *River Research and Applications*.

- Stofleth, John, Shields, Douglas Jr, and Fox, Garey. 2008. "Hyporheic and total transient storage in small, sand-bed streams". *Hydrological Processes*. 22: 1885-1894.
- Stonedahl, Susa H., Harvey, Judson W., Detty, Joel, Aubeneau, Antoine, and Packman, Aaron I. 2012. "Physical controls and predictability of stream hyporheic flow evaluated with a multiscale model". *Water Resources Research*. 48: W10513.
- Storey, Richard G., Howard, Kenneth W. F., and Williams, Dudley D. 2003. "Factors controlling riffle-scale hyporheic exchange flows and their seasonal changes in a gaining stream: A three-dimensional groundwater flow model". *Water Resources Research*. 39 (2): ARTN 1034.
- Szeftel, Pascal, Moore, R.D., and Weiler, Markus. 2011. "Influence of distributed flow losses and gains on the estimation of transient storage parameters from stream tracer experiments". *Journal of Hydrology*. 396: 277-291.
- Takahashi, Goichiro, Gomi, Takashi, and Sasa, Kaichiro. 2008. "Hyporheic flow as a potential geomorphic agent in the evolution of channel morphology in a gravel-bed river". *Catena*. 73: 239-248.
- Thackston, E.L. and Schnelle, K.B. 1970. "Predicting effects of dead zones on stream mixing". *Journal of the Sanitary Engineering Division*. 96: 319-331.
- Tonina, Daniele and Buffington, John M. 2007. "Hyporheic exchange in gravel bed rivers with pool-riffle morphology: Laboratory experiments and three-dimensional modelling". *Water Resources Research*. 43: W01421 1-16.
- Tonina, Daniele and Buffington, John M. 2009. "Hyporheic Exchange in Mountain Rivers I: Mechanics and Environmental Effects." *Geography Compass*. 3: 1063-1086.
- U.S. Geological Survey. 2000. "Using OTIS to Model Solute Transport in Streams and Rivers ". Fact Sheet FS-138-99.
- Wagner, Brian J., and Harvey, Judson W. 1997. "Experimental design for estimating parameters of rate-limited mass transfer: Analysis of stream tracer studies". *Water Resources Research*. 33 (7): 1731-1741.
- Ward, Adam S., Gooseff, Michael N., and Singha, Kamini. 2012. "How Does Subsurface Characterization Affect Simulations of Hyporheic Exchange?" *Ground Water*. 51 (1): 14-28.
- Webster, Jackson R. and Valett, H. Maurice. 2007. "Solute Dynamics". *Methods in Stream Ecology*. Edited by Hauer, F. Richard and Lamberti, Gary A. Second Edition. Academic Press, Burlington.
- Wheeler, Andrew P., Angermeier, Paul L., and Rosenberger, Amanda E. 2005. "Impacts of New Highways and Subsequent Landscape Urbanization on Stream Habitat and Biota". *Reviews in Fisheries Science*. 13:141-164.
- White, David. 1993. "Perspectives on Defining and Delineating Hyporheic Zones". *Journal of the North American Benthological Society*. 12 (1): 61-69.
- Woessner, William. 2000. "Stream and Fluvial Plain Ground Water Interactions: Rescaling Hydrogeological Thought". *Ground Water*. 38 (3): 423-429.

- Wondzell, Steven M. 2011. "The role of the hyporheic zone across stream networks". *Hydrological Processes*. 25: 3525-3532.
- Wondzell, Steven M. 2006. "Effect of Morphology and Discharge on Hyporheic Exchange Flows in Two Small Streams in the Cascade Mountains of Oregon, USA." *Hydrological Processes*. 20: 267-287.
- Wondzell, Steven M and Swanson, Frederik J. 1996. "Seasonal and Storm Dynamics of the Hyporheic Zone of a 4<sup>th</sup>-order Mountain Stream. I: Hydrologic Processes." *The North American Benthological Society*. 15: 3-19.
- Wroblicky, G.J., Campana, M.E., Valett, H.M., Dahm, Clifford N. 1998. "Seasonal variation in surface-subsurface water exchange and lateral hyporheic area of two stream-aquifer systems". *Water Resources Research*. 34(3): 317-328.
- Zimmerman, S. 2011. "Temperature as a Tracer for Studying Water Movement in the Hyporheic Zone". Bachelorarbeit thesis. University of Bonn, Bonn, Germany.

## **Appendices**

## Appendix A: Temporal Stability Calculation

The essence of temporal stability analysis is finding the relative difference for each measurement location (Martínez-Fernandez and Ceballos, 2005). The relative difference,  $\delta_{ij}$ , is calculated by **equation A1**:

$$\delta_{ij} = \frac{\Delta_{ij}}{\bar{S}_j} \quad [A1]$$

where  $\Delta_{ij}$  is the difference between steady state EC at location  $i$  and time  $j$ , and  $\bar{S}_j$  is the average steady state EC at time  $j$ :

$$\Delta_{ij} = S_{ij} - \bar{S}_j \quad [A2]$$

and

$$\bar{S}_j = \frac{1}{N} \sum_{i=1}^N S_{ij} \quad [A3]$$

where  $S_{ij}$  is the measured steady state EC at location  $i$  and time  $j$ ,  $\bar{S}_j$  is the average steady state EC at time  $j$ , and  $N$  is the number of measurement locations. Finally, the mean relative difference of each measurement location can be calculated with **equation A4**:

$$\bar{\delta}_i = \frac{1}{m} \sum_{j=1}^m \delta_{ij} \quad [A4]$$

where  $m$  is the number of tracer experiments. Locations that are the most stable are characterized by the lowest standard deviation of the mean relative difference,  $\sigma(\bar{\delta}_i)$  (Martínez-Fernandez and Ceballos, 2005). Locations with a low mean relative difference represent the average condition in the stream well.

## Appendix B: Steady State EC Maps

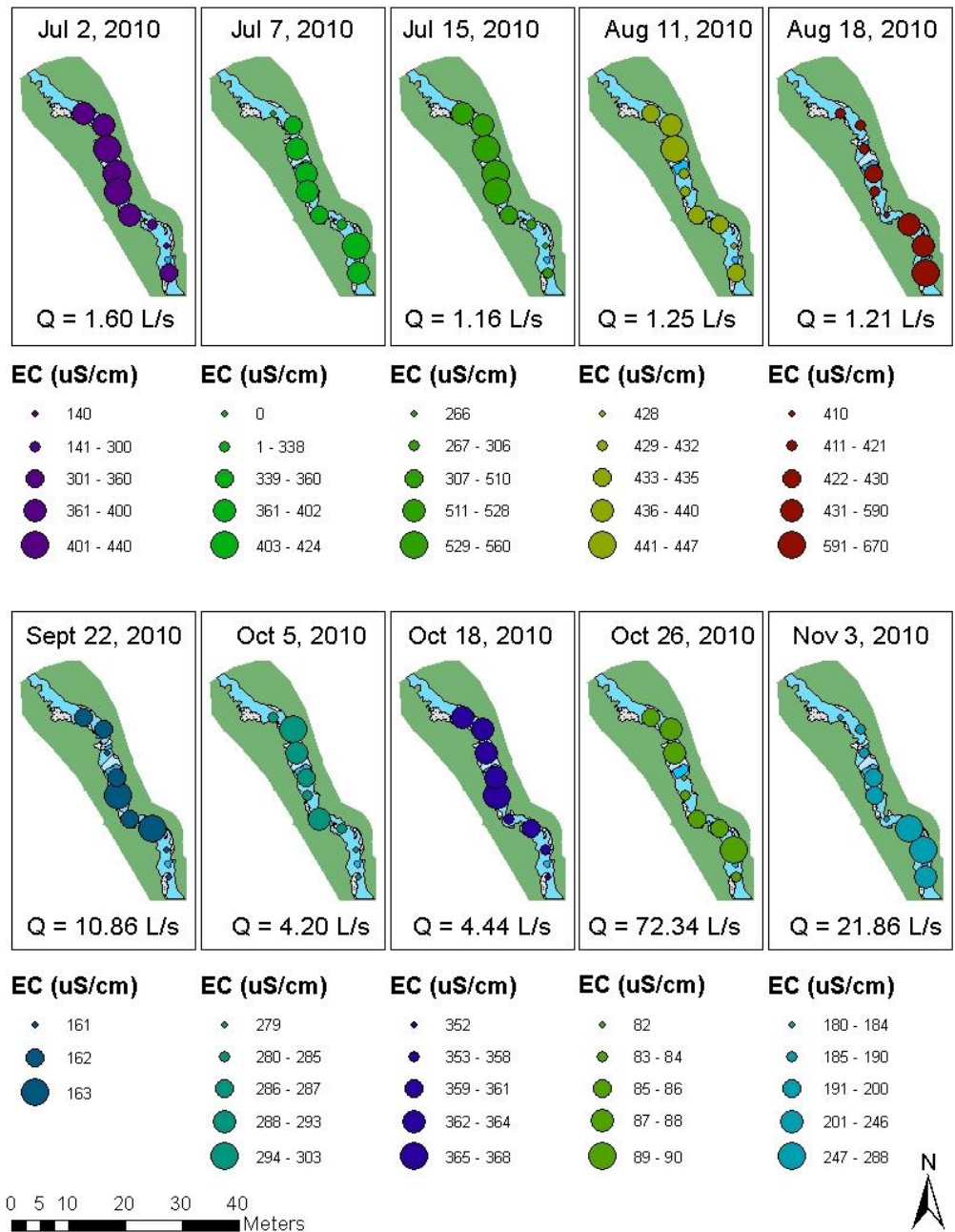
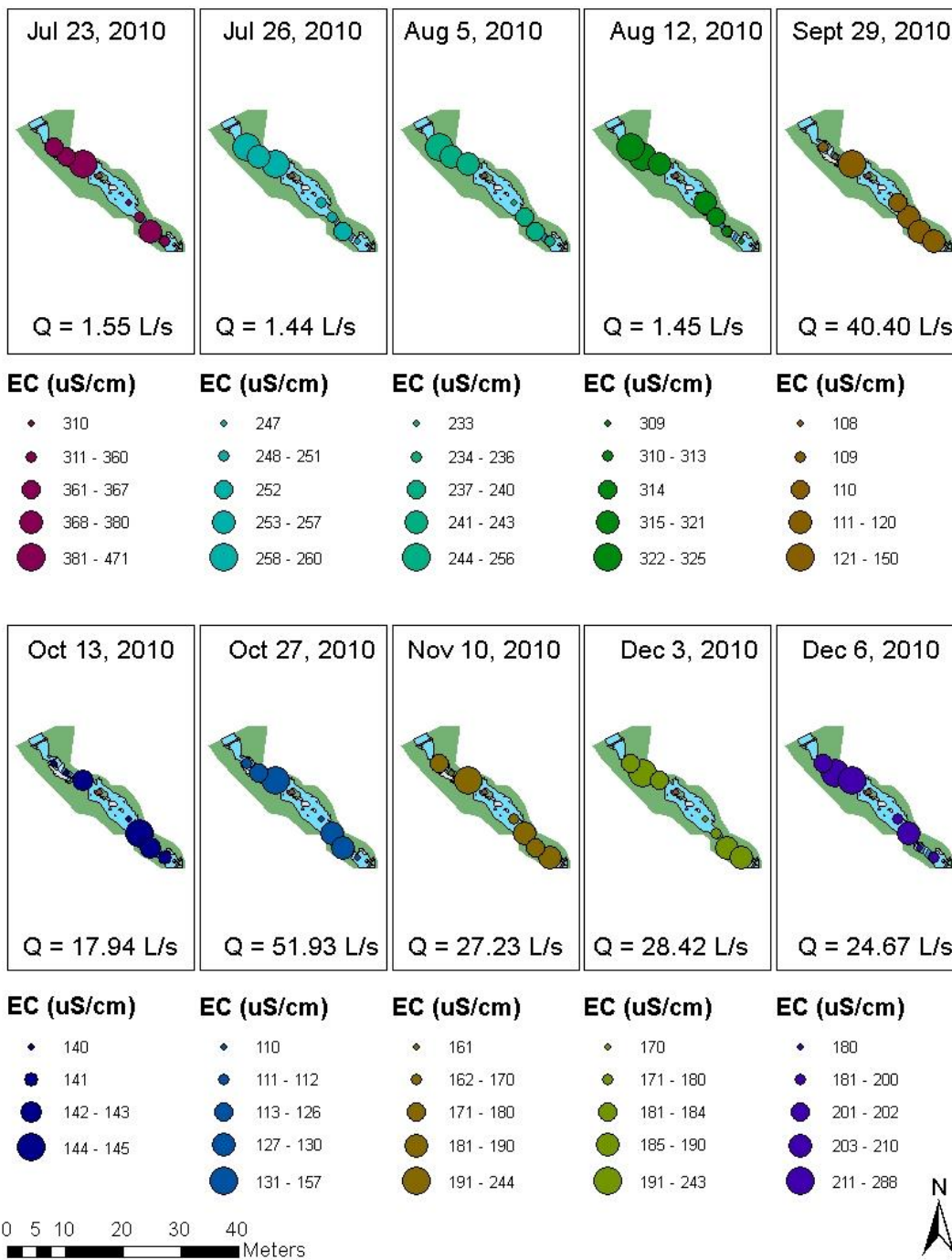


Figure B.1 Patterns of steady state EC during the tracer experiments at reach UA.



**Figure B.2 Patterns of steady state EC during the tracer experiments at reach UB.**

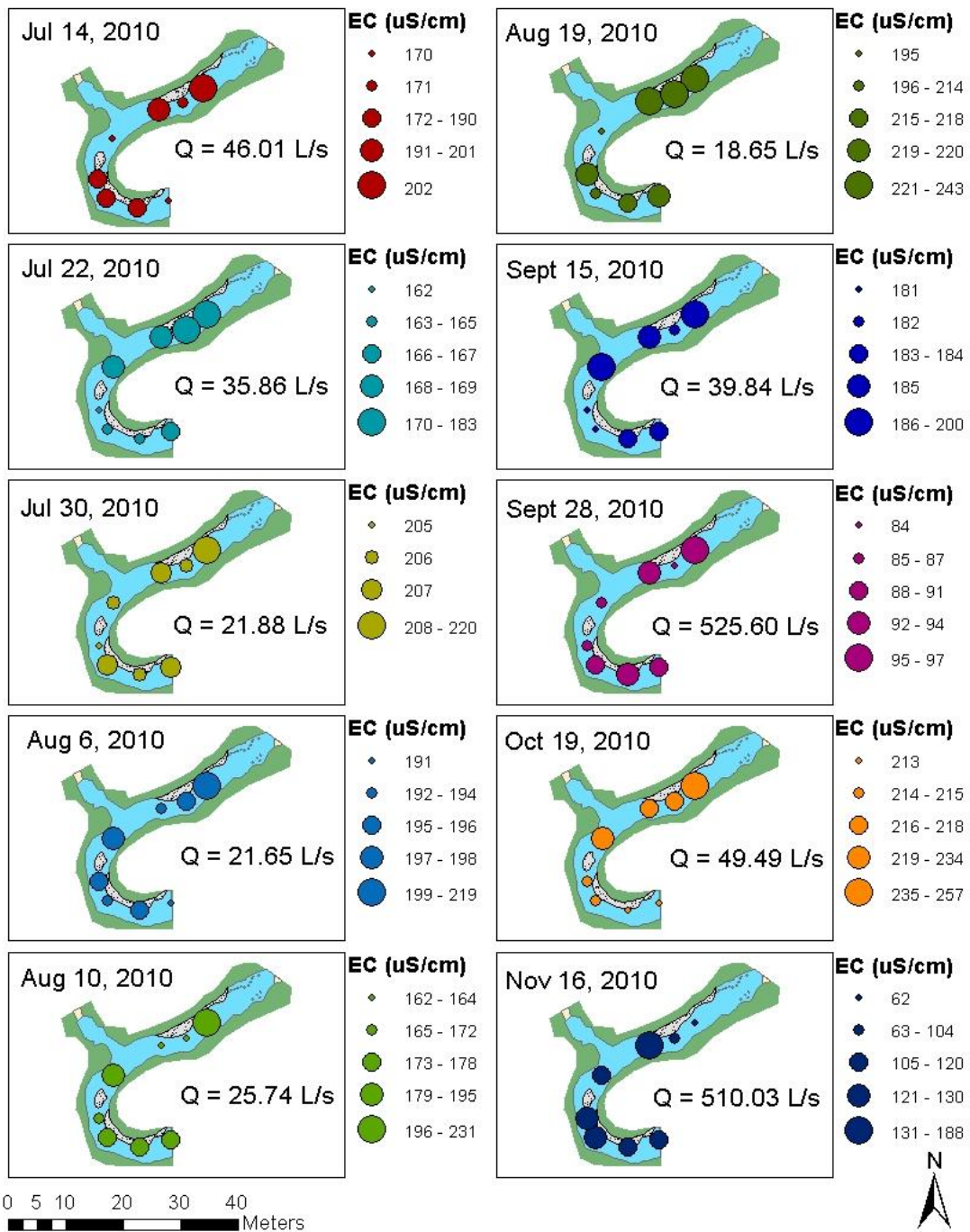
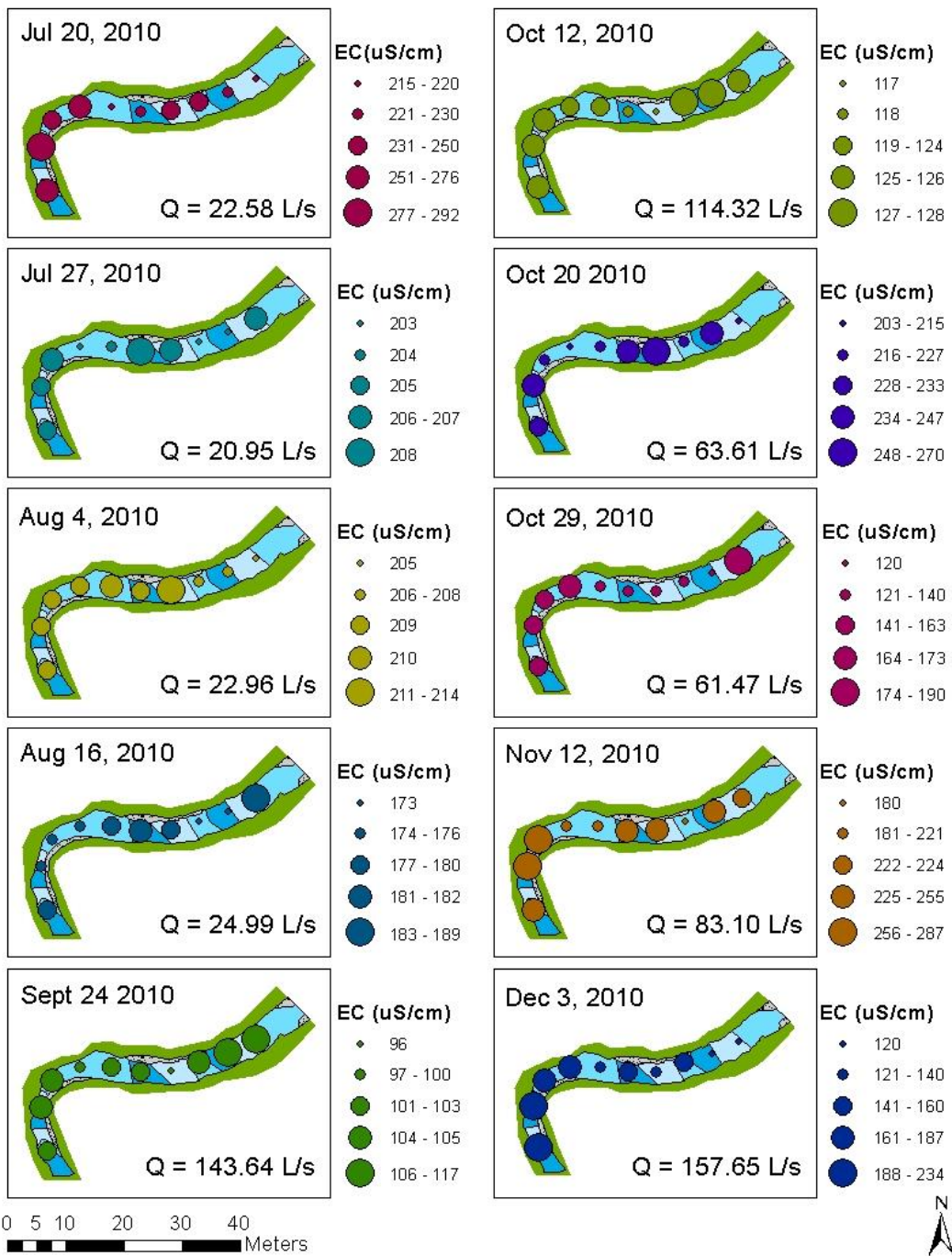
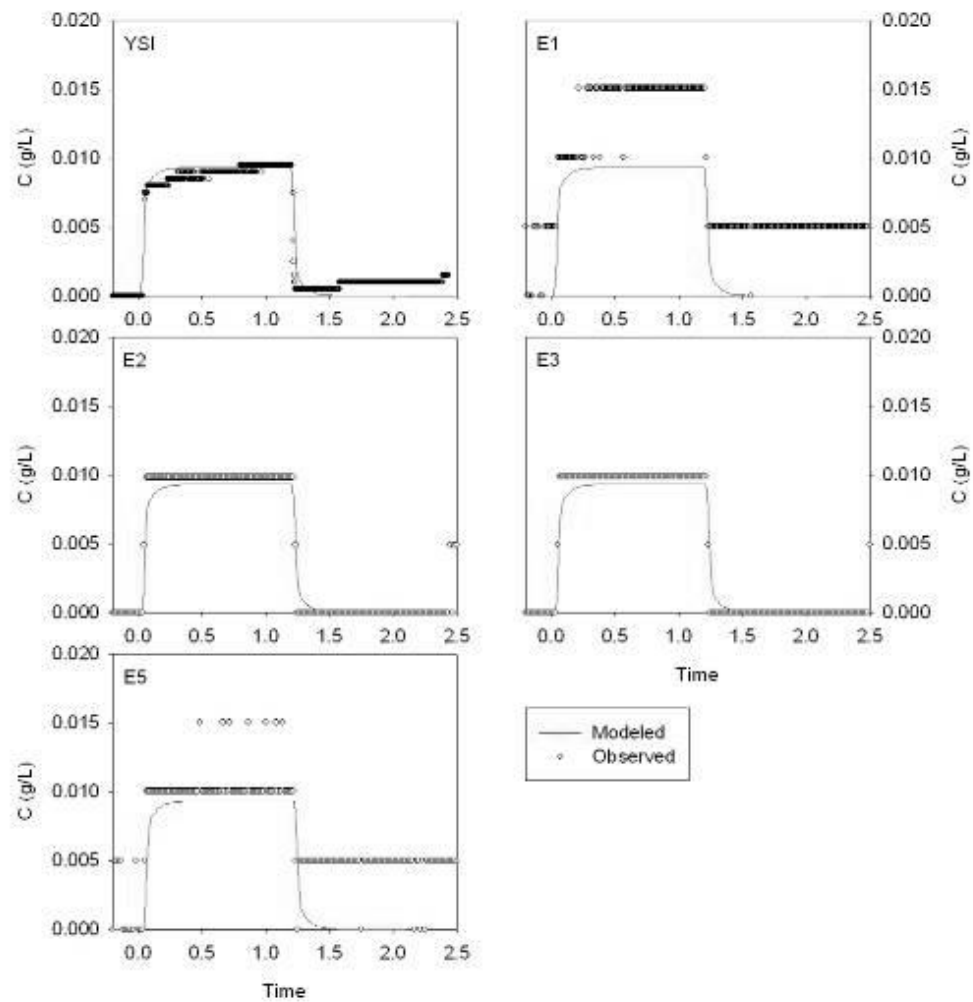


Figure B.3 Patterns of steady state EC during the tracer experiments at reach DA.



**Figure B.4 Patterns of steady state EC during the tracer experiments at reach DB.**

## Appendix C: Calibration Results



**Figure C.1** Observed and modeled tracer concentrations ( $C$  in g/L) during the tracer test at reach UA on October 26, 2010. For the goodness of fit statistics, see Table 4.7. For the location of the YSI and ECH<sub>2</sub>O 1-5 probes, see Figure 3.7.

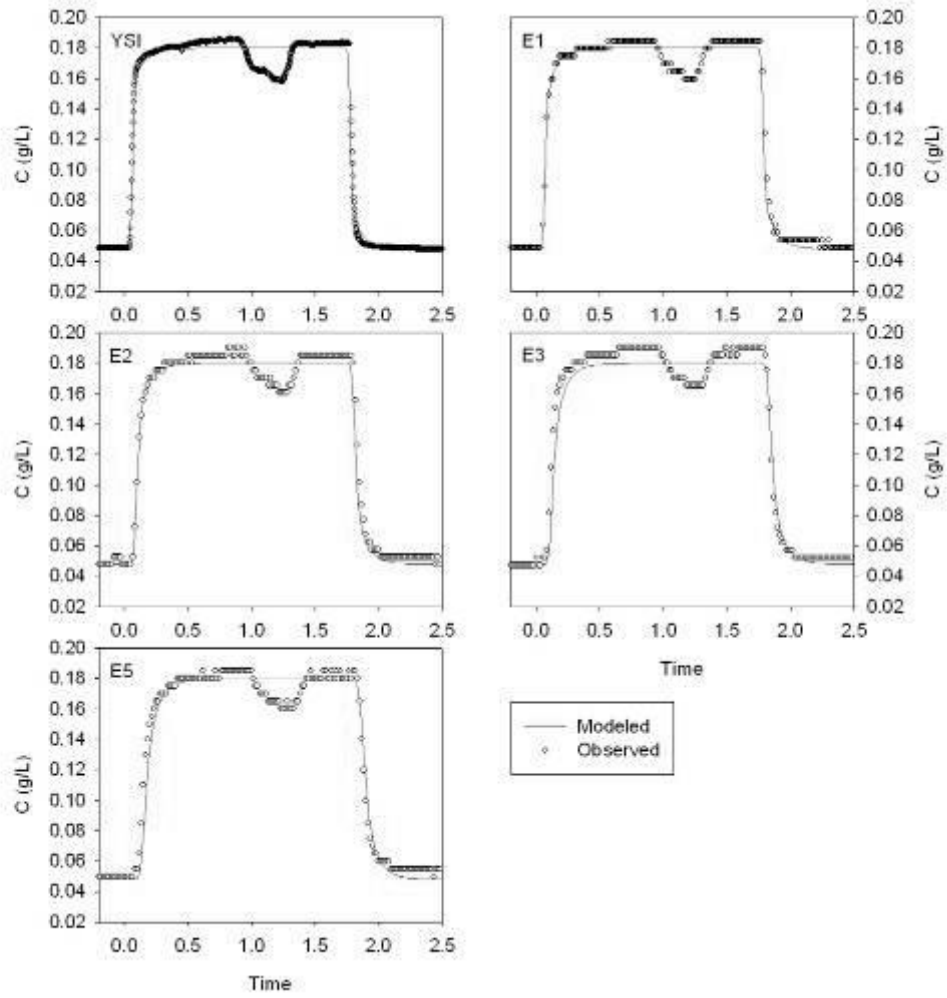


**Figure C.2** Observed and modeled tracer concentrations ( $C$  in g/L) during the tracer test at reach UA on October 18, 2010. For the goodness of fit statistics, see Table 4.7. For the location of the YSI and ECH<sub>2</sub>O 1-5 probes, see Figure 3.7.

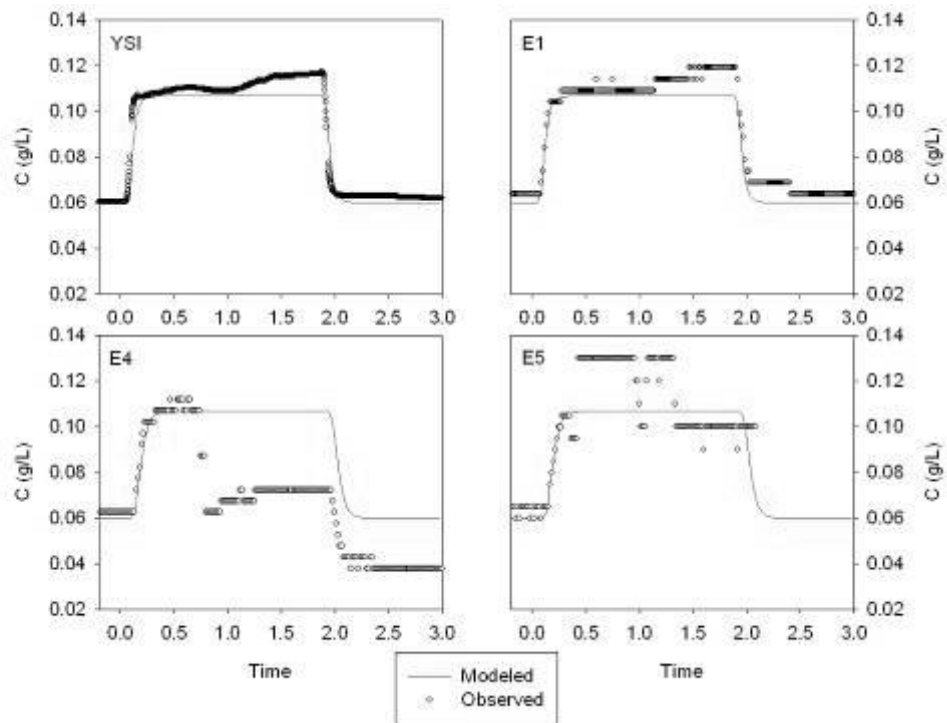


**Figure C.3** Observed and modeled tracer concentrations ( $C$  in g/L) during the tracer test at reach UA on October 5, 2010. For the goodness of fit statistics, see Table 4.7. For the location of the YSI and ECH<sub>2</sub>O 1-5 probes, see Figure 3.7. The ECH<sub>2</sub>O 5 probe stopped recording data after just over 2 hours.

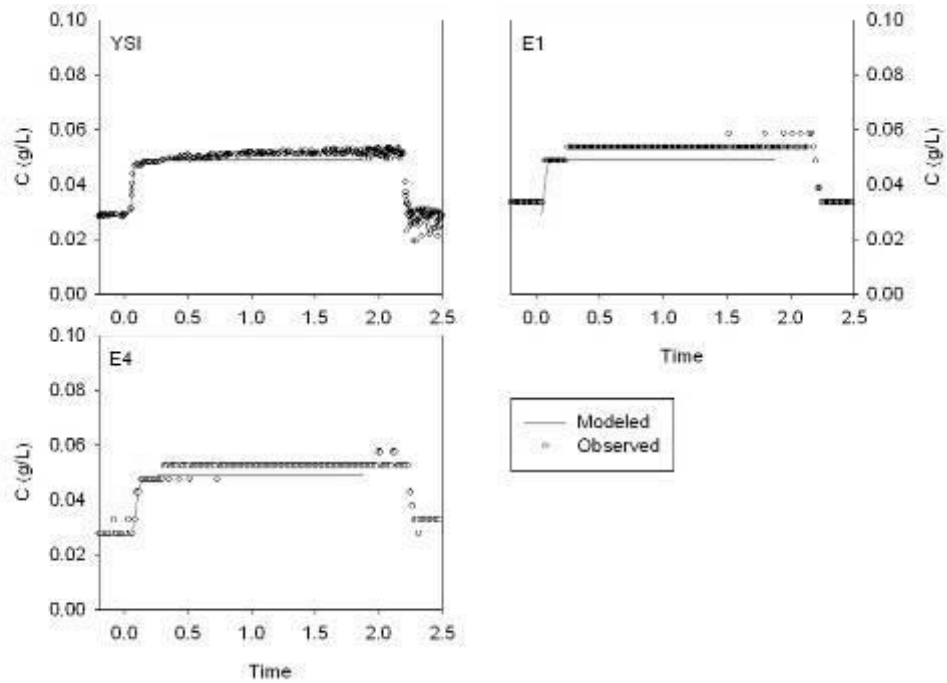


**Figure C.4** Observed and modeled tracer concentrations ( $C$  in g/L) during the tracer test at reach UA on September 22, 2010. For the goodness of fit statistics, see Table 4.7. For the location of the YSI and ECH<sub>2</sub>O 1-5 probes, see Figure 3.7.

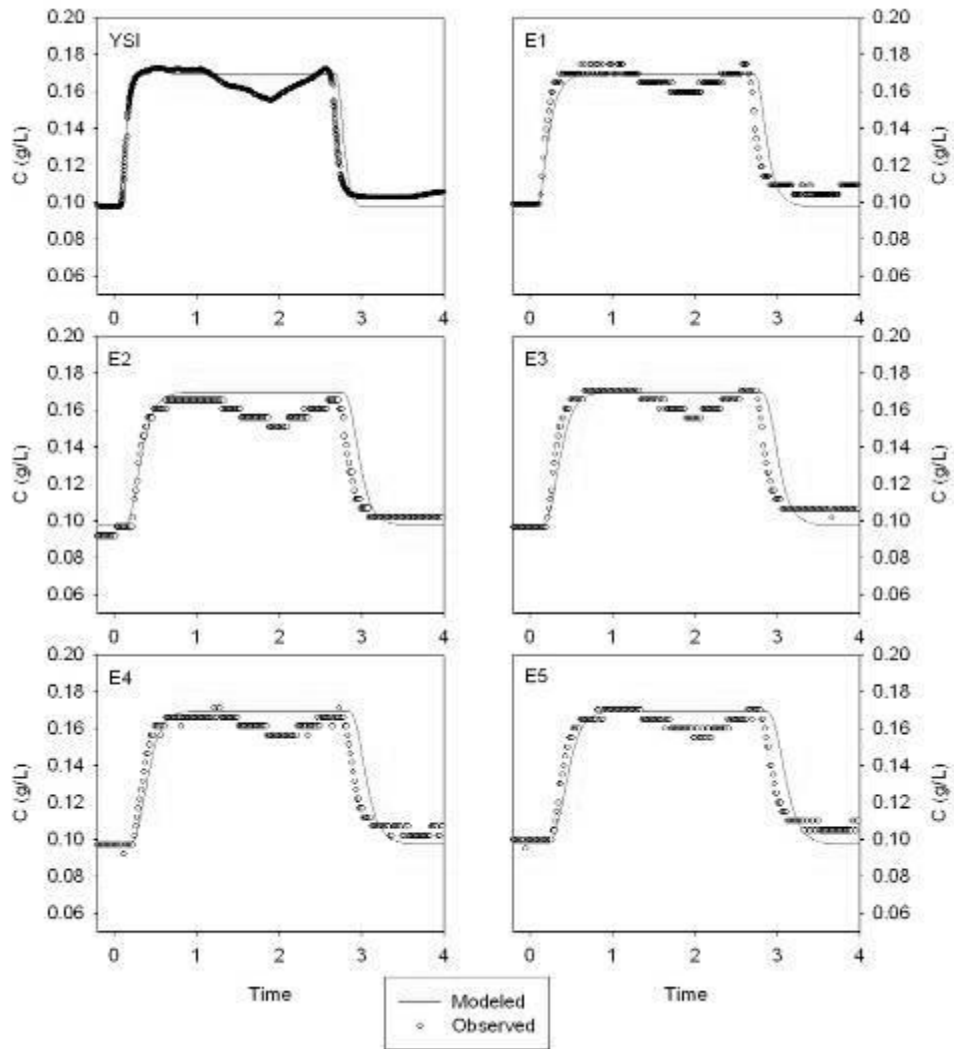


**Figure C.5** Observed and modeled tracer concentrations ( $C$  in g/L) during the tracer test at reach UA on August 18, 2010. For the goodness of fit statistics, see Table 4.7. For the location of the YSI and ECH<sub>2</sub>O 1-5 probes, see Figure 3.7.

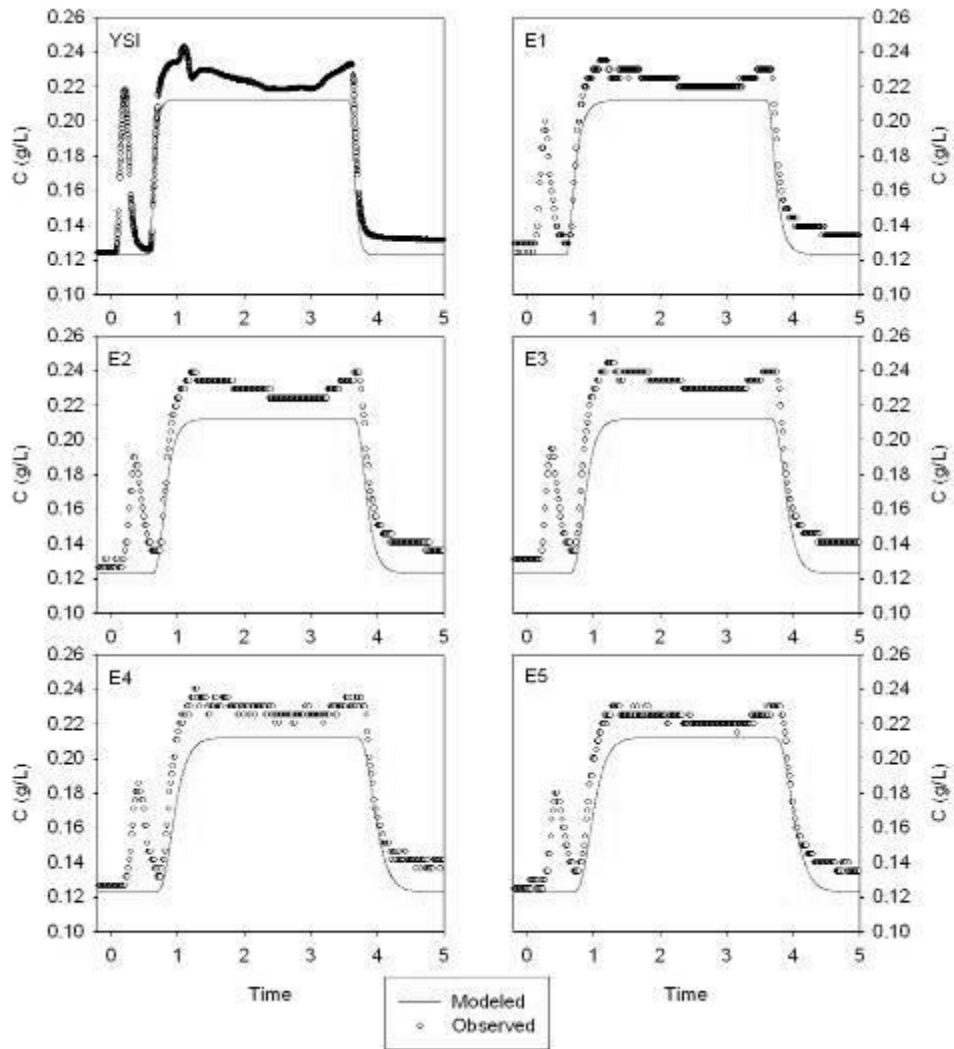


**Figure C.6** Observed and modeled tracer concentrations ( $C$  in g/L) during the tracer test at reach UA on July 15, 2010. For the goodness of fit statistics, see Table 4.7. For the location of the YSI and ECH<sub>2</sub>O 1-5 probes, see Figure 3.7. The pump stopped near the beginning, and was restarted just after 0.5 hours.

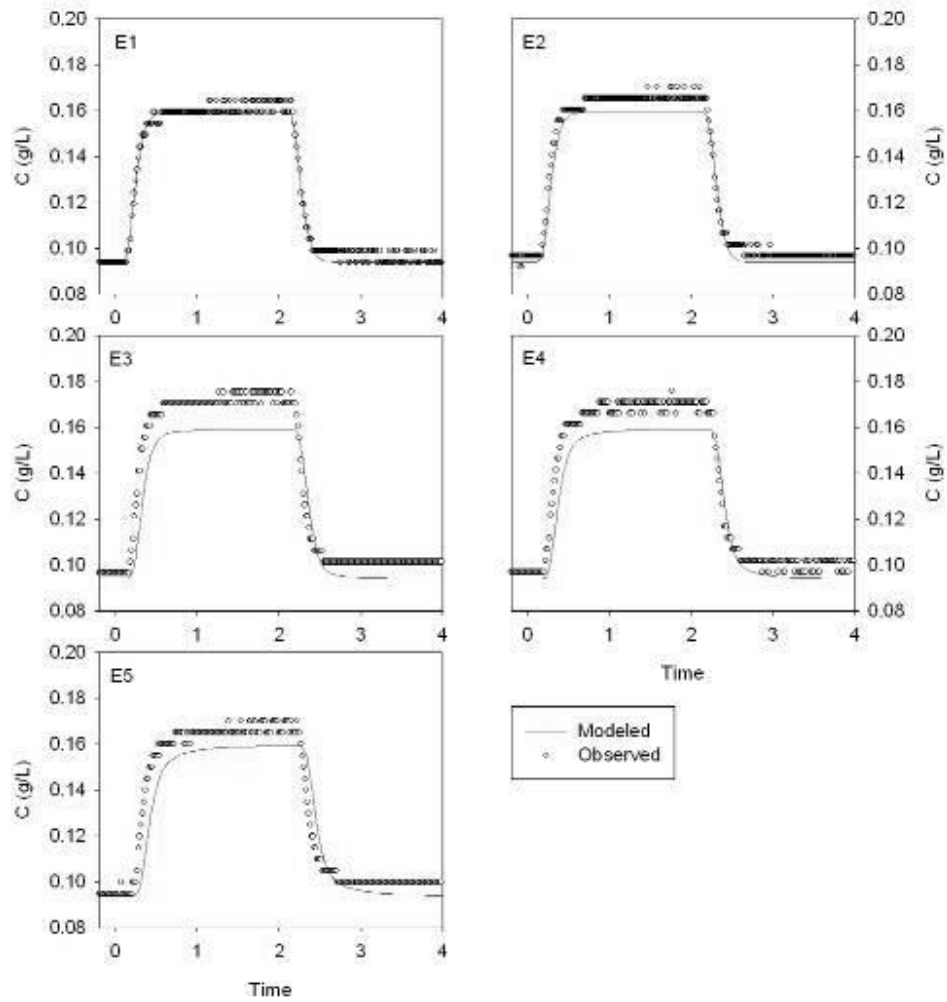


**Figure C.7** Observed and modeled tracer concentrations ( $C$  in g/L) during the tracer test at reach UA on July 2, 2010. For the goodness of fit statistics, see Table 4.7. For the location of the YSI and ECH<sub>2</sub>O 1-5 probes, see Figure 3.7.

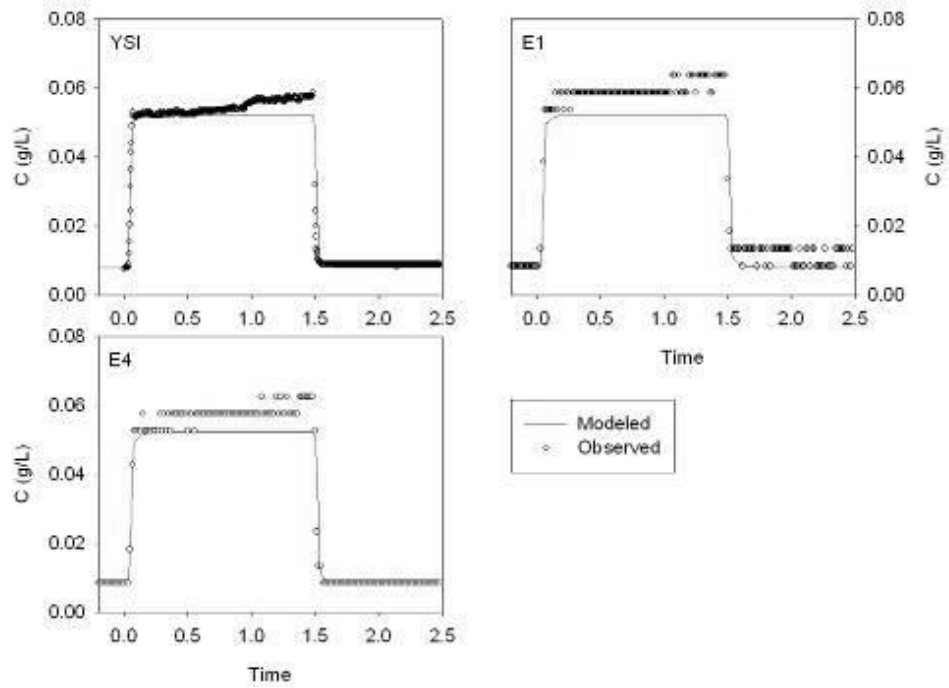


**Figure C.8** Observed and modeled tracer concentrations ( $C$  in g/L) during the tracer test at reach UA on November 3, 2010. For the goodness of fit statistics, see Table 4.7. For the location of the YSI and ECH<sub>2</sub>O 1-5 probes, see Figure 3.7.

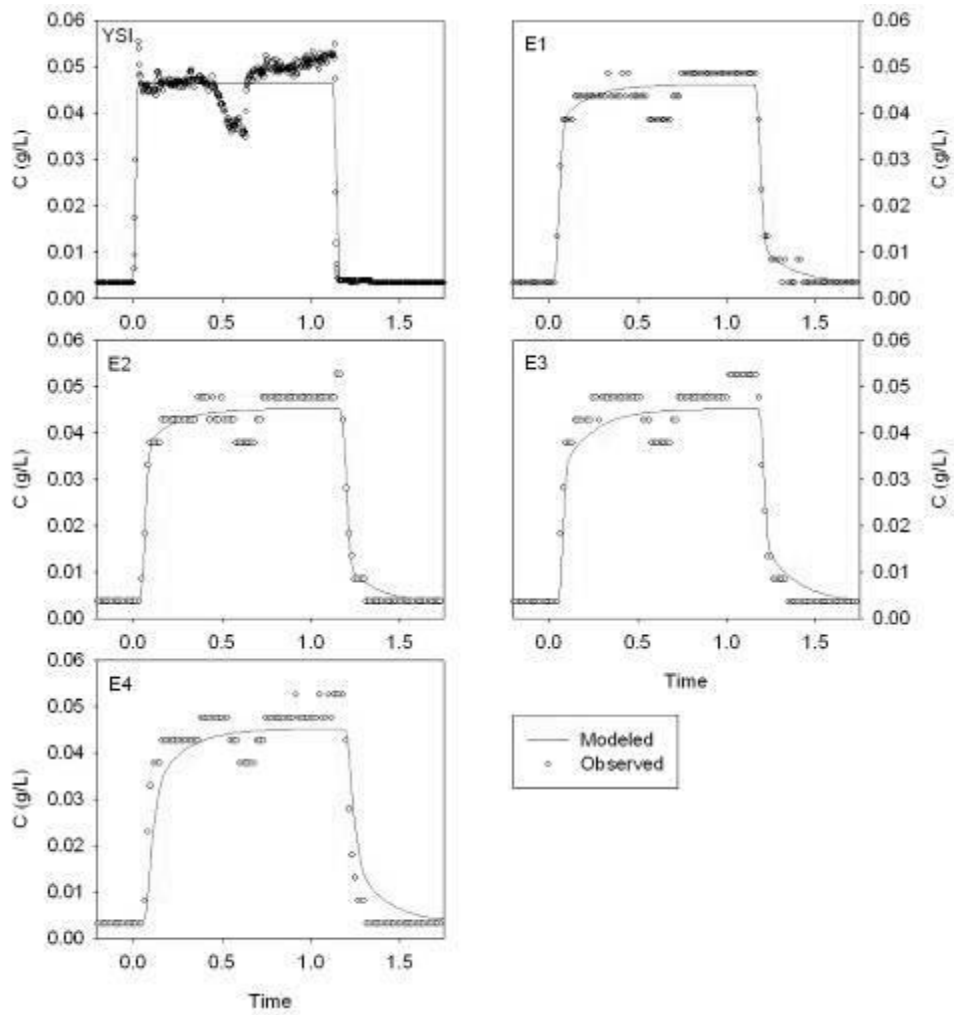


**Figure C.9** Observed and modeled tracer concentrations ( $C$  in g/L) during the tracer test at reach UB on December 4, 2010. For the goodness of fit statistics, see Table 4.8. For the location of the YSI and ECH<sub>2</sub>O 1-5 probes, see Figure 3.7.

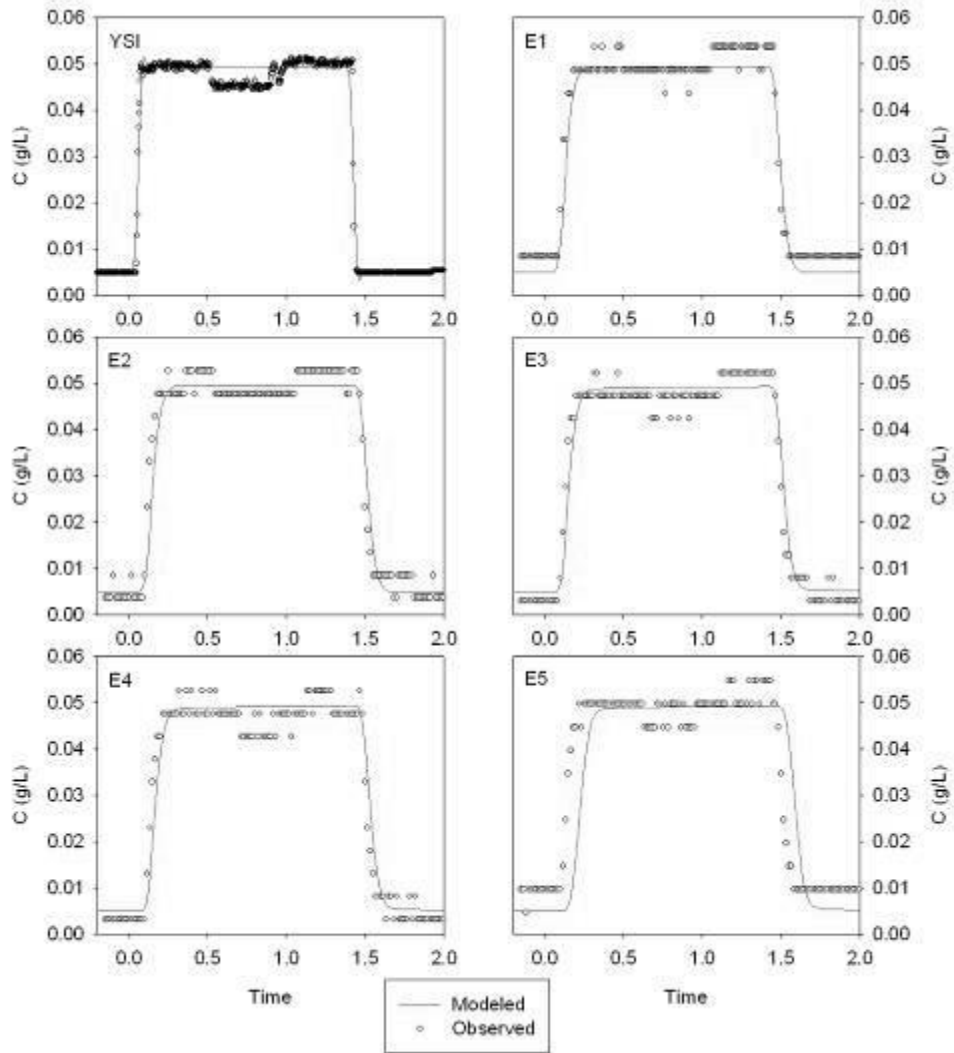


**Figure C.10** Observed and modeled tracer concentrations ( $C$  in g/L) during the tracer test at reach UB on November 10, 2010. For the goodness of fit statistics, see Table 4.8. For the location of the YSI and ECH<sub>2</sub>O 1-5 probes, see Figure 3.7.

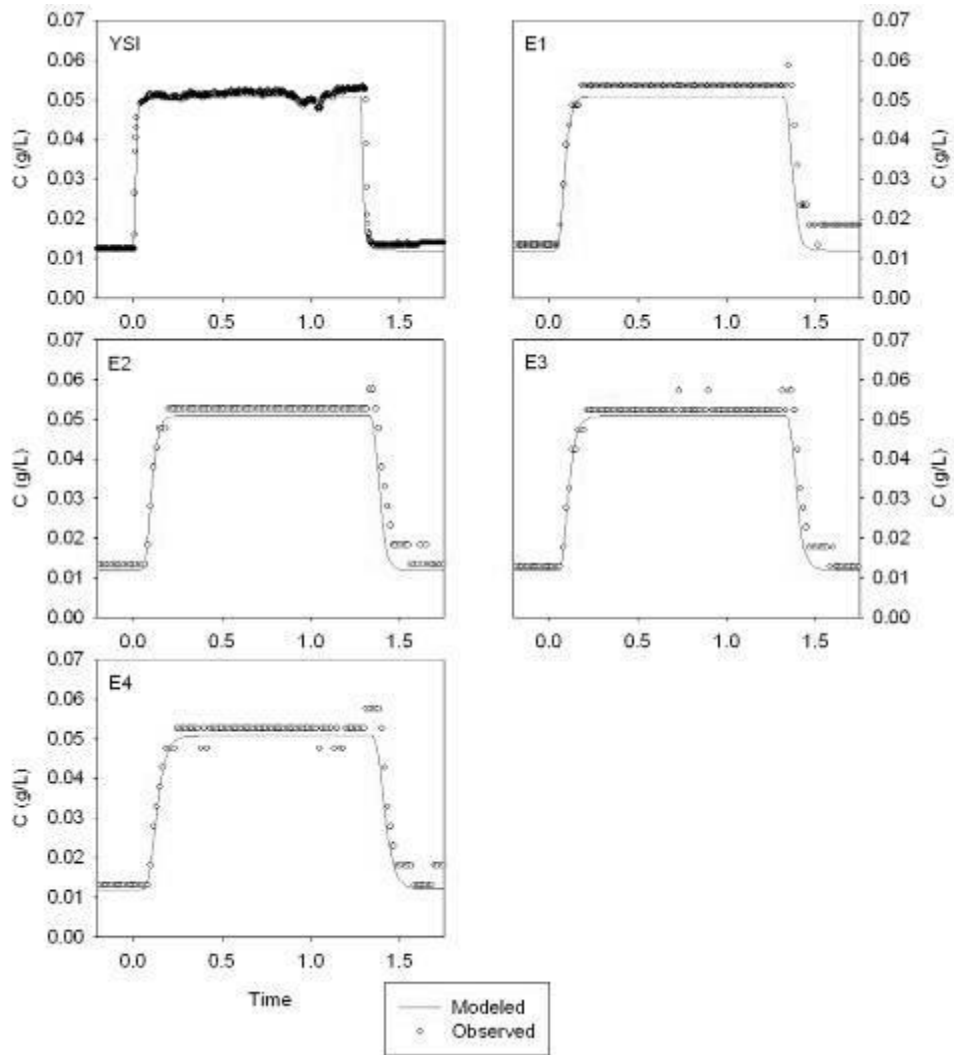


**Figure C.11** Observed and modeled tracer concentrations ( $C$  in g/L) during the tracer test at reach UB on October 13, 2010. For the goodness of fit statistics, see Table 4.8. For the location of the YSI and ECH<sub>2</sub>O 1-5 probes, see Figure 3.7.

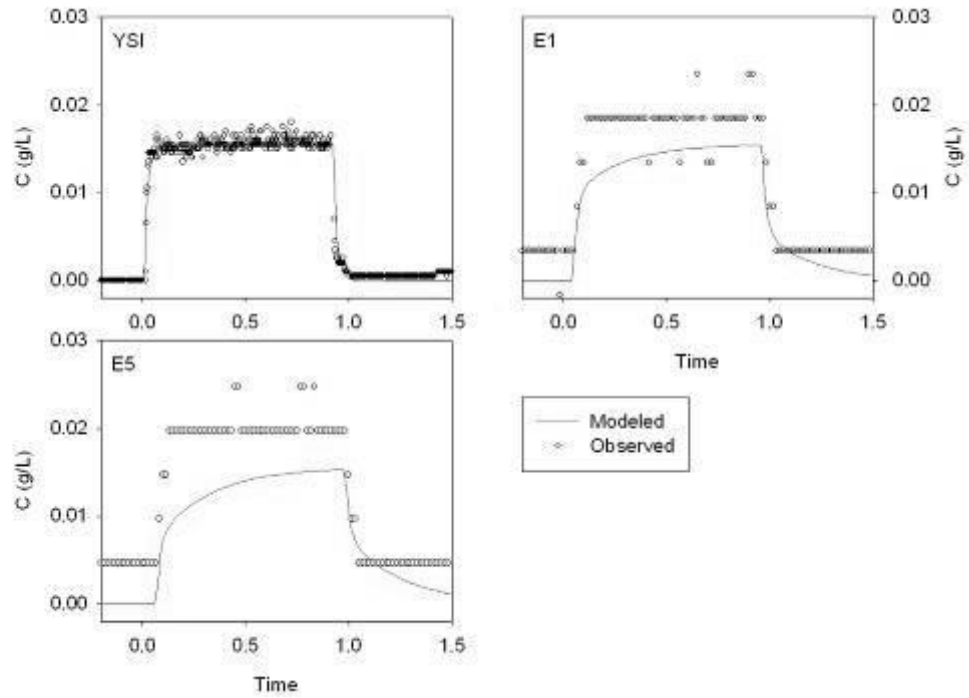


**Figure C.12** Observed and modeled tracer concentrations ( $C$  in g/L) during the tracer test at reach UB on September 29, 2010. For the goodness of fit statistics, see Table 4.8. For the location of the YSI and ECH<sub>2</sub>O 1-5 probes, see Figure 3.7.

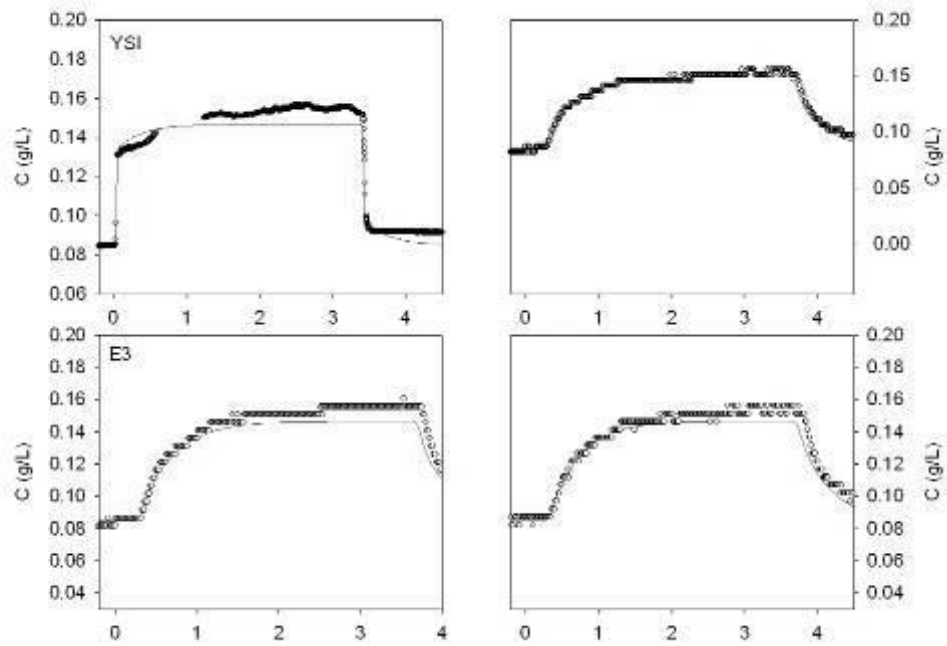


**Figure C.13** Observed and modeled tracer concentrations ( $C$  in g/L) during the tracer test at reach UB on August 12, 2010. For the goodness of fit statistics, see Table 4.8. For the location of the YSI and ECH<sub>2</sub>O 1-5 probes, see Figure 3.7.

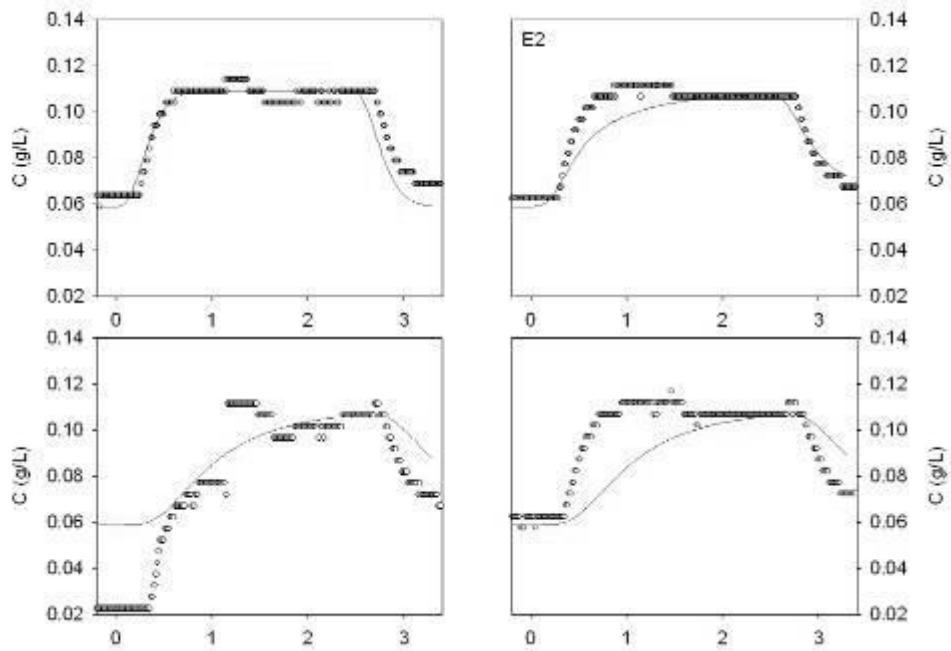


**Figure C.14** Observed and modeled tracer concentrations ( $C$  in g/L) during the tracer test at reach UB on August 5, 2010. For the goodness of fit statistics, see Table 4.8. For the location of the YSI and ECH<sub>2</sub>O 1-5 probes, see Figure 3.7.

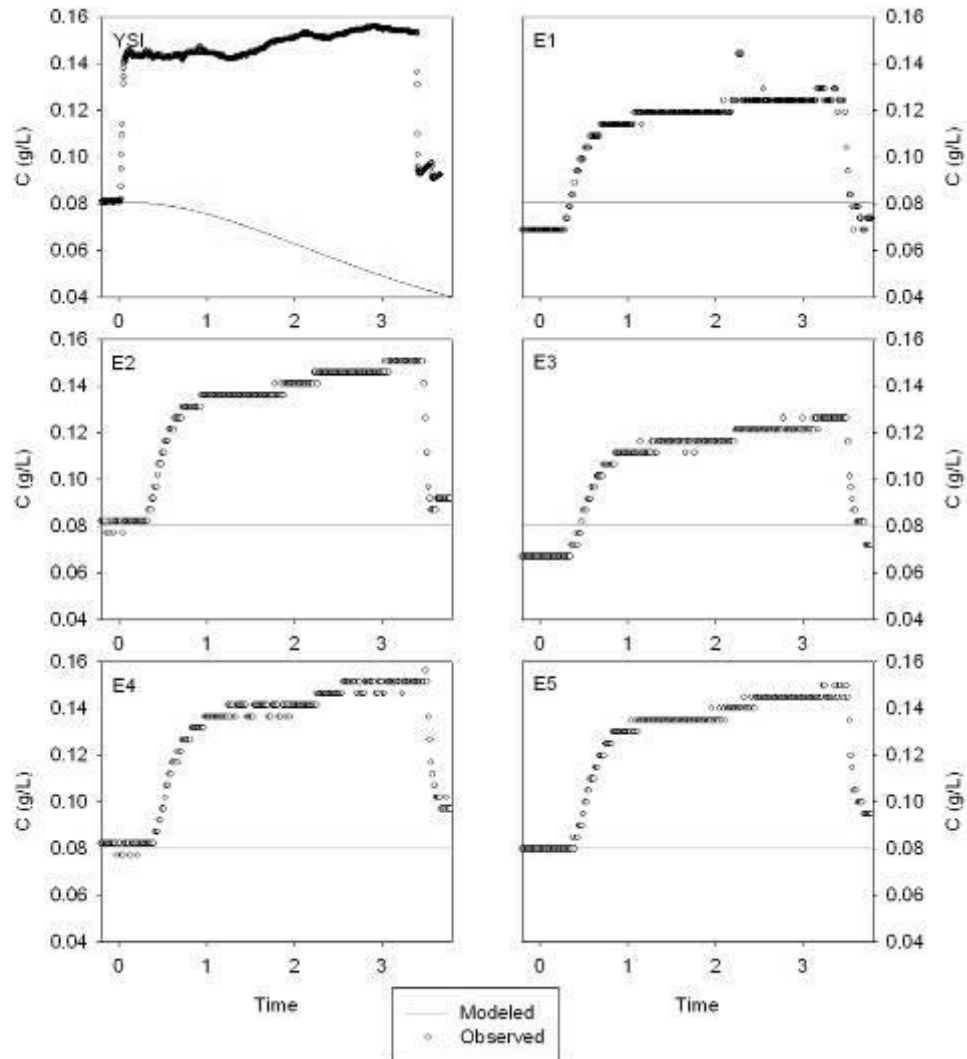


**Figure C.15** Observed and modeled tracer concentrations ( $C$  in g/L) during the tracer test at reach UB on July 23, 2010. For the goodness of fit statistics, see Table 4.8. For the location of the YSI and ECH<sub>2</sub>O 1-5 probes, see Figure 3.7. Goodness of fit is very poor, and the parameters estimated from this test are therefore considered outliers and not included in statistical analyses.

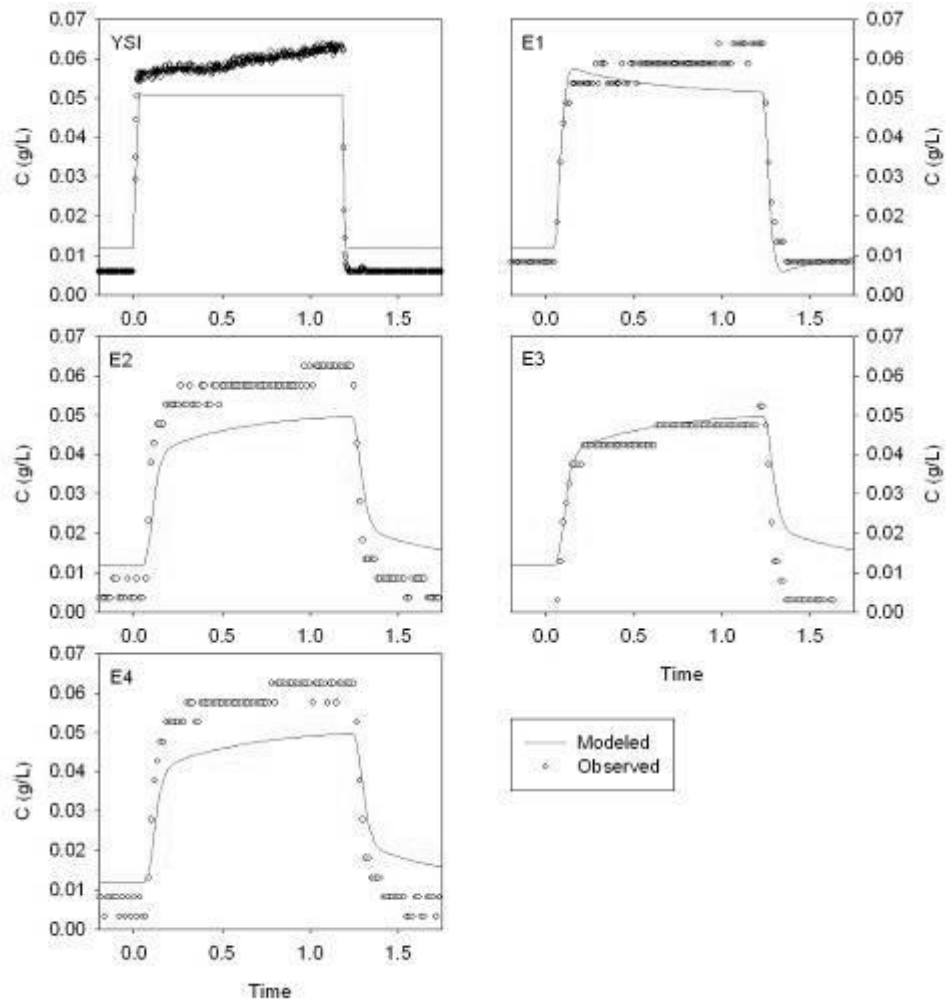


**Figure C.16** Observed and modeled tracer concentrations ( $C$  in g/L) during the tracer test at reach UB on December 6, 2010. For the goodness of fit statistics, see Table 4.8. For the location of the YSI and ECH<sub>2</sub>O 1-5 probes, see Figure 3.7.

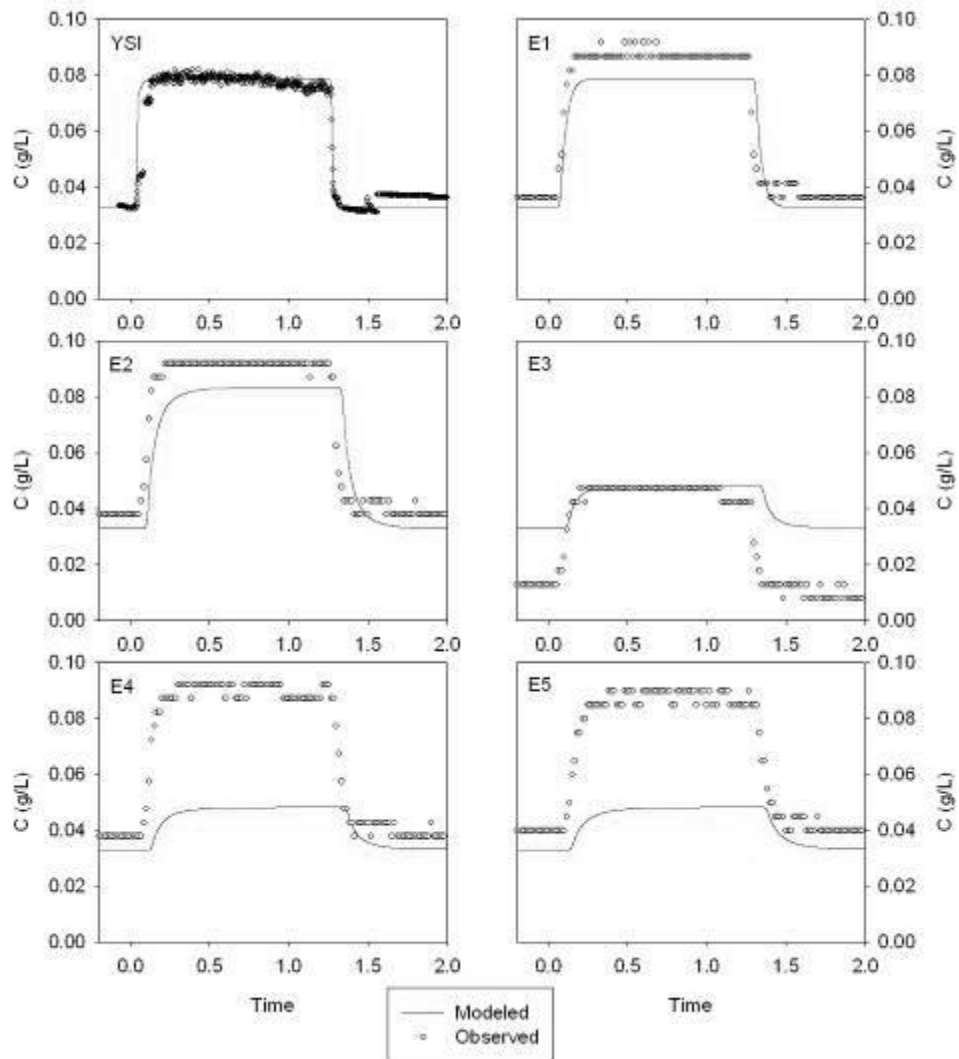


**Figure C.17** Observed and modeled tracer concentrations ( $C$  in g/L) during the tracer test at reach DA on October 19, 2010. For the goodness of fit statistics, see Table 4.9. For the location of the YSI and ECH<sub>2</sub>O 1-5 probes, see Figure 3.7.

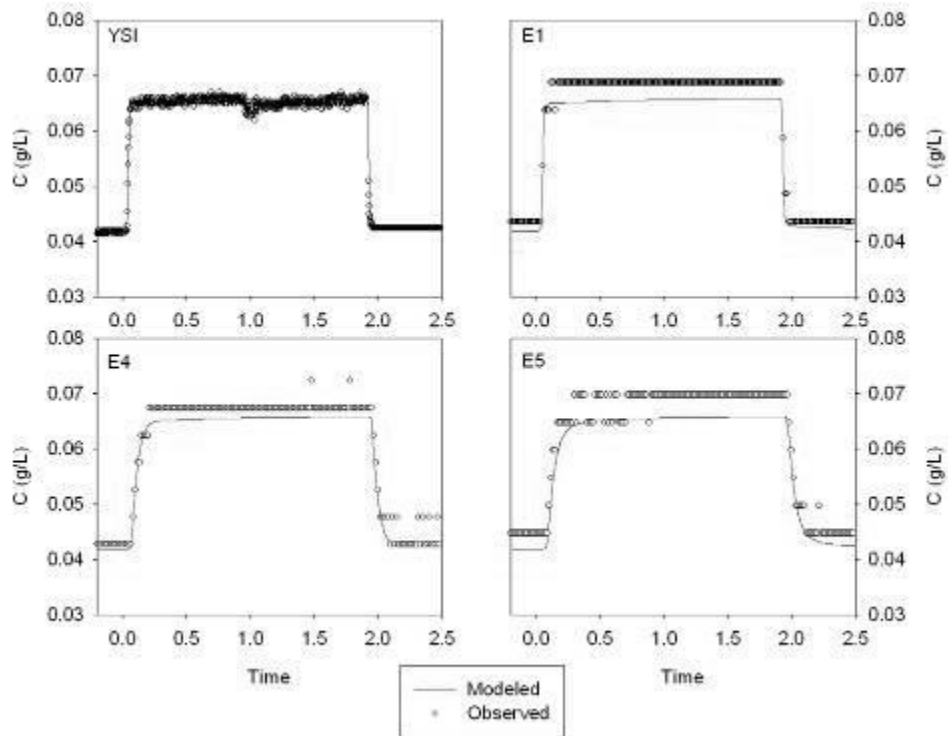


**Figure C.18** Observed and modeled tracer concentrations ( $C$  in g/L) during the tracer test at reach DA on September 15, 2010. For the goodness of fit statistics, see Table 4.9. For the location of the YSI and ECH<sub>2</sub>O 1-5 probes, see Figure 3.7.

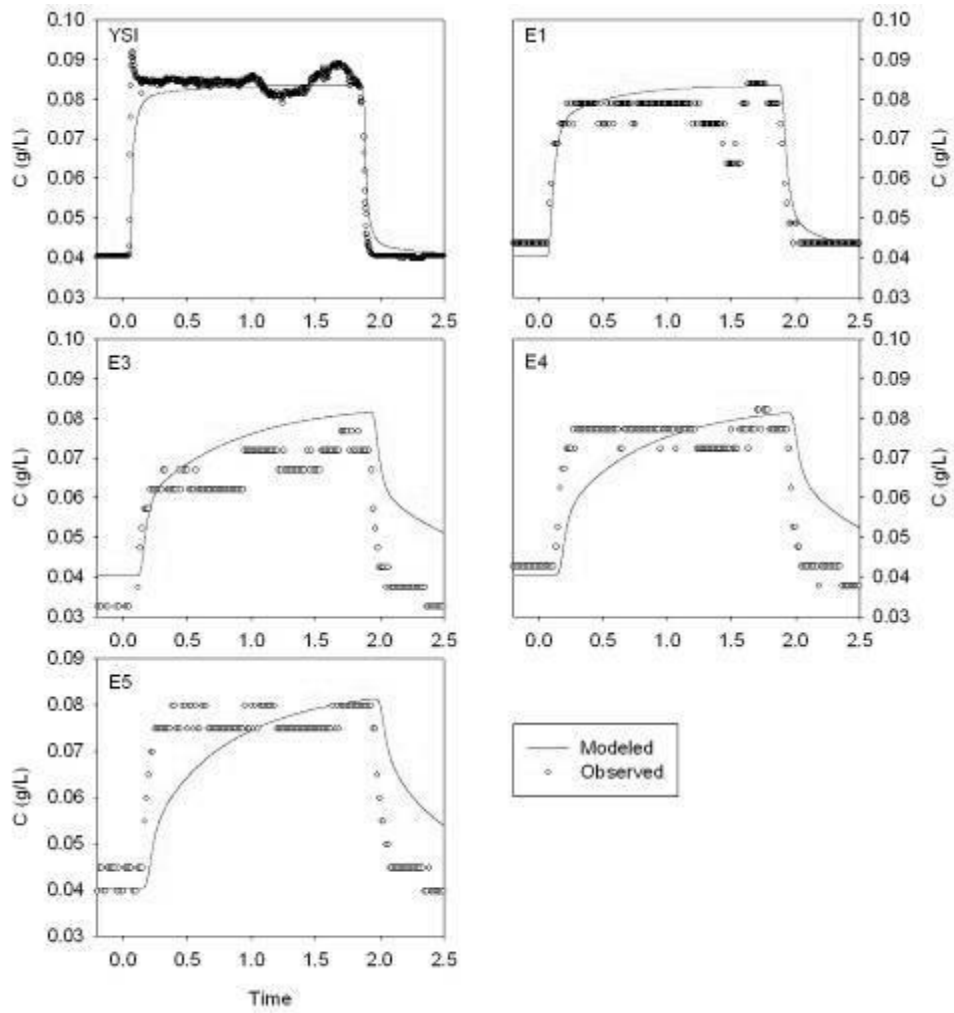


**Figure C.19** Observed and modeled tracer concentrations ( $C$  in g/L) during the tracer test at reach DA on August 19, 2010. For the goodness of fit statistics, see Table 4.9. For the location of the YSI and ECH<sub>2</sub>O 1-5 probes, see Figure 3.7.

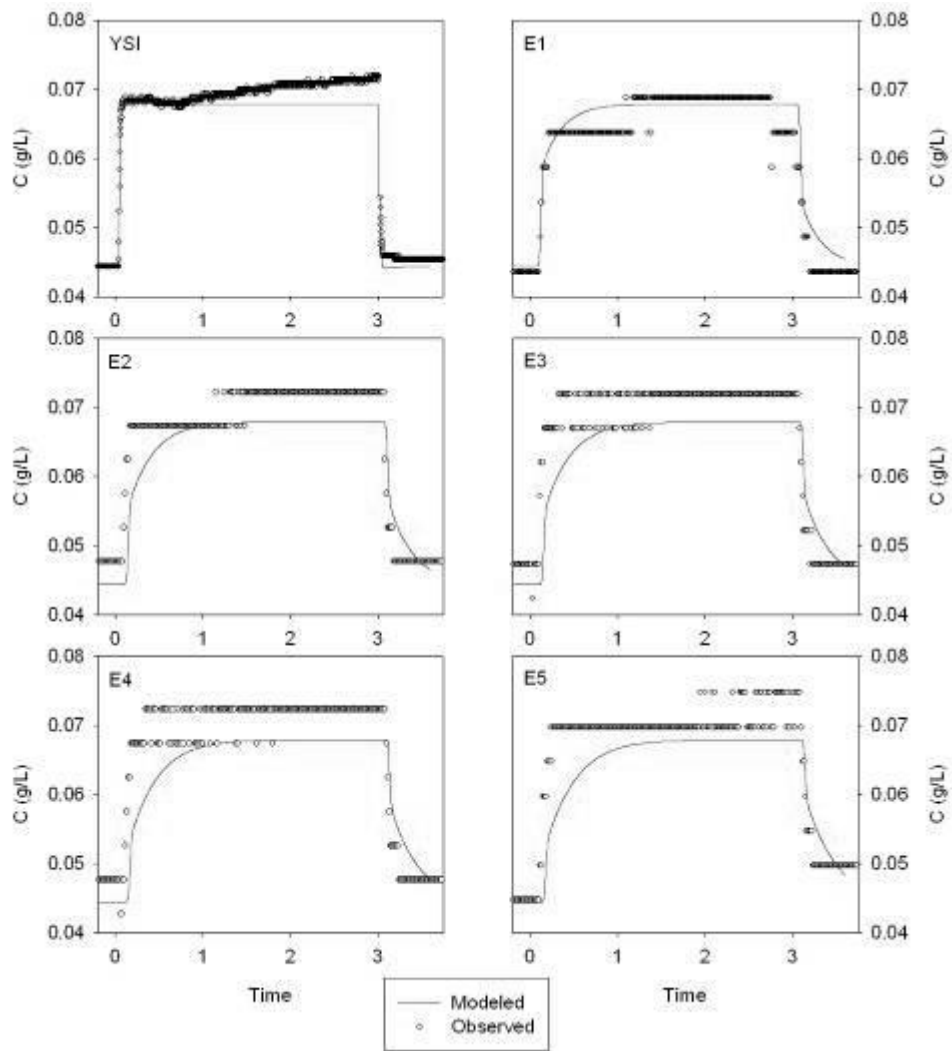


**Figure C.20** Observed and modeled tracer concentrations ( $C$  in g/L) during the tracer test at reach DA on August 10, 2010. For the goodness of fit statistics, see Table 4.9. For the location of the YSI and ECH<sub>2</sub>O 1-5 probes, see Figure 3.7.

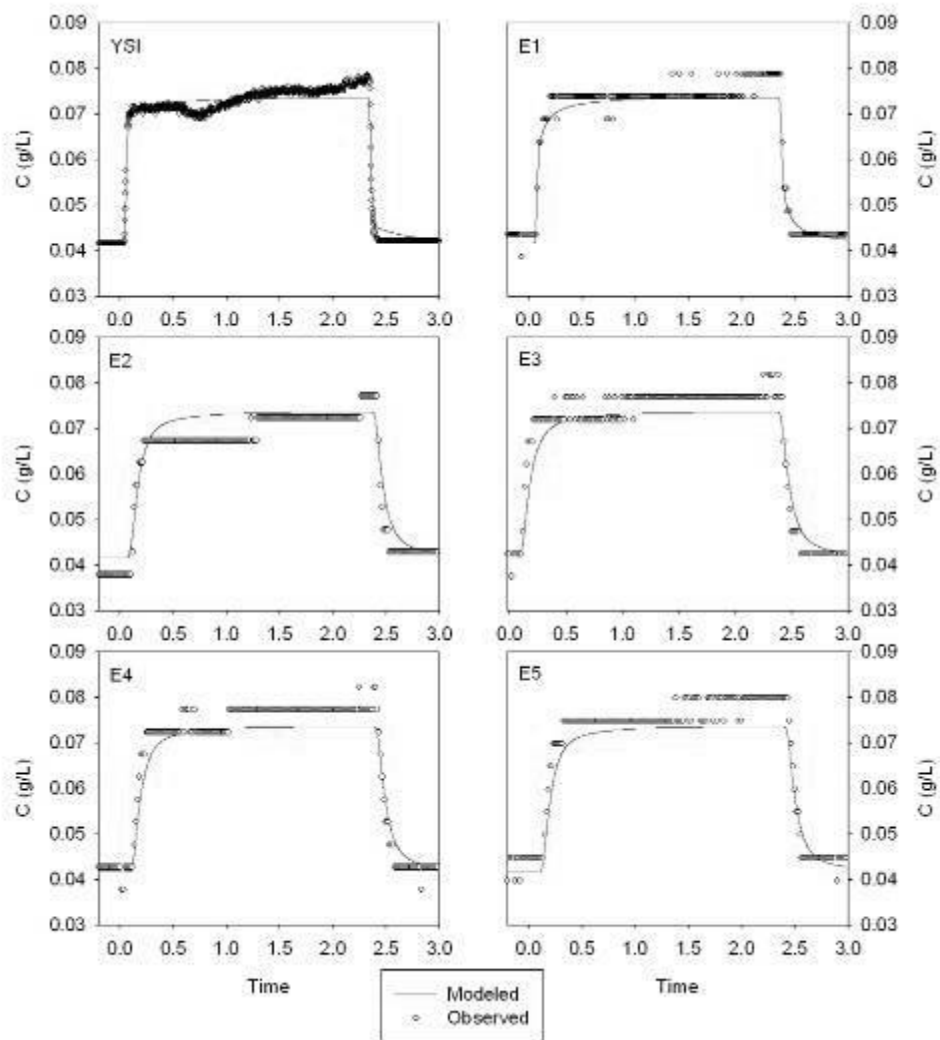


**Figure C.21** Observed and modeled tracer concentrations ( $C$  in g/L) during the tracer test at reach DA on August 6, 2010. For the goodness of fit statistics, see Table 4.9. For the location of the YSI and ECH<sub>2</sub>O 1-5 probes, see Figure 3.7.

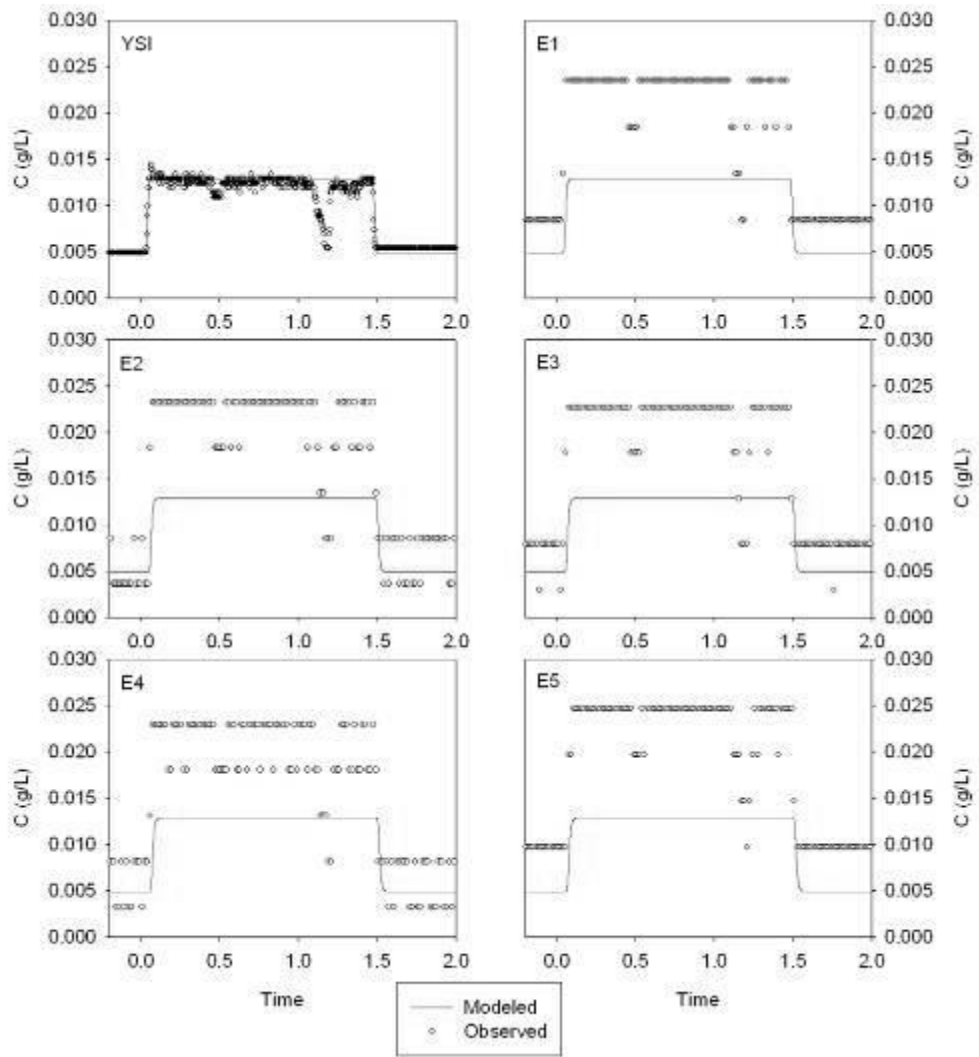


**Figure C.22** Observed and modeled tracer concentrations ( $C$  in g/L) during the tracer test at reach DA on November 16, 2010. For the goodness of fit statistics, see Table 4.9. For the location of the YSI and ECH<sub>2</sub>O 1-5 probes, see Figure 3.7.

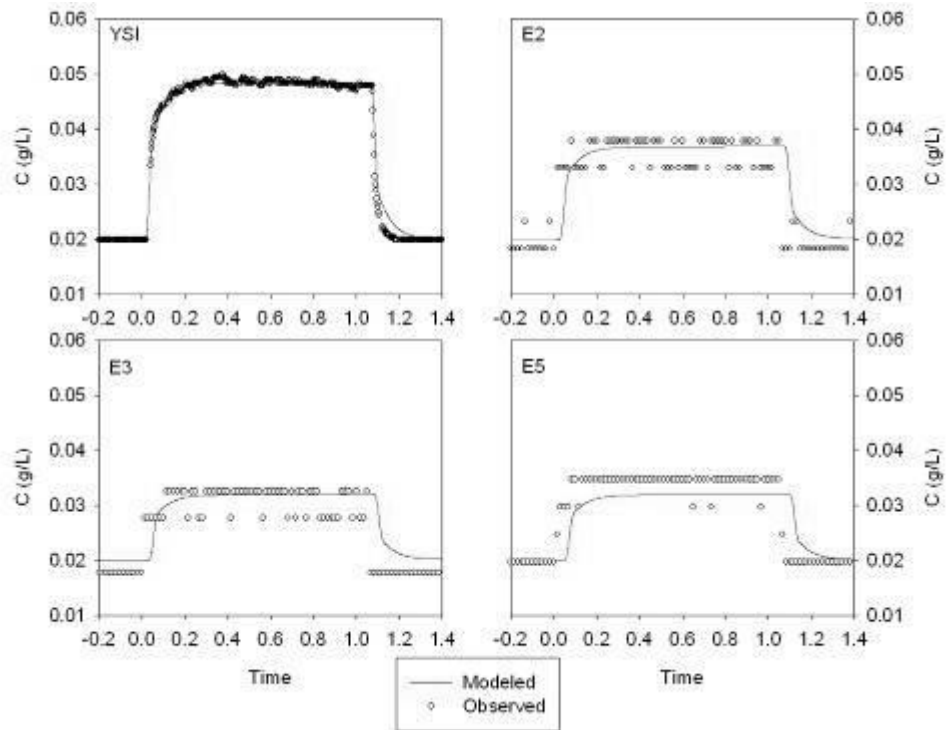


**Figure C.23** Observed and modeled tracer concentrations ( $C$  in g/L) during the tracer test at reach DB on December 3, 2010. For the goodness of fit statistics, see Table 4.10. For the location of the YSI and ECH<sub>2</sub>O 1-5 probes, see Figure 3.7.

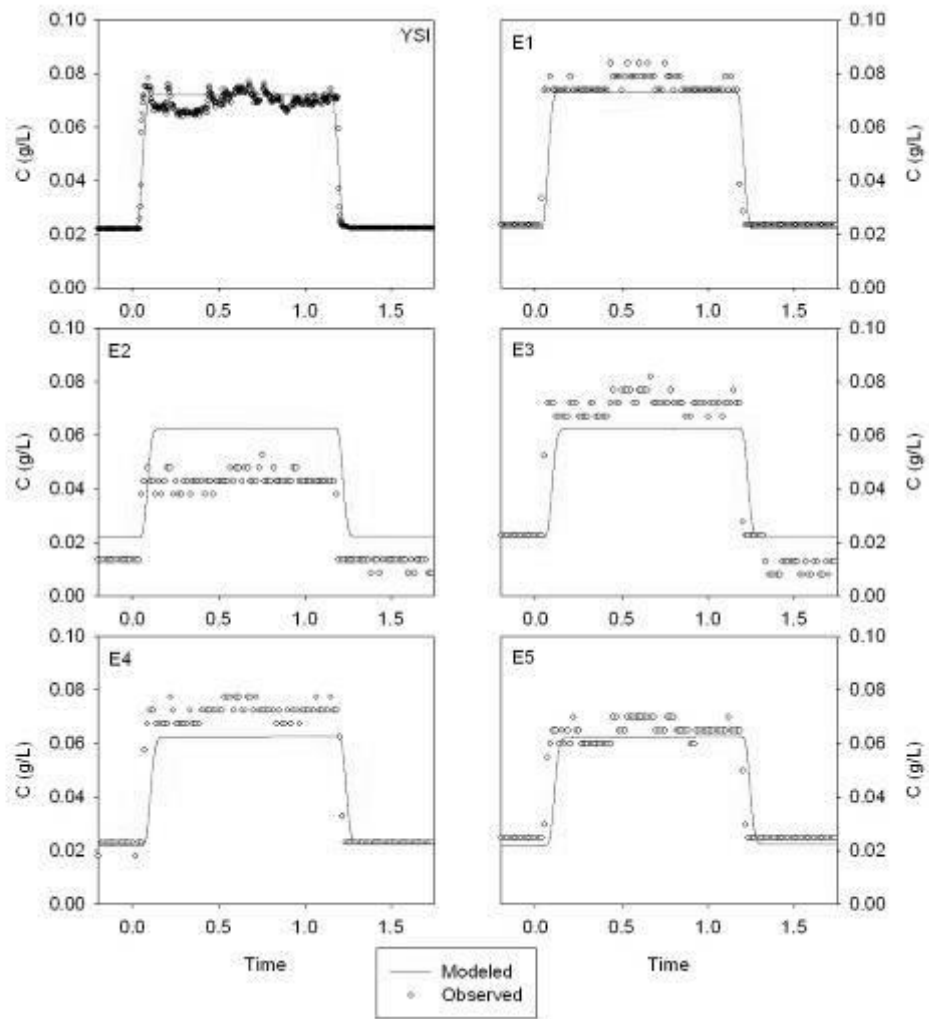


**Figure C.24** Observed and modeled tracer concentrations ( $C$  in g/L) during the tracer test at reach DB on November 12, 2010. For the goodness of fit statistics, see Table 4.10. For the location of the YSI and ECH<sub>2</sub>O 1-5 probes, see Figure 3.7.

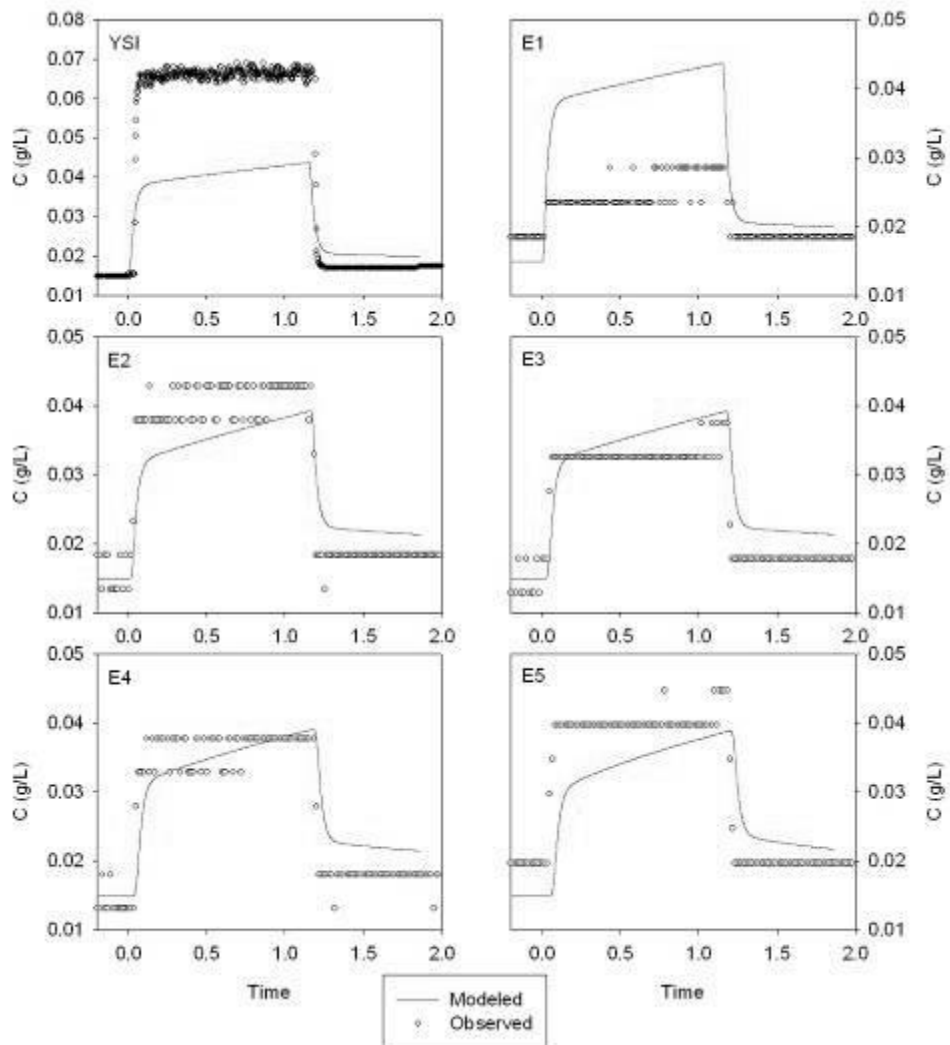


**Figure C.25** Observed and modeled tracer concentrations ( $C$  in g/L) during the tracer test at reach DB on November 12, 2010. For the goodness of fit statistics, see Table 4.10. For the location of the YSI and ECH<sub>2</sub>O 1-5 probes, see Figure 3.7.

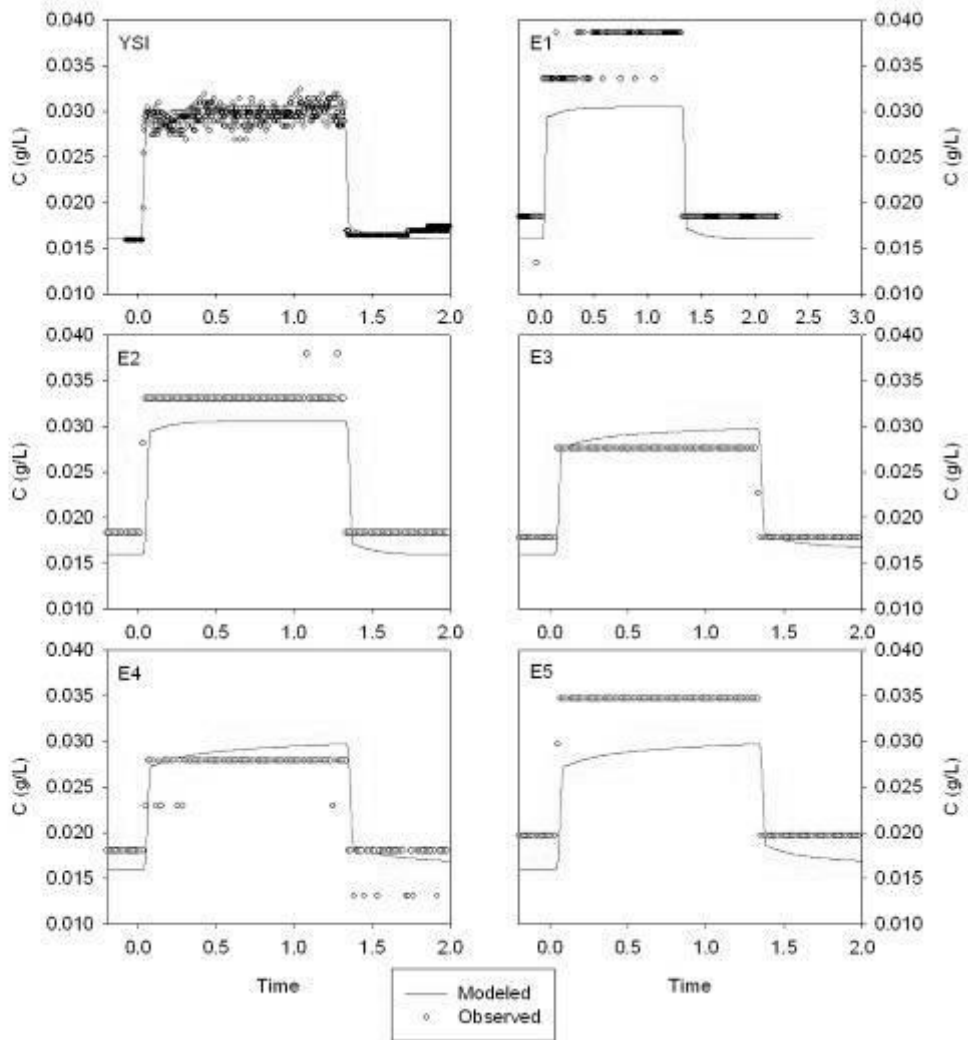


**Figure C.26** Observed and modeled tracer concentrations ( $C$  in g/L) during the tracer test at reach DB on November 12, 2010. For the goodness of fit statistics, see Table 4.10. For the location of the YSI and ECH<sub>2</sub>O 1-5 probes, see Figure 3.7.

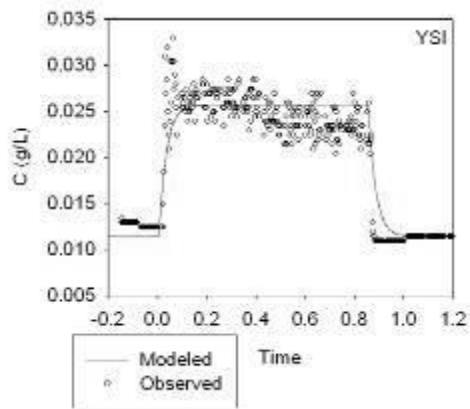


**Figure C.27** Observed and modeled tracer concentrations ( $C$  in g/L) during the tracer test at reach DB on September 24, 2010. For the goodness of fit statistics, see Table 4.10. For the location of the YSI and ECH<sub>2</sub>O 1-5 probes, see Figure 3.7.

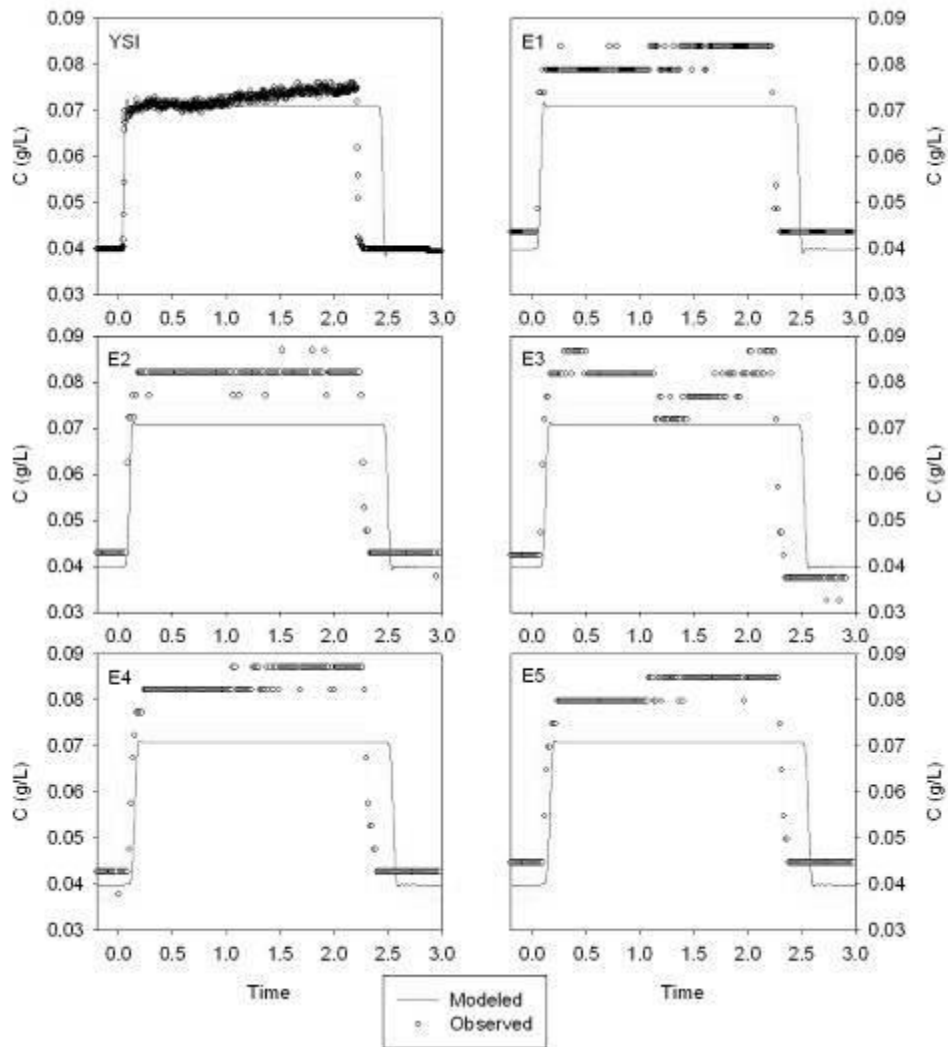


**Figure C.28** Observed and modeled tracer concentrations ( $C$  in g/L) during the tracer test at reach DB on August 16, 2010. For the goodness of fit statistics, see Table 4.10. For the location of the YSI and ECH<sub>2</sub>O 1-5 probes, see Figure 3.7.

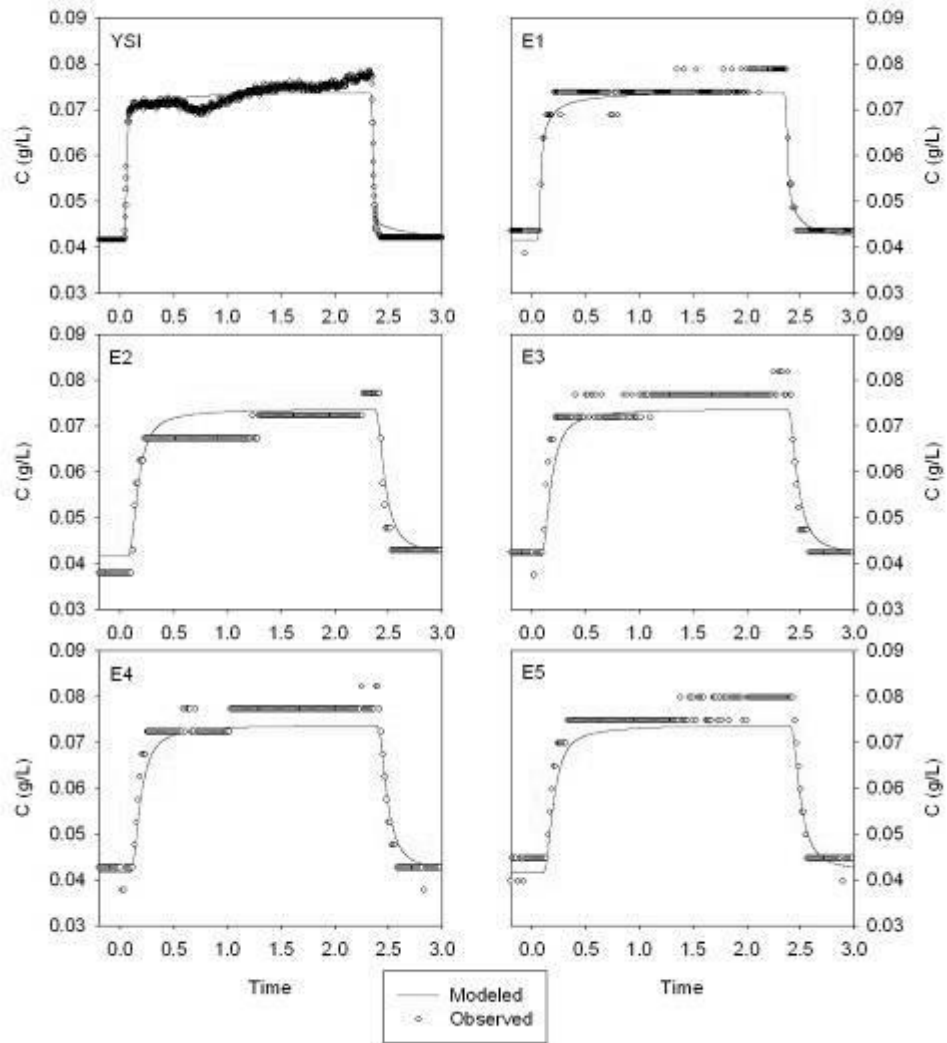


**Figure C.29** Observed and modeled tracer concentrations ( $C$  in g/L) during the tracer test at reach DB on August 4, 2010. For the goodness of fit statistics, see Table 4.10. For the location of the YSI and ECH<sub>2</sub>O 1-5 probes, see Figure 3.7.

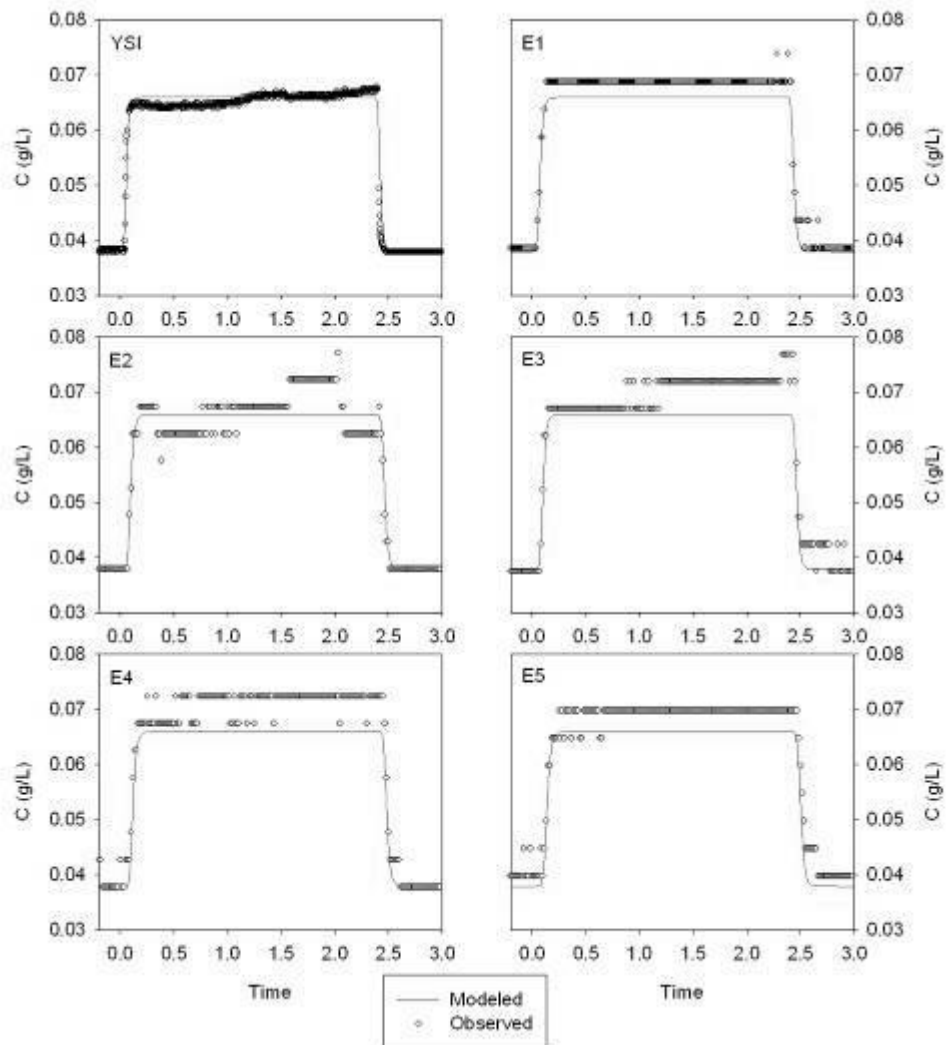


**Figure C.30** Observed and modeled tracer concentrations ( $C$  in g/L) during the tracer test at reach DB on July 27, 2010. For the goodness of fit statistics, see Table 4.10. For the location of the YSI and ECH<sub>2</sub>O 1-5 probes, see Figure 3.7.

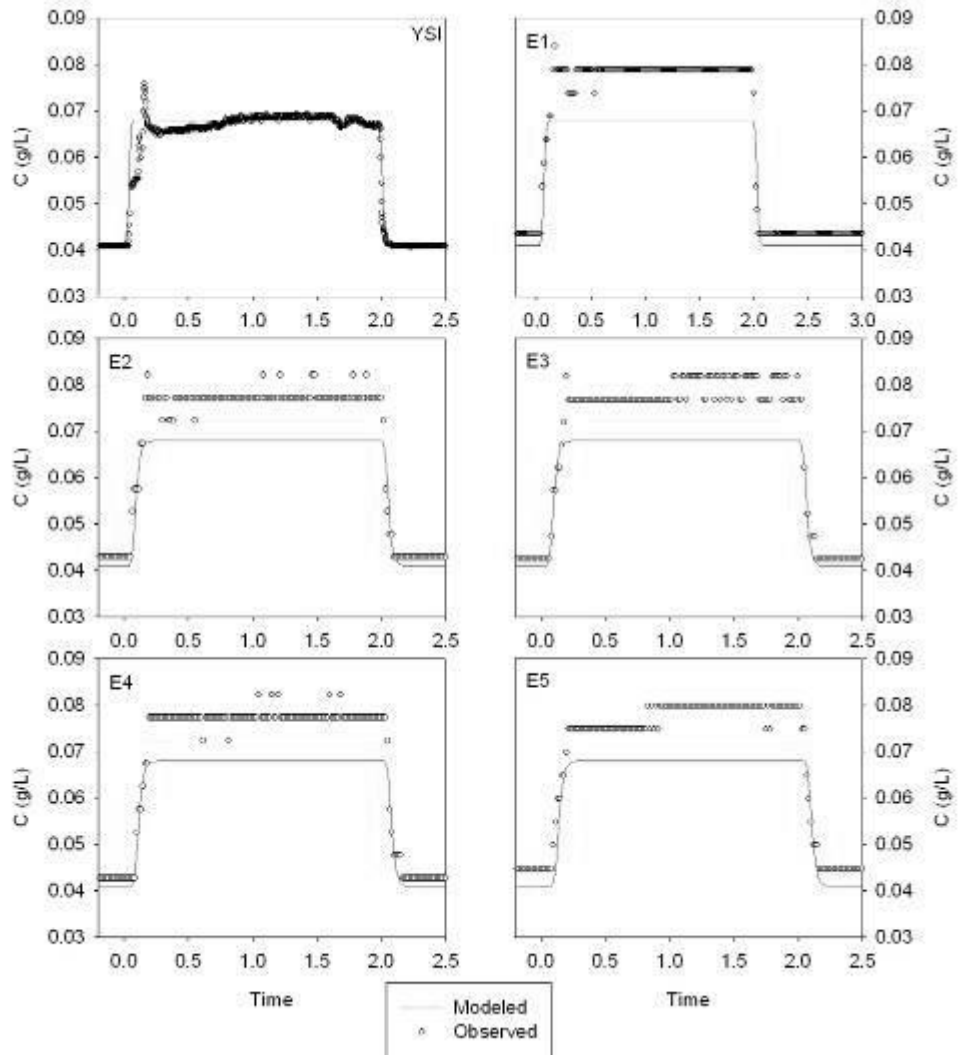


**Figure C.31** Observed and modeled tracer concentrations ( $C$  in g/L) during the tracer test at reach DB on June 20, 2010. For the goodness of fit statistics, see Table 4.10. For the location of the YSI and ECH<sub>2</sub>O 1-5 probes, see Figure 3.7.

## Appendix D: Validation Results

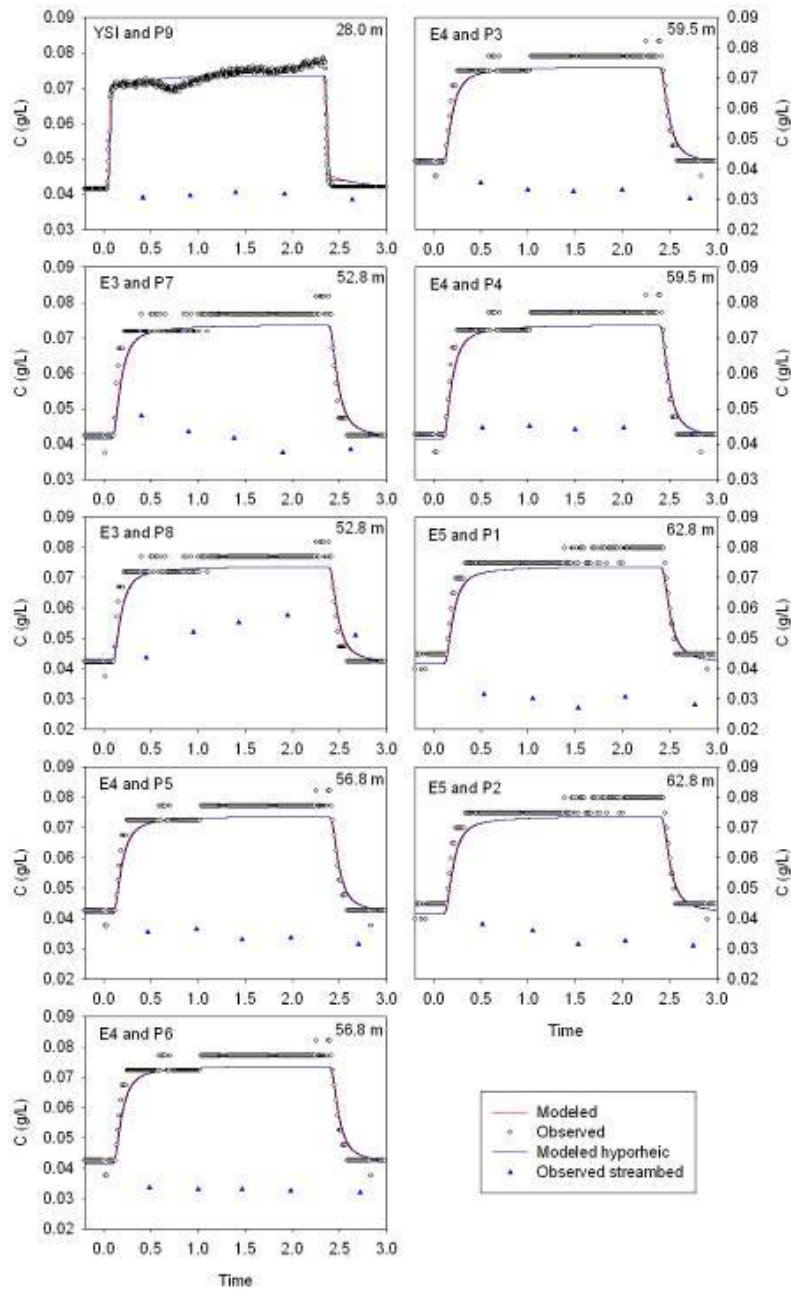


**Figure D.1** Observed and modeled tracer concentrations ( $C$  in g/L) during the tracer test at reach DA on August 6, 2010. For the goodness of fit statistics, see Table 4.16. For the location of the DEC probes and piezometers, see Figure 3.7.

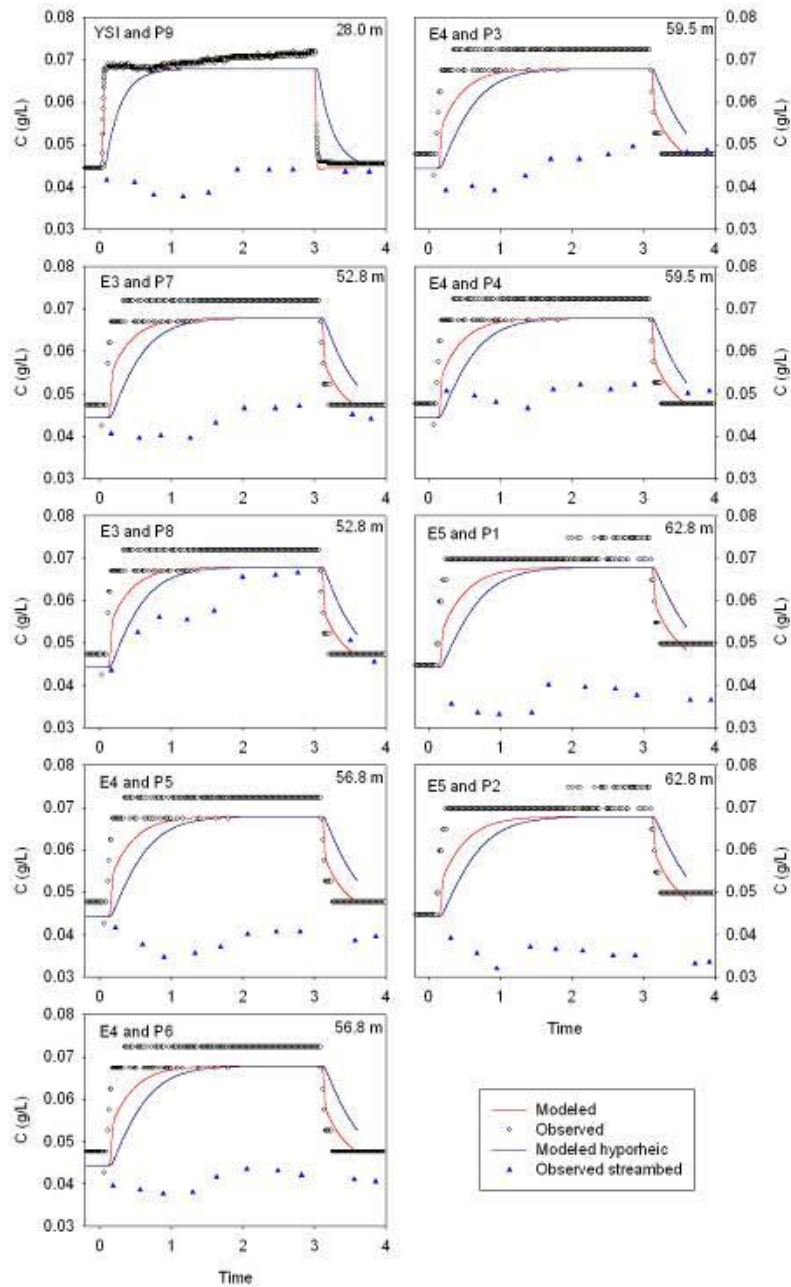


**Figure D.2** Observed and modeled tracer concentrations ( $C$  in g/L) during the tracer test at reach DA on August 10, 2010. For the goodness of fit statistics, see Table 4.16. For the location of the DEC probes and piezometers, see Figure 3.7.

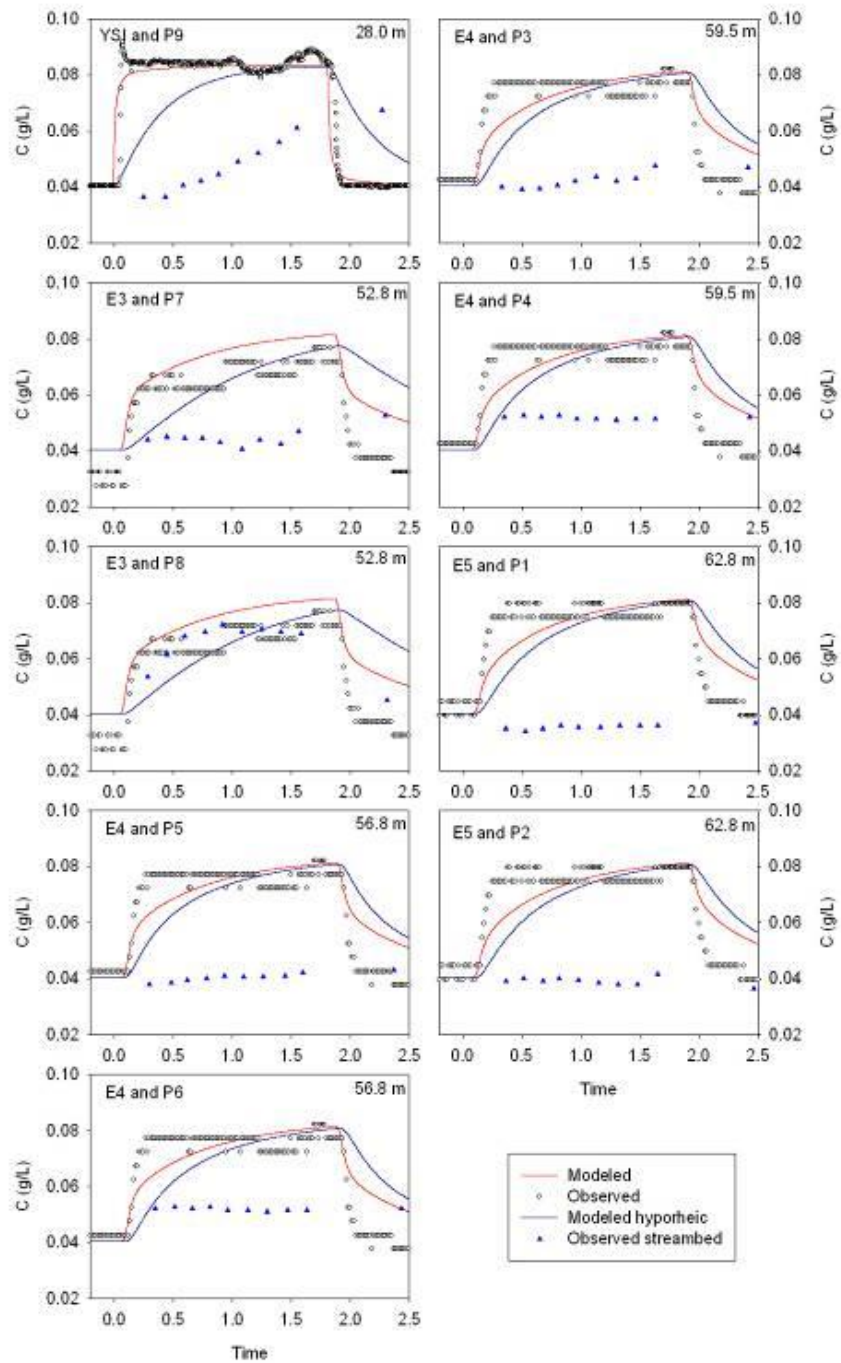


**Figure D.3** Observed and modeled tracer concentrations ( $C$  in g/L) during the tracer test at reach DA on August 19, 2010. For the goodness of fit statistics, see Table 4.16. For the location of the DEC probes and piezometers, see Figure 3.7.

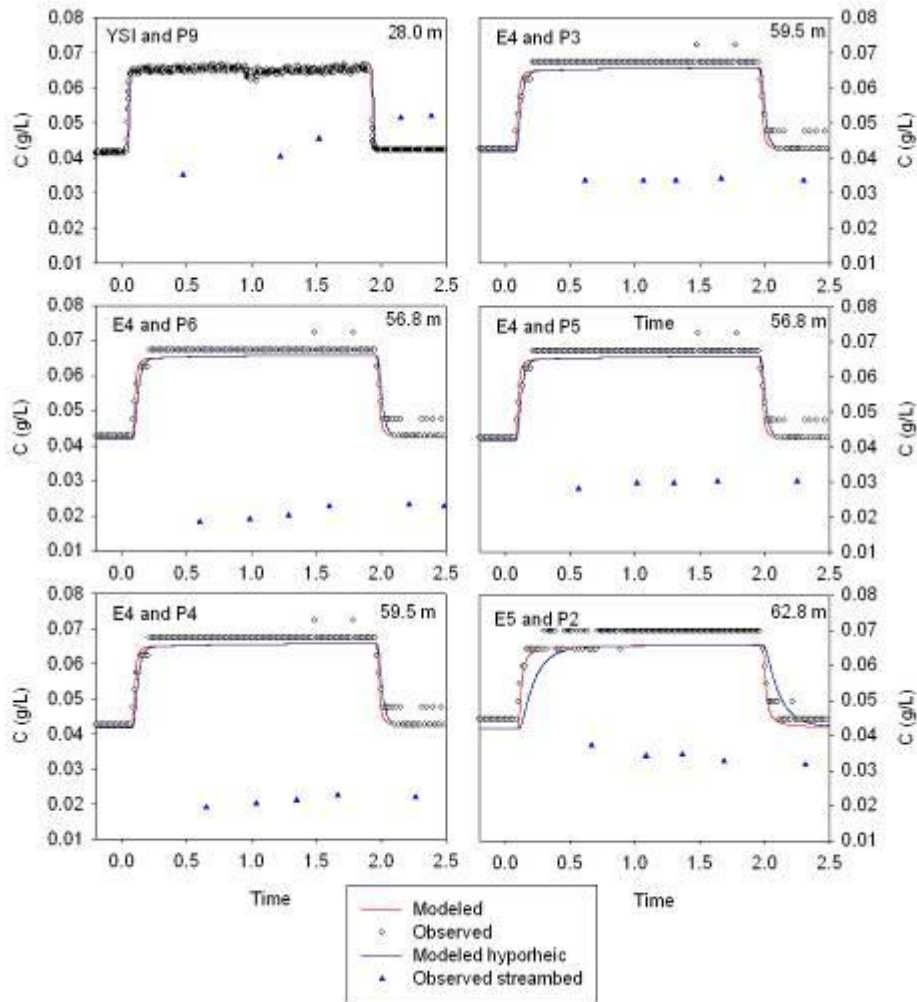


**Figure D.4** Observed and modeled tracer concentrations ( $C$  in g/L) during the tracer test at reach DA on September 15, 2010. For the goodness of fit statistics, see Table 4.16. For the location of the DEC probes and piezometers, see Figure 3.7.

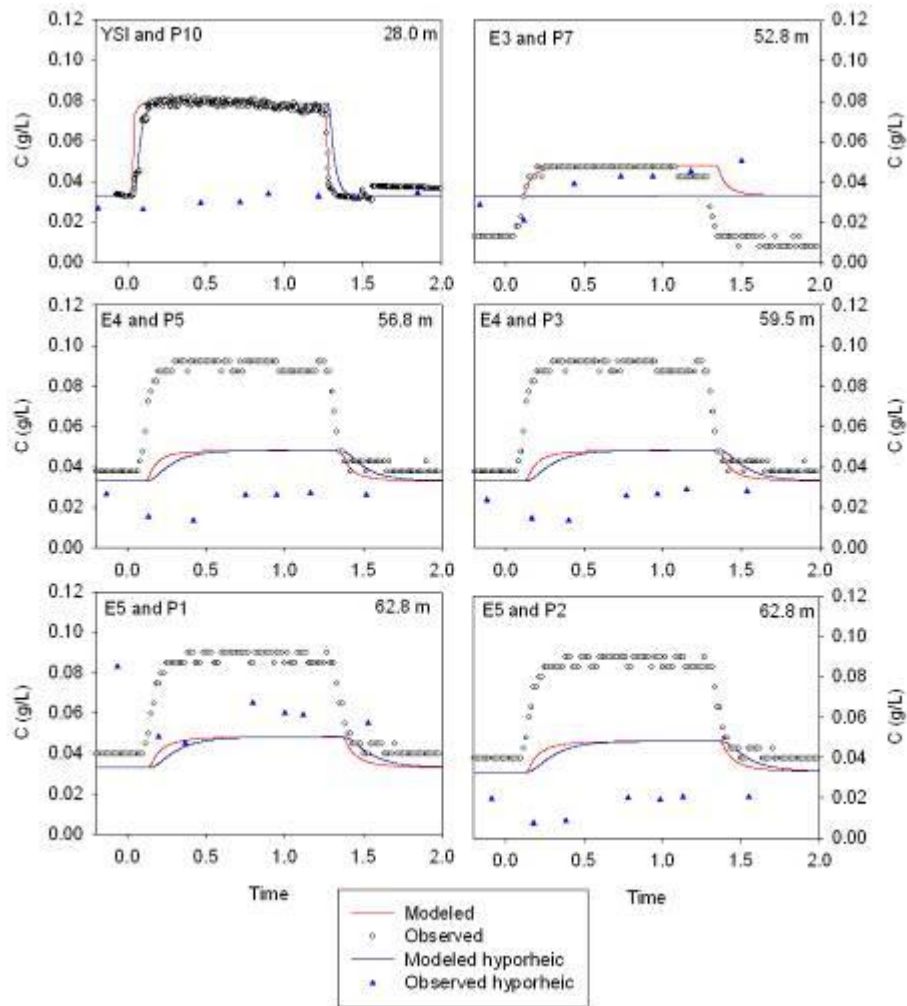


**Figure D.5** Observed and modeled tracer concentrations ( $C$  in g/L) during the tracer test at reach DA on October 19, 2010. For the goodness of fit statistics, see Table 4.16. For the location of the DEC probes and piezometers, see Figure 3.7.

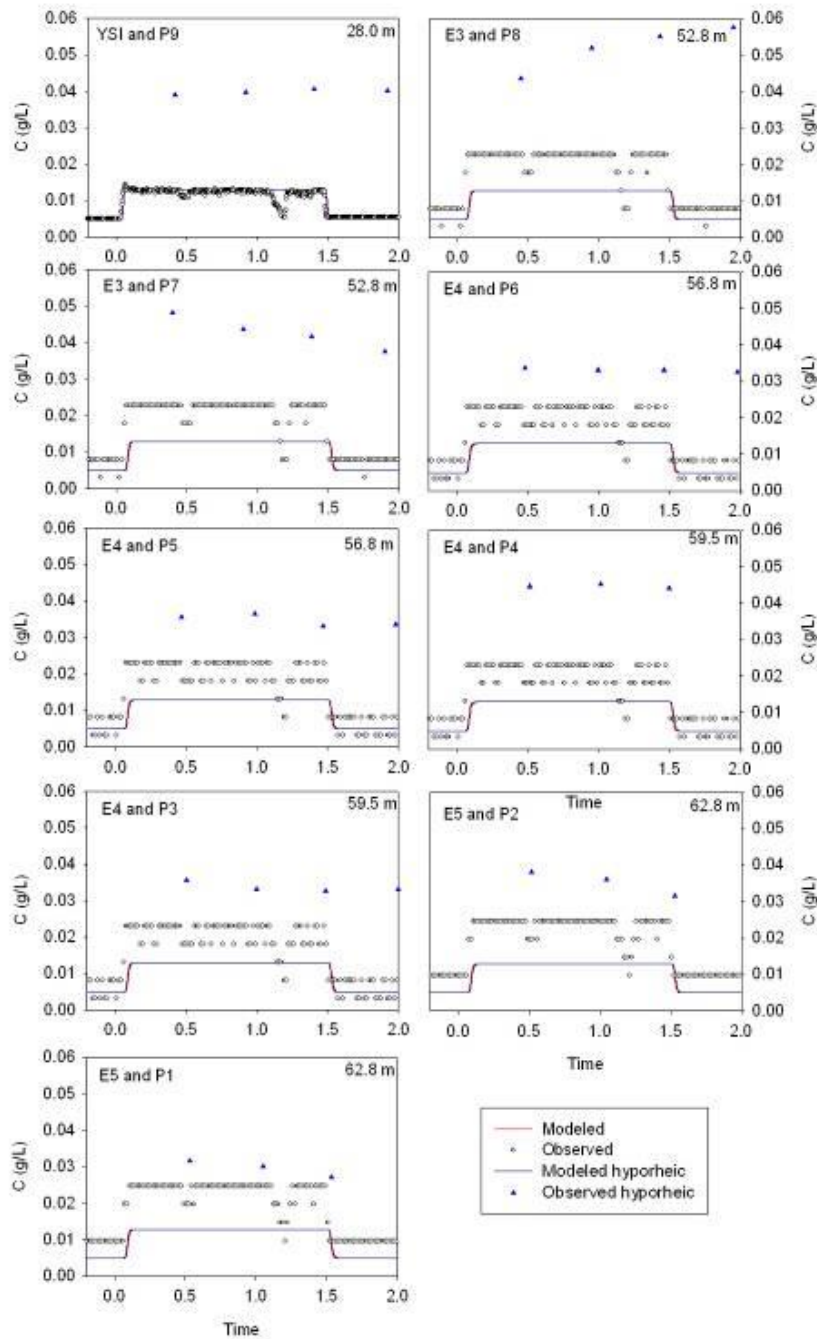


**Figure D.6** Observed and modeled tracer concentrations ( $C$  in g/L) during the tracer test at reach DA on November 16, 2010. For the goodness of fit statistics, see Table 4.16. For the location of the DEC probes and piezometers, see Figure 3.7.

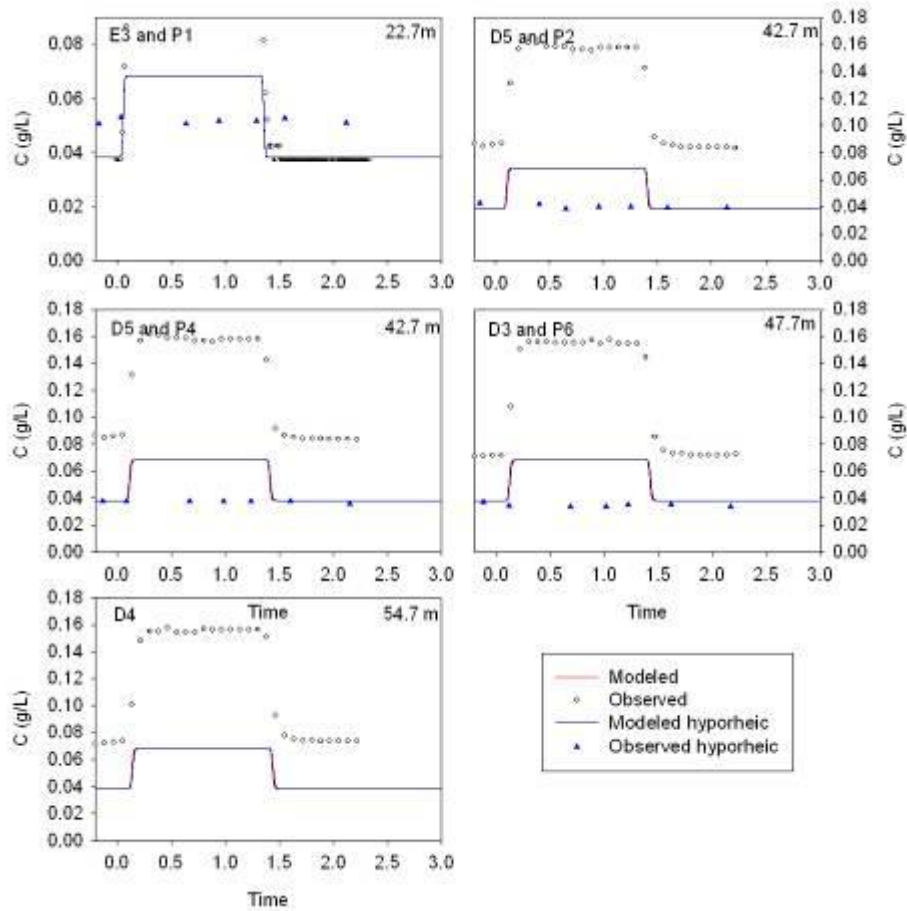


**Figure D.7** Observed and modeled tracer concentrations ( $C$  in g/L) during the tracer test at reach DB on October 20, 2010. For the goodness of fit statistics, see Table 4.16. For the location of the DEC probes and piezometers, see Figure 3.7.

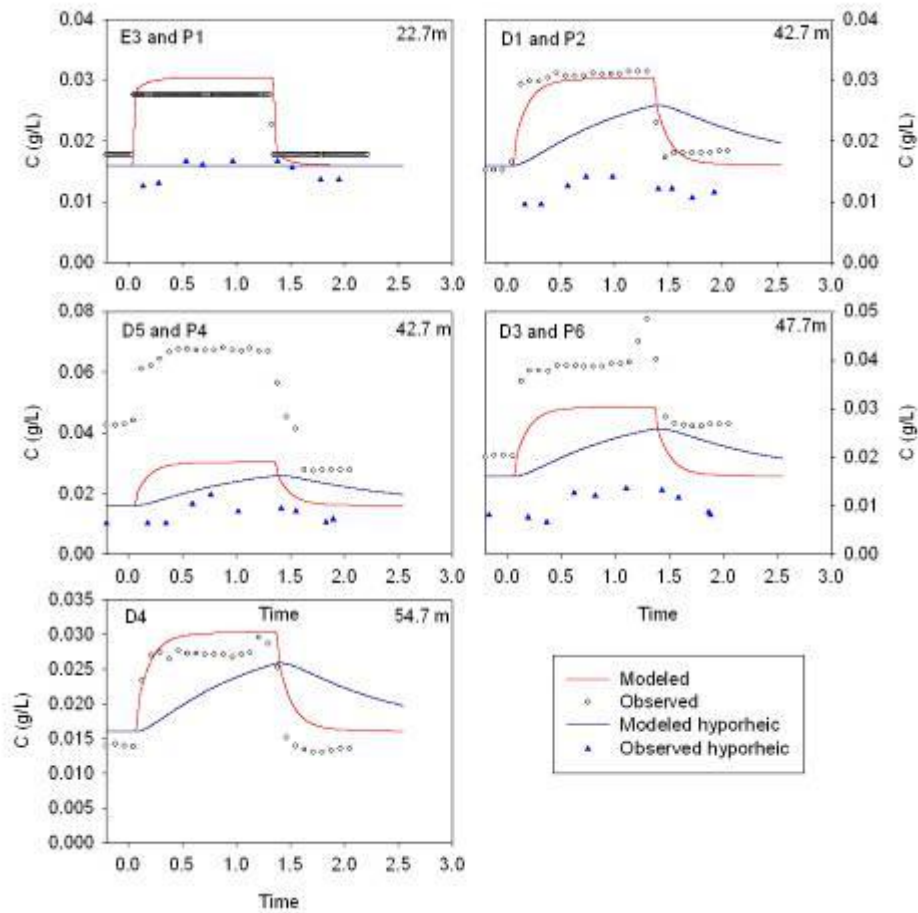


**Figure D.8** Observed and modeled tracer concentrations ( $C$  in g/L) during the tracer test at reach DB on October 12, 2010. For the goodness of fit statistics, see Table 4.16. For the location of the DEC probes and piezometers, see Figure 3.7.

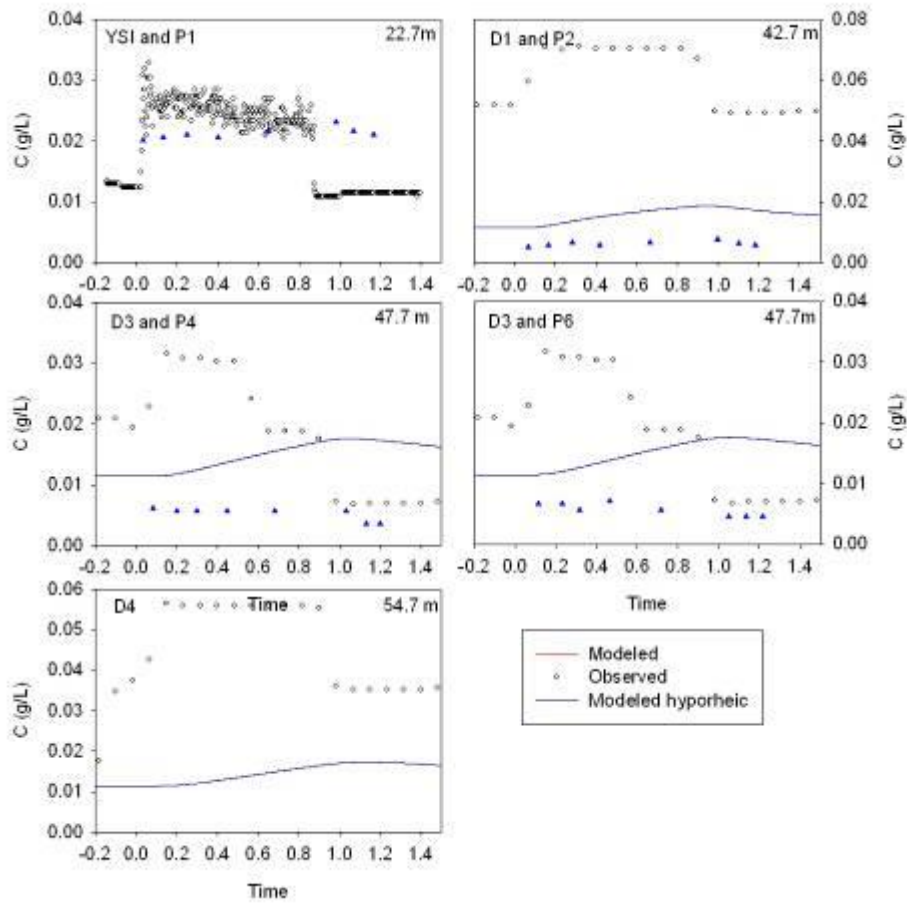


**Figure D.9** Observed and modeled tracer concentrations ( $C$  in g/L) during the tracer test at reach DB on September 24, 2010. For the goodness of fit statistics, see Table 4.16. For the location of the DEC probes and piezometers, see Figure 3.7.

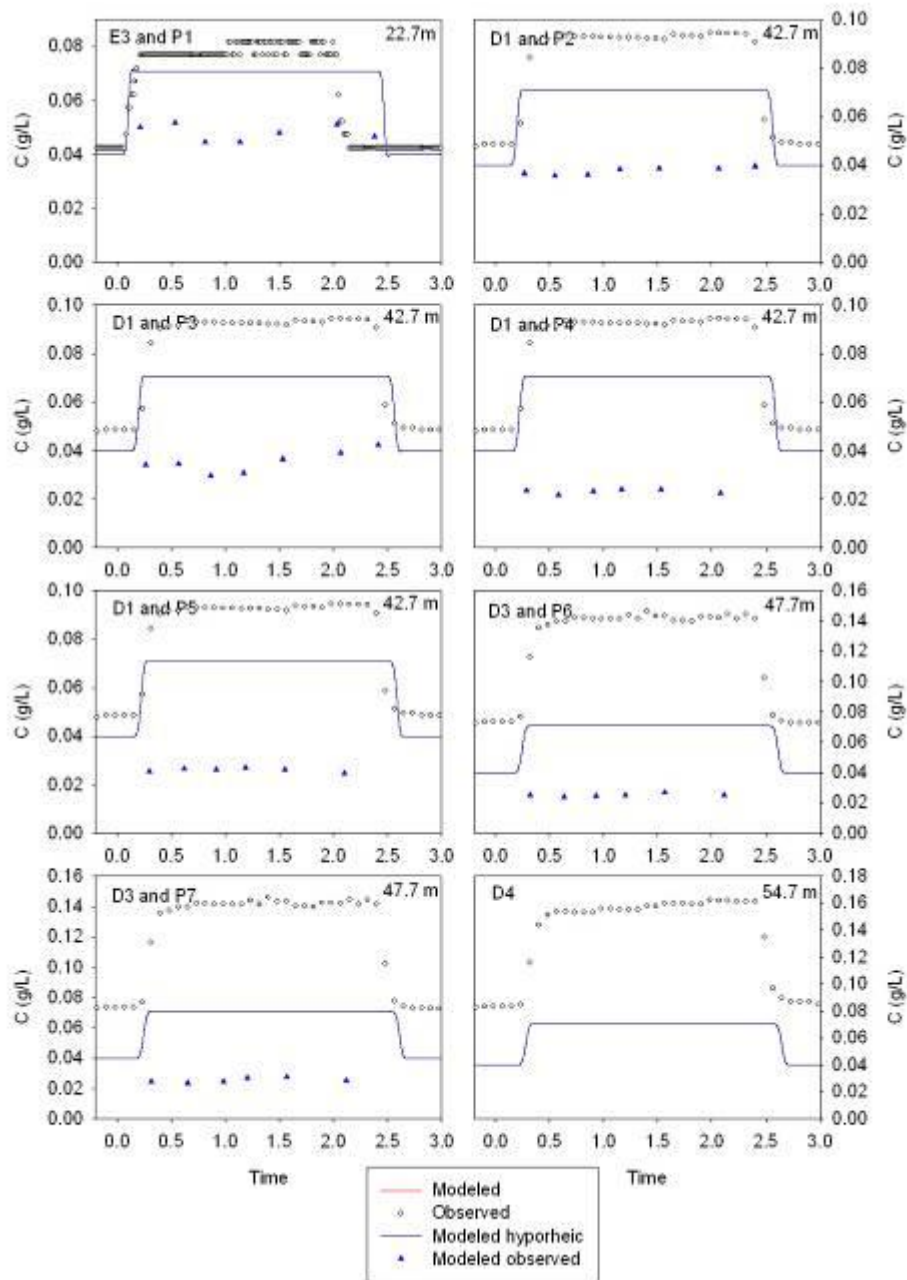


**Figure D.10** Observed and modeled tracer concentrations ( $C$  in g/L) during the tracer test at reach DB on August 16, 2010. For the goodness of fit statistics, see Table 4.16. For the location of the DEC probes and piezometers, see Figure 3.7.

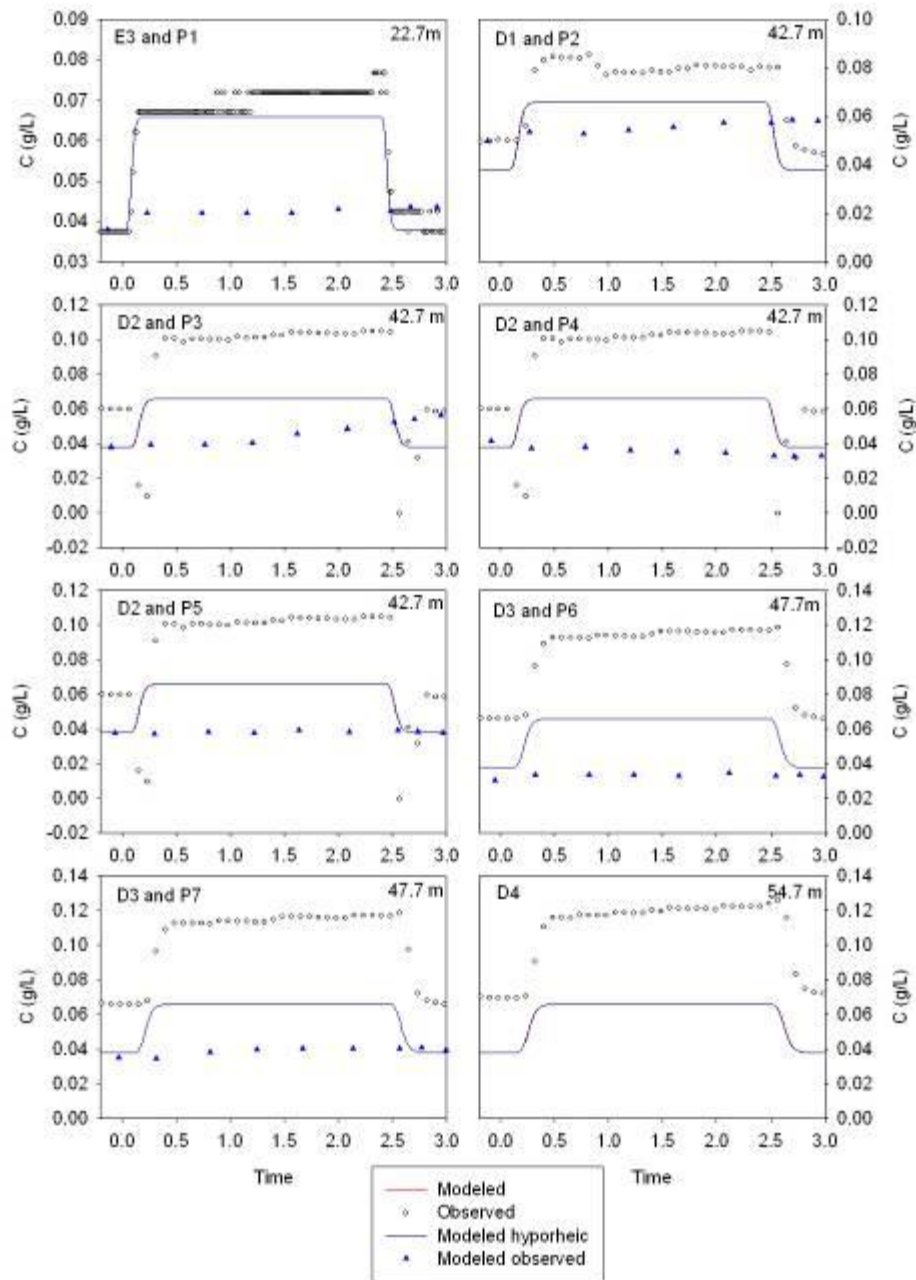


**Figure D.11** Observed and modeled tracer concentrations ( $C$  in g/L) during the tracer test at reach DB on July 27, 2010. For the goodness of fit statistics, see Table 4.16. For the location of the DEC probes and piezometers, see Figure 3.7.

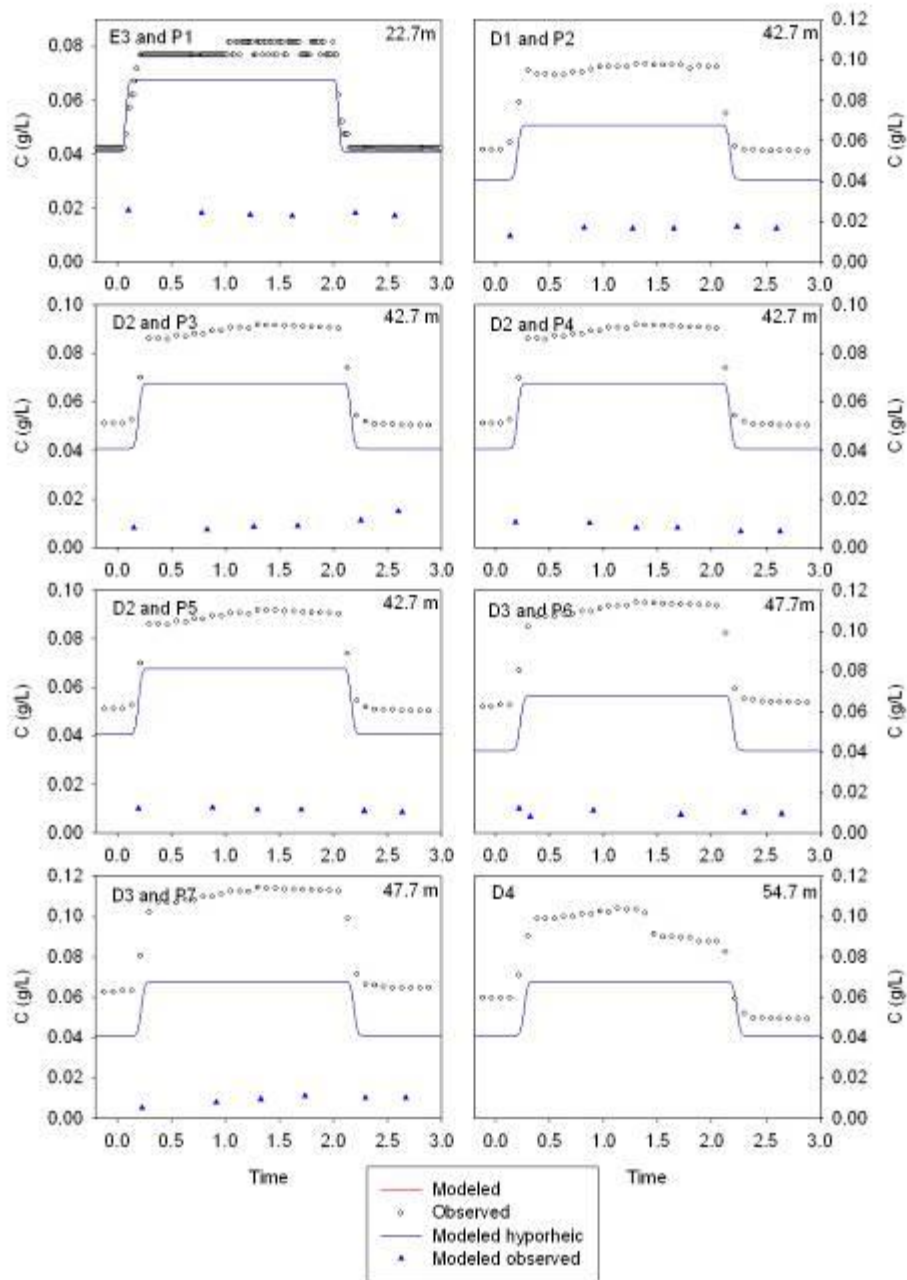


**Figure D.12** Observed and modeled tracer concentrations ( $C$  in g/L) during the tracer test at reach DB on July 20, 2010. For the goodness of fit statistics, see Table 4.16. For the location of the DEC probes and piezometers, see Figure 3.7.

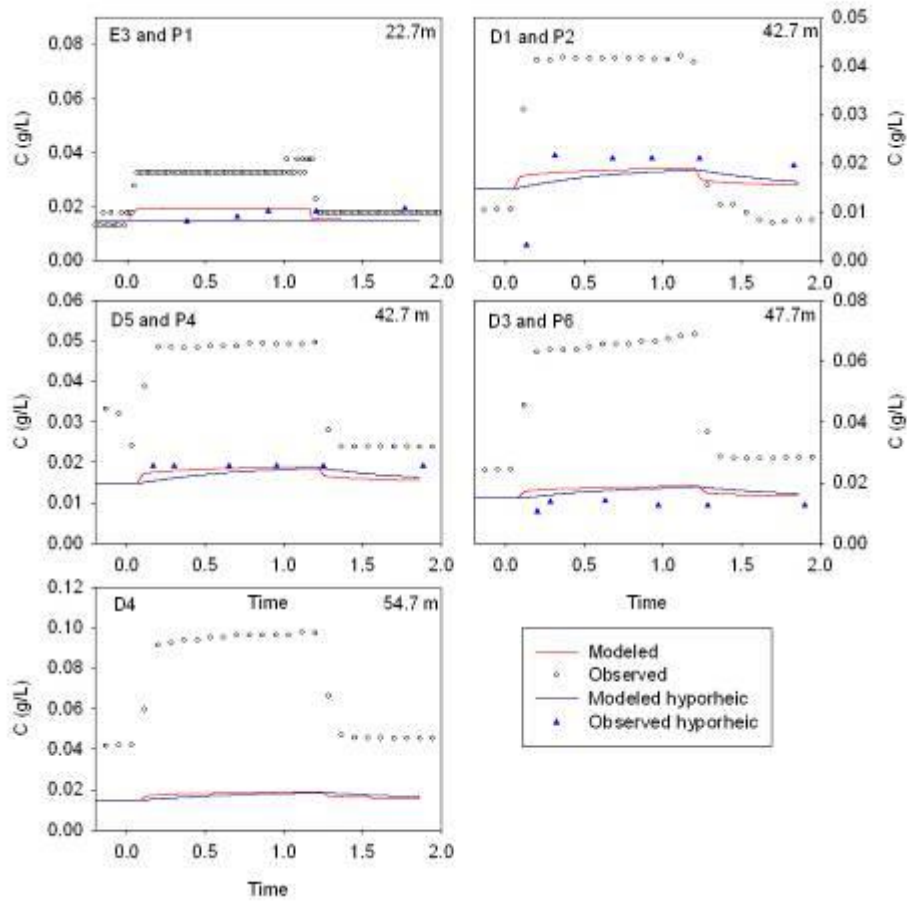


**Figure D.13** Observed and modeled tracer concentrations ( $C$  in g/L) during the tracer test at reach DB on October 29, 2010. For the goodness of fit statistics, see Table 4.16. For the location of the DEC probes and piezometers, see Figure 3.7.

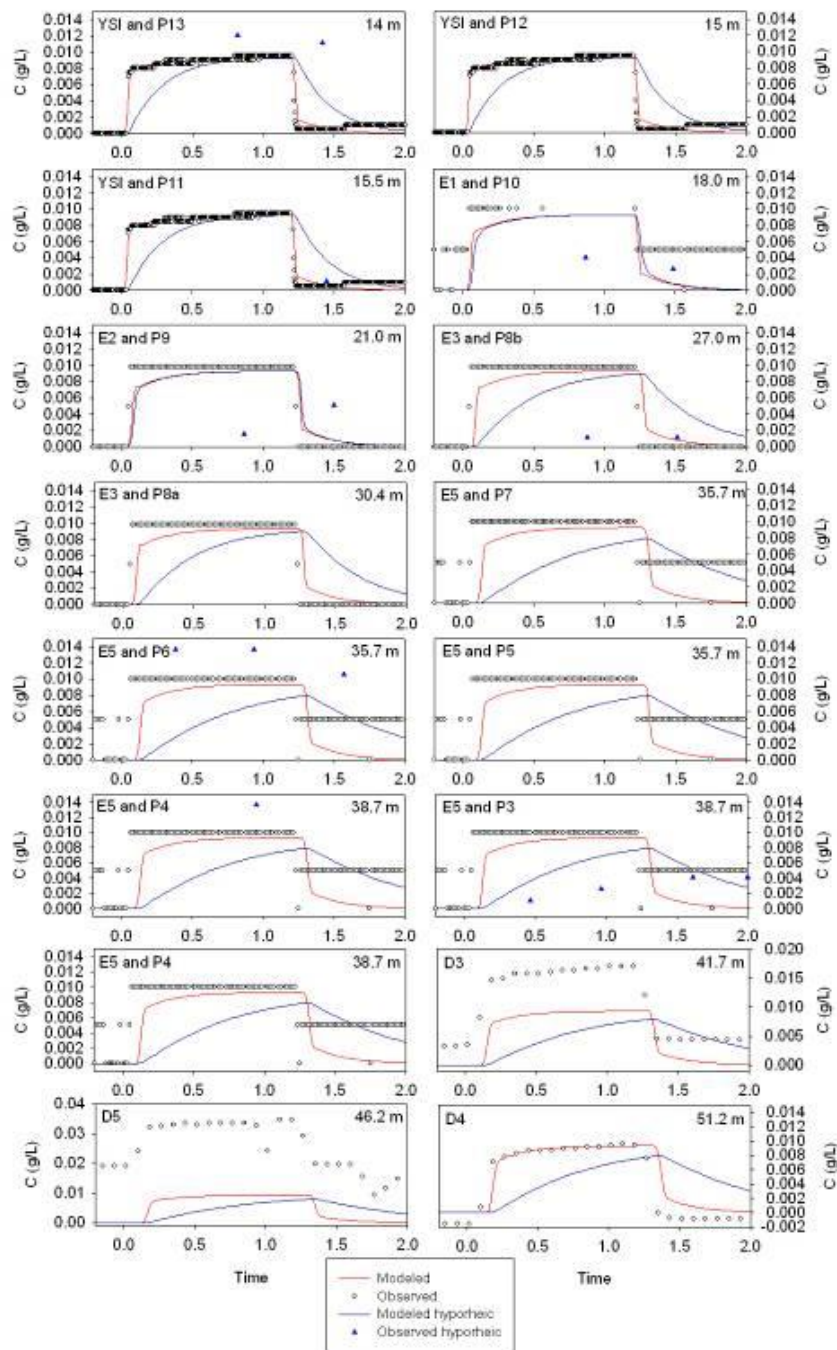


**Figure D.14** Observed and modeled tracer concentrations ( $C$  in g/L) during the tracer test at reach UA on October 26, 2010. For the goodness of fit statistics, see Table 4.15. For the location of the DEC probes and piezometers, see Figure 3.7.

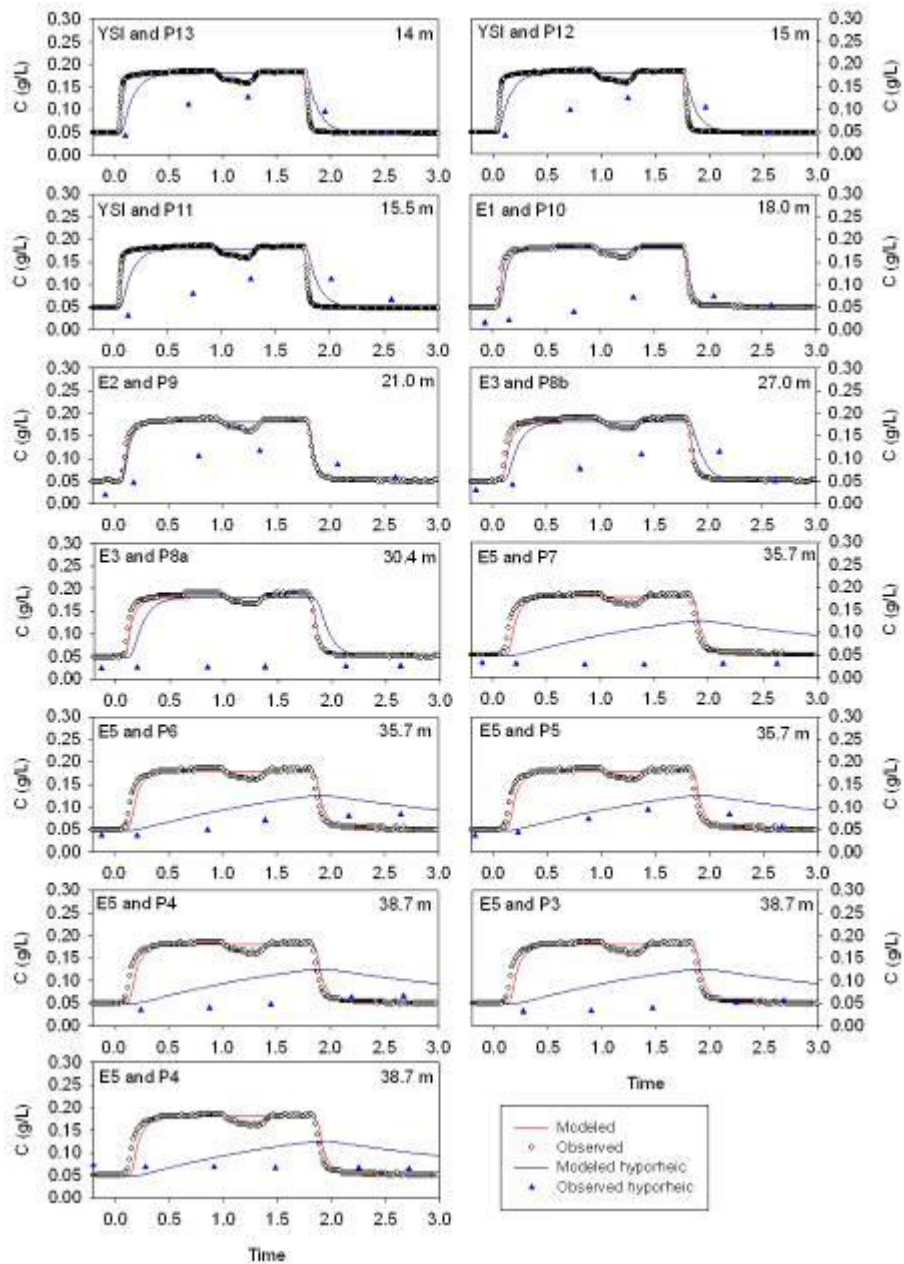


**Figure D.15** Observed and modeled tracer concentrations ( $C$  in g/L) during the tracer test at reach UA on October 18, 2010. For the goodness of fit statistics, see Table 4.15. For the location of the DEC probes and piezometers, see Figure 3.7.

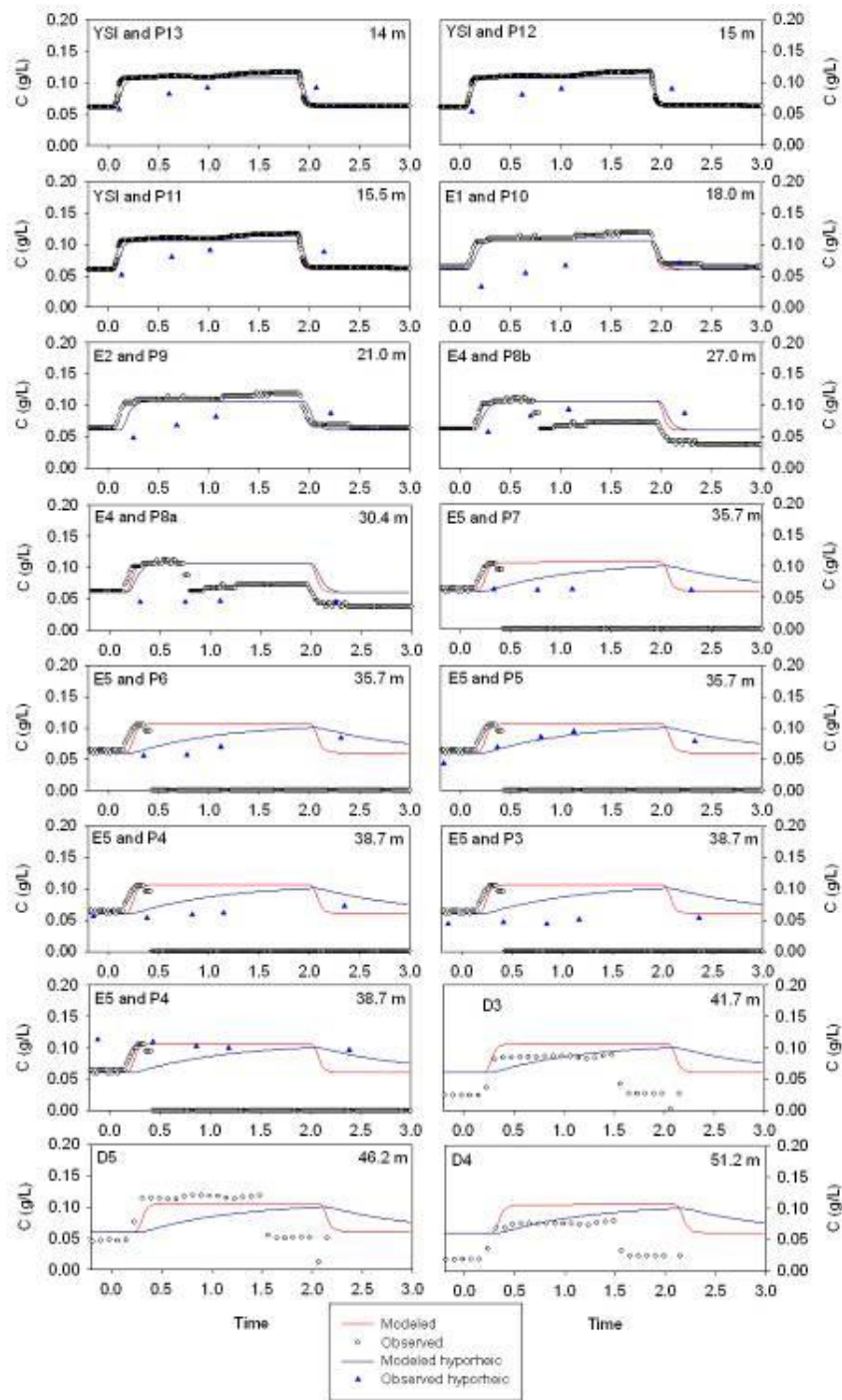


**Figure D.16** Observed and modeled tracer concentrations ( $C$  in g/L) during the tracer test at reach UA on October 5, 2010. For the goodness of fit statistics, see Table 4.15. For the location of the DEC probes and piezometers, see Figure 3.7.

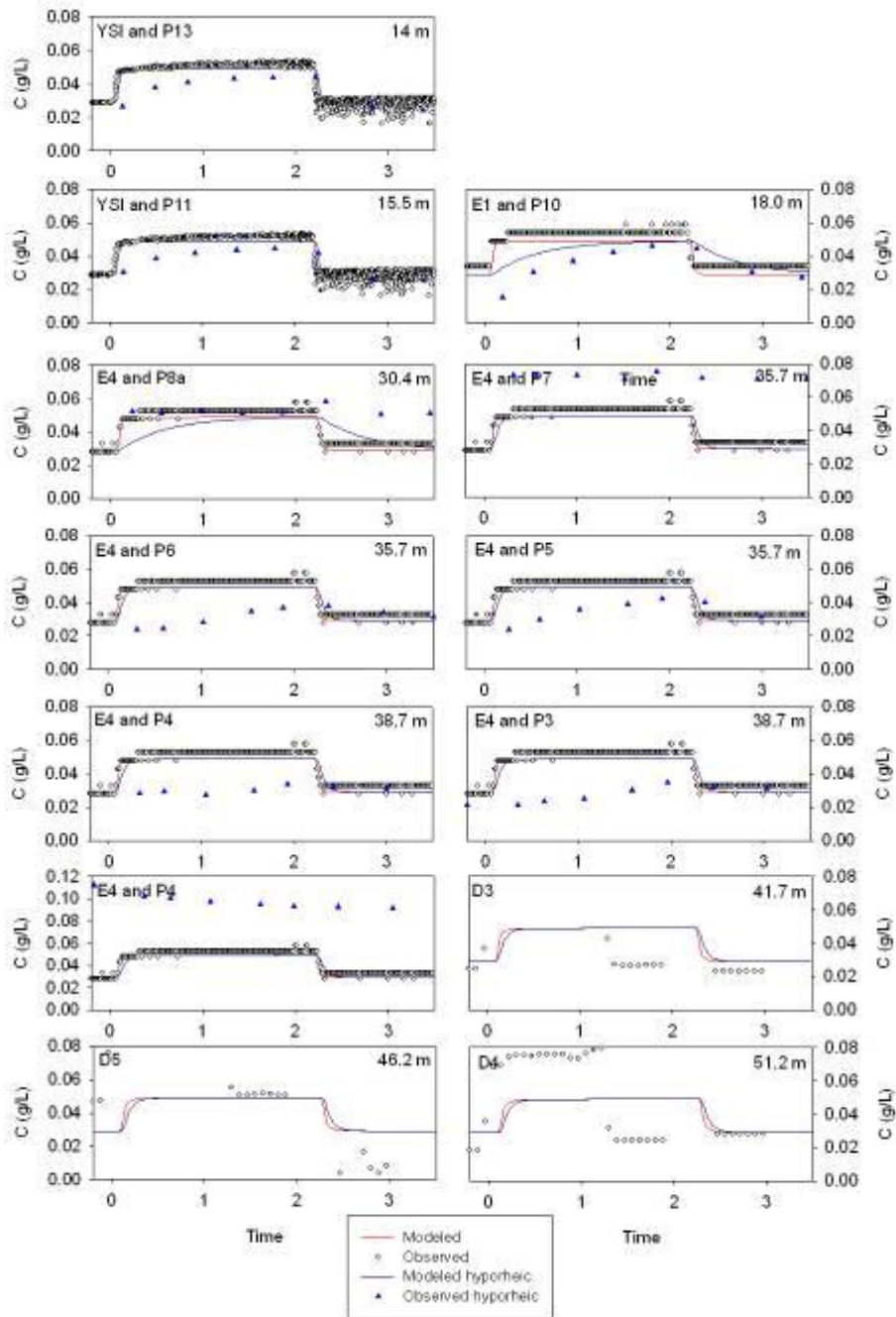


**Figure D.17** Observed and modeled tracer concentrations ( $C$  in g/L) during the tracer test at reach UA on September 22, 2010. For the goodness of fit statistics, see Table 4.15. For the location of the DEC probes and piezometers, see Figure 3.7.

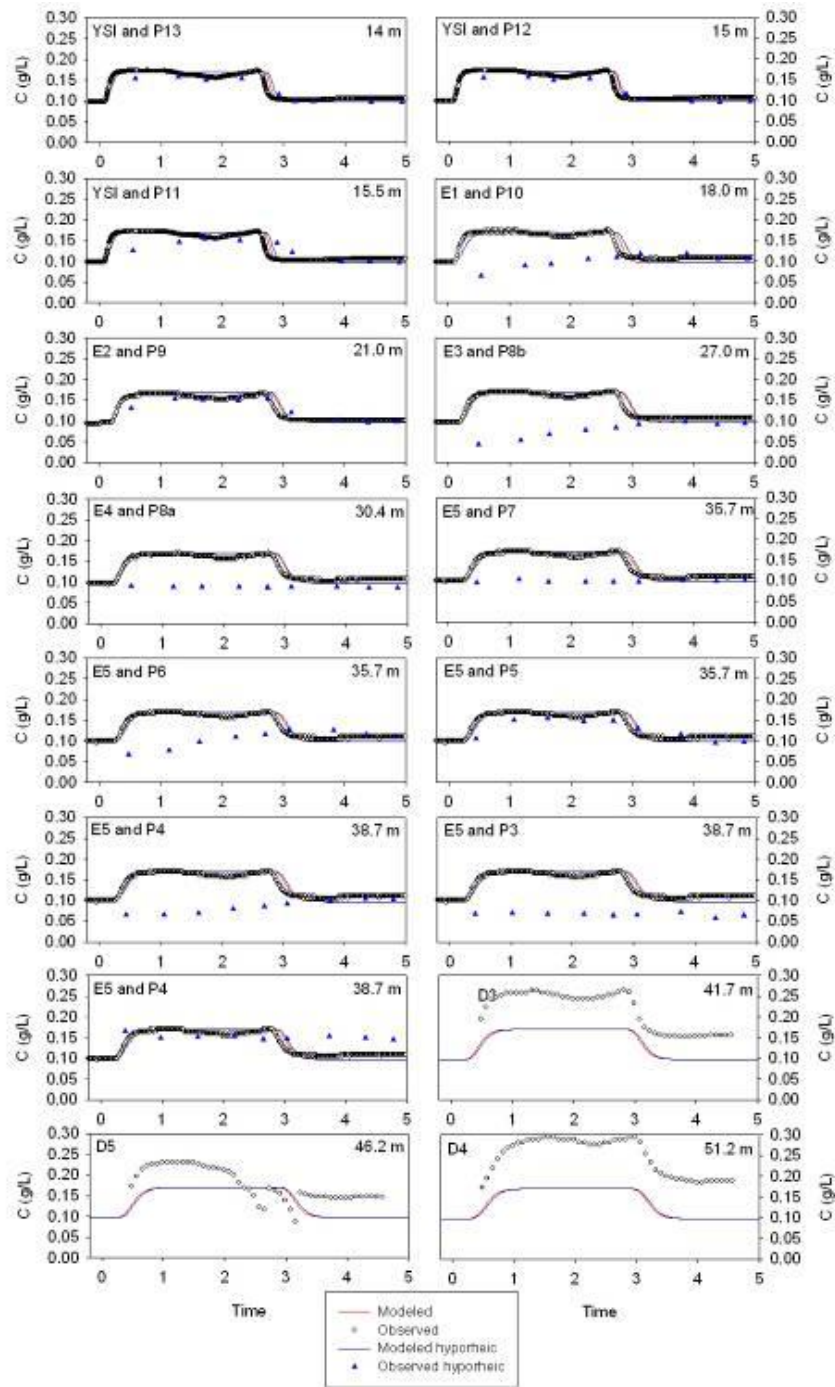


**Figure D.18** Observed and modeled tracer concentrations ( $C$  in g/L) during the tracer test at reach UA on August 18, 2010. For the goodness of fit statistics, see Table 4.15. For the location of the DEC probes and piezometers, see Figure 3.7.

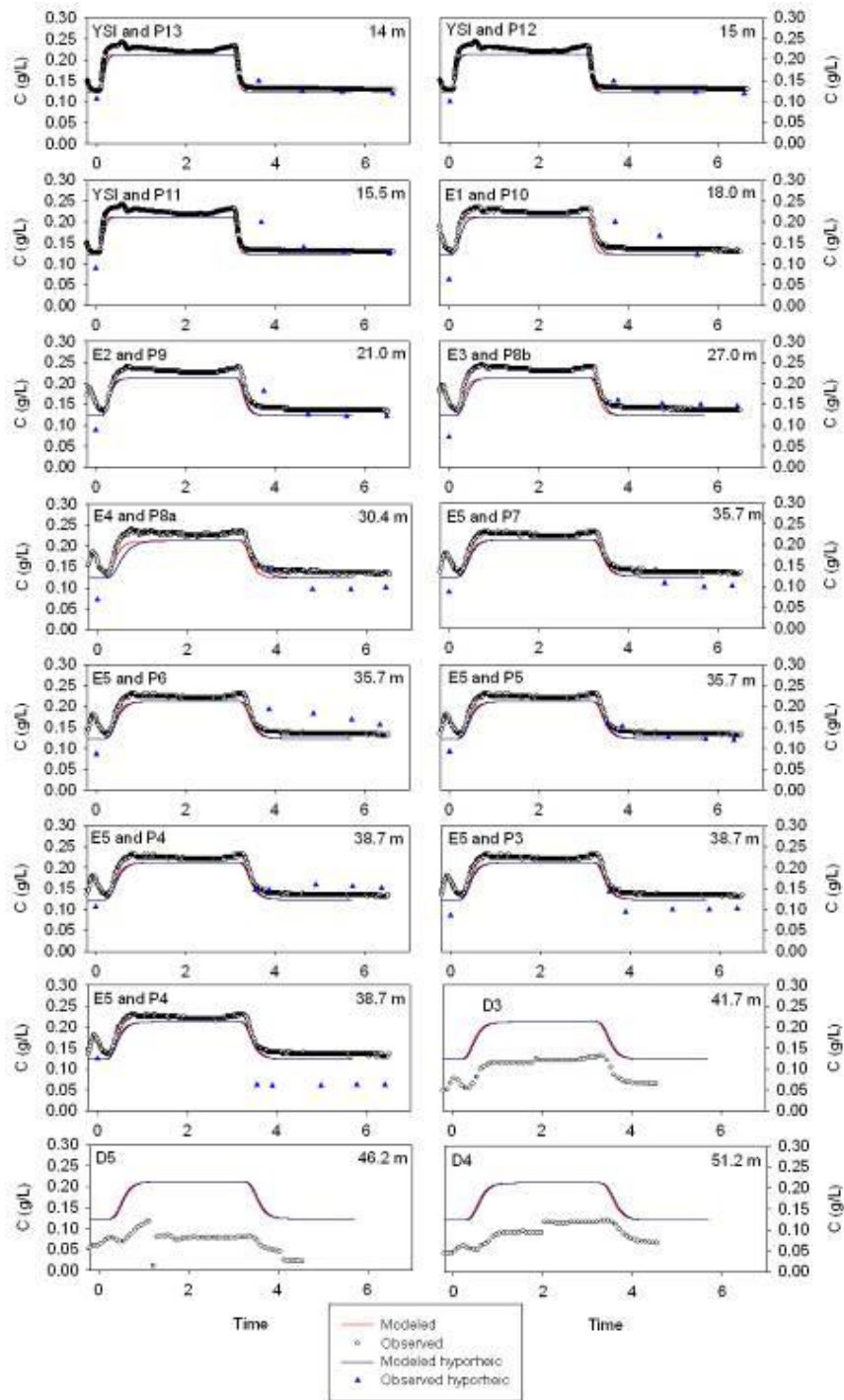


**Figure D.19** Observed and modeled tracer concentrations ( $C$  in g/L) during the tracer test at reach UA on July 15, 2010. For the goodness of fit statistics, see Table 4.15. For the location of the DEC probes and piezometers, see Figure 3.7.

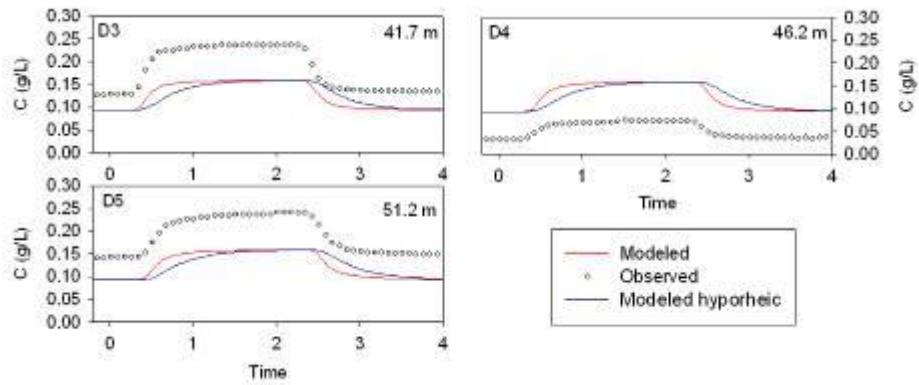


**Figure D.20** Observed and modeled tracer concentrations ( $C$  in g/L) during the tracer test at reach UA on July 2, 2010. For the goodness of fit statistics, see Table 4.15. For the location of the DEC probes and piezometers, see Figure 3.7.

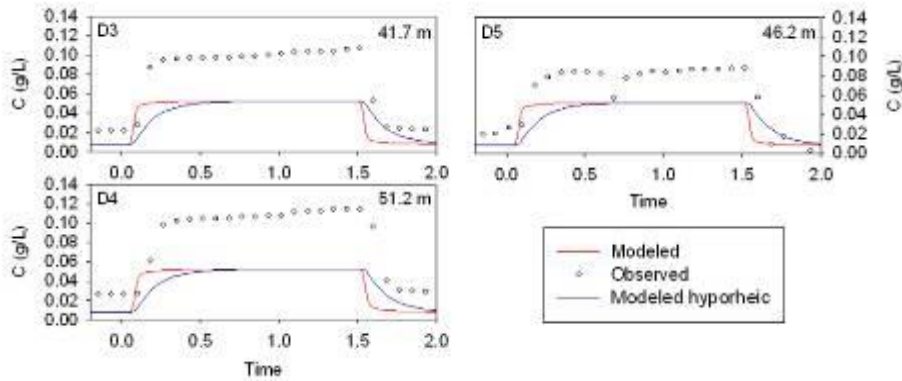


**Figure D.21** Observed and modeled tracer concentrations ( $C$  in g/L) during the tracer test at reach UA on November 3, 2010. For the goodness of fit statistics, see Table 4.15. For the location of the DEC probes and piezometers, see Figure 3.7.

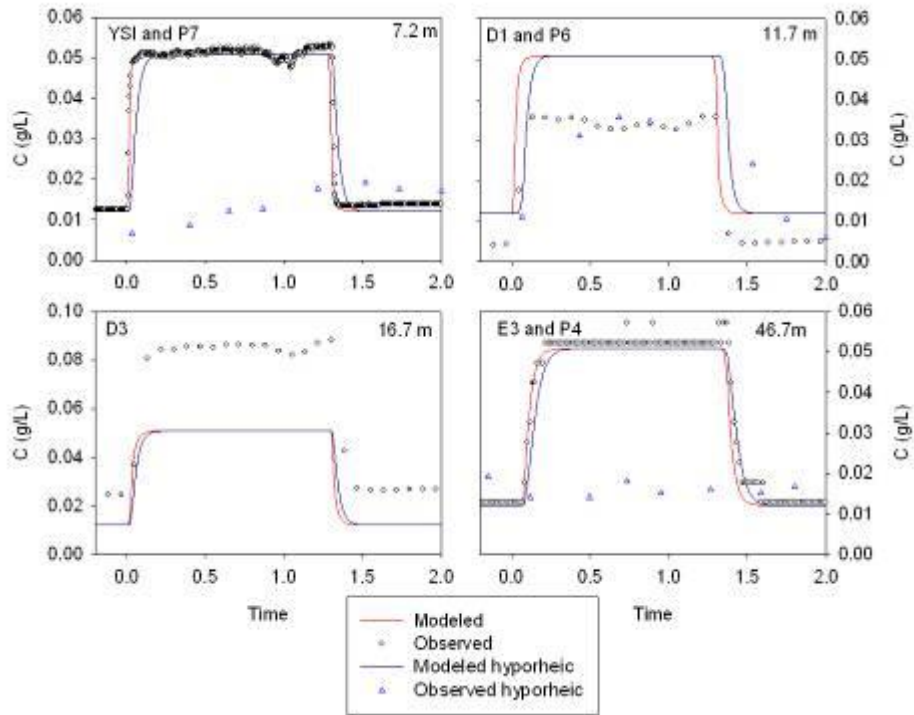


**Figure D.22** Observed and modeled tracer concentrations ( $C$  in g/L) during the tracer test at reach UB on October 13, 2010. For the goodness of fit statistics, see Table 4.15. For the location of the DEC probes and piezometers, see Figure 3.7.

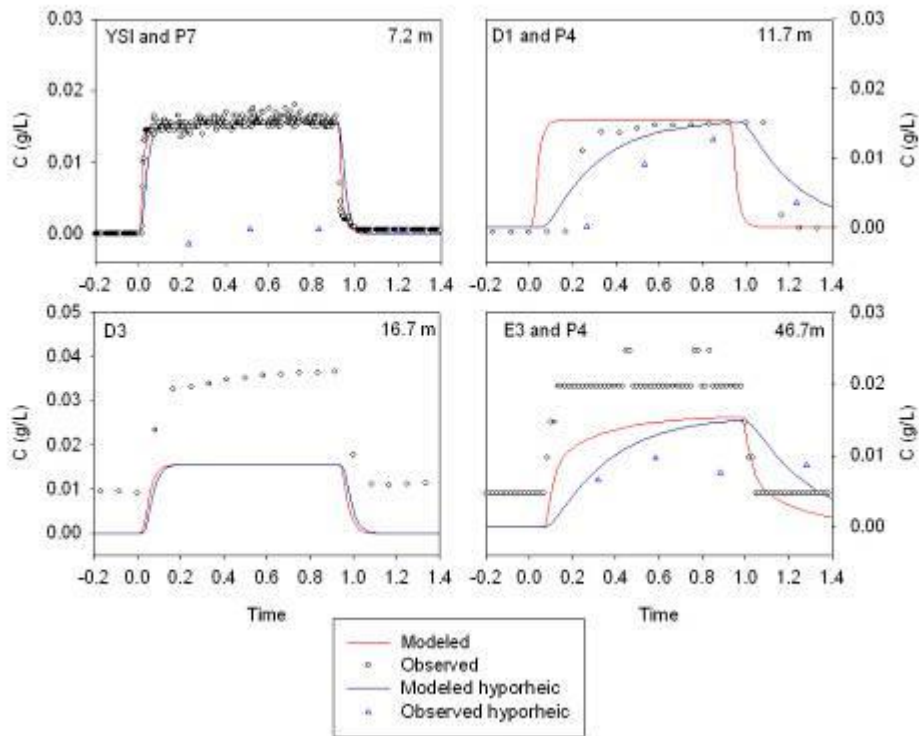


**Figure D.23** Observed and modeled tracer concentrations ( $C$  in g/L) during the tracer test at reach UB on September 29, 2010. For the goodness of fit statistics, see Table 4.15. For the location of the DEC probes and piezometers, see Figure 3.7.

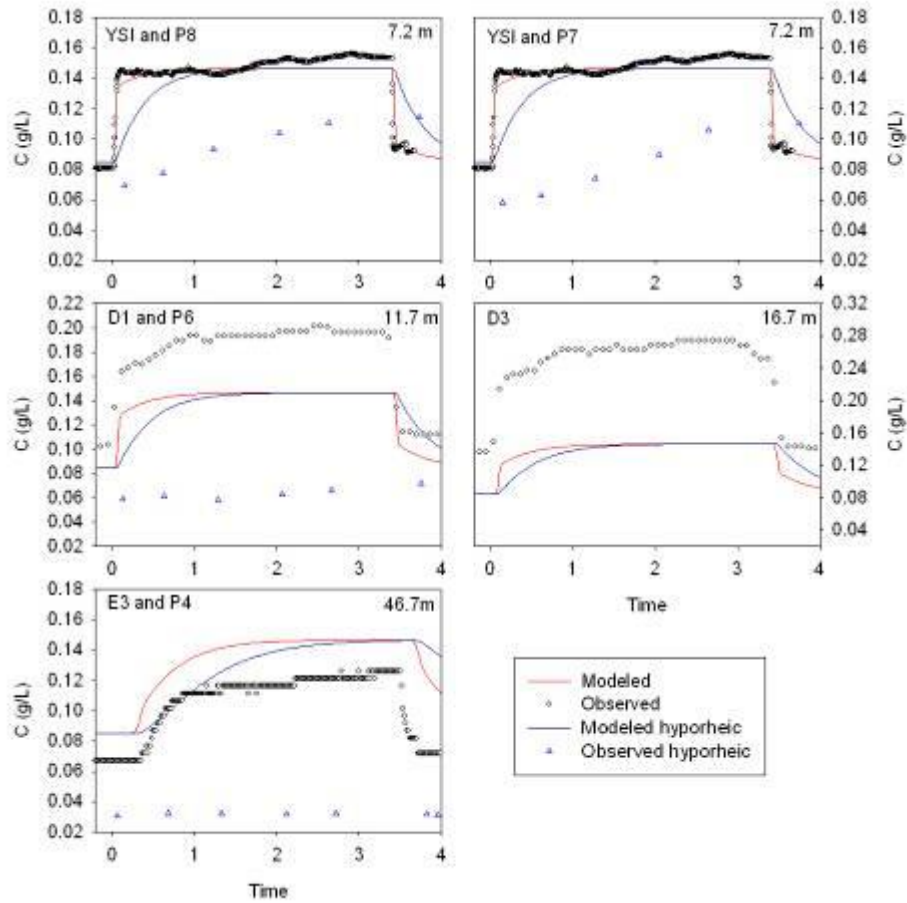


**Figure D.24** Observed and modeled tracer concentrations ( $C$  in g/L) during the tracer test at reach UB on August 12, 2010. For the goodness of fit statistics, see Table 4.15. For the location of the DEC probes and piezometers, see Figure 3.7.

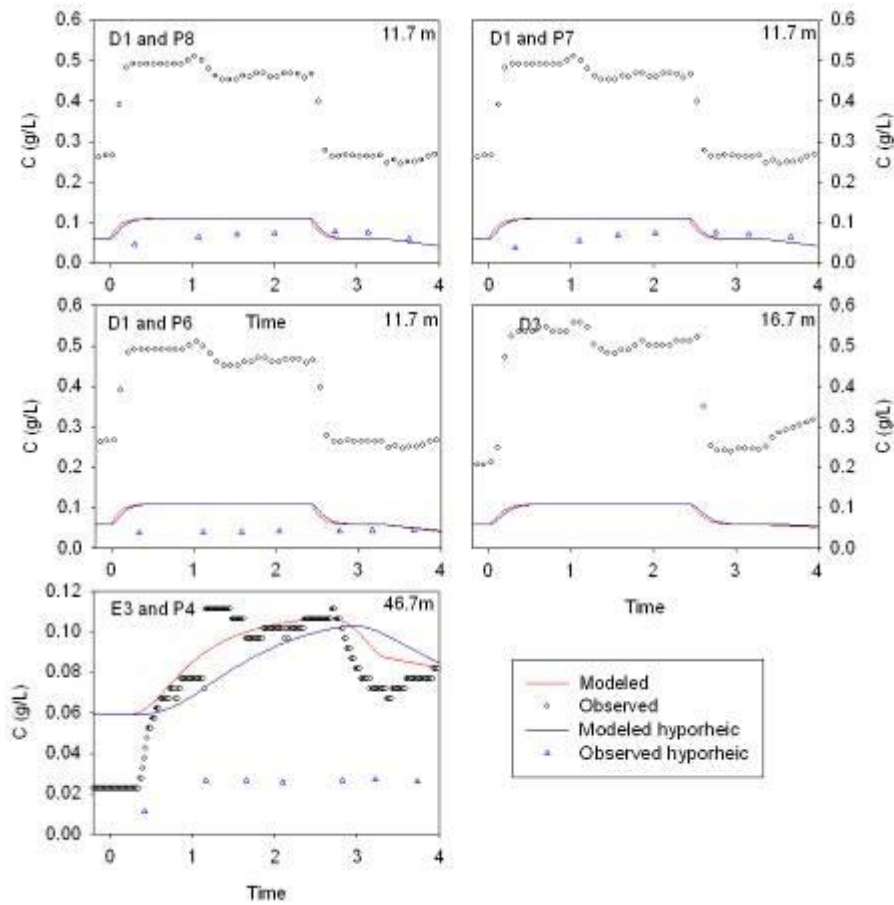


**Figure D.25** Observed and modeled tracer concentrations ( $C$  in g/L) during the tracer test at reach UB on August 5, 2010. For the goodness of fit statistics, see Table 4.15. For the location of the DEC probes and piezometers, see Figure 3.7.

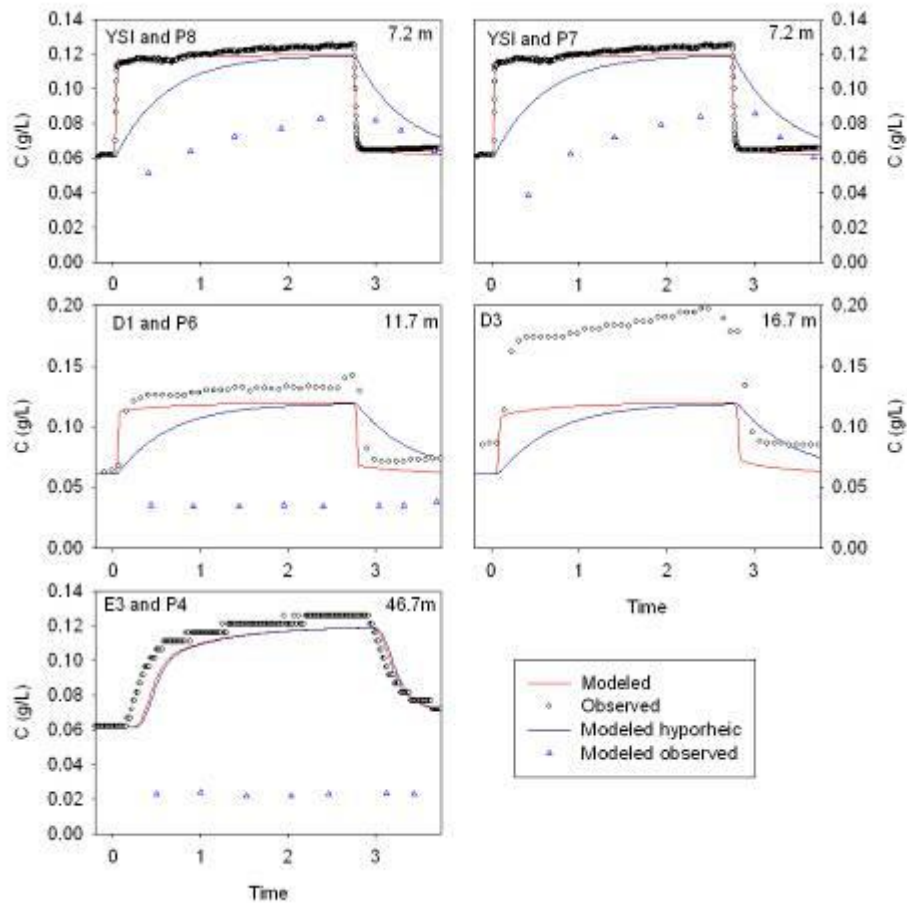


**Figure D.26** Observed and modeled tracer concentrations ( $C$  in g/L) during the tracer test at reach UB on July 26, 2010. For the goodness of fit statistics, see Table 4.15. For the location of the DEC probes and piezometers, see Figure 3.7.

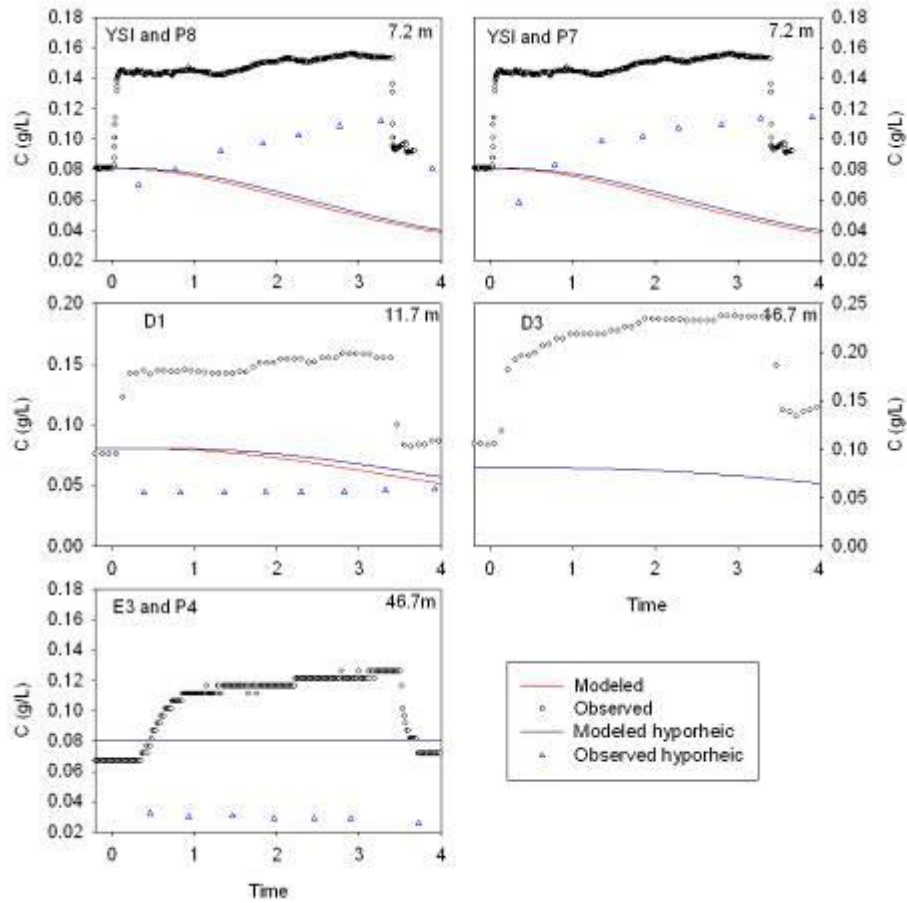


**Figure D.27** Observed and modeled tracer concentrations ( $C$  in g/L) during the tracer test at reach UB on July 23, 2010. For the goodness of fit statistics, see Table 4.15. For the location of the DEC probes and piezometers, see Figure 3.7.

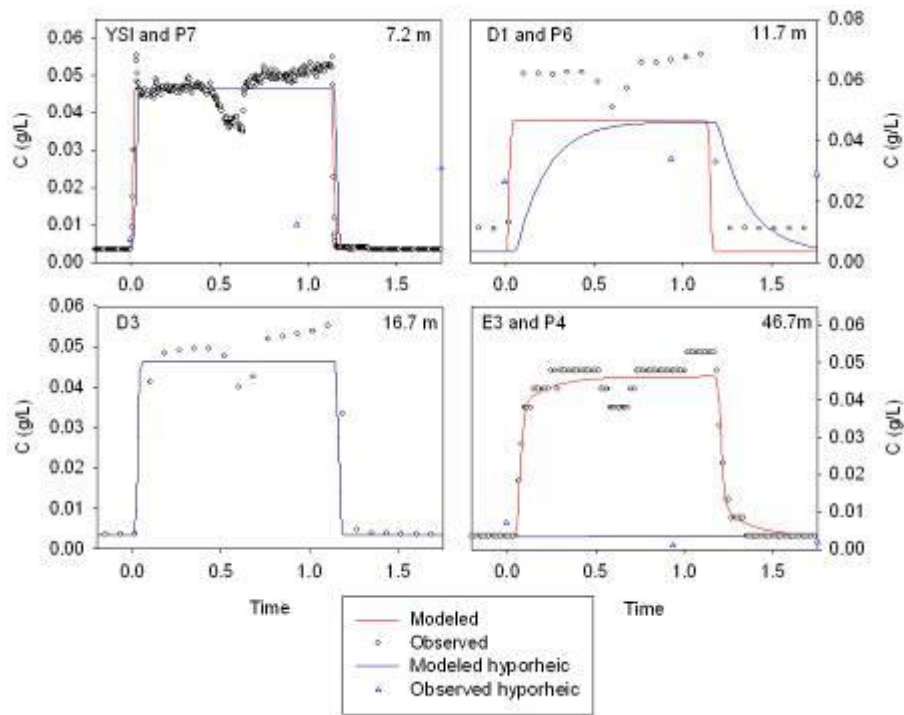


**Figure D.28** Observed and modeled tracer concentrations ( $C$  in g/L) during the tracer test at reach UB on December 4, 2010. For the goodness of fit statistics, see Table 4.15. For the location of the DEC probes and piezometers, see Figure 3.7.